Alma Mater Studiorum – Università di Bologna

DOTTORATO DI RICERCA

Scienze Chimiche

Ciclo XXI

Settore/i scientifico disciplinari di afferenza: CHIM/06

TITOLO TESI

Conformation and Stereodynamic of Hindered Aromatic Systems

Presentata da: **Dr. Michele Mancinelli**

Coordinatore Dottorato

Prof. Giuliano Longoni

Relatore

Prof. Lodovico Lunazzi

Correlatore

Dr. Andrea Mazzanti

Esame finale anno 2009

Index

Introduction

To date stereochemistry has evolved to a multifaceted and interdisciplinary field that continues to grow at an exponential rate. Chirality is a key feature of natural compounds and plays an essential role in amino acids, peptides and proteins, sugars, numerous bioactive substances, and recently it has also turned out to play a fundamental role in nanomaterials and in to drug discovery. The immense interest and activity in these areas have led to the development of new methodologies for the synthesis of chiral compounds starting from the chiral pool, by separation of racemic mixtures, or by performing asymmetric syntheses from achiral precursors, and this advance has been accompanied by significant progress in stereochemical analysis. Therefore, a wide range of analytical tools for the determination of the optical purity and absolute configurations of chiral compounds have been established in the past. Today, mechanism's knowledge of isomerization reactions, a profound understanding of the thermodynamic stability of chiral target compounds, intermediates and starting materials to racemization and diastereomerization are necessary for planning an efficient synthetic route: these studies are a fundamental aspect of dynamic stereochemistry and special emphasis is given to dynamic NMR spectroscopy.[1]

Compounds that exist as a mixture of rapidly interconverting stereoisomers are often conveniently, albeit inaccurately, viewed as one average structure. A close look reveals that organic compounds are generally fluxional and adopt more than one conformation or configuration. The low energy barrier to interconversion is often difficult to distinguish between the individual isomers of stereolabile compounds, but the interconversion of stereoisomers exhibiting anisochronous nuclei can be monitored by variable-temperature NMR spectroscopy when the process is slow on the NMR time scale.

This is the case when:

$$k = \frac{1}{t} << \pi \frac{\Delta \nu}{\sqrt{2}}$$

k = the interconversion rate constant (in s^{-1})

t = the interconversion time (in s)

Δv = the NMR shift separation of the signals (in Hz) at low temperatures at which exchange does not occur.

This equation indicates that different positions of the same nucleus can show distinct signals when the chemical shift different (*Δv*) corresponds to a time spent by the nuclei in different positions longer than the interconversion time *t*.

As the difference of the signals in Hz is proportional to the strength of the applied magnetic field, a high magnetic field NMR spectrometer can distinguish two conformations that are not distinguishable by a low field NMR spectrometer at the same temperature, withal by using a powerful instrument it is possible to observe two distinct signals at higher temperatures than with a smaller instrument. This is important when the shift separations are very small or when it is necessary to perform spectra at very low temperatures, where the solvent viscosity broadens the signals or the products are not very soluble.

Variable-temperature NMR spectroscopy has been applied extensively in kinetic studies of stereodynamic processes with energy barriers between 4.4 and 31 kcal/mol. The energy range covered by DNMR is limited by the NMR time scale, signal resolution and the practical NMR temperature range (-180 °C to +160 °C) which ultimately depends on the melting and boiling points of available solvents.

A particularly simple situation arises when two nuclei (AB case)[2] provide sharp signals with equal intensity and undergo chemical exchange resulting in line broadening and coalescence upon heating (*Figure 1*).

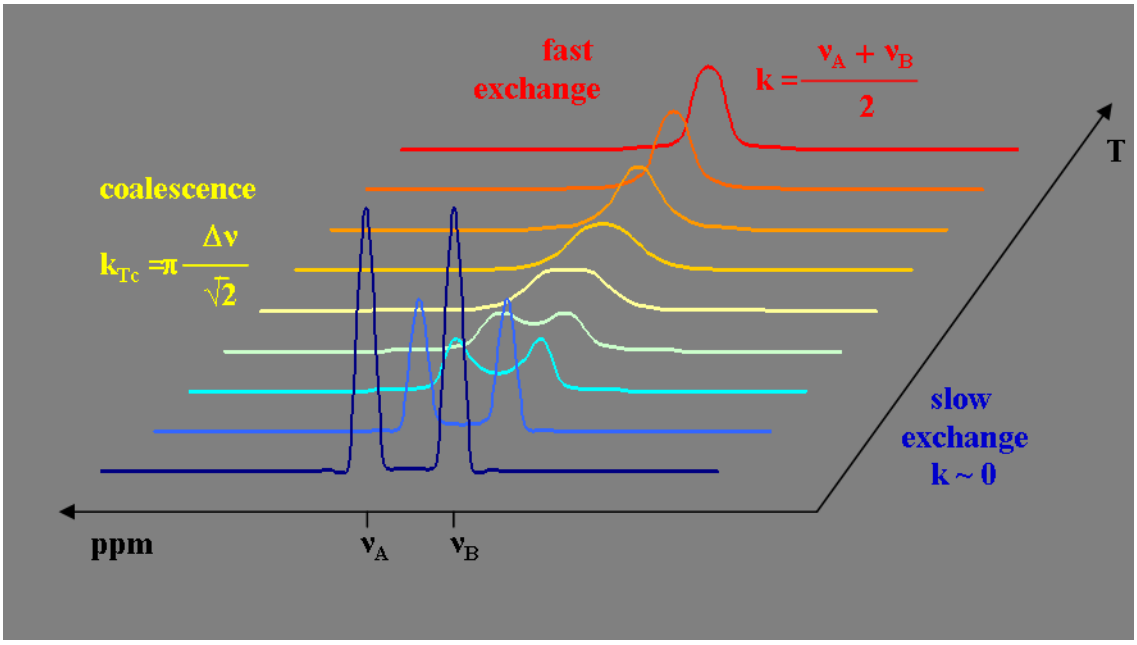

***Figure 1*:Variable-temperature NMR spectra of an uncoupled dynamic AB system**

In such a case, one can obtain well resolved signals at low temperatures where the two nuclei do not show measurable exchange (blue line, *Figure 1*). As the temperature is increased, the exchange rate becomes fast relative to the NMR time scale and only one averaged species is observed due to signal coalescence (yellow line, *Figure 1*).

In the absence of any coupling, at the coalescence temperature, the first-order interconversion rate constant can be calculated as:

$$k_{Tc} = \pi \frac{\Delta \nu}{\sqrt{2}}$$

k_{Tc} = the rate constant (s^{-1})

T_C = the coalescence temperature (in Kelvin)

$\Delta\nu$ = the difference in the chemical shifts (in Hz) of the two signals without exchange.

Further increasing to the temperature, the exchange rate is too fast and only a single signal is observed (red line, *Figure 1*) and the rate constant can be calculate as:

$$k = \frac{\nu_A + \nu_B}{2}$$

k = the rate constant (s^{-1})

ν_A = the chemical shifts (in Hz) of the signal at low field without exchange

ν_B = the chemical shifts (in Hz) of the signal at high field without exchange

By the rate constant at any temperatures and using the Eyring equation:[3]

$$k = \kappa \frac{k_B \cdot T}{h} e^{-\Delta G^{\neq} / RT}$$

h = Planck's constant ($1.584 \cdot 10^{-34}$ cal·s)

k_B = the Boltzmann constant ($3.2998 \cdot 10^{-24}$ cal/K)

R = the universal gas constant (1.9872 cal/K·mol)

κ = the transmission coefficient (can be considered equal to 1).

the free Gibbs activation energy $\Delta G^{\#}$ can be calculated in kcal·mol^{-1}:

$$\Delta G^{\neq} = 4.574 \cdot 10^{-3} \cdot T \cdot (\log \frac{T}{k} + 10.318)$$

The simplicity of the coalescence method, for this simple case, has certainly contributed to its widespread use.[2] However, this method is not applicable neither to interconversion of species with different thermodynamic stability, nor to compounds that show complicate NMR spectra with multiple coupling patterns. In these cases, the rate constants, at the different temperatures, can be obtained by NMR line shape analysis with appropriate programs.[4]

When the half-life of interconversion of these stereoisomers is greater than 1000 seconds, i.e. the time considered to be the minimum life time for a molecule to be

manipulated, they are defined atropisomers.[5] This new word, atropisomer, coined by Kuhn in 1933,[6] means stereoisomers resulting from hindered rotation about single bonds where the steric strain barrier to rotation is high enough to allow for the isolation of the conformers.[7] These molecules are very interesting because introduce an element of chirality in the absence of stereogenic atoms, and consequently atropisomers are of great importance in asymmetric synthesis and asymmetric catalysis.

In recent years the experimental study of atropisomers could be compared with the computational data. The advances of new softwares have produced programs that are easily used by any chemist to calculate the structures and properties of molecules; it is possible to find the 3D-structure of the fundamental states, the transiction states and calculated the free Gibbs activation energy $\Delta G^{\#}$, it is also possible to calculate NMR and ECD data, which are important to establish the absolute configurations.

A computational method very popular and used by chemist is the density functional theory (DFT).[8] The premise behind DFT is that the energy of a molecule can be determined from the electron density instead of a wave function. This theory originated with a theorem by Hohenberg and Kohn[9] that stated this was possible. The original theorem was applied only to find the ground-state electronic energy of a molecule. A practical application of this theory was developed by Kohn and Sham;[10] they expressed the electron density as a linear combinations of basis functions and then a determinant is formed from these functions, called Kohn-Sham orbitals. It is the electron density from this determinant of orbitals that is used to compute the energy.

For accuracy considerations, the smallest basis set used is generally 6-31G* or the equivalent. Interestingly, there is only a small increase in accuracy obtained by using very large basis sets. This is probably due to the fact that the density functional is limiting accuracy more than the basis set limitations. The accuracy of results from DFT calculations can be poor to fairly good, depending on the choice of basis set and density functional. The choice of density functional is made more difficult because creating new functionals is still

an active area of research. One popular functional is known as BLYP (from the name Becke for the exchange part and Lee, Yang and Parr for the correlation part).[11] Even more widely used is B3LYP which is a hybrid functional in which the exchange energy, in this case from Becke's exchange functional, is combined with the exact energy from Hartree-Fock theory. The best B3LYP results are obtained for a large range of compounds and particularly of organic molecules. Despite such success, the B3LYP could fail badly in describing the energies of van der Waals molecules, hydrogen bonded system, reaction barrier heights, and large molecules.[12] Therefore, it would not be surprising if this functional's dominance changed within a few years.

The preparation of conformationally hindered molecules and their study by DNMR and computational methods are my thesis's core. In the first chapter, the conformations and the stereodynamics of symmetrically ortho-disubstituted aryl carbinols and aryl ethers are described.

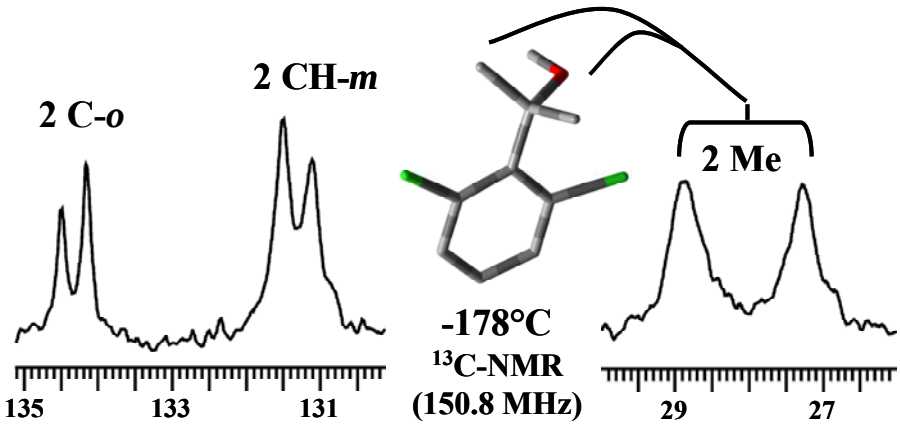

***Figure 2*: Two different signals are observed for each diastereotopic carbons when the steric barrier is slowed down.**

In the second chapter, the structures of axially chiral atropisomers of hindered biphenyl carbinols are studied.

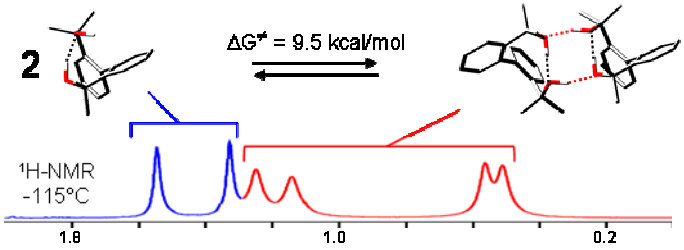

***Figure 3*: For the first time, the formation of a dimer is observed by dynamic NMR.**

In the third chapter, the steric barriers and the π-barrier of 1,8-di-aylbiphenylenes are determined.

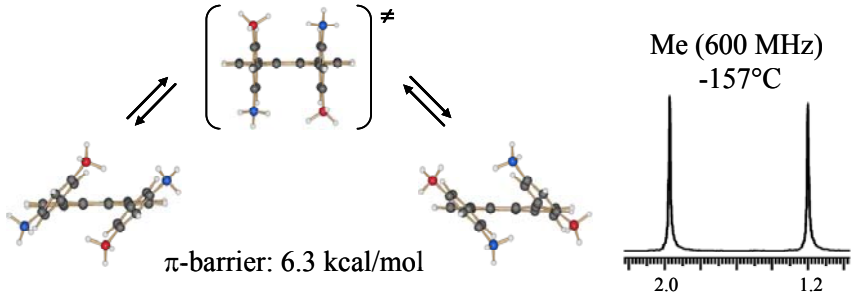

***Figure 4*: The π-barrier is observed by dynamic NMR in 1,8-bis(1,3-dimetilfenil)biphenylenes.**

Interesting atropisomers are found in the cases of arylanthrones, arylanthraquinones and arylanthracenes and are reported in the fourth chapter.

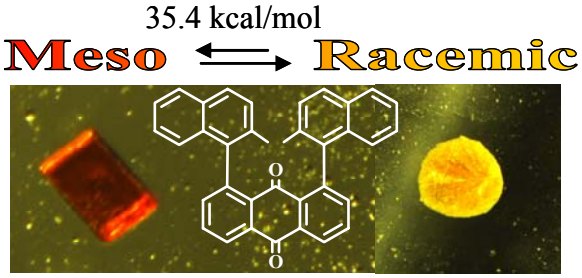

***Figure 5*: Meso (red crystal) and racemic (yellow solid) atropisomers for 1,8-bis(2-methylnapthyl)anthraquinone.**

By the combined use of dynamic NMR, ECD spectroscopy and DFT computations, the conformations and the absolute configurations of 2-Naphthylalkylsulfoxides are studied in the fifth chapter.

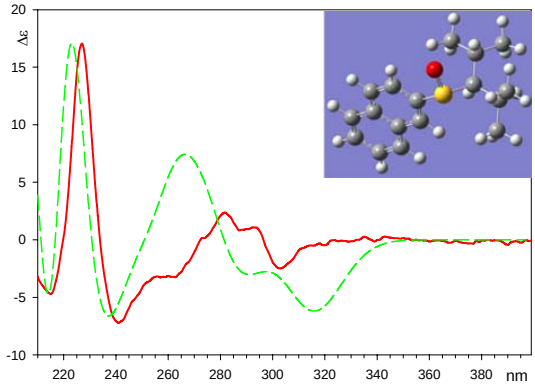

***Figure 6*: Experimental (full red trace) and DFT computed (dashed green trace) ECD spectrum of 2-S-naphthyldiisopropylmethylsulfoxide (top right).**

In the last chapter, a new synthetic route to α,α'-arylated secondary or tertiary alcohols by lithiated O-benzyl-carbamates carrying an N-aryl substituent and DFT calculations to determinate the cyclic intermediate are reported. This work was done in the research group of Prof. Jonathan Clayden, at the University of Manchester.

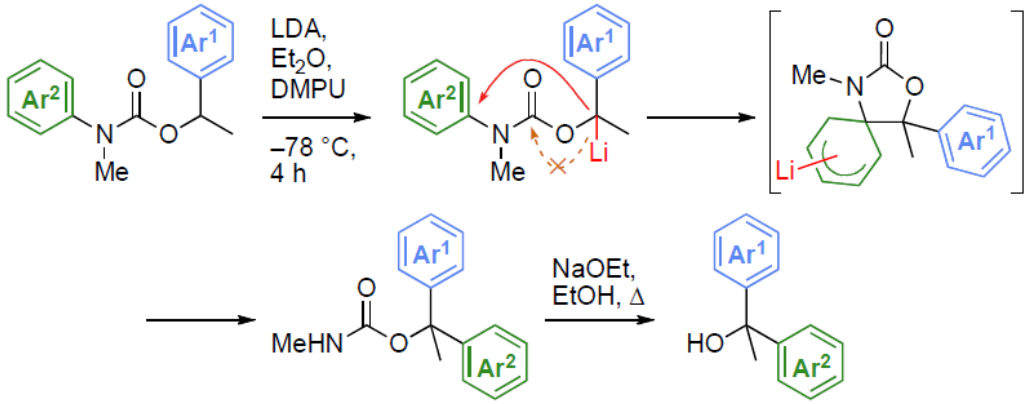

***Figure 7*: Preparation of tertiary alcohols *via* O-benzyl-carbamates rearrangement.**

Chapter 1

1.1 DNMR and DFT Study of Symmetrically Ortho-Disubstituted Aryl Carbinols and Aryl Ethers

Restricted rotation about the bond connecting the aryl groups with the sp^3 carbon atoms has been observed in a variety of aryl carbinols (Ar-C(OH)R_2) and the corresponding barriers were determined by means of variable temperature NMR spectroscopy.[13] In particular, when the aryl moiety does not exhibit a two-fold symmetry axis two atropisomers with different populations were detected and their structure assigned.[13d,n] In the case of very crowded derivatives bearing, as substituents, the *tert*-butyl or the adamantyl groups, the atropisomers could be also separated.[13f-13n] The majority of the compounds studied so far had the aryl moiety substituted by one or by two different groups.

Therefore conformational and stereodynamic properties of a number of hindered benzyl alcohols symmetrically substituted in the ortho positions are investigated; the substituents are F, Cl, Br, and Me, as shown in *Scheme 1*.[14]

Scheme 1

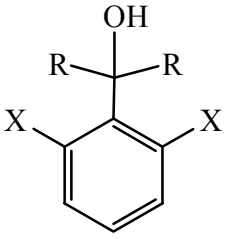

R = Me, X= F, **1** Cl, **2** Br, **3** Me, **4**

R = Et, X= F, **5** Cl, **6** Br, **7** Me, **8**

In this type of derivatives four possible situations could, in principle, be considered: in *Scheme 2* are displayed, as an example, the possible conformers one might expect in the case of compounds **1-4** (R = Me).

Scheme 2

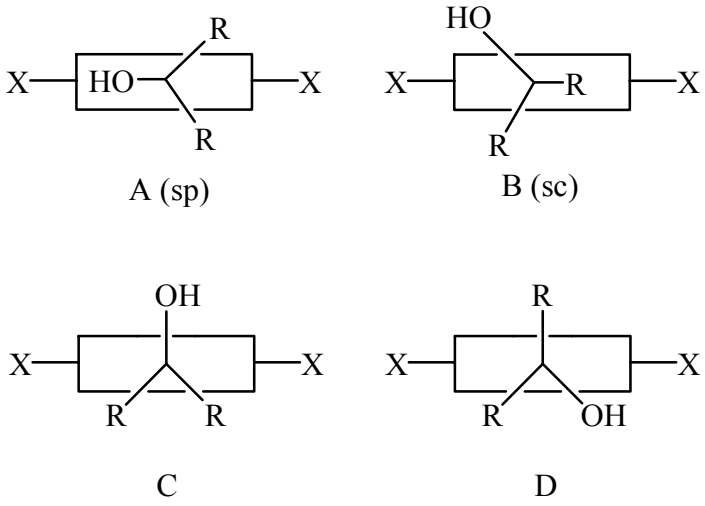

In order to decide whether they actually correspond to ground state structures, theoretical calculations were employed. The theoretical approach is also helpful for providing indications about the relative stability of these conformers.

DFT[15] computations (and Molecular Mechanics[16] as well) of **1** (X = F, R = Me) indicate that the conformations of type C (anticlinal[17]) and D (synclinal[17]) do not correspond to energy minima (actually they represent transition states[18]) and that the minimum corresponding to conformation A (synperiplanar[17]) has an energy higher (by 0.65 kcal mol^{-1}, according to DFT) than that of conformation B (synclinal[17]), indicating that the latter should be the more populated species at low temperature. The asymmetry of the most stable conformer B implies the existence of two enantiomeric forms (+sc and –sc), but the barrier for their interconversion, involving the passage through the scarcely populated conformer A (sp), is predicted to be very low: for instance the DFT computed value for **1** is 3.15 kcal mol^{-1}, as shown in *Figure 8*. The computed dihedral angle between the aromatic ring and the plane defined by the C1-C-O moiety of **1** is +48° for the most stable conformer B and +28° for the transition state D interconverting B into A, i.e. the process which is responsible for the too fast interconversion of the +sc and –sc enantiomers (*Figure 8*).

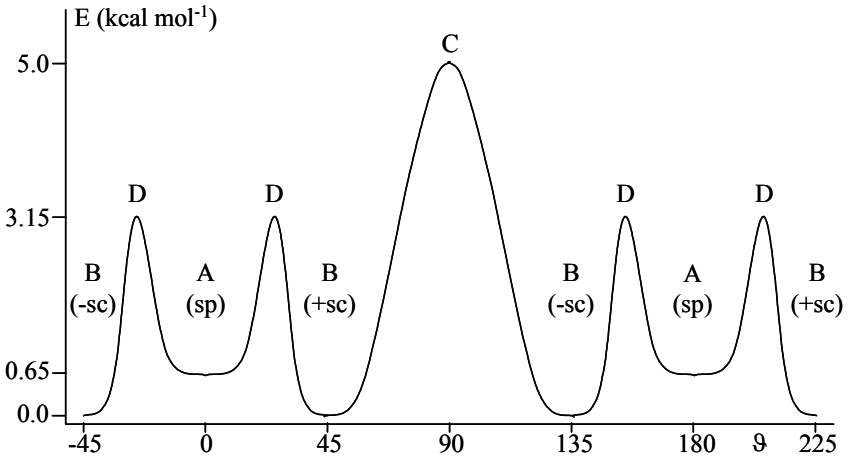

Figure 8:. **Schematic Energy Profile of *1* (E in kcal mol^{-1}) as Function of the Dihedral Angle ϑ Between the Aromatic Ring and the Plane of the C1-C-O Moiety.**

Such a low barrier does not allow the corresponding enantiomerisation process to be frozen in an NMR experiment in the case of **1**, so that, even at the lowest attainable temperature, a dynamic C_s symmetry (i.e., the same type of symmetry displayed by the synperiplanar conformer A) will be actually observed. Thus the two methyl groups of **1** will appear equivalent (enantiotopic) in the NMR timescale, even when the atoms in the ortho and meta positions become diastereotopic.

The low temperature ^{19}F spectra of **1** (*Figure 9*) show indeed how the single signal of the two ortho fluorine atoms broadens on cooling and eventually decoalesces at –169 °C into a pair of partially overlapping signals exhibiting a quite different line width: their integrated intensities indicate that the ratio is 1:1.[18] Also the ortho and meta ^{13}C signals of **1** should likewise split into a pair of lines: this feature, however, was not observed since the corresponding shift separations were smaller than the line width, which is very broad below –160 °C. From the rate constants derived from line shape simulation,[19] the free energy of activation ($\Delta G^{\neq}$ = 4.6 ± 0.3 kcal mol^{-1}) for the rotation that makes the ortho positions equivalent (homotopic) could be obtained. The relatively large experimental error of the barrier of **1** (± 0.3 kcal mol^{-1}) is a consequence of the great uncertainty in determining the intrinsic line width of the two ^{19}F lines at such low temperatures.

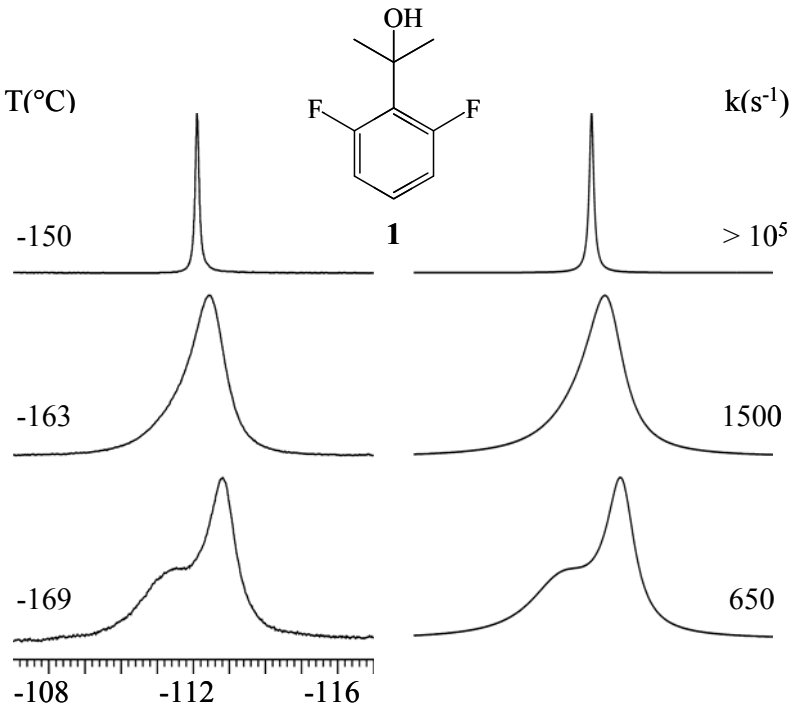

Figure 9: **Left: Temperature dependence of the ^{19}F NMR signal (564.3 MHz) of compound *1* in $CHF_2Cl/CHFCl_2$. The shifts are referred to the signal of C_6F_6 at –163 ppm. Right: Simulation obtained with the rate constants indicated.**

The corresponding DFT calculated barrier is 5.0 kcal mol^{-1}, a value in good agreement with the experiment. These calculations indicate that the transition state for this process corresponds to the structure C (anticlinal[17]), as shown in the rotation pathway reported in *Figure 8*.

The larger width observed at –169 °C (*Figure 9*) for one of the two ^{19}F signals might suggest that the process which interconverts the unequally populated conformers A (sp) and B (sc) of *Scheme 2* has a rate sufficiently slow for broadening this line, but still too fast to show the expected decoalescence, in agreement with the quite low computed barrier of 3.15 kcal mol^{-1} predicted for **1** (*Figure 8*). According to this interpretation, the greater steric hindrance of the corresponding ethyl derivative **5** should make possible the detection of this second process at an attainable temperature.

Indeed, *Figure 10* shows that at –120 °C the two fluorine atoms of **5** display two equally intense lines, due to the freezing of the same rotation process observed in **1**, the corresponding barrier being higher than that of **1**, as anticipated (6.9 rather than 4.6 kcal mol^{-1}). On further cooling, these lines broaden selectively, as observed in the case of **1**, but now they split into a pair of unequally populated peaks at –163 °C (*Figure 10*). These signals correspond, therefore, to the conformers B (sc) and A (sp) of derivative **5**, their relative proportion being approximately 80:20. Line shape simulation yields the free energy of activation required to interconvert the major into the minor conformer (5.0 kcal mol^{-1}).

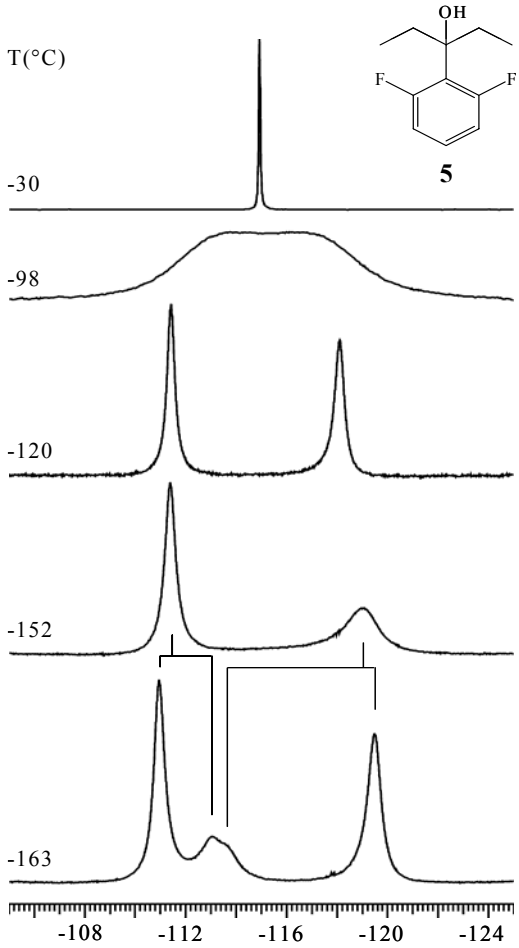

Figure 10: **Temperature dependence of the ^{19}F NMR signal (564.3 MHz) of compound *5* in $CHF_2Cl/CHFCl_2$. The shifts are referred to the signal of C_6F_6 at –163 ppm.**

Contrary to the case of **1**, DFT computations predict that the conformer A (sp) of **5** is 0.47 kcal mol^{-1} more stable than the conformer B (sc),[20] a result in agreement with the corresponding ^{13}C spectrum (*Figure 11*). The rate constants for the exchange process yield a free energy of activation $\Delta G^{\neq} = 4.95 \pm 0.15$ kcal mol^{-1}, i.e. a value equal to that obtained from the corresponding ^{19}F spectrum (*Figure 10*).

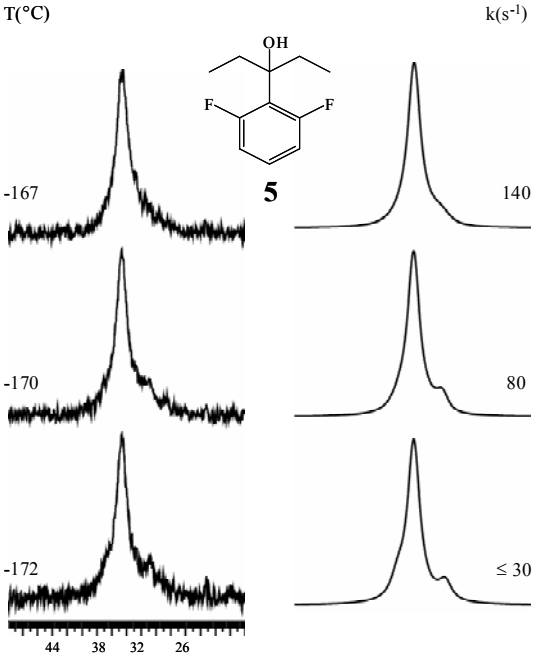

Figure 11: **Left: temperature dependence of the ^{13}C methylene signal of compound 5 at 150.8 MHz in CHF_2Cl/CF_2Cl_2. Right: computer simulation obtained by considering a single signal at 34.4 ppm (80%) and a pair of less intense signals (10% each) at 36.5 and 30.6 ppm: the conformer ratio is derived from the ^{19}F spectrum (*Figure 10*).**

At a temperature of –172 °C, in fact, the methylene carbon signal of **5** appears as a single line superimposed to a pair of equally intense lines, the single line being more intense (about 80%) than the other ones (10% each). The single major line thus corresponds to the two CH_2 carbons of the equivalent (enantiotopic) ethyl groups of conformer A (sp), whereas the two distinct lines with lower intensity are due to the two CH_2 carbons of the diastereotopic ethyl groups of conformer B (sc) of *Scheme 2*. The interconversion between the two conformers of type A and B also involves a simultaneous

rearrangement of the two ethyl groups: such a rearrangement contributes to determine the value of the measured barrier of 5 kcal mol^{-1} (the corresponding DFT computed barrier of 4.4 kcal mol^{-1} agrees well with the experiment). In the more stable conformer of type A, in fact, the two ethyl groups adopt a symmetric relative disposition (*Figure 12*), in agreement with the observation of a single CH_2 line in the mentioned ^{13}C spectrum at the –172° C. In the less stable conformer of type B, on the other hand, one of the two ethyl groups adopts a disposition different form that of its companion (*Figure 12*)[21], therefore explaing the two observed signals.

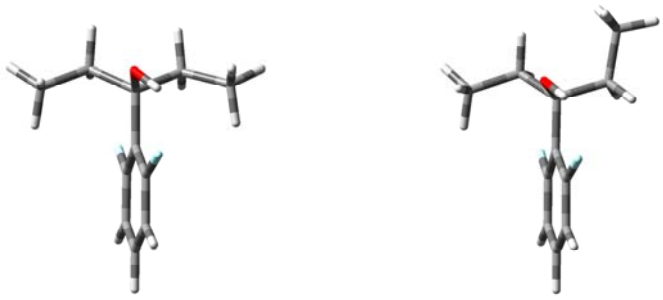

5-DFT-conformation A
sp (E = 0.0 kcal mol^{-1})

5-DFT-conformation B
sc (E = 0.48 kcal mol^{-1})

Figure 12: **DFT computed structure of the more stable sp-conformer (A type) and of the less stable sc-conformer (B type) of compound *5*.**

In the case of compounds without fluorine substituents, the exchange process was followed by monitoring the decoalescence of the ^{13}C signals of the quaternary ortho and CH meta carbons; owing to the poor solubility of **4** and **11** at temperatures lower than –120 °C, these barriers were measured by monitoring the ^{1}H signal (600 MHz) of the ortho methyl substituents.

Figure 13 displays, for instance, the temperature dependence of these lines in the case of derivative **2** (X = Cl, R = Me).

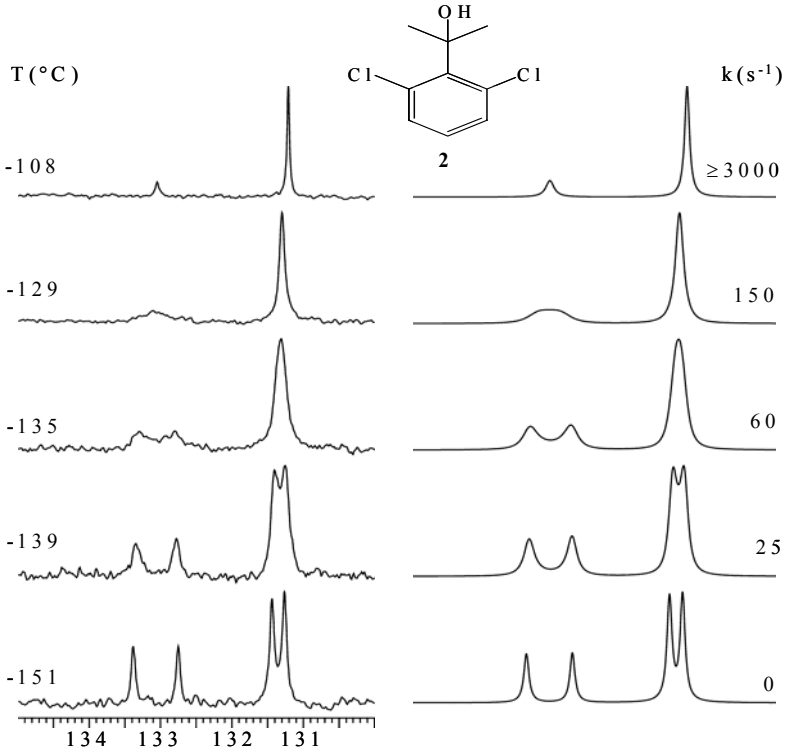

Figure 13: **Left: temperature dependence of the ^{13}C signals (150.8 MHz in $CHF_2Cl/CHFCl_2$) of the two quaternary ortho and of the two CH meta carbons of *2*. Right: simulation obtained with the rate constants indicated.**

In *Table 1* are collected the barriers,[22] measured by line shape simulation,[19] for all the compounds investigated.

Table 1: **Experimental Rotation Barriers (kcal mol^{-1}) [a] for Compounds *1-8* and DFT Computed Barriers for Compounds *1-4*.**

Compd.	1 R=Me (X=F)	2 R=Me (X=Cl)	3 R=Me (X=Br)	4 R=Me (X=Me)	5 [b] R=Et (X= F)	6 R=Et (X=Cl)	7 R=Et (X=Br)	8 R=Et (X=Me)
Exper.	4.6	6.8	7.4	6.2	6.9	9.4	10.1	8.6
Computed	5.0 [c]	7.0 [d]	7.9 [d]	7.8 [c]				

[a] in $CHF_2Cl/CHFCl_2$. [b] In *5* a second barrier of 5.0 kcal mol^{-1} has been also measured (see text). [c] B3LYP/6-31G(d) level. [d] B3LYP/6-311+G(2df,p)//B3LYP/6-31G(d) level.

As in the case of **1** and **2**, also in the other methyl alcohols investigated (**3** and **4**), the ^{13}C signals of the methyl groups bonded to the COH moiety remained equivalent (enantiotopic) at any attainable temperature, in agreement with the mentioned expectation of the related enantiomerisation process having a barrier too low to be experimentally detected. It should be pointed out that, according to calculations, the ground state (i.e. the B-type conformer of *Scheme 2*) of compounds **3** and **4** (X = Br and Me, respectively) has a value for the dihedral angle ϑ between the aryl ring and the C1-C-O plane smaller than 30°. Rather than +48° as in **1** or +40° as in **2**, this angle is predicted to be +18° in **3** and +27° in **4**: for this reason the corresponding conformer B should be indicated, in these cases, as synperiplanar (sp) rather than synclinal (sc).[17]

Single crystal X-ray diffraction of **4** (*Figure 14*, left) shows indeed that the dihedral angle ϑ between the average plane defined by the aryl group (the shape of the aromatic ring deviates from a perfect planarity by 6° in the crystal) and that identified by the C1-C-O moiety is +24°, a value very close to that (ϑ = +27°) computed for the isolated molecule (*Figure 14*, right).

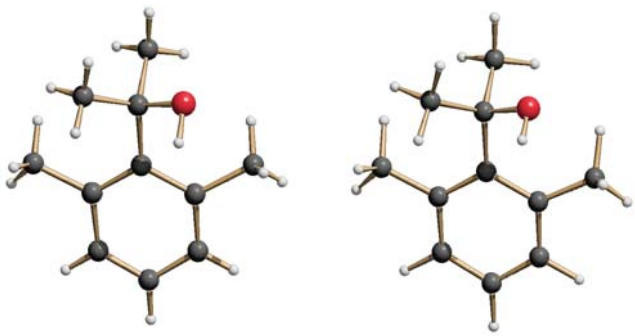

4-X-Ray **4-DFT-sp**

Figure 14: **Experimental (left) and computed (right) structure of compound *4*.**

In the case of compounds **3** and **4** computations also indicate that the A-type conformer of *Scheme 2* (i.e. that having ϑ = 0°) corresponds to a low energy transition

state rather than a ground state, as in **1** and **2**. Consequently the corresponding energy profile is of the type displayed in *Figure 15* for the case of **4** (R =X = Me).

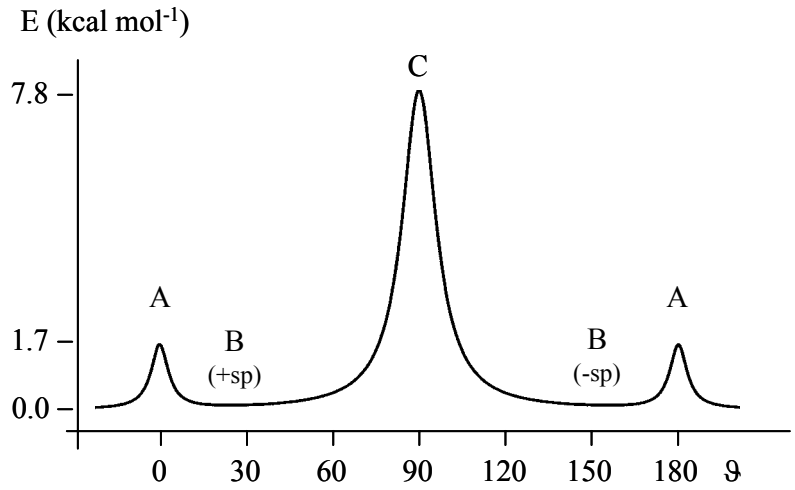

Figure 15: **Schematic Energy Profile of *4* (E in kcal mol^{-1}) as Function of the Dihedral Angle ϑ Between the Aromatic Ring and the Plane of the C1-C-O Moiety.**

In the aryl carbinols with two ethyl substituents bonded to the COH moiety (compounds **5-8**), the interconversion barrier was found to be consistently larger (by 2.45 ± 0.15 kcal mol^{-1}) than in the analogous methyl substituted derivatives **1-4**. This is a consequence of the greater bulkiness of the ethyl with respect to the methyl group. In addition, in derivatives **1-3** and **5-7** the barriers increase with the dimension of the halogen substituent: this parallels the trend of the corresponding van der Waals radii (1.47, 1.75, 1.85 for F, Cl, Br, respectively).[23]

As shown in *Table 1*, the barriers measured for compounds **4** and **8** (having two methyl groups as ortho substituents) are lower than those of the corresponding derivatives **2** and **6** that have two chlorine atoms as ortho substituents (the average difference is 0.7 kcal mol^{-1}).

This trend suggests that the steric hindrance exerted by the methyl group upon the rotation process is lower than that of the chlorine atom. This is in a qualitative agreement with the trend recently reported[24] for a pair of ortho-substituted biphenyl derivatives,

where the Ar-Ar rotation barrier was found slightly lower for the methyl than for the chlorine substituent (i.e., 7.4 vs. 7.7 kcal mol^{-1}, respectively).[25]

The present finding is at variance with the trend of the van der Waals radii indicated by Bondi,[23] who proposed a larger value for methyl with respect to chlorine (i.e. 2.0 vs. 1.75), but is in keeping with that proposed by Charton,[26] if the minimum van der Waals radius for methyl is taken into account (i.e., 1.715 for methyl vs. 1.75 for chlorine).

As previously mentioned, the process that would make diastereotopic the methyl groups is too fast in the alcohols **1-4** to be experimentally observed. However, if the OH is substituted by the OMe group (as in compounds **9-12** of *Scheme 3*), the greater steric requirement should increase the corresponding barrier, making this process amenable to an experimental detection.

Scheme 3

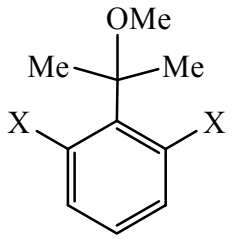

X= F, **9**
Cl, **10**
Br, **11**
Me, **12**

This prediction is supported by Molecular Mechanics calculations[16] of the energy surface as function of the previously defined dihedral angle ϑ (related to the torsion about the Ar-C(Me_2) bond, and of the dihedral angle φ formed by the C1-C(Me_2)-O and (Me_2)C-O-Me planes (this angle is related to the torsion about the C-OMe bond). As an example, such a surface is displayed in *Figure 16* for the case of **10** (X = Cl).

The computed barrier involving the transition state which renders diastereotopic the ortho and meta positions (full square in *Figure 16*) is larger than that involving the transition state which renders diastereotopic the two methyl groups (full circle in *Figure 16*); the full line describes the passage across the higher energy transition state and the dashed line that across the lower energy transition state.

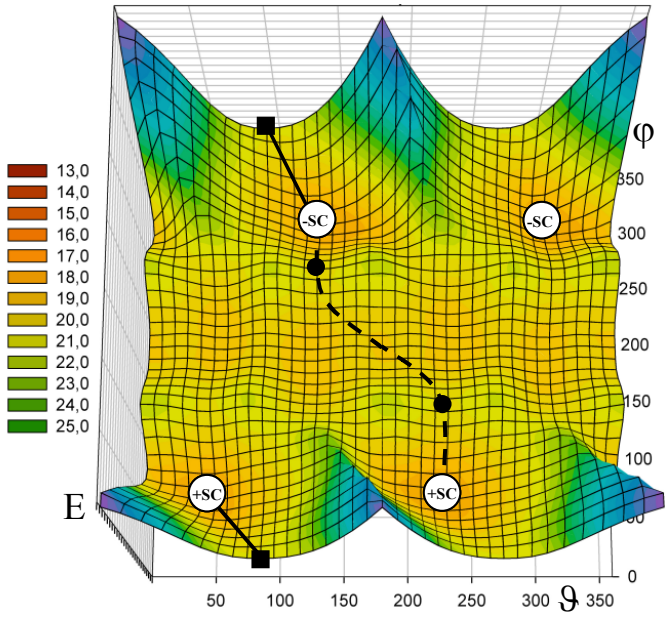

Figure 16: **MM computed energy (kcal mol^{-1}) surface of *10* as function of the dihedral angles ϑ and φ defined in the text.**

The ground states are indicated as +*sc* e –*sc*. The more accurate DFT computations (*Table 2*) indicate that the values for the two barriers should be 9.4 and 5.5 kcal mol^{-1}, respectively.[27]

Table 2: **Experimental Values of the two Barriers (kcal mol^{-1}) Measured[a] for the Rotation Processes Occurring in Ethers *9-12* (in Parenthesis the Computed Values Corresponding to the Transitions States TS-1 and TS-2).**

Compd.	**9** (X=F)	**10** (X=Cl)	**11** (X=Br)	**12** (X=Me)
Higher barrier (TS-1)	5.0 (5.5 [b])	6.9 (9.4 [c])	8.1 (10.2 [c])	7.0 (10.0 [b])
Lower barrier (TS-2)	4.7 (4.9 [b])	4.8 (5.5 [c])	5.0 (5.9 [c])	6.2 (5.5 [b])

[a] in $CHF_2Cl/CHFCl_2$ [b] B3LYP/6-31G(d) level. [c] B3LYP/6-311+G(2df,p)// B3LYP/6-31G(d) level.

These calculations therefore support the hypothesis that even the lower of these two barriers should be sufficiently high for obtaining an experimental determination (barriers larger than 4 kcal mol^{-1}, in fact, are amenable to NMR measurements).[28]

The temperature dependence of the ^{13}C signals of **10** (X = Cl), reported in *Figure 17*, shows that at –144 °C the single lines of the two ortho and of the two meta carbons split into 1:1 pairs, since the same type of process observed in the corresponding alcohol **2** has been frozen. The signal of the two methyl groups bonded to the C-OMe moiety is still a single line at -144 °C, but on further lowering the temperature to –178 °C splits into a 1:1 pair of lines, because also the second process, with the lower barrier, has been frozen at this temperature (*Figure 17).*

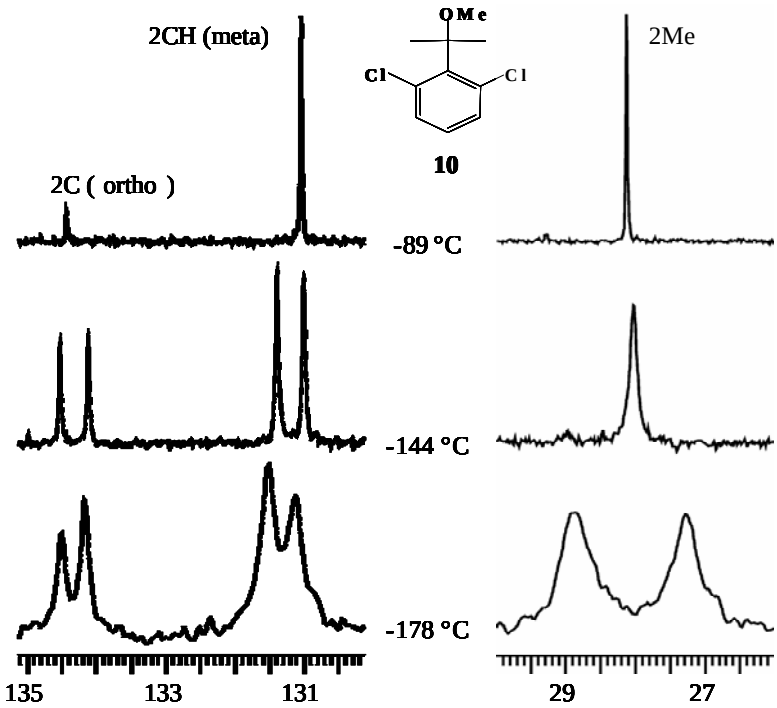

Figure 17: **Temperature dependence of ^{13}C signals (150.8 MHz) of the two ortho, two meta and two methyl carbons (bonded to the C-OMe moiety) of *10* in $CHF_2Cl/CHFCl_2$.**

Analogous results were obtained for **11** and **12** (X = Br and Me, respectively): the corresponding barriers are collected in *Table 2*.

Also in the case of **9** (X = F) the methyl groups become diastereotopic at low temperature, as predicted by calculations: within the experimental uncertainty (± 0.15 kcal mol^{-1}), however, the corresponding barrier was found equal to that measured by monitoring

the ^{19}F signals of the ortho fluorine substituents (5.0 and 4.7 kcal mol^{-1}, respectively, as in *Table 2*). This means that in compound **9** the barrier for rendering diastereotopic the ortho and meta positions is very close to that required to make diastereotopic the two methyl groups. This agrees with the DFT calculations predicting quite similar values for these two barriers (5.5 and 4.9 kcal mol^{-1}, respectively, as in *Table 2*).

The higher of the two barriers measured in the ethers **9-11** increases regularly (5.0, 6.9, 8.1 kcal mol^{-1} as in *Table 2*) with the dimension of the halogen substituent, as already observed in the corresponding alcohols **1-3** and **5-7** (*Table 1*): this trend is also predicted by the computed values of *Table 2*. The pathway responsible for this effect is due to the restriction of the Ar-C bond rotation that drives the C-OMe bond into a perpendicular position to the aryl ring (i.e., a situation analogous to that of type C of *Scheme 2*): the corresponding DFT computed transition states (indicated as TS-1) are reported at the top of *Figure 18*.

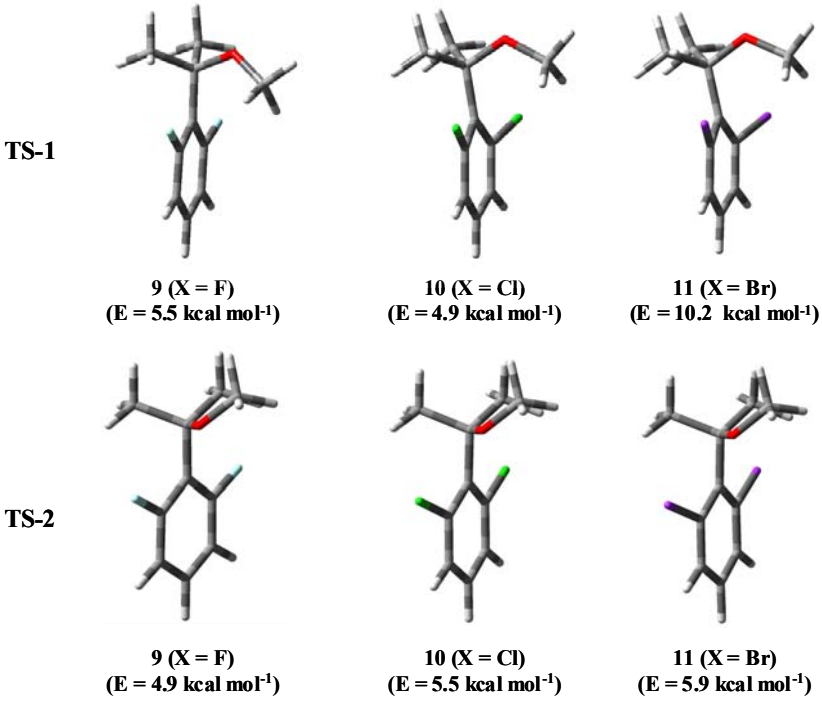

Figure 18: **Top: DFT computed transitions states TS-1 of *9-11*. Bottom: DFT computed transition states TS-2 of *9-11*. The energies reported refer to the ground state.**

On the contrary, the values of the lower barriers measured for the ethers 9-11 are equal within the experimental uncertainty (4.7-5.0 kcal mol^{-1} as in *Table 2*) and do not depend, therefore, on the dimension of the halogen substituents. This suggests that the lower barriers measured by NMR are essentially determined by the rotation process about the C-OMe bond (i.e., that indicated by the angle φ in *Figure 16*), the related transition state (TS-2) being described by the O-Me bond eclipsing one of the two C-Me bonds (this situation corresponds to the point identified by the full dot in *Figure 16* for compound 10). It is quite evident that this process cannot be affected by the dimension of the halogen groups in the ortho position, thus accounting for the observed invariance of the lower barriers in 9-11: these TS-2 transition states, resulting from DFT computations, are displayed in *Figure 18*, bottom.

Such an interpretation also accounts for the fact that in the alcohols **1-4** the diastereotopicity of the two methyl groups could not be observed in the NMR spectra, even at the same low temperatures where it was detected in the corresponding methyl ethers **9-12**: the rotation barrier about the C-OH bond of the alcohols is in fact conceivably lower than that about the C-OMe bond of the corresponding ethers.

1.2 Conclusions

As anticipated by computations, the low temperature NMR spectra of symmetrically ortho disubstituted aryl carbinols display a barrier due to the restricted rotation about the sp^2-sp^3 Ar-C bond, the threshold mechanism being that where the C-OH bond becomes perpendicular to the aryl ring: this barrier increases with the increasing dimension of the halogen substituents. The free energies of activation covered the range 4.6-10.1 kcal·mol^{-1}. DFT computations matched satisfactory the trend of these values and predicted the conformation adopted by these compounds (*Table 1*). In one case, this result could be also confirmed by the X-ray diffraction structure (*Figure 14*). In the

corresponding methyl ethers two barriers could be measured, corresponding to the passage across two distinguishable transition states: the higher barriers covered the range 5.0-8.1 kcal·mol^{-1} and the lower ones the range 4.7-6.2 kcal·mol^{-1} (*Table 2*).

1.3 Experimental Section

1.3.1 General procedure for 1-3 and 5-7. A solution of lithium diisopropylamide (LDA) was prepared in 1 hour by addition of 12.5 mL of n-butyllithium (20 mmol, 1.6 M in hexane) to a stirred solution of 2.02 g of diisopropylamine (20 mmol in 12.5 mL of anhydrous THF) kept at –5 °C. The solution was then slowly transferred into a solution of the appropriate 1,3-dihalobenzene (20 mmol in 12.5 ml of anydrous THF), kept at –78 °C. After 1.5 hours the suspension of the resulting lithiate[29] was treated either with acetone (for compounds **1-3**, 40 mmol, neat) or diethylketone (for compounds **5-7**, 40 mmol, neat). The temperature was immediately raised to ambient temperature, and the mixture treated with aqueous NH_4Cl, extracted with Et_2O and dried (Na_2SO_4). After removing the solvent, the crude was pre-purified by a silica gel chromatography column (petroleum ether/Et_2O 8/2). Yields: 73% for **1**[30], 52% for **2**, 8% for **3**, 66% for **5**, 44% for **6**, 10% for **7**. Analytically pure samples were obtained by semi-preparative HPLC on a Synergi Polar-RP column (4μm, 250x10 mm, 4 ml/min, MeOH/H_2O 80:20 v:v).

2-(2,6-Difluoro-phenyl)-propan-2-ol (1)[30]. ^{1}H-NMR (600 MHz, $CDCl_3$, 25°C, TMS): δ 1.71 (6H, t, J_{H-F} = 2.1 Hz), 3.06 (1H, t, J_{H-F} = 6.5 Hz), 6.81-6.91(2H, m), 7.13-7.22 (1H, m). ^{13}C-NMR (150.8 MHz, $CDCl_3$, 25°C, TMS): δ 30.8 (2CH_3, t, J_{C-F} = 4.0 Hz), 72.6 (Cq, t, J_{C-F} = 1.9 Hz), 112.5 (2CH, dd, J_{C-F} = 6.1 Hz, 23.7 Hz), 123.3 (Cq, t, J_{C-F} = 14.0 Hz), 128.3 (CH, t, J_{C-F} = 11.9 Hz), 160.5 (2Cq, dd, J_{C-F} = 9.0 Hz, 247.0 Hz). HRMS(ESI): m/z 195.0602 [$(M+Na)^+$ calcd for $C_9H_{10}F_2ONa$ 195.0597]. HPLC: RT = 4.85 min.

2-(2,6-Dichloro-phenyl)-propan-2-ol (2). ^{1}H-NMR (600 MHz, $CDCl_3$, 25 °C, TMS): δ 1.87 (6H, s), 3.60 (1H, s), 7.06 (1H, t, *J* = 7.9 Hz), 7.31 (2H, d, *J* = 7.9 Hz). ^{13}C-NMR (150.8 MHz, $CDCl_3$, 25 °C, TMS): δ 30.5 ($2CH_3$), 76.0 (Cq), 127.8 (CH), 131.3 (2CH), 133.5 (2Cq), 142.2 (Cq). HRMS(ESI): m/z 227.0013 [$(M+Na)^+$ calcd for $C_9H_{10}Cl_2ONa$ 227.0006. HPLC: RT = 7.96 min.

2-(2,6-Dibromo-phenyl)-propan-2-ol (3). ^{1}H-NMR (400 MHz, $CDCl_3$, 25 °C, TMS): δ 1.91 (6H, s), 3.23 (1H, s), 6.85 (1H, t, *J* = 7.9 Hz), 7.59 (2H, d, *J* = 7.9 Hz). ^{13}C-NMR (100.6 MHz, $CDCl_3$, 25 °C, TMS): δ 30.1 ($2CH_3$), 76.2 (Cq), 121.5 (2Cq), 128.5 (CH), 135.6 (2CH), 144.5 (Cq). HPLC: RT = 6.68 min.

3-(2,6-Difluoro-phenyl)-pentan-3-ol (5). ^{1}H-NMR (600 MHz, $CDCl_3$, 25°C, TMS): δ 0.88 (6H, t, *J* = 7.5 Hz), 1.77-1.83 (2H, m), 2.08-2.14 (2H, m), 3.17 (1H, t, J = 8.2), 6.85-6.88 (2H,m), 7.16-7.21 (2H,m). ^{13}C-NMR (150.8 MHz, $CDCl_3$, 25°C, TMS): δ 8.3 ($2CH_3$), 34.3 ($2CH_2$, t, J_{C-F} = 3.5 Hz), 79.6 (Cq, t, J_{C-F} = 3.0 Hz), 112.5 (2CH, d, J_{C-F} = 30.1 Hz), 120.4 (Cq, t, J_{C-F} = 13.6 Hz), 128.2 (CH, t, J_{C-F} = 12.1 Hz), 161.0 (2Cq, dd, J=9.3 Hz, 246.2 Hz). HRMS(ESI): m/z 223.0915 [$(M+Na)^+$ calcd for $C_{11}H_{14}F_2ONa$ 223.0910]. HPLC : 5.65 min.

3-(2,6-Dichloro-phenyl)-pentan-3-ol (6). ^{1}H-NMR (600 MHz, $CDCl_3$, 25°C, TMS): δ 0.85 (6H, t, *J* = 7.5 Hz), 1.85 (2H, dq, *J* = 7.4 Hz, 15.0 Hz), 2.60 (2H, dq, *J* = 7.6 Hz, 15.0 Hz), 3.39 (1H, s), 7.06 (1H, t, *J* = 7.9 Hz), 7.31 (1H, d, *J* = 7.9 Hz). ^{13}C-NMR (150.8 MHz, $CDCl_3$, 25°C, TMS): δ 8.2 ($2CH_3$), 33.2 ($2CH_2$), 82.5 (Cq), 127.8 (CH), 131.5 (2CH), 134.3 (2Cq), 139.2(Cq). HRMS(ESI): m/z 255.0321 [$(M+Na)^+$ calcd for $C_{11}H_{14}Cl_2ONa$ 255.0319]. HPLC: RT = 7.75 min.

3-(2,6-Dibromo-phenyl)-pentan-3-ol (7). ^{1}H-NMR (600 MHz, CD_2Cl_2, 25°C, TMS): δ 0.81 (6H, t, *J* = 7.3 Hz), 1.83 (2H, dq, *J* = 7.3 Hz, 14.7 Hz), 2.75 (2H, dq, *J* = 7.3 Hz, 14.7 Hz), 2.88 (1H, s), 6.87 (1H, t, *J* = 7.9 Hz), 7.63 (2H, d, *J* = 7.9 Hz). ^{13}C-NMR (150.8 MHz, CD_2Cl_2, 25°C, TMS): δ 8.7 ($2CH_3$), 33.5 ($2CH_2$), 82.8 (Cq), 123.1 (2Cq), 129.3 (CH), 136.7 (2CH), 142.2 (Cq). HPLC : RT = 8.63 min.

1.3.2 Procedure for 2-(2,6-Dimethyl-phenyl)-propan-2-ol (4) and 3-(2,6-Dimethyl-phenyl)-pentan-3-ol (8). 12.5 ml of BuLi (20 mmol, 1.6M in hexane) was added to a solution of 1-bromo-2,6-dimethyl-benzene (20 mmol in 15 ml of dry THF) at –78 °C. The solution was stirred for 60 min and then treated with acetone or diethylketone (40 mmol in 5 ml of dry THF). After stirring for 10 min, the mixture was warmed to 25°C and treated with aqueous NH_4Cl, extracted with Et_2O and dried (Na_2SO_4). The crude obtained after removal of the solvent was purified by a silica gel chromatography column (petroleum ether/Et_2O 8/2) to give **4**(65%)[31] and **8**(58%). Analytically pure samples were obtained by semi-preparative HPLC on a Synergi Polar-RP column (4µm, 250x10 mm, 4 ml/min, MeOH/H_2O 80:20 v:v). In the case of compound **4**, crystals suitable for X-ray diffraction were obtained by slow evaporation from $CHCl_3$.

2-(2,6-Dimethyl-phenyl)-propan-2-ol (4)[31]. ^{1}H-NMR (600 MHz, $CDCl_3$, 25°C, TMS): δ 1.67 (1H, s), 1.73 (6H, s), 2.54 (6H, s), 6.98-7.00 (3H, m). ^{13}C-NMR (150.8 MHz, $CDCl_3$, 25°C, TMS): δ 25.4 ($2CH_3$), 31.9 ($2CH_3$), 76.2 (Cq), 126.3 (CH), 131.3 (2CH), 136.1 (2Cq), 145.5 (Cq). HRMS(ESI): m/z 187.1093 [$(M+Na)^+$ calcd for $C_{11}H_{16}ONa$ 187.1099]. HPLC: RT = 5.89 min.

Crystal Data

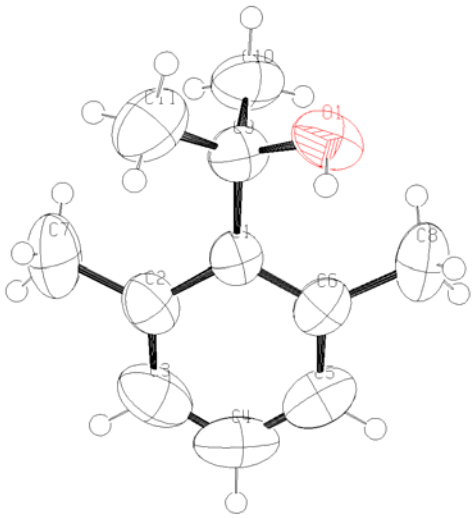

Molecular formula: $C_{11}H_{16}O$, M_r = 164.24, Tetragonal, space group I-4 (No. 82), a = 16.5954(15), c = 8.2166(11) Å, V = 2262.9(4) Å^3, T = 298(2) K, Z = 8, ρ_c = 1.139 g cm^{-3}, F(000) = 836, graphite-monochromated $Mo_{K\alpha}$ radiation (λ = 0.71073 Å), $\mu(Mo_{K\alpha})$ = 0.241 mm^{-1}, colourless brick (0.4 × 0.4 × 0.2 mm^3), empirical absorption correction with SADABS (transmission factors: 0.9099 – 0.9535), 1800 frames, exposure time 10 s, 2.77 ≤ θ ≤ 24.99, –19 ≤ h ≤ 18, –19 ≤ k ≤ 19, –9 ≤ l ≤ 9, 8057 reflections collected, 1986 independent reflections (R_{int} = 0.0238), solution by direct methods (SHELXS97[32]) and subsequent Fourier syntheses, full-matrix least-squares on F_o^2 (SHELX97[32]), hydrogen atoms refined with a riding model, data / restraints / parameters = 1986 / 6 / 138, $S(F^2)$ = 1.023, $R(F)$ = 0.0502 and $wR(F^2)$ = 0.1270 on all data, $R(F)$ = 0.0449 and $wR(F^2)$ = 0.1213 for 1777 reflections with $I > 2\sigma(I)$, weighting scheme $w = 1/[\sigma^2(F_o^2) + (0.0614P)^2 + 0.7035P]$ where $P = (F_o^2 + 2F_c^2)/3$, largest difference peak and hole 0.153 and –0.130 e Å^{-3}. The unit cell contains one disordered $CHCl_3$ molecule, which has been split in two parts and refined using anisotropic displacement parameters restraints.

3-(2,6-Dimethyl-phenyl)-pentan-3-ol (8). ^{1}H-NMR (300 MHz, $CDCl_3$, 25°C, TMS): δ 0.84 (6H, t, *J* = 7.4 Hz), 1.65 (1H, s), 1.75 (2H, dq, *J* = 7.4 Hz, 14.8 Hz), 2.25 (2H, dq, *J* = 7.4 Hz, 14.8 Hz), 2.52 (6H, s), 6.96-6.98 (3H, m). ^{13}C-NMR (75.4 MHz, $CDCl_3$, 25°C, TMS): δ 8.2 ($2CH_3$), 25.2 ($2CH_2$), 34.4 ($2CH_3$), 81.8 (Cq), 125.9 (CH), 131.3 (2CH), 136.4 (2Cq), 141.9 (Cq). HRMS(ESI): m/z 215.1406 [$(M+Na)^+$ calcd for $C_{13}H_{20}ONa$ 215.1412]. HPLC : 7.50 min.

1.3.3 General procedure for 9,10 and 12 To a suspension of NaH (95% powder, about 10 mmol in 5 ml of dry THF), kept at 0°C, a solution of the appropriate alcohol (2 mmol in 2 ml of dry THF) was added dropwise. After 10 minutes the stirred suspension was treated with excess MeI (1 ml). After warming to ambient temperature, the reaction was cautiously quenched with aqueous NH_4Cl, extracted with Et_2O and dried (Na_2SO_4). After removing the solvent, the crude was pre-purified by a silica gel chromatography column (petroleum ether/Et_2O 20/1) to give **9** (72%)**, 10** (65%) and **12** (58%). Analytically pure samples were obtained by semi-preparative HPLC on a Synergi Polar-RP column (4μm, 250x10 mm, 4 ml/min, MeOH/H_2O 80:20 v:v) in the case of compound **10**, and on a Luna C18(2) column (5μm, 250x10 mm, 4 ml/min, ACN/H_2O 95:5) in the case of compounds **9** and **12**.

1,3-Difluoro-2-(2-methoxypropan-2-yl)benzene (9). ^{1}H-NMR (600 MHz, $CDCl_3$, 25°C, TMS): δ 1.69 (6H, t, J_{H-F} = 2.4 Hz), 3.15 (3H, s), 6.84-6.87 (2H, m), 7.19-7.21 (H, m). ^{13}C-NMR (150.8 MHz, $CDCl_3$, 25°C, TMS): δ 28.2 ($2CH_3$, t, J_{C-F} = 4.6 Hz), 51.2 (OCH_3, s), 77.2 (Cq, t, J_{C-F} = 2.9), 112.5 (2CH, dd, J_{C-F} = 5.6 Hz, 23.9 Hz), 119.6 (Cq, t, J_{C-F} = 14.3 Hz), 128.8 (CH, t, J_{C-F} = 11.6 Hz), 161.5 (2Cq, dd, J_{C-F} = 9.1 Hz, 251.2 Hz). HRMS(ESI): m/z 209.0745 [$(M+Na)^+$ calcd for, $C_{10}H_{12}F_2ONa$ 209.0754]. HPLC: RT = 4.62 min.

1,3-Dichloro-2-(2-methoxypropan-2-yl)benzene (10). ^{1}H-NMR (600 MHz, $CDCl_3$, 25°C, TMS): δ 1.85 (6H, s), 3.04 (3H, s), 6.83 (1H, t, *J* = 7.9 Hz), 7.61 (2H, d, *J* = 7.9 Hz). ^{13}C-NMR (150.8 MHz, $CDCl_3$, 25 °C, TMS): δ 28.6 ($2CH_3$), 50.5 (OCH_3), 80.2 (Cq), 127.9 (CH), 131.4 (2CH), 135.1 (2Cq), 139.0 (Cq). HRMS(ESI): m/z 241.0173 [$(M+Na)^+$ calcd for, $C_{10}H_{12}Cl_2ONa$ 241.0163]. HPLC : RT = 8.57 min.

2-(2-Methoxypropan-2-yl)-1,3-dimethylbenzene (12). ^{1}H-NMR (600 MHz, $CDCl_3$, 25°C, TMS): δ 1.68 (6H, s), 2.48 (6H, s), 3.06 (3H, s), 6.98-6.70 (3H, m). ^{13}C-NMR (150.8 MHz, $CDCl_3$, 25°C, TMS): δ 24.6 ($2CH_3$), 29.2 ($2CH_3$), 49.9 (OCH_3), 80.3 (Cq), 126.1 (CH), 131.2 (2CH), 136.9 (2Cq), 142.1 (Cq). HRMS(ESI): m/z 179.1438 [$(M+H)^+$ calcd for $C_{12}H_{19}O$ 179.1436]. HPLC: RT = 5.98 min.

1.3.4 Procedure for 1,3-Dibromo-2-(2-methoxypropan-2-yl)benzene (11). A solution of LDA was prepared in 1 hour by addition of 12.5 mL of n-butyllithium (20 mmol, 1.6 M in hexane) to a stirred solution of 2.02 g of diisopropylamine (20 mmol in 12.5 mL of anhydrous THF) kept at –5°C. The solution was then slowly transferred into a solution of 1,3-dibromobenzene (20 mmol in 12.5 ml of anhydrous THF) kept at –78°C. After 1.5 hours the suspension of the resulting lithiate was treated with acetone (40 mmol, neat). The temperature was immediately raised to 25°C, and the mixture transferred into a solution of MeI (1 ml) in anhydrous DMF (10 ml). After 1 hour the solvents and DMF were removed by distillation at reduced pressure and the crude was pre-purified by a silica gel chromatography column (petroleum ether/Et_2O 20/1) to obtain **11** (overall Yield: 3%, ≈ 30% on the intermediate alcohol). Analytically pure samples were obtained by semi-preparative HPLC on a Luna C18(2) column (5μm, 250x10 mm, 4 ml/min, ACN/H_2O 80:20 v:v).

1,3-Dibromo-2-(2-methoxypropan-2-yl)benzene (11). ^{1}H-NMR (600 MHz, $CDCl_3$, 25°C, TMS): δ 1.87 (6H, s), 3.60 (3H, s), 7.06 (1H, t, *J* = 7.9 Hz), 7.29 (2H, t, *J* = 7.9 Hz). ^{13}C-NMR (150.8 MHz, $CDCl_3$, 25°C, TMS): δ 28.4 ($2CH_3$), 50.2 (OCH_3), 80.3 (Cq), 122.7 (2Cq), 128.6 (CH), 135.7 (2CH), 141.7 (Cq). HPLC : RT = 12.42 min.

1.4 NMR Spectroscopy

The spectra were recorded at 300, 400 and 600 MHz for ^{1}H and 75.45, 100.6 and 150.8 MHz for ^{13}C, and 564.3 MHz for ^{19}F. The external standard C_6F_6 (neat, set at –163.0 ppm) in the ^{19}F spectra was used as reference. The assignments of the ^{13}C signals were obtained by DEPT and bi-dimensional experiments (gHSQC[33] and gHMBC[34] sequences). The samples for obtaining spectra at temperatures lower than –100 °C were prepared by connecting to a vacuum line the NMR tubes containing the compound and some C_6D_6 for locking purpose and condensing therein the gaseous CHF_2Cl and $CHFCl_2$ (4:1 v/v) under cooling with liquid nitrogen. The tubes were subsequently sealed *in vacuo* and introduced into the precooled probe of the spectrometer. The temperatures were calibrated by substituting the sample with a Cu/Ni thermocouple before the measurements.

1.5 Calculations

Computations were carried out at the B3LYP/6-31G(d) or at the B3LYP/6-311+G(2df,p)//B3LYP/6-31G(d) level by means of the Gaussian 03 series of programs[15]: the standard Berny algorithm in redundant internal coordinates and default criteria of convergence were employed. The reported energy values are not ZPE corrected. Harmonic vibrational frequencies were calculated for all the stationary points. For each optimized ground state the frequency analysis showed the absence of imaginary frequencies, whereas each transition state showed a single imaginary frequency.

Chapter 2

2.1 Hindered Biphenyl Carbinols: For The First Time Dimer Formation is Observed by DNMR

Enantiomerism generated by axial chirality has been receiving increasing attention, as reported in a recent comprehensive review by Bringmann at al.[35] This is because structures having a biaryl axis represent the basis for reagents or catalysts employed in the asymmetric synthesis.[35] Biphenyl derivatives exhibiting axial chirality can be either configurationally stable or can give raise to stereolabile atropisomers, depending on the extent of the steric effects of their substituents.

Dynamic NMR spectroscopy has been used as an efficient tool to investigate conformational enantiomers generated by axial chirality due to restricted Ar-Ar bond rotation.[36,37] In the recent past stereolabile atropisomerism arising from restricted rotation about the sp^2-sp^3 bond in a number of hindered aryl carbinols and ethers were also investigated.[13p,38]

It was thus attractive to study the atropisomerism occurring in derivatives bearing both a sp^2-sp^2 and a sp^2-sp^3 chiral axis, i.e. biphenyls substituted by one or two carbinol moieties, as those displayed in *Scheme 4*.

Scheme 4

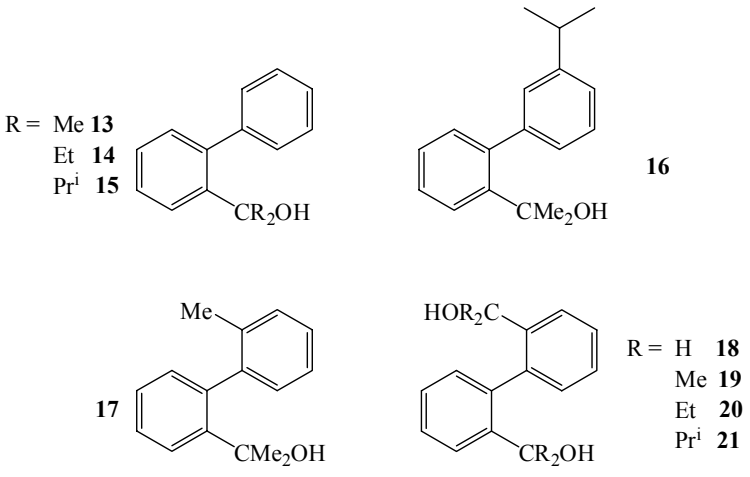

Contrary to the case of analogously hindered ortho substituted benzyl carbinols,[13p] the low temperature (down to –170 °C) NMR spectra of **13** (R = Me) do not exhibit the two groups of signals expected for the two possible conformers displayed in *Scheme 5* (antiperiplanar and synperiplanar).[17]

Scheme 5

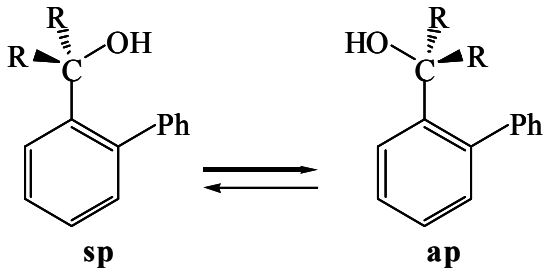

DFT calculations[15] suggest that the relative stability of the two conformational isomers is the result of a delicate balance between the steric hindrance exerted by the two aliphatic groups on the phenyl ring in the ortho position, and the possibility of an energy stabilization due the position of the some hydrogen atoms over the π-system of the orthogonal phenyl ring. In the case of compound 13, calculations indicate that both conformers correspond to energy minima and should have essentially the same stability (*Figure 19*).

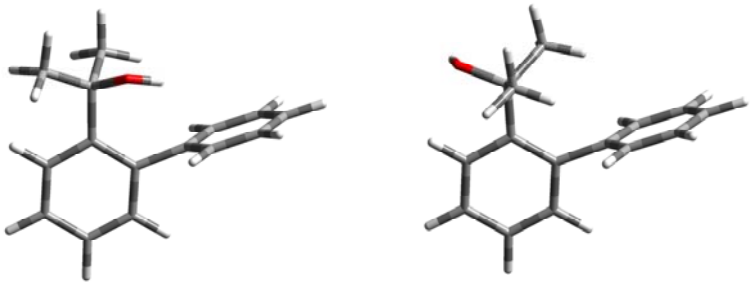

13-sc (E = 0.0 kcal mol^{-1}) **13-ap (E = 0.011 kcal mol^{-1})**

Figure 19: **DFT computed structures of the two atropisomers of compound *13*. In this case the *syn* structure might be rather called synclinal (sc): according to computations, in fact, the corresponding O-C(Me2)-C1-C2 dihedral angle (+47°) exceed +30°.**[17]

However the barrier calculated for the interconversion occurring *via* the Ar-CMe_2 bond rotation, is predicted to be quite low (about 5 kcal mol^{-1}), thus accounting for the failure of detecting separate NMR signals for the two conformers at any attainable temperature. The presence of both the *syn* and *anti* conformers in rapid equilibrium is also demonstrated by NOE experiments (*Figure 20*).

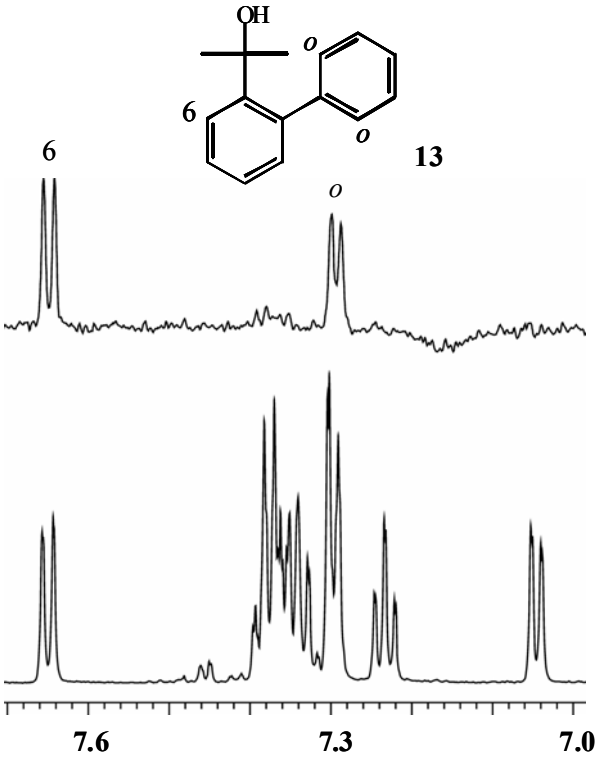

Figure 20: **Bottom: ^{1}H NMR aromatic signals (600 MHz) of *13* in $CDCl_3$ at –30 °C. Top: the NOE spectrum, obtained by irradiating the OH signal, shows the enhancement of the signal of the hydrogen in position *6* and of the two hydrogens in position ortho. Assignment obtained by means of the COSY bi-dimensional sequence.**

As shown in *Figure 20*, irradiation of the OH signal of **13** enhances that of the single aromatic hydrogen in position ortho to the CMe_2OH moiety, indicating the presence of the *anti* (*ap*) conformer, as well as that of the two ortho hydrogens within the unsubstituted phenyl ring, indicating the presence of the *syn* conformer.

DFT computations[15] also predict that the Ar-Ar rotation barrier of **13** should be relatively high (14.5 kcal mol^{-1}), but this motion is NMR invisible in **13** owing to the molecular symmetry. In order to detect experimentally such a process an isopropyl group was introduced in the meta position of the unsubstituted phenyl ring, yielding compound **16**: the substitution in this position, in fact, should not affect significantly the value of the Ar-Ar rotation barrier. At –40 °C the ^{13}C methyl signals of both the isopropyl (*Figure 21*) and CMe_2OH moieties of **16** split into 1:1 pairs.

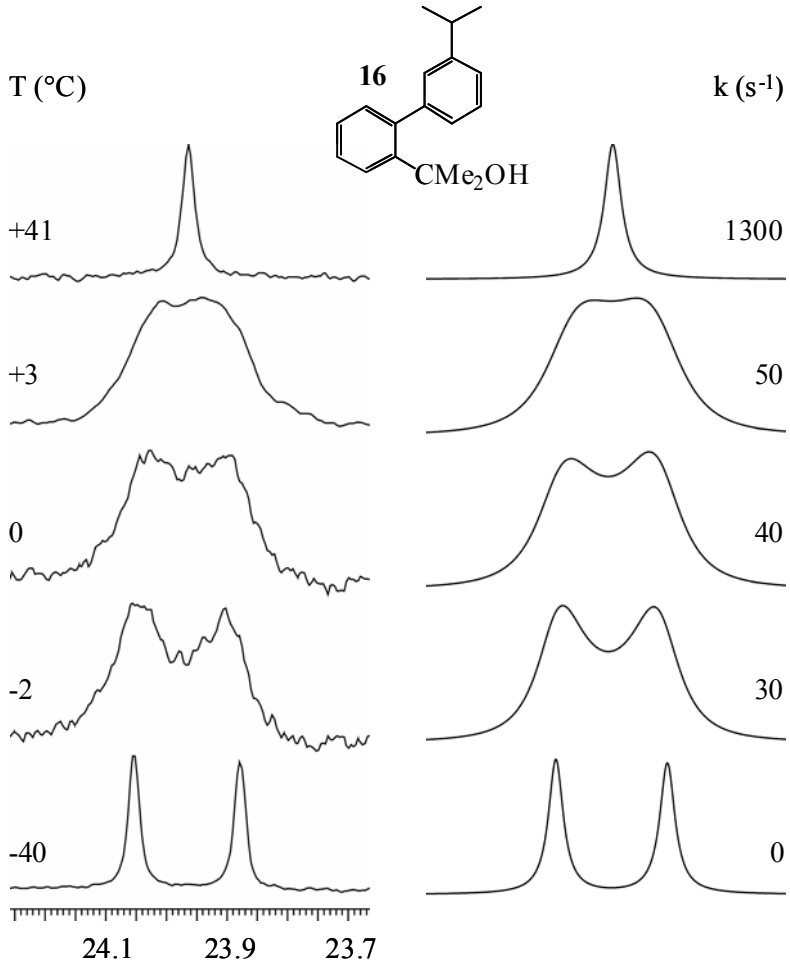

Figure 21: **Left: Temperature dependence of the ^{13}C (150.8 MHz) of the isopropyl methyl signals of *16* in $CDCl_3$; Right: simulation obtained with the rate constants indicated.**

This proves that the Ar-Ar rotation rate has become slow in the NMR time scale and that the molecule has adopted an asymmetric (C_1 point group) conformation where the two aryl groups are nearly orthogonal to each other. The low temperature observation of anisochronous signals for these diastereotopic methyl groups[39] implies the presence of two stereolabile atropisomers due to the chirality axis: the corresponding enantiomerisation barrier, brought about by the Ar-Ar rotation, was determined by line shape simulation (*Figure 21*). The resulting value of $13.9_5 \pm 0.15$ kcal mol^{-1} (*Table 3*) is indeed very close to that anticipated by calculations (14.7 kcal mol^{-1}).

Table 3: **Barriers for the Dynamic Processes Measured in 14-16 and 19.**

Compd.	**$\Delta G^{\neq}$ (kcal mol^{-1})**	**Dynamic Process**
14	7.5 ± 0.15	Ph-CEt_2OH rotation
15	6.4 ± 0.15	Me_2CH-C(OH)Ar rotation
16	13.9_5 ± 0.15	Ar-Ar rotation
19	9.5 ± 0.3	Dimerization

The greater steric hindrance occurring in compound **14** (R = Et) with respect to **13** allowed the detection of separate NMR signals for the corresponding *sp* and *ap* conformers. In *Figure 22*, the ^{13}C lines of two aromatic quaternary carbons are displayed as function of temperature: the ratio of the two atropisomers appears to be 70:30.

Computations predict that the relative energies of the two isolated *sp* and *ap* atropisomers are essentially equal, (*Figure 23*), thus the unequal proportion observed should be attributed to the effect of the condensed phase.

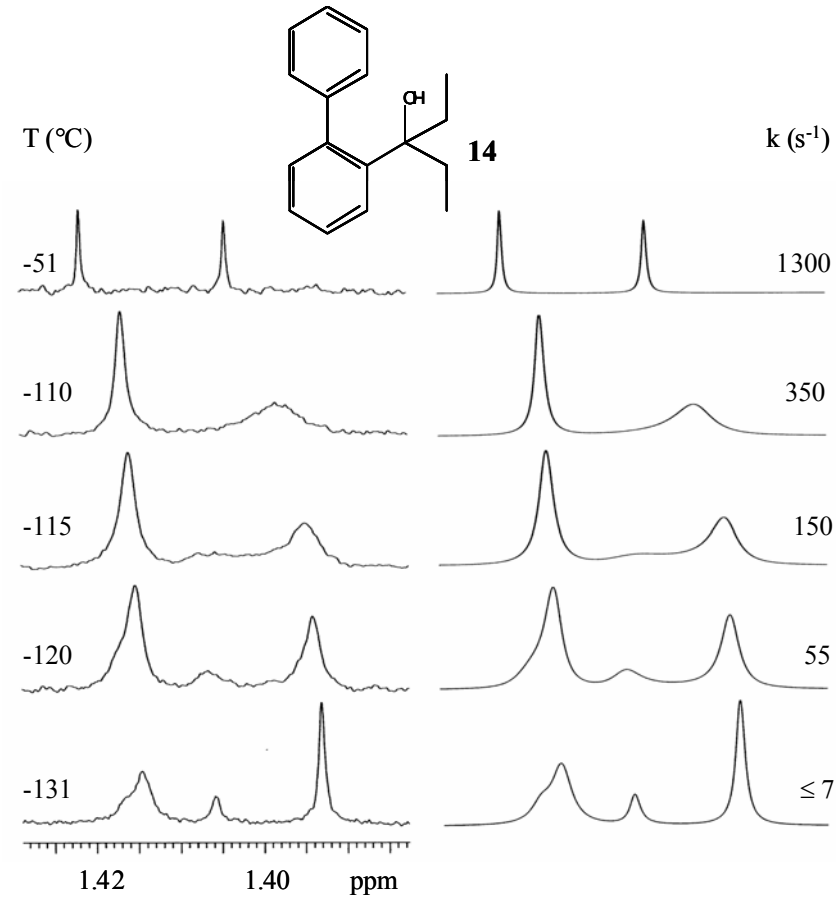

Figure 22: **Left: temperature dependence of the ^{13}C NMR signals (150.8 MHz) of the lines of two aromatic quaternary carbons of *14* in $CHF_2Cl/CHFCl_2$. Right: simulation obtained with the rate constants indicated.**

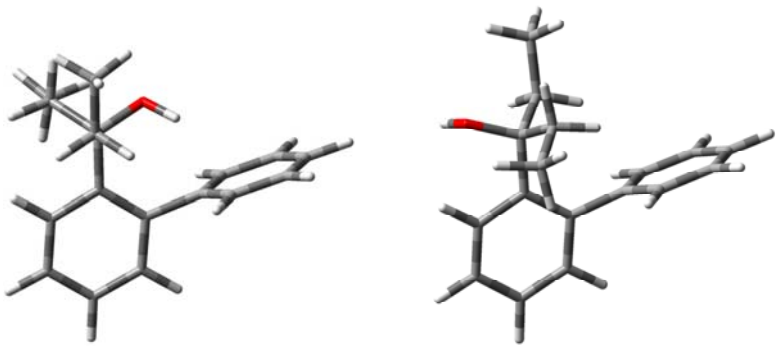

14-sp (E = 0.0 kcal mol^{-1}) **14-ap (E = 0.005 kcal mol^{-1})**

Figure 23: **DFT computed structures of the two atropisomers of compound *14*.**

Nonetheless the *ap* structure has been assigned to the more populated of the two conformers on the basis of the chemical shift predicted by DFT computations. In fact the aromatic quaternary carbon ortho to the CEt_2OH moiety, the aliphatic quaternary carbon and the CH_2 carbon are all predicted to have shifts at higher field in the *ap* with respect to the corresponding carbons of the *sp* conformer. The computed differences between the shifts of these carbons are 1.1, 1.5 and 1.4 ppm, to be compared with the corresponding experimental differences (measured at –131 °C) of 1.26, 2.56 and 1.70 ppm, respectively. The other carbons either have shift differences too small to be significant or are overlapped by the signals of the solvent ($CHF_2Cl/CHFCl_2$). In all these cases the experimental spectrum shows that the upfield is more intense than the downfield ^{13}C signal (see *Figure 22* and *Figure 24*).

From the line shape simulation of the spectrum of *Figure 22* the barrier for the interconversion of the major (*ap*) into the minor (*sp*) conformer is derived (7.5 ± 0.15 kcal mol^{-1}, as in *Table 3*): the same value was also obtained by simulating the ^{13}C signals of the CH_2 carbon (*Figure 24*).

Although the greater steric requirements of **15** (R = *i*-Pr) would suggest a barrier for the interconversion larger than that of **14** (R = Et), the corresponding ^{13}C NMR spectrum does not show the two expected sets of unequally intense signals, even at –152 °C. This means that in the case of **15** only one of the two possible conformers is appreciably populated.

Calculations actually show that the *sp* form has an energy 3.2 kcal mol^{-1} lower than that of its *ap* companion, thus accounting for the negligible population of the latter. The structure computed for the more stable *sp* conformer of **15** indicates that the two isopropyl groups are locked in two different spatial situations (*Figure 25*) since they exhibit two different values (+58° and +170°) for the H-C(Me_2)-C(OH)-C_{isop} dihedral angles.

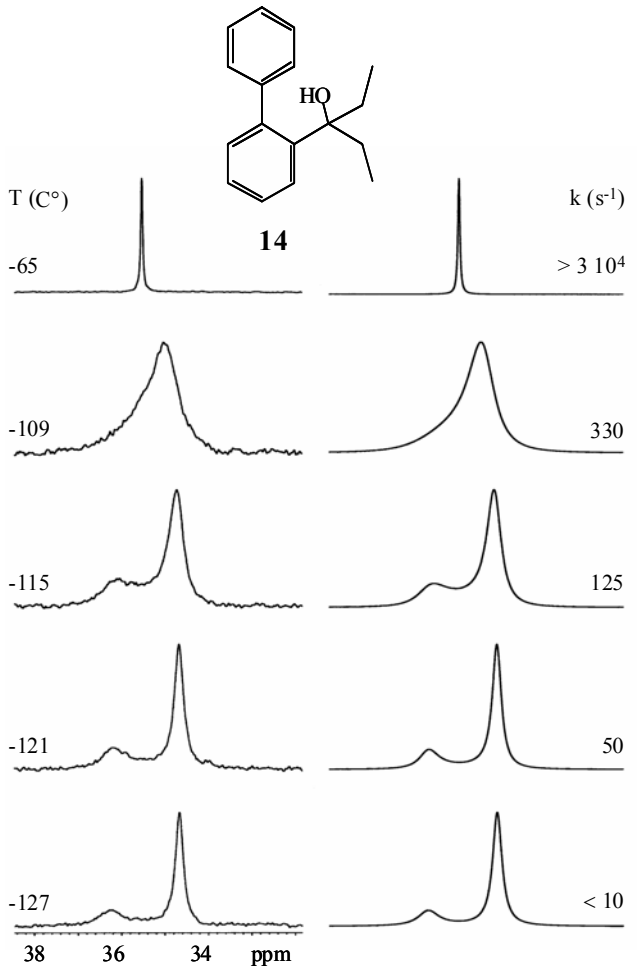

Figure 24: **Left: Experimental ^{13}C NMR signals of the CH_2 carbons of *14* (150.8 MHz in $CHF_2Cl/CHFCl_2$) as function of temperature; Right: simulation obtained with the rate constants indicated.**

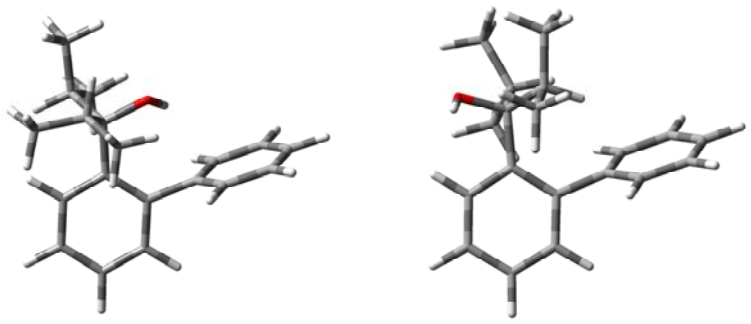

15-sp (E = 0.0 kcal mol^{-1}) **15-ap (E = 3.17 kcal mol^{-1})**

Figure 25: **DFT computed structures of the two atropisomers of compound *15*.**

Indeed the ^{13}C spectrum of 15 at –152 °C displays two equally intense signals for the two isopropyl CH carbons (*Figure 26*) and, in addition, also one of the two lines, due to the two pairs of methyl carbons (that are already diastereotopic at ambient temperature[39]), is further split into 1:1 lines at –152 °C (the additional splitting, expected for the other diastereotopic methyl line, have a shift difference too small to be detected).

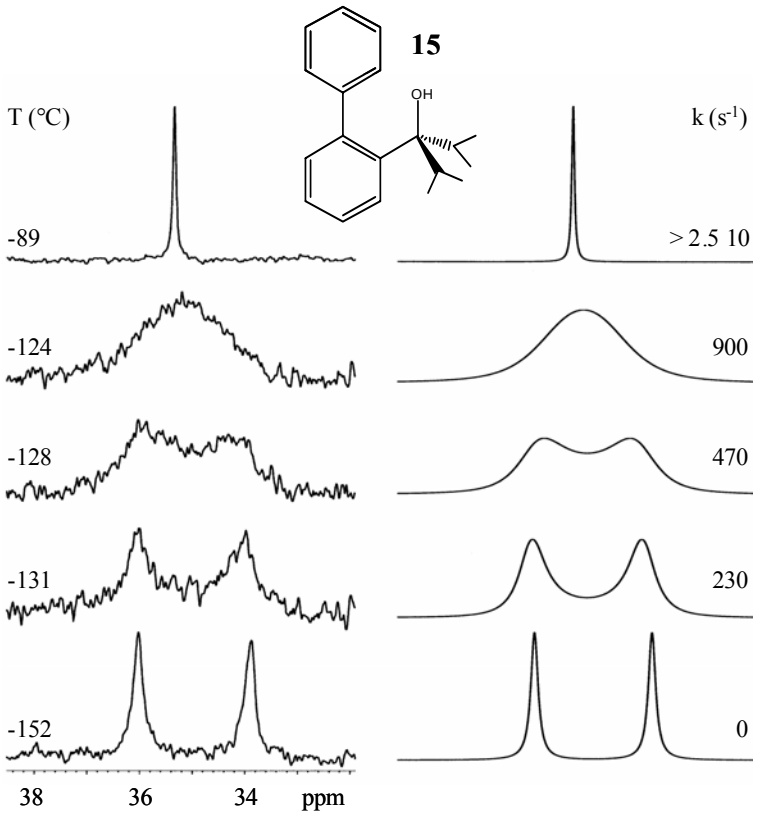

Figure 26: **Left: temperature dependence of the CH isopropyl signal of *15* (^{13}C NMR at 150.8 MHz) in $CHF_2Cl/CHFCl_2$. Right: simulation obtained with the rate constants indicated.**

The line shape simulation of the signals of *Figure 26* yields a barrier of 6.5 kcal mol^{-1} for the rotation process of the isopropyl substituents about the HOC-$CHMe_2$ bond this value is in keeping with that (6.4 kcal mol^{-1}) determined in an analogous case.[13p]

The presence of an ortho methyl substituent in the phenyl moiety of compound **17** enhances the Ar-Ar rotation barrier and, at the same time, renders the molecule asymmetric since the two aryl rings adopt an orthogonal arrangement, as anticipated by DFT

calculations. For this reason the ambient temperature NMR spectrum of **17** displays two anisochronous lines for the methyl groups because they have been made diastereotopic[39] by the chirality of the molecule. Even at higher temperature (+120 °C in DMSO-d_6) these lines do not undergo an exchange process, indicating that the Ar-Ar rotation barrier, required to interconvert the two enantiomers, is, at least, higher than 21-22 kcal mol^{-1} (DFT computations predict a barrier of 25.1 kcal mol^{-1}). As already observed in the case of compounds **13** and **16**, low temperature spectra (*Figure 27*) do not show any dynamic feature due to slow rotation of the C-Me_2OH moiety.

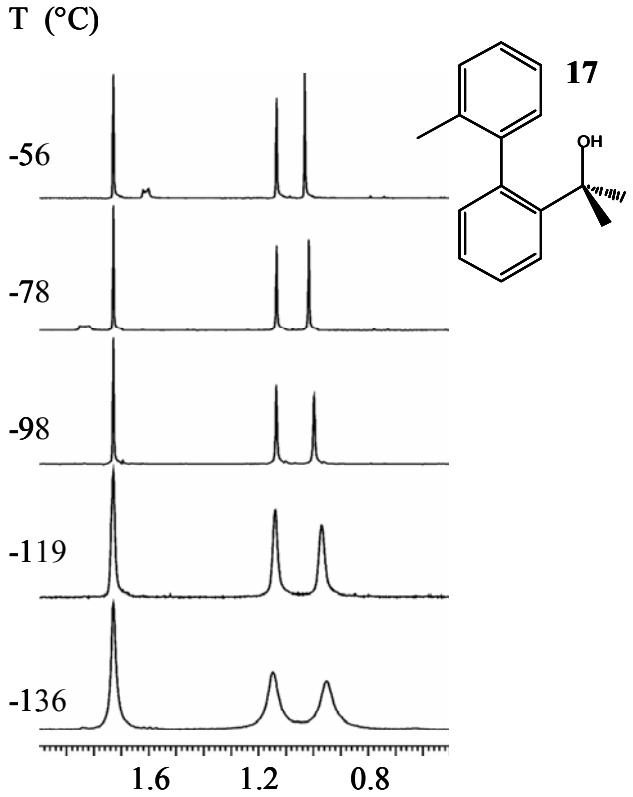

Figure 27: **Experimental ^{1}H spectra of the Me signals of *17* (600 MHz in $CHF_2Cl/CHFCl_2$) as function of temperature.**

In the case of biphenyls bearing two equal CR_2OH substituents in the ortho and ortho' positions (*Scheme 4*), the Ar-Ar rotation barrier is likewise quite high, so that two relatively stable atropisomers are expected to occur. For instance, derivative **18** (R = H)

displays at ambient temperature an AB-type spectrum for the diastereotopic methylene hydrogens of the CH_2OH moiety[40] (*Figure 28*, top): even on warming well above ambient temperature this diastereotopicity is maintained.

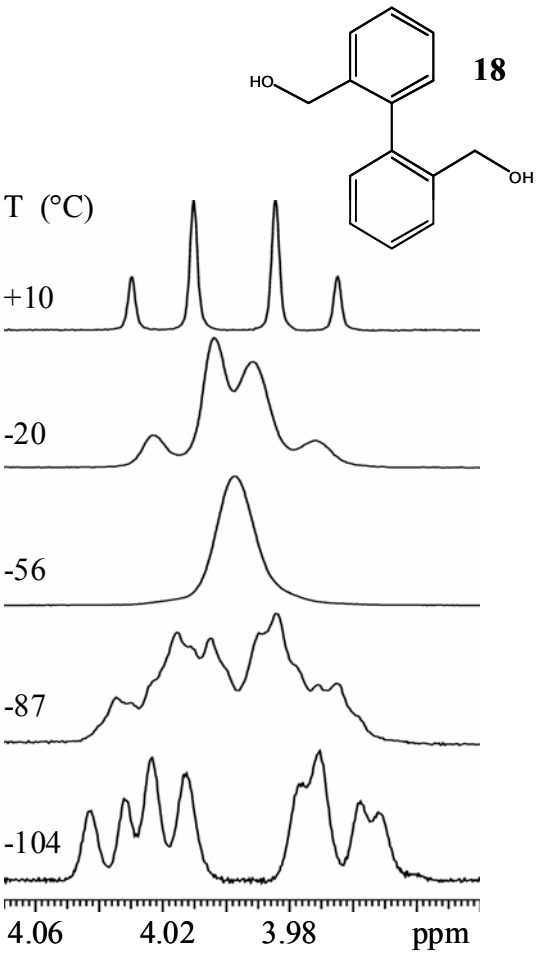

Figure 28: **Temperature dependence of the ^1H signals (600 MHz) of the methylene hydrogens of *18* (ca. 0.07 M in CD_2Cl_2/CHF_2Cl 9:1 v/v).**

Molecular Mechanical conformational analysis has revealed the presence of three energy minima, and the following optimization by DFT[15] for **18** and **19** are displayed in *Scheme 6*. As conceivable, the computed Ar-CH_2OH rotation barrier, required to interconvert these conformers, is so low (less than 4 kcal mol^{-1}) as to be NMR invisible at any attainable temperature. The computed minimum of energy corresponding to the *sp,ac*

is much lower than for the other two structures (i.e. *sp*,*sp* and *ap*,*ap*), thus derivatives **18** is expected to adopt essentially this conformation.

Scheme 6: **DFT Computed Relative Energies (kcal mol^{-1}) for the Conformers of *18* and *19* (dotted lines indicate hydrogen bonds).**

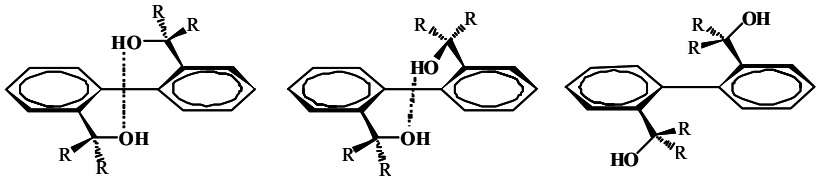

	(sp, sp)	(sp, ac)	(ap, ap)
R = H, **18**	E = 3.2	E = 0.0	E = 4.8
R= Me, **19**	E = 0.0	E = 3.8	E = 7.0

On lowering the temperature, the spectral lines of **18** broaden and, subsequently, sharpen again, in a way typical of an exchange process (*Figure 28*). Since, as mentioned, the barrier to freeze the Ar-CH_2OH rotation is NMR invisible, the observed dynamic process could be attributed to the exchange of the *sp*,*ac* monomer with a dimer, assembled by two intermolecular H-bond interactions between the pairs of the OH groups of two *sp*,*ac* conformers.

DFT calculations[15] indicate, in fact, that a heterochiral dimer, formed by a *M* and a *P* enantiomer of the *sp*,*ac* conformer, corresponds to a minimum, with an energy value much lower than that of the homochiral dimer formed by two *M* (or two *P*) enantiomers (*Figure 29*): thus only the heterochiral dimer (*meso*) should be present, whereas the *M*,*M* (or *P*,*P*) homochiral dimer (racemic) should not be populated. The static symmetry of the dimer of **18** (*Figure 29*) is C_i, but the rapid rotation about the C-OH bonds in this *meso* structure makes the dynamic symmetry higher, thus rendering equivalent (i.e. isochronous) the shifts (both ^{13}C and ^{1}H) of the four CH_2OH moieties of the dimer. Within each CH_2OH moiety, however, the two methylene hydrogens would always remain diastereotopic.

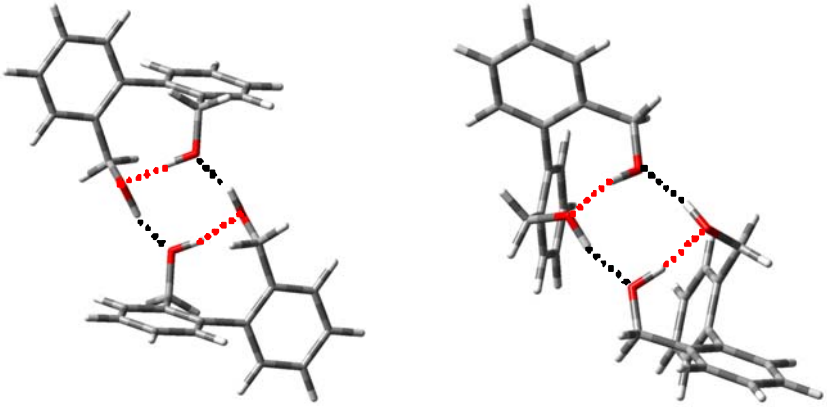

18-MP-dimer
(E = 0.0 kcal mol^{-1})

18-PP-dimer
(E = 6.8 kcal mol^{-1})

Figure 29: **Structures of compound *18*. Left: more stable heterochiral dimer obtained by DFT calculations; Right: less stable homochiral dimer obtained by DFT calculations. The dotted lines indicate intramolecular (red) and intermolecular (black) hydrogen bonds.**

Also the known[41] crystal structure of compound **18**, obtained on crystals grown from acetone, shows that the molecule exists essentially as a dimer formed by a pair of heterochiral molecules kept together by H-bond; the dimers are then linked together to form a supramolecular chain. To avoid the possibility of polymorphism induced by the solvent, crystals were also obtained from a very low polarity solvent (hexane). The crystal structure obtained is exactly equal to the reported one (*Figure 30*).

Such an experimental result thus confirms the theoretical computations and also agrees with the interpretation of the NMR spectra in solution. There is a slight deviation in the shape of the preferred conformer in the solid state as compared to that computed for the isolated molecule, this being a consequence of the lattice interactions experienced by the dimer in the crystalline state.

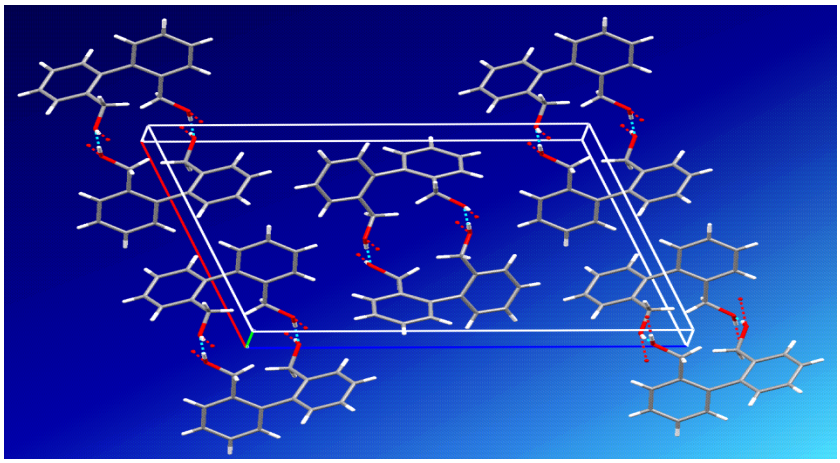

Figure 30: **Single crystal X-ray structure of compound *18* (crystals obtained from hexane) showing the preference for a dimeric form (cyan dotted lines indicate the H-bonds).**

In solution, at ambient temperature, the amount of the dimer is conceivably quite small with respect to the monomer and, in any case, the exchange with the monomer is fast, so that only a four line AB-spectrum can be observed by ^{1}H-NMR (*Figure 28*, top trace). On lowering the temperature, the amount of the dimer increases progressively and, at the same time, the exchange rate diminishes, yielding spectra with lines broadened by the exchange. The complexity of the variable temperature spectra arises from the fact that in the range –20 °C to –60 °C the shift separation of the AB spectrum of the monomer changes and, furthermore, its lines are broadened by the exchange with an increasing amount of the dimer, until a single broad line is observed at –56 °C. In the range –60 °C to –85 °C both the spectrum of the dimer and that of the monomer begin to appear as superimposed traces, with the widths of the lines still broadened by the exchange. At –87 °C approximately 12 broad humps are observed, due to the 4 lines of the monomer superimposed to the 8 lines of the dimer in a slow exchange regime: simulation of this spectrum (*Figure 31*) indicates that the dimer/ monomer ratio is 88/12.

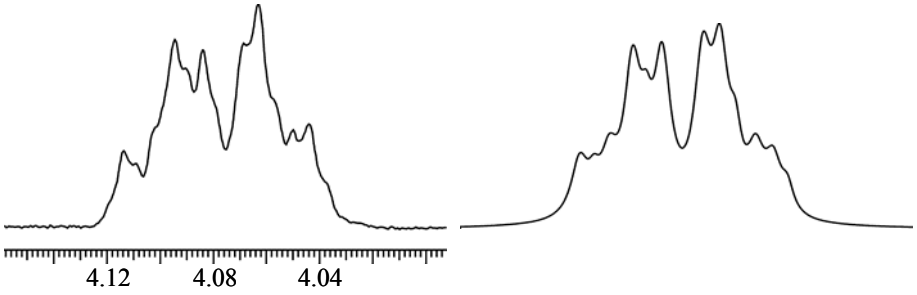

Figure 31: **Left: Experimental ^{1}H NMR spectrum (600 MHz) of compound *18* at –87 °C (ca. 0.07 M in CD_2Cl_2/ CHF_2Cl) as in *Figure 28*. Right: Respective simulation.**

The latter appear as an ABX-type spectrum, since at such low temperature the diastereotopic methylene hydrogens also display two different J couplings with the OH hydrogen, therefore the computer simulation (*Figure 31*, right) is obtained with 88% of the 8-line spectrum of the AB portion of the ABX system of the dimer ($\Delta\nu$ = 23 Hz, J_{AB} = -11.7 Hz, J_{AX} = 6.7 Hz, J_{BX} = 3.7 Hz) superimposed to 12% of the 4-line AB spectrum of the monomer ($\Delta\nu$ = 29 Hz, J_{AB} = -11.5 Hz). The spectrum of the monomer is 2.5 Hz at higher field with respect to that of the dimer, the line widths being 4.5 Hz for the spectrum of the dimer and 3.2 Hz for that of the monomer.

Such an observation allowed us to rule out the possibility that the dynamic process is due to solely to the mobility of the OH hydrogen (moving from one OH to another), because this motion alone cannot produce a spectrum with more than 8 lines. Only below -100 °C could a well resolved spectrum be observed, since the only species present at this temperature is that of the dimer (*Figure 28*, bottom trace). In the latter the coupling with the OH hydrogen could be detected because these hydrogens are not mobile: they are firmly bonded to the oxygen, because the OH groups are involved in the strong intermolecular hydrogen bonds required to form the dimer. In the monomer, on the contrary, the OH hydrogens, not involved in a strong hydrogen bonds, are very mobile and can rapidly exchange among the various molecules, thus making such a coupling invisible.[42]

Decoupling of the OH single broad line transforms, in fact, the 8-line ABX spectrum into a 4-line AB spectrum. It should be also pointed out that when CD_3OD is used as solvent this process does not occur and only the 4-line AB spectrum of the monomer is detected, even at very low temperature: the possibility for **18** of making a strong H-bond with this solvent makes formation of the dimer unlikely.[43]

The NMR spectral traces of **18**, however, are too complex to allow a quantitative interpretation of the process, whereas derivative **19**, which yields simpler spectra, is better suited for obtaining a quantitative determination of the exchange dynamics (*Figure 32*).

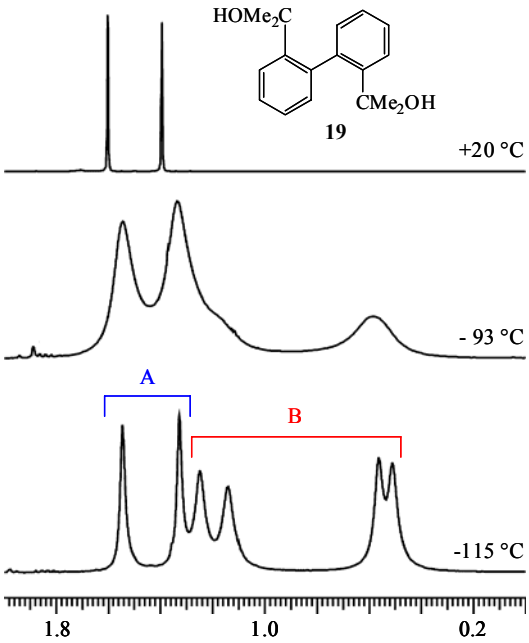

Figure 32: **^{1}H NMR signals (600 MHz in CD_2Cl_2/CHF_2Cl 9:1 v/v) of the diastereotopic methyl groups of *19* (top trace). On lowering the temperature these lines broaden (central trace) and at -115 °C (bottom trace) the spectrum displays two lines for the form A (33%) and four lines for the form B (67%).**

In the latter derivative the two ^{1}H lines of the diastereotopic methyl groups broaden on cooling, as observed in the spectrum of 18, but, in this case, two well resolved spectra, due to two species with unequal populations, are observed at low temperature (33/67 in CD_2Cl_2/CHF_2Cl at –115 °C, as in *Figure 32*). One such spectrum displays two equally

intense lines (indicated as *A*), the other spectrum shows four equally intense integrated lines (indicated as *B*). The ratio of these two forms is greatly dependent on the type of solvent employed, up to the point of reversing their relative proportions, as summarized in *Table 4*.

Table 4: **Relative Proportion of the two Spectral Traces of the Methyl Groups of *19* in Various Solvents at –115 °C.**

Solvent	CD_2Cl_2 [a]	Toluene-d_8 [a]	CD_3OD [a]	$CHFCl_2/CHF_2Cl$
Two-lines Spectrum (A)	33%	10%	100%	84%
Four-lines Spectrum (B)	67%	90%	0%	16%

[a] **To lower the freezing point of the solutions a small amount of CHF_2Cl (≈ 10% v/v) was added.**

The two lines of the spectrum, indicated as A, should correspond to the diastereotopic methyl groups within the two equal CMe_2OH moieties of the most stable *sp*,*sp* conformer of *Scheme 6*, essentially in the monomeric situation. The four line spectrum (labelled B) are again attributed to a dimer, formed by two intermolecular H-bond interactions between the pairs of OH groups of two *sp*,*sp* conformers.

The crystal structure of **19** (*Figure 33*) confirms the presence of an extended network of H-bond; however, at variance with **18**, the *sp*,*sp* conformation of the molecule of **19** in the solids indicates the presence of an intramolecular H-bond and an intermolecular H-bond with another molecule of opposite chirality. This arrangement should correspond to a weaker intermolecular interaction with respect to the case of **18**, in which each molecule has two intermolecular H-bond. This agrees with the fact that in solution distinguishable NMR spectra are observed for the monomer and the dimer of **19** at low temperature, whereas in the case of **18** only the spectrum of the dimer is present at low temperature.

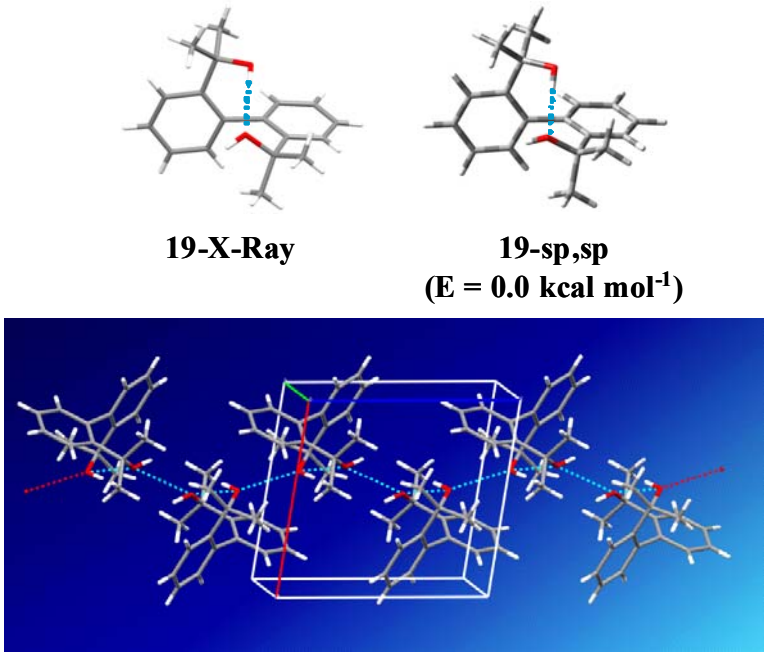

Figure 33: **Top: X-ray structure (left) and DFT computed structure (right) of compound *19*. Bottom: crystallographic cell showing the presence of both intra and intermolecular H-bond (dotted cyan lines).**

DFT calculations[15] indicate that the energy of the homochiral dimer (*M,M* or *P,P*) is much lower than that of the heterochiral *M,P* (*meso*) dimer (*Figure 34*), thus the latter should not be populated.

In the most stable *M,M* (or in the isoenergetic *P,P*) chiral dimer, the eight methyl groups experience four different spatial environments, because there are two pairs of diastereotopic CMe_2OH moieties, each bearing two diastereotopic methyl groups. Four different shifts are, accordingly, expected for the methyl groups: since the homochiral dimer of ***19*** is racemic (C_2 static symmetry), even the rapid rotation about the C-OH bonds maintain diastereotopic the two pairs of CMe_2OH moieties, contrary to the case of the CH_2OH moieties of the *meso* dimer of **18**). The four-line spectrum displays two lines at a field quite higher than the other two spectra (in CD_2Cl_2 the shifts are, respectively, 0.50, 0.55 and 1.13, 1.24 ppm). As evident from the computed structure of the *M,M* dimer

(*Figure 34*), two pairs of methyl groups lie above the aryl rings and thus experience the well known upfield shift due to the aromatic ring current.[44] The DFT-computed shifts for the *M,M* dimer display an analogous trend, i.e., 1.51, 1.21 ppm for the two pairs of methyls at lower field and 1.16, 1.14 ppm for the two pairs of methyls at higher field, the latter actually corresponding to the methyls lying above the phenyl rings.

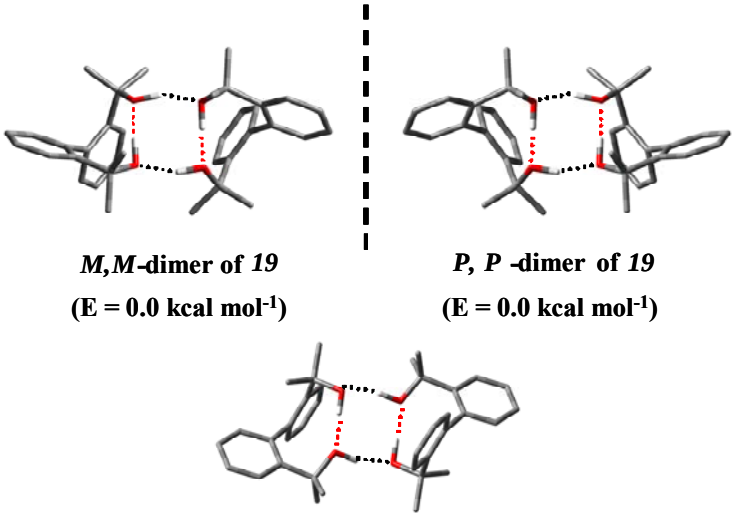

Figure 34: **DFT computed structures of the two possible dimers derived from the association between two enantiomers of the most stable conformer (*sp,sp*) of compound *19*. Red dotted lines indicate intramolecular hydrogen bonds. Black dotted lines indicate intermolecular ones.**

As previously mentioned, the amount of a dimer is conceivably quite small with respect to the monomer at higher temperatures and, being the exchange with the monomer fast, only the two-lines spectrum can be observed. On lowering the temperature, the amount of the dimer increases progressively and, at the same time, the rate of exchange diminishes. As a consequence the lines begin to broaden and finally yield distinguishable spectra for the monomer and the dimer, the proportion of the latter growing, as

conceivable, on further lowering the temperature (for instance, from 46% at –100 °C to 72% at –120 °C in CD_2Cl_2/CHF_2Cl).

The following experimental evidences further support the hypothesis of a monomer/dimer equilibrium:

i) When very diluted (less than 10^{-3} molar) solutions of **19** are examined, only the two-lines spectrum is invariably observed in any solvent at any low temperature. In these conditions, in fact, the probability of forming a dimer has become negligible and only the spectrum of the monomer is therefore present (*Figure 35*).

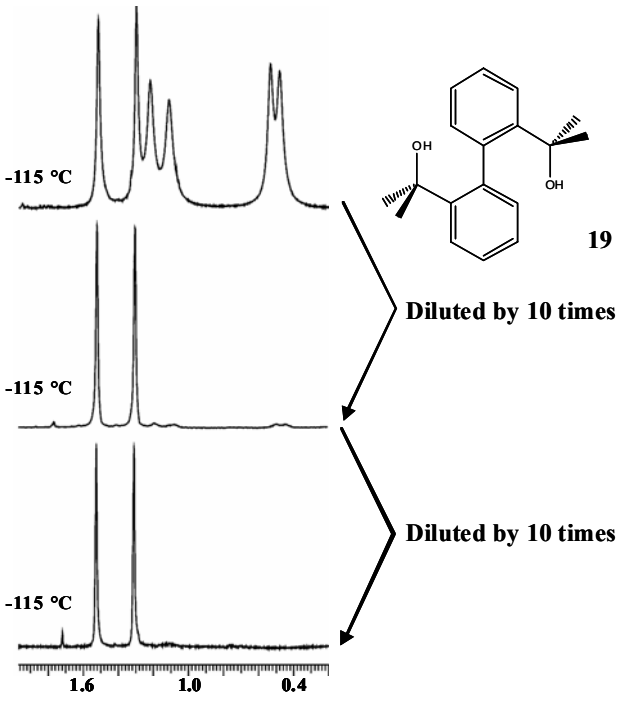

Figure 35: **Spectra of the ^{1}H methyl region of compound *19* (600 MHz in CD_2Cl_2/CHF_2Cl 9:1 v/v), diluted 10 and 100 times, showing the disappearance of the four-line species at lower concentration.**

ii) At any concentration in CD_3OD solutions only the two-lines spectrum is observed, as reported for **19**. As mentioned, it is more likely that the H-bond takes place with methanol, thus preventing the occurrence of the H-bond between two molecules to produce the dimer.[43] Likewise, when a wholly fluorinated solvent is employed

($CHF_2Cl/CHFCl_2$) it is possible to have H-bonds between OH and fluorine.[45] This type of H-bond is weaker than in the case of methanol,[46] and thus accounts for the quite small, although not negligible, proportion of the four-lines spectrum observed in this solution (*Table 4*).

iii) When the possibility of making hydrogen bond with the solvent is negligible (as in the case of toluene and methylene chloride) the proportion of the dimer in toluene (*Table 4*), which has a small dielectric constant, is larger, at a given temperature, than in methylene chloride, which has a larger dielectric constant: this is in keeping with the computed value of the dipole moment of the *M*,*M* (or *P*,*P*) dimer (0.3 D) which is lower than that computed for the *sp*,*sp* monomer (2.3 D).

iv) In absence of exchange, the lines of the four-lines spectrum B are broader than those of the two-lines spectrum A (see the traces at –115 °C and -121 °C of *Figure 32* and *Figure 36*, respectively). It is well known that the line widths of molecules of larger dimensions are broader than those of smaller molecules, due to the longer correlation time,[47] this feature being particularly evident at very low temperatures. This agrees with the hypothesis that the four-line spectrum corresponds to a dimer which, obviously, has a larger dimension, thus broader lines, than the monomer.

v) A Diffusion Ordered Spectroscopy NMR (DOSY)[48] experiment was performed in a diluted (10^{-3} M) and in a concentrated (10^{-1} M) solution of **19** in toluene-d_8. In the latter solution a certain amount of dimer should be present at the equilibrium with the monomer and indeed a lower diffusion coefficient ($8.7 \pm 0.1\ 10^{-10}$ $m^2\ s^{-1}$) was measured with respect to the diluted solution ($9.6 \pm 0.1\ 10^{-10}$ $m^2\ s^{-1}$) where the dimer is absent. The hydrodynamic volume obtained for the concentrated (359 $Å^3$) was accordingly larger than for the diluted solution (272 $Å^3$), confirming the presence of a certain amount of a form with a larger molecular size.[49]

The process interconverting the two monomers into a dimer depends on the concentration, according to a second order rate constant. As an example, the spectral simulation for a 0.13 M solution of **19** in $CHF_2Cl/CHFCl_2$ is displayed in *Figure 36*.

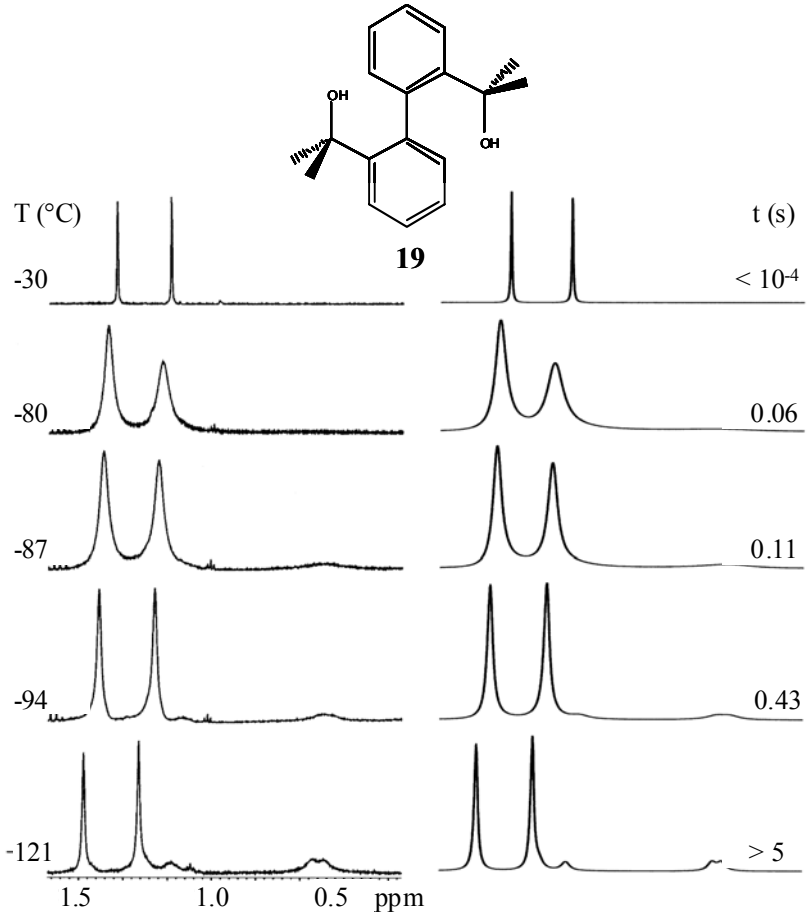

Figure 36: **Left: Experimental methyl signals of *19* (600 MHz in $CHF_2Cl/CHFCl_2$) as function of temperature; Right: simulation obtained with the rate constants reported.**

From the lifetime (τ) values, a $\Delta G^{\neq}$ of 9.5± 0.3 kcal mol^{-1} was obtained in the temperature range –80 °C to –94 °C: to the best of our knowledge this is the first example of a quantitative NMR determination of a dynamic process involving a monomer/dimer exchange.

In all derivatives bearing two equal CR_2OH substituents (18-21), the high Ar-Ar rotation barrier entails the lack of a plane or centre of symmetry, thus leading to *M* and *P*

enantiomers, that can be made visible by taking the NMR spectrum in a chiral environment, that was made of a 11:1 molar excess of the enantiopure (R)-(-)-2,2,2-trifluoro-1-(9-anthryl)ethanol (also called Pirkle's alcohol)[50]. For instance the bottom trace of *Figure 37* displays four methyl lines, i.e. a pair of lines for each of the two diastereotopic methyl groups of 19.

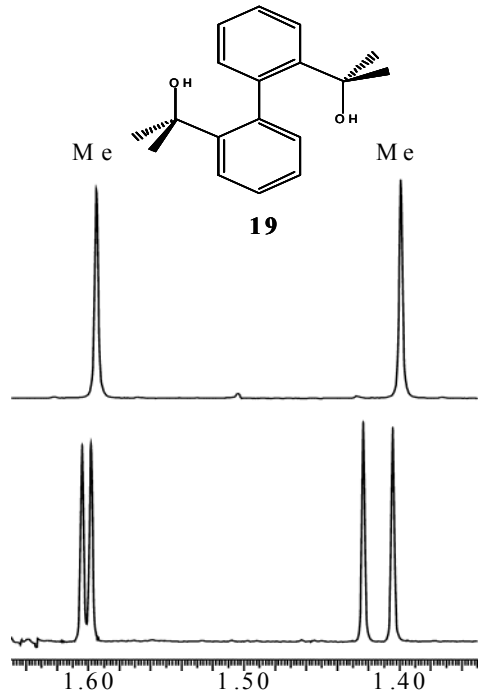

Figure 37: **Top: ambient temperature ^{1}H-NMR signals (600 MHz) of the diastereotopic methyl groups of *19*. Bottom: the same spectrum in a chiral environment, showing the line splitting due to the distinguishable *M* and *P* enantiomers.**

The observation that the NMR lines of the R groups appear anisochronous at any attainable high temperature, agrees with the results of calculations[15] predicting very high enantiomerisation barriers (for instance 38.2 kcal mol^{-1} in the case of **19**). This implies that these types of atropisomers are configurationally stable and indeed we were able to achieve a physical separation in the case of **19** by means of the enantioselective HPLC technique, with a Chiralcel OJ-H 250x4.6 mm column, at a flow rate of 1.0 mL/min, using

hexane/iPr_2O 85:15 v:v as eluent (*Figure 38*, a). The corresponding Electronic Circular Dicroism (CD)[53] spectra display the expected opposite phased traces (*Figure 38*, b).

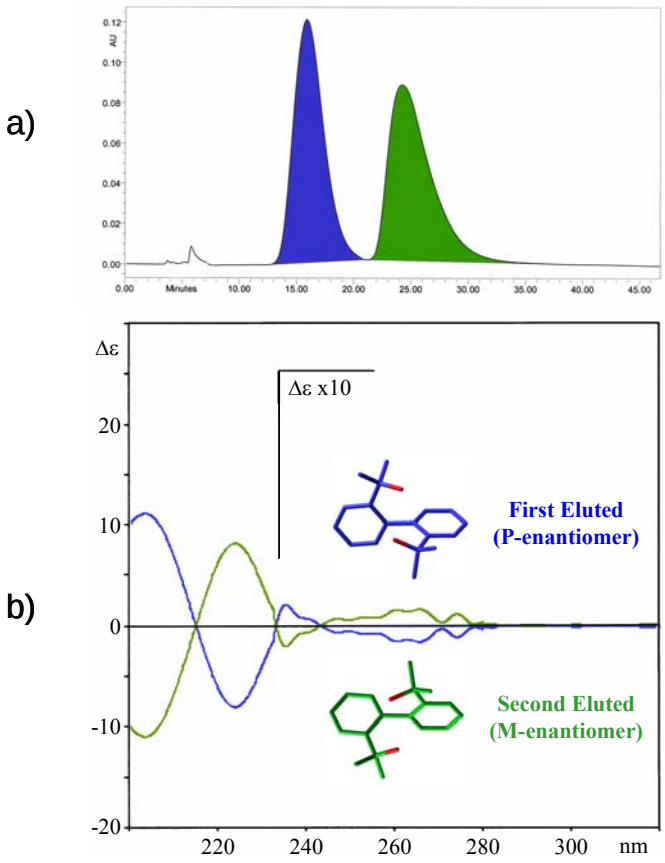

Figure 38:

a) Enantioselective HPLC separation of the enantiomers of compound *19*, obtained at 24°C. UV detection was fixed at 225 nm.

b) ECD spectra of the two enantiomers. The blue trace is that of the first eluted (absolute configuration P), the green trace is that of the second eluted (absolute configuration M).

Electronic circular dichroism is based on the fact that left and right circular polarized light is absorbed differently by chiral molecules. Therefore, two different extinction coefficients can be observed whose difference $\Delta\varepsilon = \varepsilon_l - \varepsilon_r$ is plotted in a CD spectrum.[51] Because this difference can become positive or negative, the absorption bands in a CD spectrum can also exhibit different signs. Compared to conventional UV/Vis

spectroscopy, this is an additional, useful spectral dimension, since it makes the CD technique more sensitive to geometric and electronic properties of the analyzed molecule.

The experimental CD and absorption spectra of the first eluted enantiomer of **19** are reported in *Figure 39*.

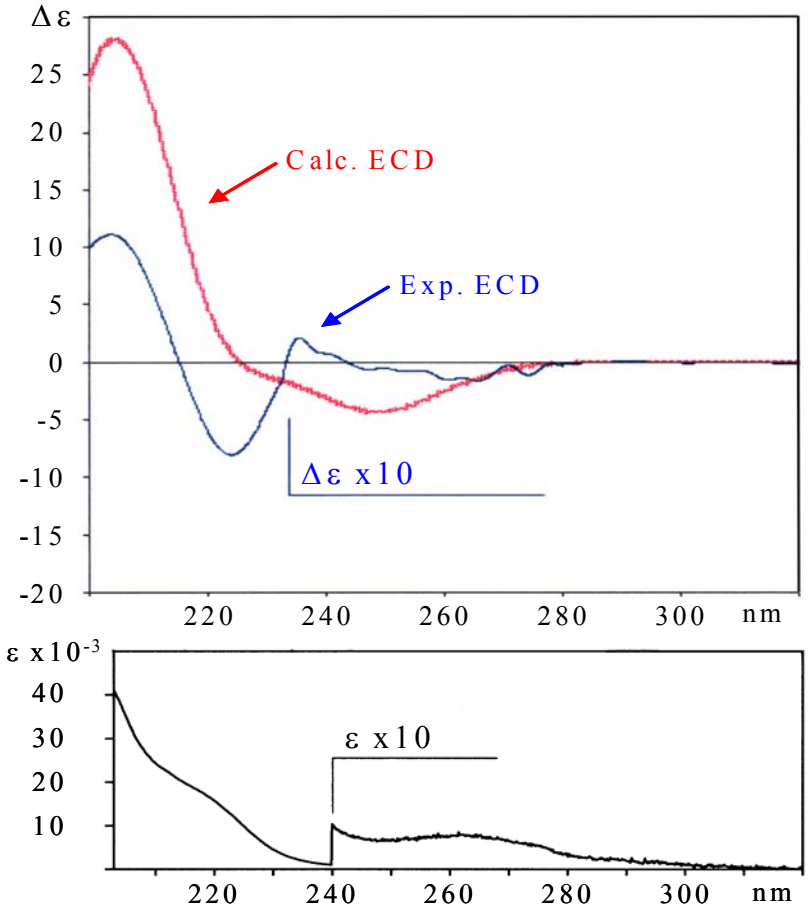

Figure 39: **Absorption (lower trace, black) and experimental CD (upper trace, blue) spectra in acetonitrile of the first eluted enantiomer of *19*. The red trace is the computed one.**

The absorption spectrum shows a weak ($\varepsilon \approx 200$) band centred around 265 nm, a clear shoulder 220 nm (with $\varepsilon \approx 12000$) followed by a monotonic increase of the absorption down to 200 nm where $\varepsilon \approx 40000$. These data are typical of a benzene chromophore[52] and very different from those of a conjugated biphenyl chromophore. This

confirms that in compound **19** the two benzene rings are completely non conjugated or, in other words, the dihedral angle defined by the two aromatic planes is of the order of 90°, in full agreement with the previous analysis based on the NMR behaviour. The CD spectrum shows very weak bands (of both the signs) in the range 280-250 nm, a weak positive ($\Delta\varepsilon$ = +0.15) band at 240 nm, followed by two Cotton effects at 222 nm ($\Delta\varepsilon$ = -7.8) and at 200 nm ($\Delta\varepsilon$ = +11), respectively.

In order to deduce the absolute configuration (AC) of the first eluted enantiomer of **19** we simulated by theoretical methods the experimental CD spectrum, assuming arbitrarily one of the two absolute configurations, and comparing the predicted result with that of the experiment.[53]

If the shape of the theoretical spectrum is comparable with the experimental one, the assumed AC should correspond to the true configuration: on the contrary, if the data are in an almost mirror age relationship, the true molecular AC is opposite to that assumed for the calculations.

To this aim exitation energies and dipole and rotational strengths for the optimized structure were calculated based on time-dependet DFT. The TD-DFT/B3LYP method (implemented in the Gaussian 03 program[15]), has been employed successfully several times[54] to simulate ECD spectra. The geometries of the three best structures have been already optimised at the B3LYP/6-31G(d) level, leading to the relative energies reported in *Scheme 6*.

The most stable conformer is characterized by a dihedral angle θ between the aromatic rings of about 90°, by intermolecular hydrogen bond between the two –OH groups and by the fact that the two methyl groups are placed far away, reducing completely the steric repulsions.

The most stable *sp*,*sp* conformer of **19**, according to DFT computations and to X-ray data, should be the only populated species (about 99%), therefore all the ECD calculations have been carried out solely for this structure.

The theoretical CD spectrum (red trace) for the *P* configuration of **19** is compared to the experimental spectrum (blue trace) in *Figure 39*.

The positions of the CD intensity maxima in the theoretical spectrum do not perfectly match those of the experimental spectrum and the predicted ECD intensities are in general larger than the experimental data. Nevertheless, the experimental spectrum shows a sequence of very weak negative, positive bands followed by a much stronger negative Cotton effect followed, in turn, by a positive CD band at about 205 nm. The same features are reproduced in the theoretical spectrum, in particular the sequence of the most intense negative/positive Cotton effects (we could not record a further negative CD band predicted below 200 nm). In conclusion, it is quite safe to state that the first eluted enantiomer of **19** possesses the absolute configuration *P* and thus the second eluted has the configuration *M*, as shown in *Figure 38*.

Also compounds 20 and 21, having ortho substituents R larger than those of 18, yield spectra exhibiting, respectively, diastereotopic ethyl and isopropyl groups at ambient temperature. Contrary to the case of 18 and 19 however, they do not display at low temperatures the signals attributable to the dimer, indicating that only the monomer is present (*Figure 40*).

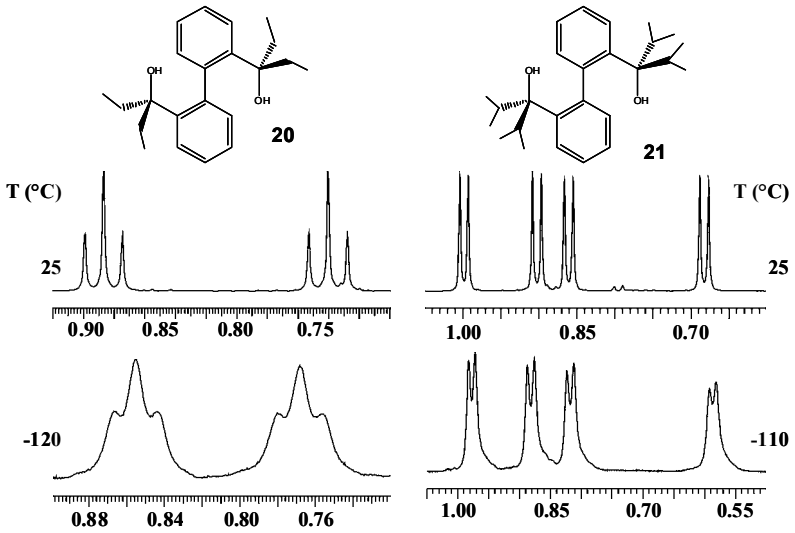

Figure 40: **Experimental methyl ^{1}H NMR signals of *20* and *21* (600 MHz in $CHF_2Cl/CHFCl_2$) as function of temperature.**

The larger dimensions of these compounds makes in fact too difficult to realize the close approach of the OH groups of two molecules, as required to produce a sufficiently stable dimer. According to calculations the most stable conformer in both 20 and 21 has the same type of *sp*,*sp* structure as that of the corresponding conformer of 19, due to the presence of the intramolecular hydrogen bond (*Figure 41, right*).

The single crystal X-ray structure of compound 21 shows the presence of the intramolecular H-bond, but it does not show the existence of any intermolecular H-bond (*Figure 41*, *left*), thus preventing the formation of a dimer, a feature in good agreement with the result of the NMR spectra. In derivative 21 the two isopropyl moieties are diastereotopic because of the chirality of the molecule (due to the highly hindered Ar-Ar rotation), so that the ^{1}H and ^{13}C signals of the corresponding CH moieties are anisochronous even at ambient temperature. Since these lines are already split, it is not possible to observe the splitting due to the restricted rotation of the isopropyl groups at low temperature, as it had been done in the case of 15 (*Figure 26*). In addition, the *sp*,*sp* conformation predicted by the theory turns out to be very close to that found by X-ray diffraction (*Figure 41*).

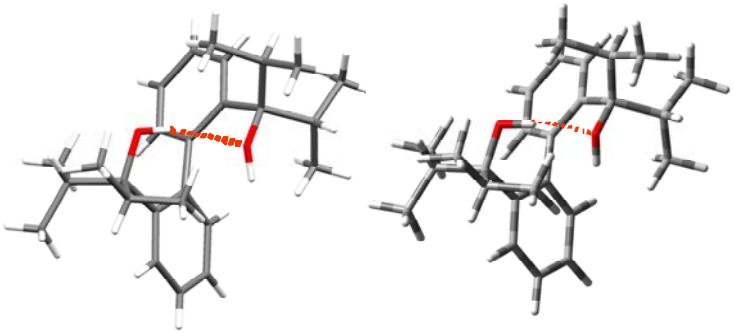

21-X-Ray **21-DFT**
Sp,sp (E=0.0 kcal mol^{-1})

Figure 41: **Left: Single crystal X-ray structure of compound *21* Right: DFT computed structure of its most stable conformer (*sp*,*sp*).**

2.2 Conclusions

Biphenyl derivatives bearing a single CR_2OH substituent in the ortho position exist as *sp* and *ap* conformers, due to the restricted rotation about the Ar-CR_2OH bond. Introduction of the prochiral *i*-Pr group in the position 3' allowed the determination of the enantiomerisation barrier due to the Ar-Ar bond rotation. DFT computations of the barriers and on the relative stability of the two conformational isomers were all in agreement with the experiments.

Biphenyls bearing two CR_2OH groups in the 2,2' positions were found to exist as configurationally stable enantiomers: when R=Me (**19**) they were separated by enantioselective HPLC and the absolute configuration assigned on the basis of simulation of the corresponding CD spectra.

Compounds **18** (R = H) and **19** (R= Me) were found to originate dimers in solution, due to intermolecular H-bond interactions. In the case of **19**, the free energy of activation (9.5 kcal mol^{-1}) for the exchange of the monomers with the dimer could be measured by dynamic NMR. The conformational preferences, predicted by computations, were confirmed by X-ray diffraction in the case of R = H (**18**), R = Me (19) and R = *i*-Pr (**21**).

2.3 Experimental Section

2.3.1 2,2'-Dibromobiphenyl[55] was prepared according to the literature.

2-bromobiphenyl and **2,2'biphenyl-dimethanol** (**18**) were commercially available. Compound **18** was further purified by semi-preparative HPLC on a C18 column (5μm, 250x10 mm, 5 ml/min, ACN/H_2O 80:20 v:v RT = 5.22 min), crystals suitable for X-ray diffraction were obtained from hexane.

Crystal Data

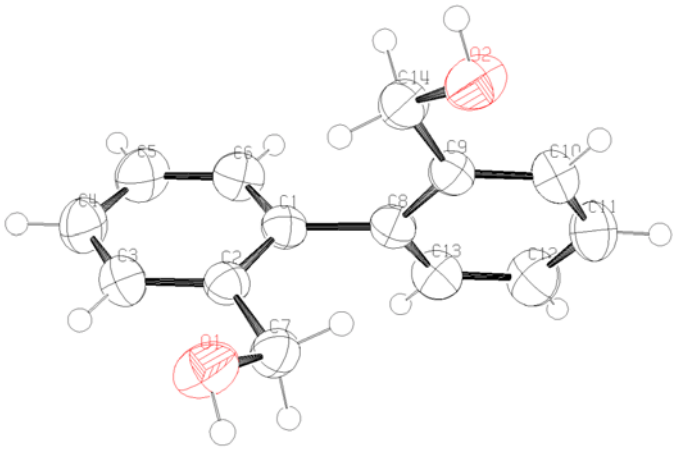

Crystals obtained from hexane, molecular formula: $C_{14}H_{14}O_2$, M_r = 214.25, monoclinic, space group $P2_1/n$ (No. 14), a = 12.7902(10), b = 5.0003(4), c = 18.5981(14) Å, β = 109.2360(10), V = 1122.85(15) Å^3, T = 298(2) K, Z = 4, ρ_c = 1.267 g cm^{-3}, F(000) = 456, graphite-monochromated $Mo_{K\alpha}$ radiation (λ = 0.71073 Å), $\mu(Mo_{K\alpha})$ = 0.084 mm^{-1}, colourless needle (0.5 × 0.2 × 0.2 mm^3), empirical absorption correction with SADABS (transmission factors: 0.9835 – 0.9594), 2400 frames, exposure time 10 s, $1.70 \leq \theta \leq 28.73$, $-16 \leq h \leq 16$, $-6 \leq k \leq 6$, $-24 \leq l \leq 24$, 12247 reflections collected, 2737 independent reflections (R_{int} = 0.0181), solution by direct methods (SHELXS97[32]) and subsequent Fourier syntheses, full-matrix least-squares on F_o^2 (SHELX97[32]), hydrogen atoms refined with a riding model except for the two hydroxyl hydrogens, that were experimentally located, data / restraints / parameters = 2737 / 0 / 154, $S(F^2)$ = 1.105, $R(F)$ = 0.0509 and $wR(F^2)$ = 0.1291 on all data, $R(F)$ = 0.0421 and $wR(F^2)$ = 0.1240 for 2194 reflections with $I > 2\sigma(I)$, weighting scheme $w = 1/[\sigma^2(F_o^2) + (0.0701P)^2 + 0.1224P]$ where $P = (F_o^2 + 2F_c^2)/3$, largest difference peak and hole 0.251 and –0.202 e Å^{-3}.

2.3.2 General Procedure for 13-15

A solution of 2-lithiumbiphenyl was prepared in 1 hour by addition of 6.3 mL of n-butyllithium (10 mmol, 1.6 M in hexane) to a stirred solution of 1.08 g of 2-bromobiphenyl (10 mmol in 40 mL of anhydrous THF) kept at –78°C. To the solution was then slowly added a solution of the appropriate ketone (aceton, diethylketone, di-isopropyl ketone, 8

mmol in 30 ml of anhydrous THF). After 1 hour at -78°, the mixture was warmed to ambient temperature and quenched with aqueous NH_4Cl. The extracted organic layer (Et_2O) was dried (Na_2SO_4) and evaporated, and the crude was purified by chromatography on silica gel (Hexane/Et_2O 10:1) to obtain compounds **1-3**. Analytically pure samples were obtained by semi-preparative HPLC on a C18 column (5μm, 250x10 mm, 5 ml/min, ACN/H_2O 70:30 v:v for **13**-**14** and 80:20 v:v for **15**).

2-(biphenyl-2-yl)propan-2-ol (13) ^{1}H-NMR (600 MHz, $CDCl_3$, 25°C, TMS): δ 1.47 (6H, s), 7.07 (1H, dd, J = 7.5, 1.6 Hz), 7.24 (1H, td, J = 7.5, 1.4 Hz), 7.30-7.40 (6H, m), 7.63 (1H, dd, J = 8.1, 1.4 Hz). ^{13}C-NMR (150.8 MHz, $CDCl_3$, 25°C, TMS): δ 32.6 (CH_3), 74.0 (q), 125.8 (CH), 126.0 (CH), 127.0 (CH), 127.4 (CH), 127.8 (CH), 129.5 (CH), 132.1 (CH), 139.9 (q), 143.0 (q), 146.1 (q). HRMS(EI): m/z calcd for $C_{15}H_{16}O$: 212.12011; found 212.1204. HPLC: RT = 6.99 min.

2-(biphenyl-2-yl)propan-2-ol (14) ^{1}H-NMR (600 MHz, $CDCl_3$, 25°C, TMS): δ 0.73 (6H, t, J= 7.4 Hz), 1.57 (1H, s, OH), 7.07 (1H, dd, J = 7.5, 1.6 Hz), 7.24 (1H, td, J = 7.5, 1.4 Hz), 7.30-7.40 (6H, m), 7.63 (1H, dd, J = 8.1, 1.4 Hz). ^{13}C-NMR (150.8 MHz, $CDCl_3$, 25°C, TMS): δ 32.6 (CH_3), 74.0 (q), 125.8 (CH), 126.0 (CH), 127.0 (CH), 127.4 (CH), 127.8 (CH), 129.5 (CH), 132.1 (CH), 139.9 (q), 143.0 (q), 146.1 (q). HRMS(EI): m/z calcd for $C_{17}H_{20}O$: 240.15141; found 240.1518. HPLC: RT = 12.76 min.

3-(biphenyl-2-yl)-2,4-dimethylpentan-3-ol (15) ^{1}H-NMR (600 MHz, $CDCl_3$, 25°C, TMS): δ 0.78 (6H, d, J = 7.0 Hz), 0.87 (6H, d, J = 6.8 Hz), 1.53 (1H, s, OH), 2.19 (1H, septet, J = 6.9 Hz), 6.99 (1H, dd, J = 7.7, 1.6 Hz), 7.17 (1H, td, J = 7.4, 1.5 Hz), 7.24-7.35 (6H, m). ^{13}C-NMR (150.8 MHz, $CDCl_3$, 25°C, TMS): δ 16.9 (CH_3), 18.1 (CH_3), 35.7 (CH), 84,24 (q), 125.1 (CH), 126.4 (CH), 126.6 (CH), 126.8 (CH), 127.5 (2CH), 128.6

(2CH), 132.3 (CH), 140.8 (q), 141.4 (q), 144.8 (q). HRMS(EI): m/z calcd for $C_{19}H_{24}O$: 268.18271; found 240.1826. HPLC: RT = 20.4min.

2.3.3 2-(3'-isopropylbiphenyl-2-yl)propan-2-ol (16).

A solution of Me-Li (5 mmol, 1.5M in Et2O) was slowly added to a solution of 1-(3'-isopropylbiphenyl-2-yl)ethanone[56] (2 mmol in THF), kept at -78°C. After 1 hour at -78°, the mixture was warmed to ambient temperature and quenched with aqueous NH_4Cl. The extracted organic layer (Et_2O) was dried (Na_2SO_4) and evaporated, and the crude was purified by chromatography on silica gel (Hexane/Et_2O 10:1). to obtain compound **16**. Analytically pure samples were obtained by semi-preparative HPLC on a C18 column (5μm, 250x10 mm, 5 ml/min, ACN/H_2O 80:20 v:v)

2-(3'-isopropylbiphenyl-2-yl)propan-2-ol (16). ^{1}H-NMR (600 MHz, $CDCl_3$, 25°C, TMS): δ 1.26 (6H, d, J = 7.0 Hz), 1.46 (6H, s), 1.89 (1H, s, OH), 2.93 (1H, septet, J = 7.9 Hz), 7.09 (1H, dd, J = 7.5, 1.5 Hz), 7.14 (1H, ddd, J = 7.4, 1.7, 1.2 Hz), 7.18 (t, 1H, J=1.8 Hz), 7.21(1H, d, J = 7.7 Hz) , 7.24 (1H, td, J = 7.4, 1.4 Hz), 7.31 (t, 1H, J = 7.6 Hz), 7.34 (1H, ddd, J = 8.0, 7.4, 1.5 Hz), 7.63 (1H, dd, J = 8.0, 1.3 Hz). ^{13}C-NMR (150.8 MHz, $CDCl_3$, 25°C, TMS): δ 23.9 (CH_3), 32.5 (CH_3), 34.0 (CH), 74,0 (q), 125.3 (CH), 125.8 (CH), 126.0 (CH), 127.0 (CH), 127.3 (CH), 127.7 (CH), 127.8 (CH), 132.0 (CH), 140.2 (q), 143.5 (q), 146.2 (q), 148.5 (q). HRMS(EI): m/z calcd for $C_{18}H_{22}O$: 254.16706; found 254.1671. HPLC: RT = 8.90 min.

2.3.4 2-(2'-methylbiphenyl-2-yl)propan-2-ol (17).

A solution of (2'-bromobiphenyl-2-yl)lithium was prepared in 1 hour by addition of 6.5 mL of n-butyllithium (10,4 mmol, 1.6 M in hexane) to a stirred solution of 3.12 g of 2,2'-dibromobiphenyl (10 mmol in 40 mL of anhydrous THF) kept at –78°C. To this solution was then slowly added a solution of Me-I (2.84 g, 20 mmol in 10 ml of anhydrous THF). After 1 hour at -78°, the mixture was warmed to ambient temperature and quenched

with aqueous NH_4Cl. The formation of 2-bromo-2'-methylbiphenyl was checked by GC-MS (m/z 246). The extracted organic layer (Et_2O) was then dried (Na_2SO_4) and evaporated. To a cooled (-78°C) solution of the crude (2.2g, about 9 mmol in 40 mL of THF), was then added 6.5 mL of n-butyllithium (10,4 mmol, 1.6 M in hexane) and, after 1 hour, a solution of acetone (1.16 g, 20 mmol in 5 ml of THF). After 1 hour at -78°, the mixture was warmed to ambient temperature and quenched with aqueous NH_4Cl. The extracted organic layer (Et_2O) was dried (Na_2SO_4) and evaporated, and the crude was purified by chromatography on silica gel (Hexane/Et_2O 10:1) to obtain compound **17**. Analytically pure samples were obtained by semi-preparative HPLC on a C18 column (5μm, 250x10 mm, 5 ml/min, ACN/H_2O 80:20 v:v).

2-(2'-methylbiphenyl-2-yl)propan-2-ol (17). ^{1}H-NMR (600 MHz, $CDCl_3$, 25°C, TMS): δ 1.41 (3H, s), 1.49 (3H, s), 1.78 (1H, s, OH), 2.07 (3H, s), 6.98 (1H, d, J = 7.5 Hz), 7.17-7.28 (5H, m), 7.34 (t, 1H, J = 7.8 Hz), 7.61 (1H, dd, J = 8.0, 1.2 Hz). ^{13}C-NMR (150.8 MHz, $CDCl_3$, 25°C, TMS): δ 20.7 (CH_3), 31.8 (CH_3), 32.4 (CH), 74,1 (q), 125.1 (CH), 126.1 (CH), 126.3 (CH), 127.3 (CH), 127.5 (CH), 129.5 (CH), 130.1 (CH), 131.5 (CH), 136.6 (q), 138.6 (q), 142.8 (q), 146.0 (q). HRMS(EI): m/z calcd for $C_{16}H_{18}O$: 226.13576; found 226.1352. HPLC: RT = 6.24min.

2.3.5 General Procedure for 19-21

A solution of the 2,2'-dilithiobiphenyl was prepared in 1 hour by addition of 14.0 mL of n-butyllithium (22,4 mmol, 1.6 M in hexane) to a stirred solution of 3.12 g of 2,2'-dibromobiphenyl. (10 mmol in 40 mL of anhydrous THF) kept at –78 °C. To this solution was then slowly added a solution of the appropriate electrofile (acetone, diethylketone or di-isopropyl ketone, 30 mmol in 10 ml of anhydrous THF). After 1 hour at -78 °C, the mixture was warmed to ambient temperature and quenched with aqueous NH_4Cl. The extracted organic layer (Et_2O) was dried (Na_2SO_4) and evaporated, and the crude was purified by chromatography on silica gel (Hexane/Et_2O 10:1). to obtain compounds **19-21**.

Analytically pure samples were obtained by semi-preparative HPLC on a C18 column (5µm, 250x10 mm, 5 ml/min, ACN/H_2O 80:20 v:v for **19** and 90:10 v:v for **20-21**). Crystals suitable for X-ray diffraction were obtained by slow evaporation in the case of **19** (from toluene) and **21** (from acetonitrile).

2,2'-(biphenyl-2,2'-diyl)dipropan-2-ol (19). ^{1}H-NMR (600 MHz, $CDCl_3$, 25°C, TMS): δ 1.44 (6H, s), 1.63 (6H, s), 2.92 (2H, s, OH), 7.02 (2H, dd, J = 7.6, 1.5 Hz), 7.20 (td, 2H, J = 7.5, 1.4 Hz), 7.30 (1H, ddd, J = 8.1, 7.4, 1.5 Hz), 7.44 (2H, dd, J = 8.1, 1.4 Hz). ^{13}C-NMR (150.8 MHz, $CDCl_3$, 25°C, TMS): δ 31.9 (CH_3), 33.4 (CH_3), 74.5 (q), 125.7 (CH), 126.3 (CH), 127.2 (CH), 131.5 (CH), 141.0 (q), 145.2 (q). HRMS(EI): m/z calcd for $C_{18}H_{22}O_2$: 270.16198; found 270.1622. HPLC: RT = 10.61 min.

Crystal Data

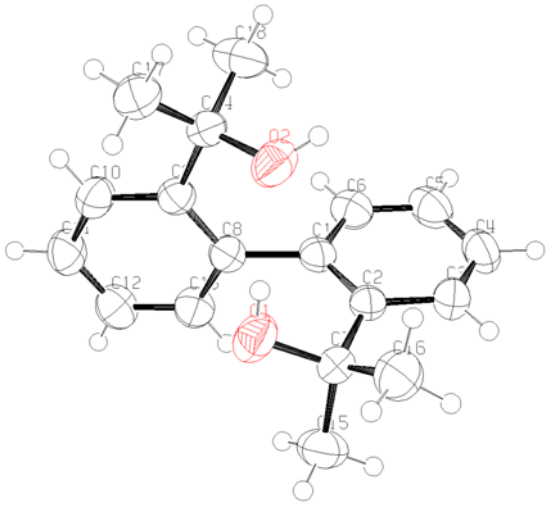

Crystals obtained from toluene, molecular formula: $C_{18}H_{22}O_2$, M_r = 270.36, triclinic, space group P-1 (No. 2), a = 8.9963(13), b = 9.9418(14), c = 10.2139(14) Å, α = 118.0260(10), β = 94.944(2), γ = 101.472(2), V = 769.52(19) Å^3, T = 298(2) K, Z = 2, ρ_c = 1.167 g cm^{-3}, F(000) = 292, graphite-monochromated $Mo_{K\alpha}$ radiation (λ = 0.71073 Å), µ($Mo_{K\alpha}$) = 0.074 mm^{-1}, colourless brick (0.4 × 0.2 × 0.1 mm^3), empirical absorption

correction with SADABS (transmission factors: 0.9926 – 0.9709), 2400 frames, exposure time 20 s, $2.32 \leq \theta \leq 25.00$, $-10 \leq h \leq 10$, $-11 \leq k \leq 11$, $-12 \leq l \leq 12$, 7332 reflections collected, 2701 independent reflections (R_{int} = 0.0156), solution by direct methods (SHELXS97[32]) and subsequent Fourier syntheses, full-matrix least-squares on F_o^2 (SHELX97[32]), hydrogen atoms refined with a riding model, data / restraints / parameters = 2701 / 0 / 185, $S(F^2)$ = 1.121, $R(F)$ = 0.0484 and $wR(F^2)$ = 0.1306 on all data, $R(F)$ = 0.0413 and $wR(F^2)$ = 0.1260 for 2296 reflections with $I > 2\sigma(I)$, weighting scheme $w = 1/[\sigma^2(F_o^2) + (0.0719P)^2 + 0.1103P]$ where $P = (F_o^2 + 2F_c^2)/3$, largest difference peak and hole 0.223 and –0.331 e Å^{-3}.

3,3'-(biphenyl-2,2'-diyl)dipentan-3-ol (20) ^{1}H-NMR (600 MHz, $CDCl_3$, 25°C, TMS): δ 0.74 (6H, t, J = 7.6 Hz), 0.89 (6H, t, J=7.4 Hz), 1.64-1.78 (3H, m), 2.11(1H, dq, J = 14.6, 7.4 Hz), 2.76 (2H, s, OH), 6.96 (2H, dd, J = 7.5, 1.5 Hz), 7.18 (td, 2H, J = 7.4, 1.4 Hz), 7.20 (2H, dd, J = 8.1, 1.4 Hz), 7.27 (1H, ddd, J = 8.1, 7.2, 1.5 Hz),. ^{13}C-NMR (150.8 MHz, $CDCl_3$, 25°C, TMS): δ 7.8 (CH_3), 8.9 (CH_3), 31.9 (CH_2), 36.48 (CH2), 79.6 (q), 125.3 (CH), 126.4 (CH), 127.8 (CH), 131.9 (CH), 141.6 (q), 142.4 (q). HRMS(EI): m/z calcd for $C_{22}H_{28}O_1$ (M^{+} - H_2O): 308.21401; found 308.2144. HPLC: RT = 20.78 min.

3,3'-(biphenyl-2,2'-diyl)bis(2,4-dimethylpentan-3-ol) (21). ^{1}H-NMR (600 MHz, $CDCl_3$, 25°C, TMS): δ 0.68 (6H, d, J = 6.7 Hz), 0.86 (6H, d, J = 7.0 Hz), 0.90 (6H, d, J = 7.0 Hz), 1.00 (6H, d, J = 6.5 Hz), 2.02 (2H, septet, J = 7.0 Hz), 2.61 (2H, septet, J = 6.7 Hz), 2.62 (2H, s, OH), 7.01 (2H, dd, J = 7.7, 1.5 Hz), 7.13 (2H, ddd, J = 7.7, 6.7, 1.5 Hz), 7.20 (2H, dd, J = 8.1, 1.8 Hz), 7.23 (2H, ddd, J = 8.1, 6.7, 1.5 Hz). ^{13}C-NMR (150.8 MHz, $CDCl_3$, 25°C, TMS): δ 16.5 (CH_3), 18.2 (CH_3),), 18.8 (CH_3), 19.4 (CH_3), 33.7 (CH), 37.0 (CH), 83.58 (q), 124.5 (CH), 125.5 (CH), 127.6 (CH), 135.0 (CH), 140.8 (q), 143.8 (q). HRMS(EI): m/z calcd for $C_{26}H_{38}O_2$: 382.28718; found 382.2873. HPLC: RT = 19.25min.

Crystal Data

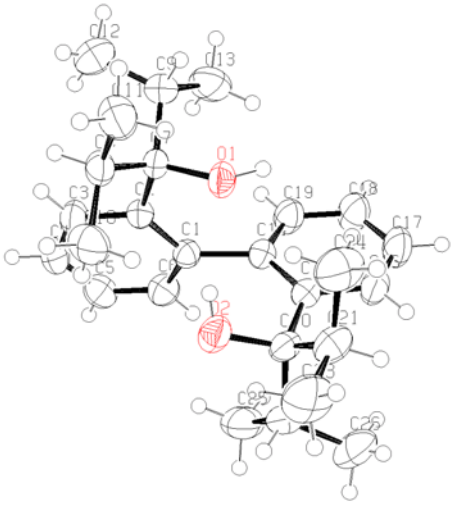

Crystals obtained from acetonitrile, molecular formula: $C_{26}H_{38}O_2$, M_r = 382.56, monoclinic, space group $P2_1/n$ (No. 14), a = 9.0332(9), b = 23.745(2), c = 11.0309(11) Å, β = 103.9570(10), V = 2296.2(4) Å^3, T = 298(2) K, Z = 4, ρ_c = 1.107 g cm^{-3}, $F(000)$ = 840, graphite-monochromated $Mo_{K\alpha}$ radiation (λ = 0.71073 Å), $\mu(Mo_{K\alpha})$ = 0.068 mm^{-1}, colourless brick (0.8 × 0.3 × 0.3 mm^3), empirical absorption correction with SADABS (transmission factors: 0.9800 – 0.9479), 2400 frames, exposure time 10 s, $1.72 \leq \theta \leq 27.50$, $-11 \leq h \leq 11$, $-30 \leq k \leq 30$, $-14 \leq l \leq 14$, 25552 reflections collected, 5256 independent reflections (R_{int} = 0.0281), solution by direct methods (SHELXS97[32]) and subsequent Fourier syntheses, full-matrix least-squares on F_o^2 (SHELX97[32]), hydrogen atoms refined with a riding model except for the two hydroxyl hydrogens, that were experimentally located, data / restraints / parameters = 5256 / 0 / 270, $S(F^2)$ = 1.729, $R(F)$ = 0.0555 and $wR(F^2)$ = 0.1699 on all data, $R(F)$ = 0.0484 and $wR(F^2)$ = 0.1639 for 4452 reflections with $I > 2\sigma(I)$, weighting scheme $w = 1/[\sigma^2(F_o^2) + (0.0768P)^2 + 0.0000P]$ where $P = (F_o^2 + 2F_c^2)/3$, largest difference peak and hole 0.282 and –0.189 e Å^{-3}.

2.4 NMR Spectroscopy

The spectra were recorded at 400 and 600 MHz for ^{1}H and 100.6 and 150.8 MHz for ^{13}C. The assignments of the ^{13}C signals were obtained by bi-dimensional experiments (edited-gHSQC[33] and gHMBC[34] sequences). The samples for obtaining spectra at temperatures lower than –100 °C were prepared by connecting to a vacuum line the NMR tubes containing the compound and a little amount of C_6D_6 (for locking purpose), and condensing therein the gaseous CHF_2Cl and $CHFCl_2$ (4:1 v/v) under cooling with liquid nitrogen. The tubes were subsequently sealed in vacuo and introduced into the precooled probe of the spectrometer. The temperatures were calibrated by substituting the sample with a Cu/Ni thermocouple before the measurements. Low temperature ^{13}C spectra were acquired with a 5 mm dual probe, without spinning, with a sweep width of 38000 Hz, a pulse width of 4.9 μs (70° tip angle), and a delay time of 2.0 s. Proton decoupling was achieved with the standard Waltz-16 sequence. A line broadening function of 1-5 Hz was applied to the FIDs before Fourier transformation. Usually 512 to 1024 scans were acquired. The line shape simulations were performed by means of a PC version of the QCPE program DNMR 6 n° 633, Indiana University, Bloomington, IN. The NOE experiments were obtained by means of the DPFGSE-NOE[57] sequence. To selectively irradiate the desired signal, a 50 Hz wide shaped pulse was calculated with a refocusing-SNOB shape[58] and a pulse width of 37 ms. DOSY experiments were obtained in toluene-d_8 at +22°C by means of the BPLED pulse sequence[59] with a delay diffusion of 0.020 and 0.025 s. Gradient strength was varied from 0.4 to 66 g/cm. Gradient calibration was obtained on a HDO/D_2O sample, for which the diffusion coefficient was known[60] ($19.2 \cdot 10^{-10}$ m^2s^{-1}). The diffusion coefficient D was obtained from the Stejskal-Tanner equation, and the hydrodynamic radius was evaluated by the Stokes-Einstein equation, using a viscosity value for toluene[61] equal to 0.575 mPa·s.

2.5 Calculations

Computations were carried out at the B3LYP/6-31G(d) level by means of the Gaussian 03 series of programs[15]: the standard Berny algorithm in redundant internal coordinates and default criteria of convergence were employed. The reported energy values are not ZPE corrected. Harmonic vibrational frequencies were calculated for all the stationary points. For each optimized ground state the frequency analysis showed the absence of imaginary frequencies, whereas each transition state showed a single imaginary frequency. Visual inspection of the corresponding normal mode was used to confirm that the correct transition state had been found. NMR chemical shift calculation were obtained with the GIAO method at the Pw1Pw91/6-311+G(2d,p)//B3LYP/6-31G(d) level. TMS, calculated at the same level of theory, was used as reference to scale the absolute shielding value.

Chapter 3

3.1 1,8-Di-arylbiphenylenes: Steric Barriers and Unprecedented Detection of the Enantiomerisation π-Barriers

When equal aryl substituents, lacking a local C_2-aymmetry axis, are bonded in appropriate positions of planar frameworks (such as benzene,[62,37a,b] naphthalene,[63] phenanthrene,[64] anthracene,[65] acenaphthene,[66] acenaphthylene[67]), configurationally stable cis/trans isomers, or stereolabile *syn*/*anti* conformers, are originated, depending on the extent of the steric hindrance. In the case of 1,8-di-o-tolylnaphthalene[63a], the existence of cis and trans isomers is the consequence of the planes of the two tolyl substituents being twisted with respect to the plane of naphthalene, so that one methyl can stay either on the same or on the opposite side of the other methyl group. The trans to cis interconversion requires the passage through a transition state where one tolyl is coplanar with the naphthalene ring (steric barrier[68]), corresponding to a 180° rotation.[63a] It was also pointed out[63a] that the twisted disposition of the two tolyl substituents would make the cis form to originate a pair of enantiomers, that interconvert through a transition state where the tolyl groups are nearly orthogonal to the naphthalene ring (π-barrier[68]): this process corresponds to a torsion (also called flipping process[63a]) of approximately 90°. In the case of the trans form, on the other hand, this nearly 90° torsion would create two conformers of different stability, identified as *anti-in* and *anti-out*. This because the two methyl groups are directed either inward or outward with respect to the naphthalene moiety (*Scheme 7*).[63a]

Scheme 7

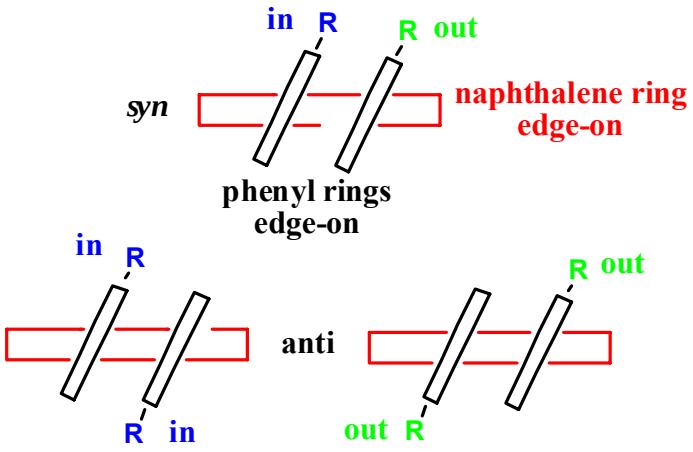

Each of these conformers too exists as a pair of enantiomers, but their enantiomerisation requires the passage through the cis isomer, i.e. the 180° rotation involving the steric barrier.

Whereas there are many reports[63-68] concerning the determination of cis/trans (or *syn*/*anti*) interconversion involving the steric barrier, the so called π-barrier has not been detected in this type of compounds. This is due to the fact that such enantiomerisation barrier is expected to be very low,[37a,63a] thus usually not amenable to NMR observation.

For this purpose a number of aryl moieties bearing, in the meta or ortho positions, alkyl groups of various sizes in the 1,8 positions of biphenylene are prepared (*Scheme 8*).

DFT computations[15] (at the B3LYP/6-31G(d) level) of 1,8-di-m-tolylbiphenylene (compound **22**) show that there are three energy minima,[69] corresponding to the mentioned *anti-in*, *syn* and *anti-out* conformations. The computed ground state energy for the *anti-in* is 0.4 kcal mol^{-1} lower than that of the *syn*, and 0.7_5 kcal mol^{-1} lower than that of the *anti-out* (*Figure 42*). According to the DFT energies the *anti-in* should be therefore the most stable and the *anti-out* the least stable conformer.

The greater stability of the *anti-syn* conformer might be due to the so-called CH/π interactions[70] that are possible in the *anti-syn* but not in the *anti-out*.

Scheme 8

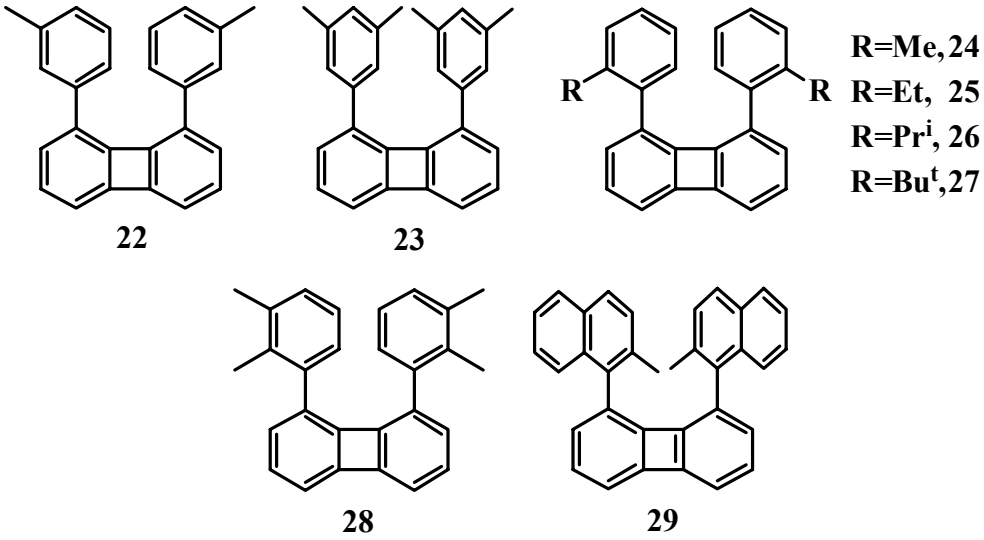

Also, the *anti-out* might be destabilized by the H/H repulsion between the methyl groups and the hydrogen protruding from the biphenylene ring, situation which does not occur in the *anti-syn* conformer;[71] the *syn* conformer have an intermediate stability.

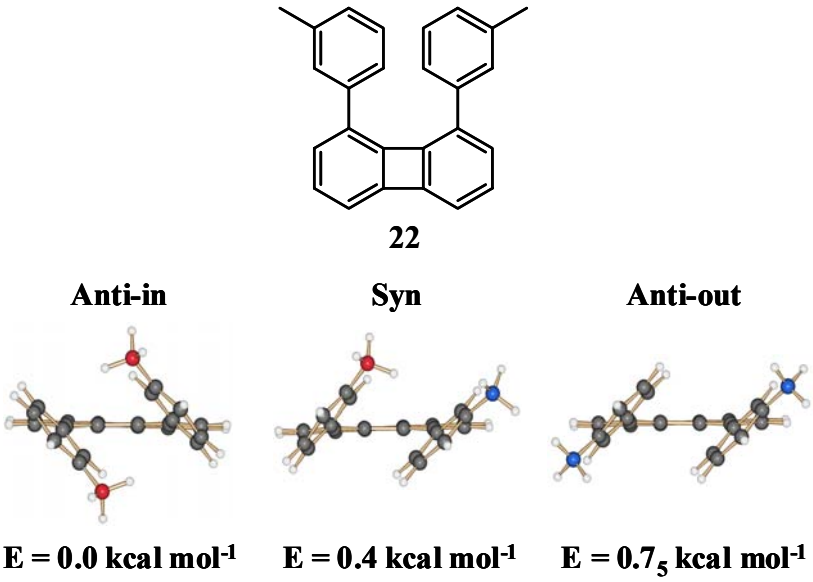

Figure 42: **DFT computed structures of the three possible conformers of *22*, having dihedral angles of 44° between the planes of toluene and biphenylene (only one of the two enantiomers is displayed for convenience).**

As mentioned above, these conformers interconvert according to the circuit displayed in *Figure 43*. Within each of the two *anti* conformers, the hydrogens and carbons of one tolyl would always display NMR signals coincident (isochronous) with those of the other tolyl group, owing to the C_2 symmetry of these forms. In the *syn* conformer, on the other hand, these signals will be coincident only if the enantiomerisation process (occurring via the 90° torsion involving the π-barrier) is fast.

When this process is frozen, the signals of one tolyl group of the *syn* will be different (anisochronous) with respect to those of the other, due to the C_1 symmetry: at the same time, distinct signals with different intensities should become observable for the *anti-in* and the *anti-out* conformers (*Figure 43*).

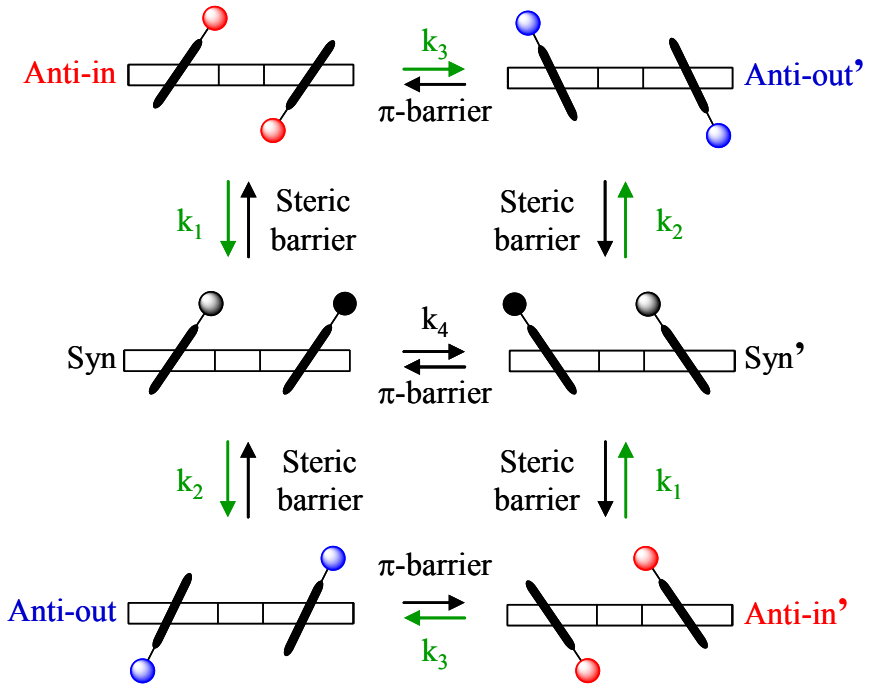

Figure 43: **Representation of the Conformers, Enantiomers and Equilibrium Processes for Compound *22*. The circles represent the methyl: within each form they have the same colours when enantiotopic (conformers *anti*) and different colours when diastereotopic (conformer *syn*). The primes indicate enantiomeric structures.**

The steric barrier computed[15] for the *anti-in* to *syn* interconversion is 6.3_5 kcal mol^{-1} and that for the *syn* to *anti-out* interconversion is 5.9_5 kcal mol^{-1}, the difference being equal to the computed energy separation between the two corresponding ground states (i.e., 0.4 kcal mol^{-1} as in *Figure 42*). In *Figure 45* only one of the two possible transition states for the 180° rotation pathway (steric barrier) is reported, i.e. the one in which the tolyl plane, coplanar with that of biphenylene, places its methyl group opposite to the other tolyl (see TS-1 in *Figure 44*). In fact, the pathway for the alternative transition state, having the methyl on the same side of the other tolyl (see: TS-1' in *Figure 44*), has a higher energy (7.25 vs. 6.35 kcal mol^{-1}) and therefore can be considered as "forbidden". In the allowed pathway only one of the two tolyl rings becomes, alternatively, coplanar with biphenylene, whereas the other remains close to its original position: the rotation processes of the tolyl substituents are thus independent of each other. The computed π-barrier for the exchange between the two enantiomers of *syn*, and that for the interconversion of the *anti-in* into the *anti-out* conformer, are 3.5 and 4.0 kcal mol^{-1}, respectively. The energy of the transition state for the enantiomerisation (*syn* to *syn'* interconversion, i.e. 90° torsion *via* π-barrier) is not necessarily equal to that for the interconversion of the two *anti* conformers: two different transition states thus imply two different π-barriers, as predicted by calculations (*Table 5, Figure 44* and *Figure 45*).

The pathways for the 90° torsion (π-barriers) take place through transition states where both the tolyl rings move away simultaneously from their original positions, reaching dispositions where both are tilted by the same dihedral angle with respect to biphenylene, (see: TS-2 and TS-3 of *Figure 44*). The corresponding single imaginary normal modes involve the movement of both *m*-tolyl rings; accordingly, the 90° torsion processes should be considered examples of correlated motions. As a further indication, it should be pointed out the computations show that situations where *only one* of the two tolyl groups has moved across to the nearly orthogonal position do not correspond to transition states.

The corresponding computed transition states are shown in *Figure 44*.

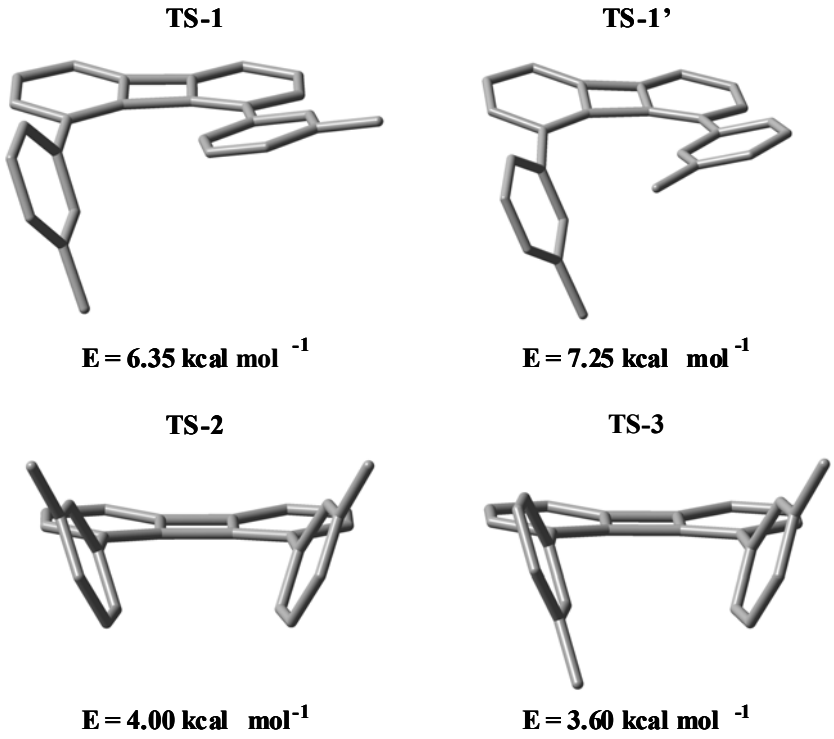

Figure 44: **DFT computed transition states of compound 22 (B3LYP/6-31G(d) level).**
Top: the two possible transition states (TS-1 and TS-1') computed for the 180° rotation pathway (steric barrier).
Bottom: TS-2 and TS-3 transition states for the two 90° torsion pathways (π-barriers).

Transition state TS-1' has an energy greater than TS-1, thus the latter (allowed) corresponds to the pathway actually followed by the 180° rotation (see *Figure 45*). Such a 180° rotation cannot take place through the higher energy TS-1' state (forbidden). Transition state TS-2 corresponds to the *anti-in* to *anti-out* interconversion (π-*anti* of *Figure 45* and *Table 5*), and TS-3 corresponds to the *syn* to *syn* enantiomerisation (π-*syn* of *Figure 45* and *Table 5*).

On this basis one should first observe separate NMR methyl signals at low temperature for the *syn* (in rapid exchange between the two enantiomeric forms) and for

the *anti* conformers (in rapid exchange between the *anti-in* and *anti-out*). On further lowering the temperature one should then identify a pair of signals (with equal intensity) for the *syn*, and single signals (with different intensity) for the *anti-in* and *anti-out* conformers (see the pathway displayed in *Figure 45).*

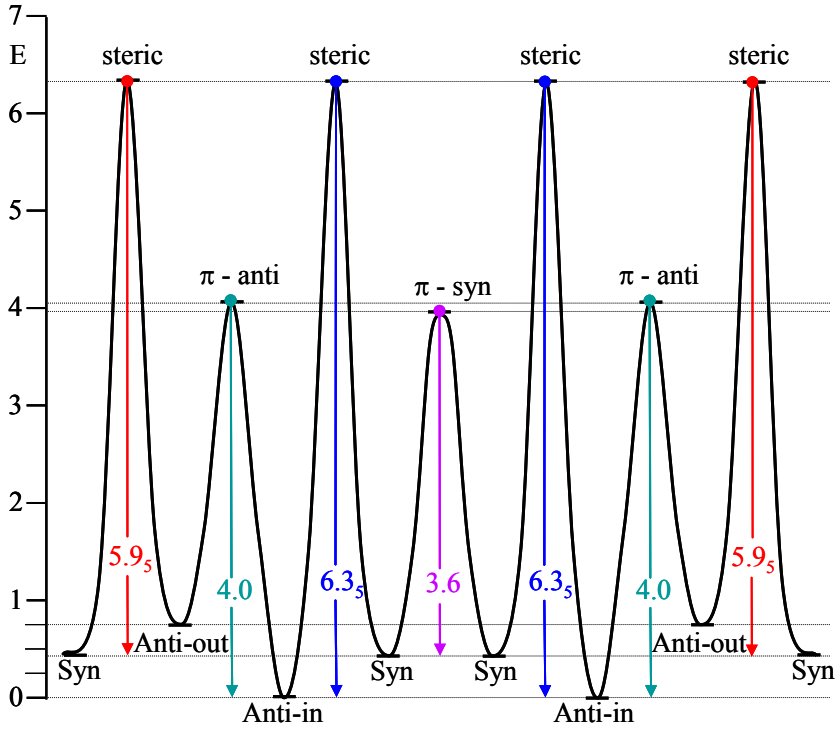

Figure 45: **DFT Computed Energy Profile for the Interconversion Pathways Occurring in Compound *22* (the Energy Values are in kcal mol^{-1}).**

The ^{13}C signal of the quaternary carbon of the four-membered ring, ortho to the tolyl substituent, broadens on cooling and splits, at -162 °C, into two lines, with an intensity ratio of about 35:65 (*Figure 46*).

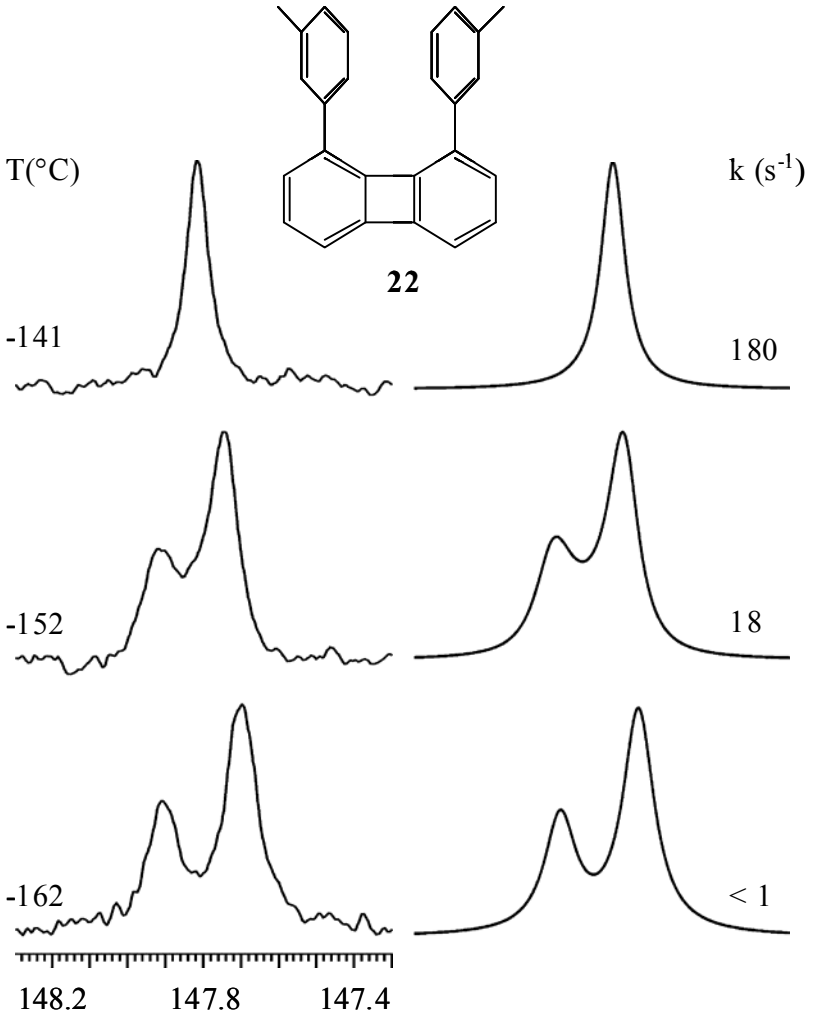

Figure 46: **Left: Temperature dependence of the ^{13}C signal (150.8 MHz in $CHF_2Cl/CHFCl_2$) of the quaternary carbons of the four membered ring ortho to the tolyl groups of compound *22*. Right: spectral simulation obtained with a 35:65 intensity ratio and with the rate constants reported.**

The spectral simulation provides a steric barrier of 6.2 ± 0.15 kcal mol^{-1} for the interconversion of the rapidly exchanging *anti* conformers (major line) into the rapidly exchanging *syn* enantiomers (minor line). Contrary to the prediction, however, the minor line does not split on further cooling, because the difference between the shifts of the two expected diastereotopic carbons of the frozen asymmetric form *syn* is less than the line width.

This splitting, however, is observed in the case of the methyl carbon spectrum, where the corresponding single line first splits at -152 °C into a pair of partially overlapped signals of unequal intensity, separated by about 30 Hz (*Figure 47*), the major corresponding to the *anti* conformers and the minor, broader signal, to the rapidly exchanging *syn* enantiomers.

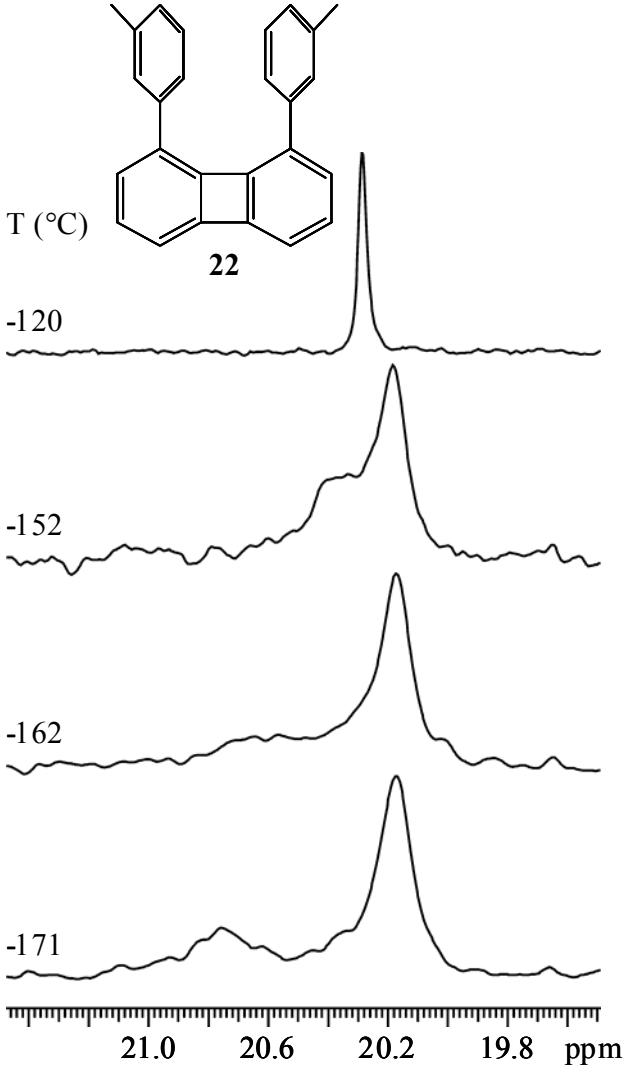

Figure 47: **Temperature dependence of the methyl carbon signal (150.8 MHz in $CHF_2Cl/CHFCl_2$) of compound *22*.**

The latter signal broadens further on cooling, and at -171 °C splits into a pair of lines, one of which is invisible being overlapped by the major signal. This is proved by the

fact that the visible downfield minor line is now separated from its major companion by 85 Hz and also by the observation that its relative intensity is approximately reduced by a factor of two, whereas that of the major is correspondingly higher. The relative intensity of the *syn*, in fact, has diminished (and that of the *anti* increased) because one of the two lines of the *syn* is superimposed on that of the *anti*. This feature thus indicates that, in addition to the steric barrier, also the mentioned π-barrier has been frozen. The spectrum does not display, however, the small line expected for the less stable *anti-out* conformer, either because of insufficient signal to noise ratio, or because this small line is hidden under one of the two observed lines (most likely the minor one, because it has a larger width than the major).

Likewise the ^{1}H signal of the methyl groups (*Figure 48*) splits, at –141 °C, into two partially overlapped lines (a feature also observed in *Figure 46* and *Figure 47*), with an approximate 35/65 ratio. On further cooling to -173 °C, also this spectrum shows that the minor broad signal of the *syn* conformer is split into a pair of widely separated lines: one (that upfield) is again overlapped by the major signal of the *anti-in* conformer, whereas the other (downfield with respect to the two overlapped lines) is clearly visible. At this temperature the ^{1}H spectrum exhibits an additional small methyl line (also involved in the exchange process) which is due to the least stable *anti-out* conformer (*Figure 48*).

The shift of this small line is close to that of the downfield line of the *syn*, because both these methyl groups point outward with respect to the biphenylene ring, thus experiencing similar environments. Indeed the relative methyl shifts predicted by computations[15] agree with the experimental trend: the *anti-in* and the upfield line of the *syn* are predicted to be at 1.82 and 1.78 ppm, respectively, thus are close enough ($\Delta\nu$ = 0.04 ppm) to overlap, as observed. The downfield line of the *syn* and that of the *anti-out* are predicted to be at 2.40 and 2.52 ppm, respectively, i.e. a difference ($\Delta\nu$ = 0.12 ppm) compatible with the detection of two separate lines.

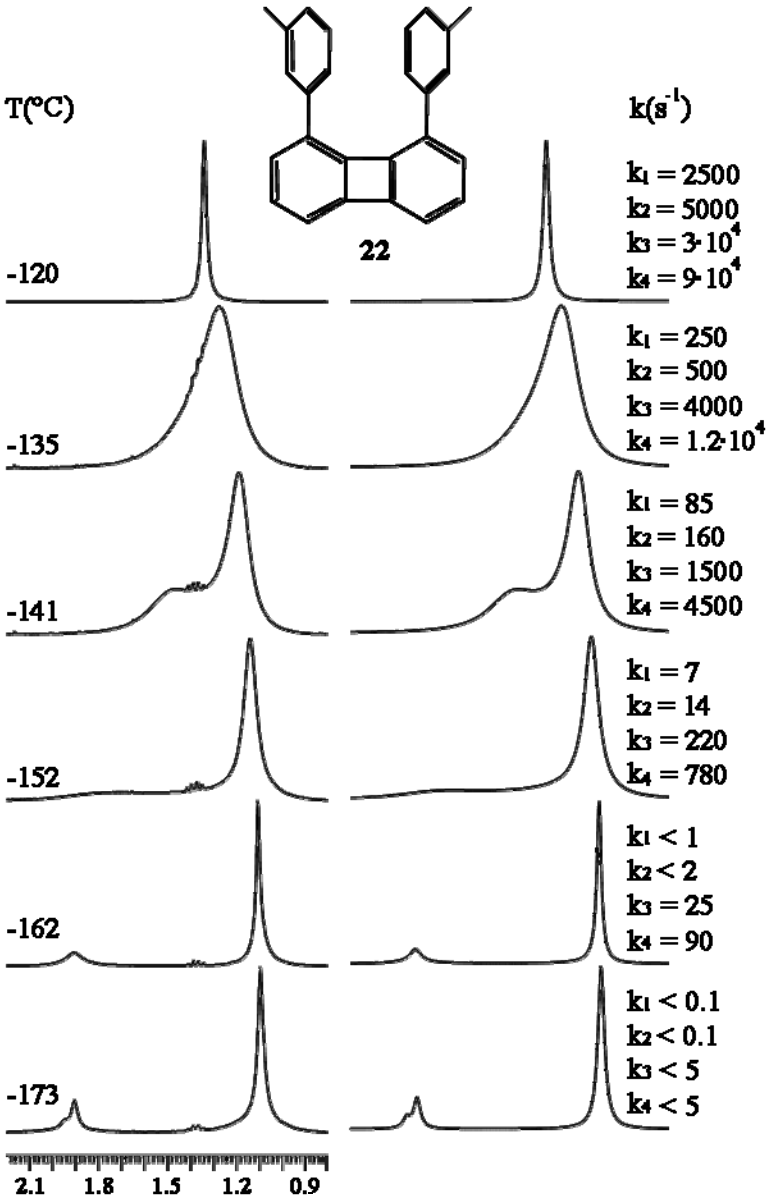

Figure 48: ***Left:*** **Temperature dependence of the ^{1}H methyl signal of *22* (600 MHz in $CHF_2Cl/CHFCl_2$). Right: Spectra simulated with the k values employed, where k_1 interconverts the *anti-in* into the *syn*, k_2 the *syn* into the *anti-out*, k_3 the *anti-in* into the *anti-out* and k_4 the *syn* into its enantiomeric form.**

The computed[15] shift differences of the methyl groups are quite close to the experimental differences, although their absolute values are consistently downfield by about 0.65 ± 0.1 ppm with respect to the corresponding experimental data. The previous

assignment of the *anti-in* structure of **22** as more stable than the *anti-out* (based upon the 0.75 kcal mol^{-1} lower computed energy, as in *Figure 42*) is further confirmed by the computed methyl shifts, that are predicted to be upfield for the *anti-in* (1.82 ppm) with respect to the *anti-out* (2.52 ppm): such a computed difference (0.70 ppm) agrees with the difference (0.87 ppm) observed in the experimental spectrum, where the most intense signal is likewise upfield with respect to the least intense one (1.08 and 1.95 ppm, respectively, as in the -173 °C trace of *Figure 48*). The relative intensities of the lines in the –173 °C spectrum are about 5:15:(65+15), corresponding to a proportion of the three conformers approximately equal to 5:30:65, for the *anti-out*, *syn* and *anti-in*, respectively. The experimental relative ΔG° values are 0.51, 0.15 and 0 kcal mol^{-1}, a trend which parallels that of the corresponding DFT computed energies (0.75, 0.4, 0 kcal mol^{-1}).

Since this spectrum displays lines for every one of the three species taking part in the exchange process, all the four rate constants (k_1, k_2, k_3, k_4, as in *Figure 43*) involved had to be used for describing the line shape. The three rate constants (k_1, k_2, k_3) are needed for describing the direct interconversion of the three conformers, the fourth (k_4) for describing the direct interconversion of the two enantiomers within the *syn* conformation (see *Figure 43*).

Two constraints should be however taken into account:

i) the rate for the steric process transforming *anti-in* into *syn* (k_1) must differ from the rate interconverting *syn* into *anti-out* (k_2) by an amount corresponding to the experimental ΔG° value of the *anti-in* and *syn* ground states (i.e., ca. 0.15 kcal mol^{-1} as mentioned above);

ii) the rate k_1, must yield a steric barrier equal, within the experimental errors, to that (6.2 ± 0.15 kcal mol^{-1}) determined from the signals of *Figure 46*.

The rates used for the simulation of *Figure 48* reproduce the experimental shape and also fulfil these constraints. The barriers derived from these rates are collected in *Table 5* and, as anticipated, the π-barriers are found lower than the steric barrier.

Table 5: **Experimental and Computed Barriers (kcal mol^{-1}) for the Interconversion Processes in Compound *22*.**

	Steric Barrier	**π-Barriers**	
	Anti-in* to *Syn	***Anti-in* to *Anti-out* (*π-anti*)**	**Enantiomerisation (*π-syn*)**
Experimental	6.4	5.6	5.3
Computed	6.3_5	4.0	3.5

The pathways for the *anti-in* to *syn* and for the *syn* to *anti-out* steric interconversion share the same transition state (see *Figure 45*), thus the corresponding $\Delta G^{\neq}$ values (derived from the rate constants k_1 and k_2, i.e. 6.4 and 6.2 kcal mol^{-1}, respectively) differ solely by the $\Delta G°$ value between the ground states of *anti-in* and *syn* (experimental value 0.15 kcal mol^{-1}). Thus, in practice, there is only one steric barrier, corresponding to the higher of these two $\Delta G^{\neq}$ values, i.e. 6.4 ± 0.15 kcal mol^{-1}, as in *Table 5*.

The experimental $\Delta G^{\neq}$ values of 5.6 and 5.3 kcal mol^{-1} (corresponding to the π-*anti* and π-*syn* barriers of *Table 5*) derive from the two values of rate constants (k_3 and k_4) that have at least a 3:1 ratio (*Figure 48*). If equal values are assumed for these rates, a proper simulation could not be achieved. Since these rate constants are obtained from spectra taken at the very same temperature, their differences are certainly meaningful. Consequently it is also meaningful the small difference between the corresponding $\Delta G^{\neq}$ values, because they are not affected by the uncertainty on the temperature (errors due solely to the simulation are less than 0.1 kcal mol^{-1}).[72] Of course, when comparing $\Delta G^{\neq}$ values obtained from spectra taken at different temperatures, experimental errors of about ±0.15 kcal mol^{-1} should be taken into account.

The interpretation proposed for these experiments implies that in a more symmetric compound, as 1,8-di-m-xylyl biphenylene (**23**), the steric barrier will be NMR invisible. In fact the 180° rotation of one xylyl group (across the transition state where the xylyl groups are alternatively coplanar with the biphenylene ring) will reproduce the same conformer with identical chemical shifts (homomerisation). When these types of situations are encountered in dynamic NMR processes, the effects of the higher barrier are invisible until also the lower barrier is frozen.[73]

Therefore, if a dynamic process will be nonetheless observed**,** one is led inexorably to assign it to the enantiomerisation process involving the ~ 90° torsion, *via* the π-barrier, as shown in *Figure 49*.

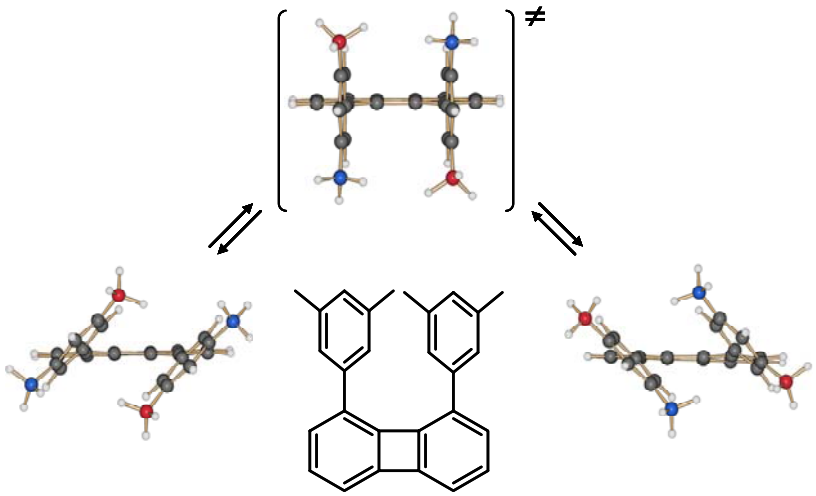

Figure 49: **DFT computed structures (bottom) of the conformational enantiomers of *23* (having dihedral angles of 43° between the planes of xylene and biphenylene). They exchange their inner and outer methyl groups passing across the orthogonal transition state (top), having a computed relative energy of 4.6 kcal mol^{-1}, *via* a ~ 90° torsion (π-barrier).**

The steric barrier for the 180° rotation process of 23 can be only obtained, as mentioned, by means of theoretical methods (the DFT computed value is 7.1 kcal mol^{-1}, as

in *Table 6*): these calculations also predict a π-barrier (4.6 kcal mol^{-1}, as in *Table 6*) which is at least 0.6 kcal mol^{-1} higher than the corresponding π-barriers computed for compound 22 (*Table 5*).

Table 6: **Experimental and Computed Barriers (kcal mol^{-1}) for the Interconversion Processes in Compound *23*.**

	Steric Barrier	**π-Barrier**
Experimental	Not measurable[a)]	6.3
Computed	7.1	4.6

NMR invisible owing to the molecular symmetry (see text).

This is due to the fact that in the computed transition state for the enantiomerisation of **23** (*Figure 49*) the two xylyl rings are both exactly orthogonal to the biphenylene plane, whereas this is not the case for the tolyl groups in **22** (see *Figure 44*). The perfect orthogonality of the two xylyl rings eliminates any contribution of conjugation with biphenylene, as compared to the case of **22**, thus enhancing the energy of the transition state, hence the corresponding barrier. Since the π-barriers measured in **22** are 5.3-5.6 kcal mol^{-1} (*Table 5*), the corresponding barrier in **23** (which is computed to be 0.6 kcal mol^{-1} higher) is expected to become about 6 kcal mol^{-1}. Such a value is well within the range accessible to dynamic NMR experiments, particularly because computations[15] predict a shift separation for the ^{1}H lines of the methyl groups as large as 0.77 ppm. The calculations also indicate that the upfield line will correspond to that of the methyls in the inner position: in this situation, in fact, these groups can experience the shielding effect due the aromatic ring currents.[44]

Actually, the ^{1}H methyl signal of **23** broadens on lowering the temperature and eventually decoalesces into a pair of equally intense sharp lines at -157 °C (***Figure 50***),

separated by 0.775 ppm: a shift difference in excellent agreement with the theoretical prediction.

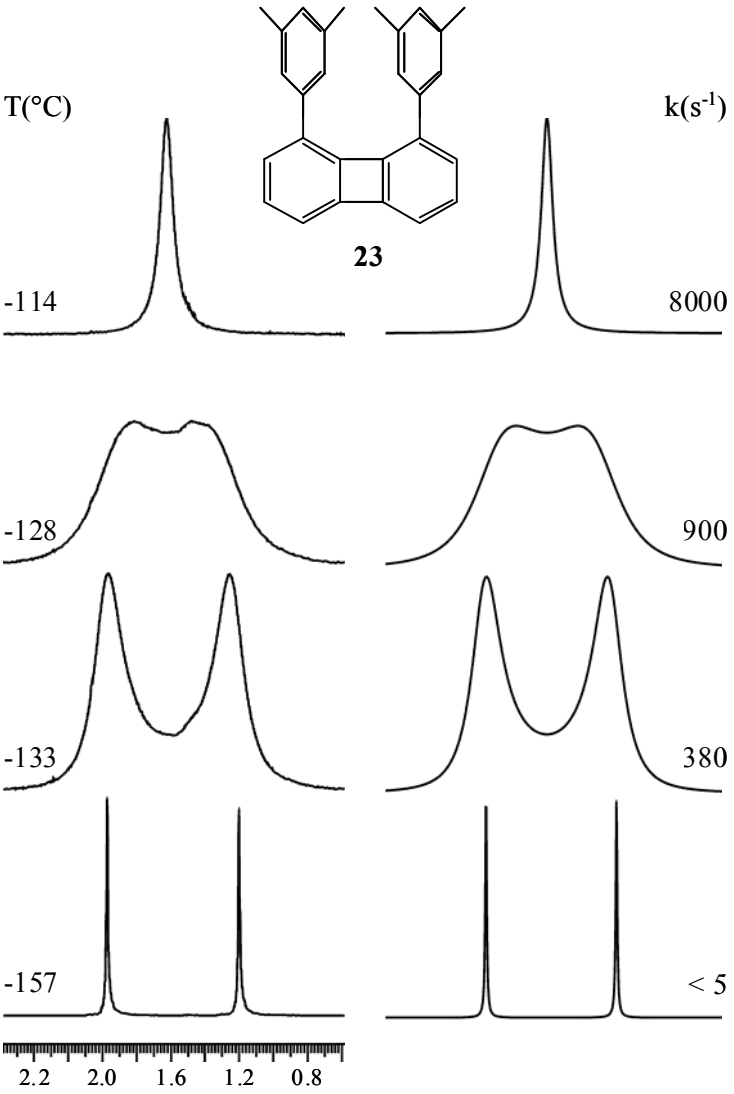

Figure 50: **Left: Temperature dependence of the ^{1}H methyl signal of *23* (600 MHz in $CHF_2Cl/CHFCl_2$). Right: simulations obtained with the rate constants indicated.**

No other exchange processes are observed, as conceivable, on further cooling to -175 °C. Spectral simulations afforded rate constants corresponding to an enantiomerisation π-barrier ($\Delta G^{\neq}$) of 6.3 kcal mol^{-1} (*Table 6*), in agreement with the anticipation.

Also in the case of **24**, in which the aryl groups are *o*-tolyl, DFT computations[15] actually predict the existence of three energy minima,[69] corresponding to the conformers displayed in *Figure 51*.

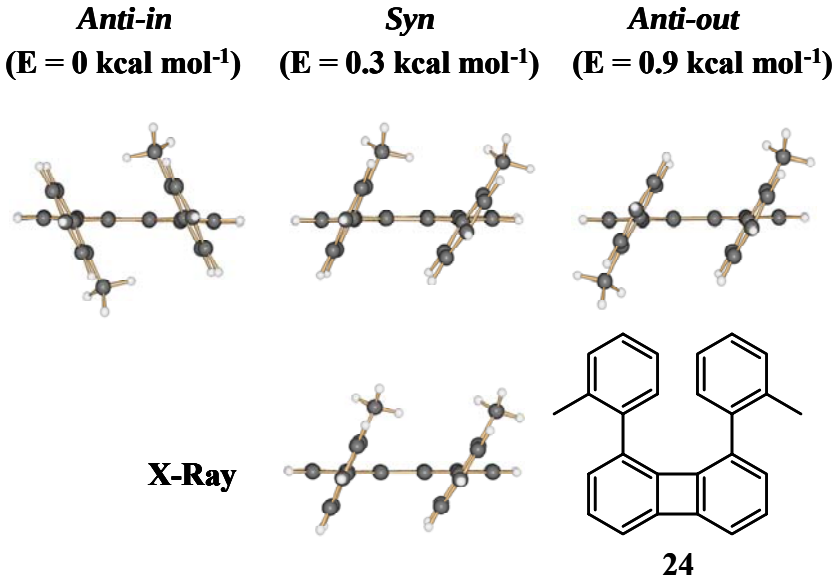

Figure 51: **Top: DFT computed structures of the conformers of *24* (for convenience only one of the two enantiomeric forms is displayed). Bottom: experimental structure obtained by single crystal X-ray diffraction.**

On the contrary of the less hindered compounds **22-23**, in the compound **24** the π-barrier is predicted to be significantly lower (1.7 kcal mol^{-1}, according to DFT computations), so that the 90° torsion processes are much faster and only the 180° rotation, which interconverts the rapidly exchanging *anti* conformers into the rapidly exchanging *syn* enantiomers, displays a barrier of 10.5 kcal mol^{-1} (by DFT computations) high enough to make the corresponding pathway accessible to a direct NMR detection.

Indeed the ^{1}H methyl signal of **24** broadens on cooling and eventually splits, at -92 °C , into a pair of lines in a 60:40 proportion (*Figure 52*), one corresponding to the rapidly interconverting *anti* conformers, the other to the rapidly interconverting enantiomers of *syn* conformers: owing to the fast 90° torsion process mentioned above,

both the *anti* and the *syn* conformers display a single methyl line (other exchange processes are not observed, even when cooling the sample to -175 °C).

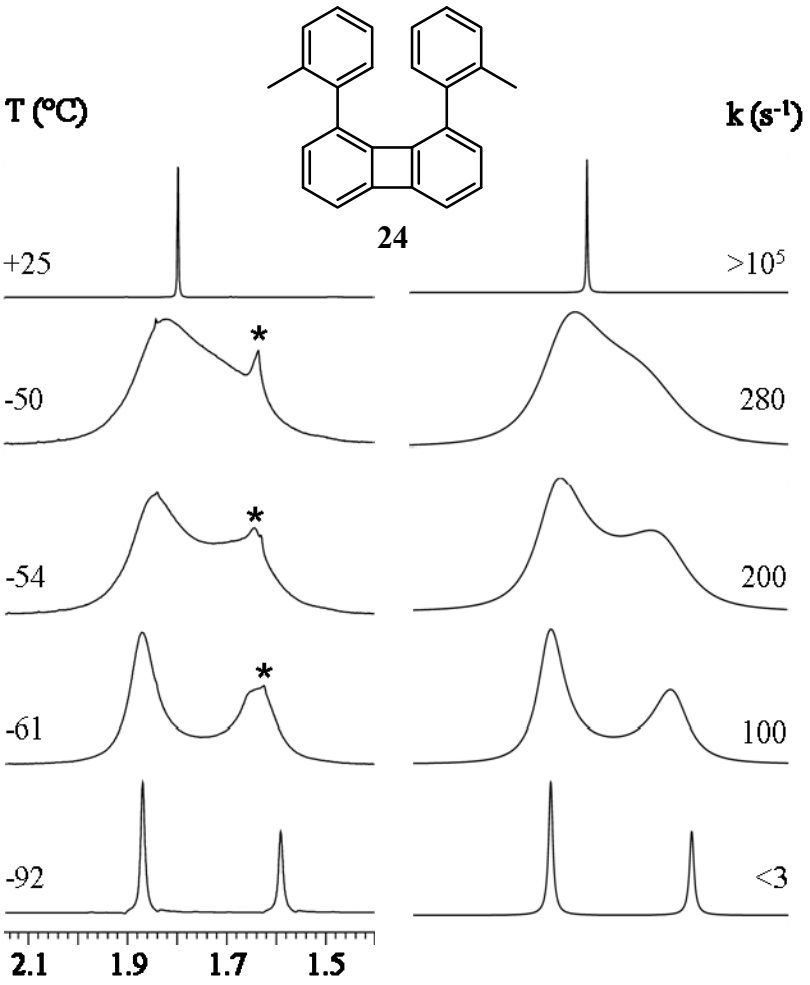

Figure 52: **Left: experimental NMR ^{1}H signal (600 MHz in CD_2Cl_2) of the methyl group of *24* as function of temperature (the starred line is a trace of HDO present in the solvent). Right: line shape simulation obtained with the rate constants indicated.**

Line shape simulation of the methyl signals as function of temperature yielded the rate constants for the interconversion of the major into the minor conformer; from these values a free energy of activation ($\Delta G^{\neq}$)[22] equal to 10.3± 0.15 kcal mol^{-1} is obtained, a result which agrees well with that predicted by DFT computations (*Table 7*).

Table 7: **Experimental and DFT Computed Barriers (kcal mol^{-1}) for the interconversion of the Major into the Minor Conformer in Compounds *24-29*.[a)]**

Compd.	24	25	26	27	28	29
Experimental (% of *anti*)	10.3 (40%)	11.4 (60%)	13.9 (87%)	17.0 [b)] (80%)	13.0 (62%)	34.5 [c)] (64%) [c)]
Computed	10.5	11.9	13.7	16.8	13.3	34.7

a) In parenthesis is reported the proportion of the conformer *anti* in compounds *24-28*, measured at the equilibrium in CD_2Cl_2 at appropriate low temperatures.

b) For the NMR determination of the large barrier of *27*, it is necessary to use a solvent (tetrachloroethane-d_2) with a higher boiling point than the solvent (CD_2Cl_2) employed for measuring the barriers of compounds *24-26* and *28*.

c) Determined in DMSO at +140 °C (see text).

Single crystal X-ray diffraction shows that in the solid state the structure of compound **24** is essentially equal to that computed for the *syn* conformation (*Figure 51*): this might be due to the existence of a more stable crystal lattice when the molecule adopts a *syn* disposition,[74,37a] but could also reflect the fact that, despite the higher computed energy, the *syn* might have a larger population in solution as a consequence of its higher entropy relative to the more symmetric *anti* form. It has to be taken into account that the *syn* conformer exists as four degenerate forms (two identical pairs of enantiomers), whereas the *anti-in* exists solely as two degenerate forms, corresponding to a pair of enantiomers (the presence of the *anti-out* can be, in practice, neglected, since its higher relative energy of 0.9 kcal mol^{-1} would correspond to a proportion lower than 8% at –92 °C). Owing to the greater probability, the actual population of the *syn* conformer might be higher than expected solely on the basis of its computed energy.

When the proportions are so close to 50/50, the approximations involved in the computed energy do not allow one to obtain a reliable assignment for the situation in solution because, in these conditions, even a small solvent effect might cause a reversal of the assignment.

Actually, the DFT computations of chemical shifts[15] predict that the *syn* should have the ^{1}H methyl signal at a field lower (by 0.23 ppm) than the *anti-in*. As shown in *Figure 52*, the more intense methyl line is 0.28 ppm at lower field with respect to its less intense companion: this feature seems to support the hypothesis that the *syn* is actually the more populated conformer in solution. For this reason an unambiguous experimental assignment of the two conformers observed in solution had to be undertaken.

To solve this problem a NOE experiment is carried out at a quite low temperature (-118 °C), in order to make negligible the saturation transfer effects:[75] at this temperature, in fact, the rate constant for the exchange is predicted to be as low as 0.01 s^{-1}. As shown in *Figure 53*, irradiation of the major methyl signal (trace b) yields significant enhancements only on two signals of the major conformer, i.e., those of H3,3' in the tolyl rings and of H2,7 in the biphenylene ring.

On the other hand irradiation of the minor methyl signal (trace c, *Figure 53*) yields significant enhancement on three signals of the minor conformer: in addition to the H3,3' signal in the tolyl rings and the H2,7 signal in the biphenylene ring, also the signal of the hydrogens in positions 6,6' in the tolyl rings is significantly enhanced. The latter effect can only occur in the *anti* conformer because the methyl in position 2 of one tolyl ring is close to the H6' in the second tolyl ring (and likewise the methyl in position 2' is close to H6 in the second ring). Thus the minor conformer, displaying three large NOE enhancements, must have the *anti* structure whereas the major, displaying only two large NOE enhancements, must have the *syn* structure. There is no doubt, therefore, that the *syn* is the more populated conformer of **24** in solution, as it is in the crystalline state (*Figure 51*, bottom).

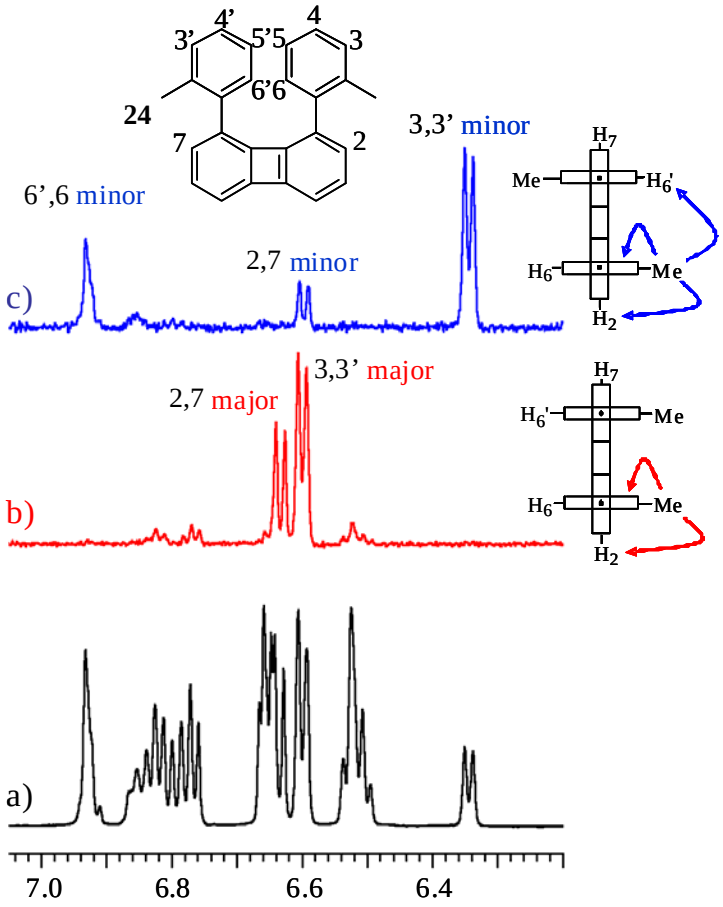

Figure 53:

***Trace a*: aromatic region (600 MHz at -118 °C in CD_2Cl_2) displaying ^1H signals for the major and minor conformers of *24*.**

***Trace b*: NOE due to irradiation of the major methyl signal (1.87 ppm), showing significant enhancement for two aromatic signals of the major conformer (*syn*).**

***Trace c*: NOE due to irradiation of the minor methyl signal (1.59 ppm), showing significant enhancements for three aromatic signals of the minor conformer (*anti*).**

When the dimension of the *ortho* substituent is increased, as in derivative **25** (R = Et), the situation is reversed in that the more stable conformer in solution appears to be the less hindered *anti* form (about 60%). This is proved by an analogous low temperature NOE experiment (*Figure 54*) where opposite effects, with respect to the case of **24**, are observed. In fact simultaneous irradiation of the two major signals of the diastereotopic

methylene hydrogens yields enhancement on three aromatic signals of the more intense spectrum, whereas only two aromatic signals of the less intense spectrum are enhanced when irradiating the two minor signals of the diastereotopic methylene hydrogens.[39]

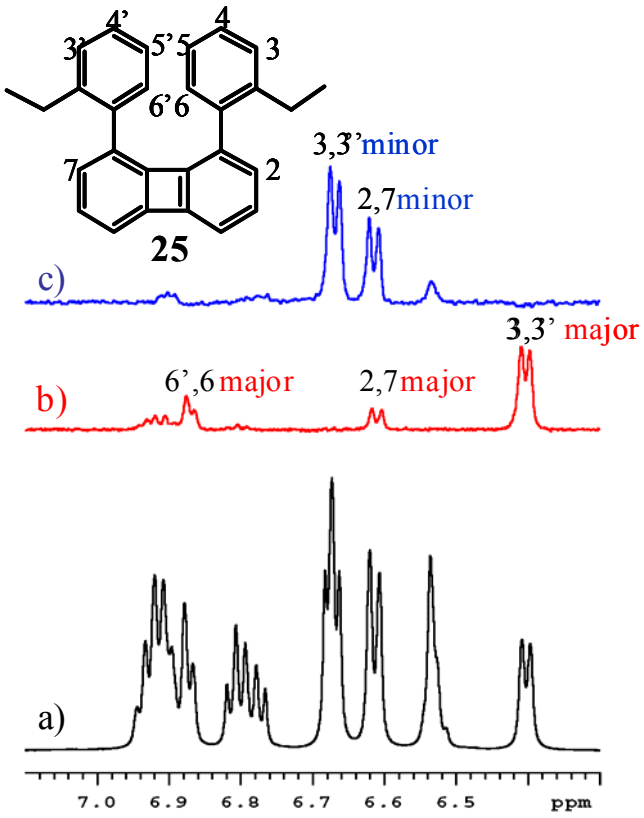

Figure 54:

Trace a: **aromatic spectral region (600 MHz at -108 °C in CD_2Cl_2) of *25*, displaying signals for the major (60%) and minor (40%) conformer.**

Trace b: **NOE due to simultaneous irradiation of the two major signals of the diastereotopic methylene hydrogens, showing significant enhancements for three aromatic doublet signals of the major conformer (i.e. *anti*).**

Trace c: **NOE due to simultaneous irradiation of the two minor signals of the diastereotopic methylene hydrogens, showing significant enhancement of two aromatic doublet signals of the minor conformer (i.e. *syn*).**

The effect of steric hindrance in controlling the relative stability of the *anti* and *syn* conformers is also noticed in the case of derivative 28. Here the introduction of an

additional methyl group in the *meta* position of the aryl ring produces the so called buttressing effect,[76] which generates a steric hindrance more similar to that of the ethyl groups in 25 than to that of the methyl groups in 24, thus making higher the rotation barrier ($\Delta G^{\neq}$ = 13.0 kcal mol^{-1} as in *Table 7*). The increased steric hindrance also renders the *anti* conformer of 28 more stable than the *syn*, (as proved by the low temperature NOE experiments in *Figure 55*), contrary to the case of the apparently similar compound 24.

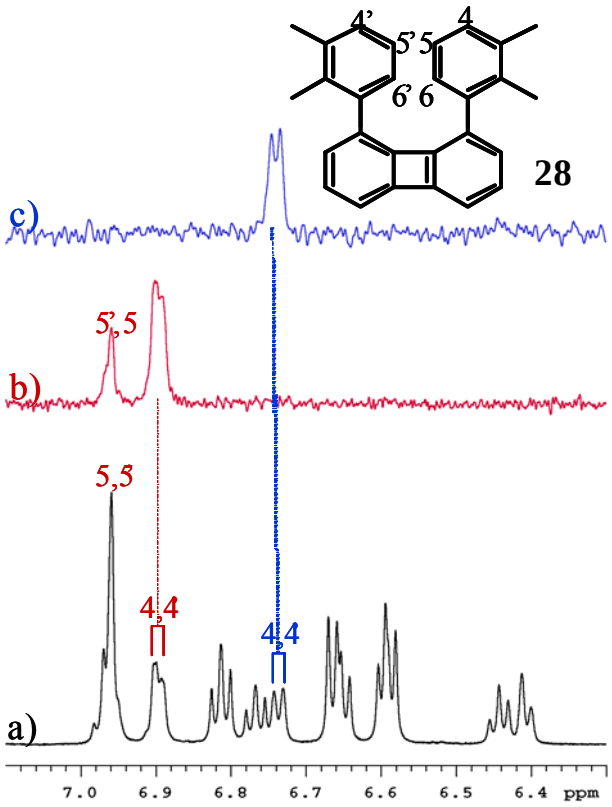

Figure 55:

Trace a: **aromatic spectral region (600 MHz at -90 °C in CD_2Cl_2) of *28*, showing separate signals for the major (62%) and minor (38%) conformer.**

Trace b: **NOE spectrum due to irradiation of the major signal of the methyls in position 3,3' of the xylyl rings, showing enhancement of two aromatic signals in the major spectrum (those of the hydrogens 5,5' and 4,4' of the *anti* conformer).**

Trace c: **irradiation of the minor signal of the methyls in position 3,3' enhances solely a single aromatic signal in the minor spectrum (that of the hydrogens in position 4,4' of the *syn* conformer).**

Irradiation (*Figure 55*) of the major signal of the methyls in position 3,3' of the xylyl rings (1.67 ppm) of **28**, yields enhancement for the major signal of the corresponding hydrogens in position 4,4' (6.90 ppm) of the same xylyl rings and for the major signal of the hydrogens in positions 5',5 (6.96 ppm) of the other ring, as expected for an *anti* conformer, where the latter distance is short enough to produce NOE effects. On the contrary irradiation of the minor signal (1.86 ppm) of the methyls in position 3,3' of the xylyl rings, enhances solely the minor signal of the corresponding hydrogens in position 4,4' of the same ring (6.74 ppm). Likewise irradiation of the major signals of the methyl in positions 2,2' of the xylyl rings (1.37 ppm) enhances the corresponding signals of the hydrogens in positions 2,7 of the biphenylene moiety (6.59 ppm) and also that of the hydrogens in positions 6',6 of the other xylyl ring (6.96 ppm). On the contrary, irradiation of the minor signal of the methyl groups (1.76 ppm) enhances solely the corresponding H2,H7 minor signal of biphenylene (6.60 ppm), as expected for a *syn* conformer where the distance between the hydrogens of the methyl in position 2 of one ring and the hydrogen in position 6' of the other ring is too large to yield a NOE effect.

This assignment is further confirmed by the observation that the DFT computed shifts of the two methyl groups for the *anti* conformer of **28** correspond to the more intense pair of the experimental methyl lines, whereas the shifts computed for the *syn* conformer correspond to the less intense lines of the experimental spectrum.

In the even more hindered derivative **26** (R = isopropyl), the proportion of the minor *syn* conformer[77] is further reduced (13%) and the interconversion barrier, obtained by line shape simulation (*Figure 56*), is increased (13.9 kcal mol^{-1}, *Table 7*).

On lowering the temperature the isopropyl methyl groups become diastereotopic, thus yielding two equally intense doublets in both the *anti* (more stable) and *syn* (less stable) conformer.

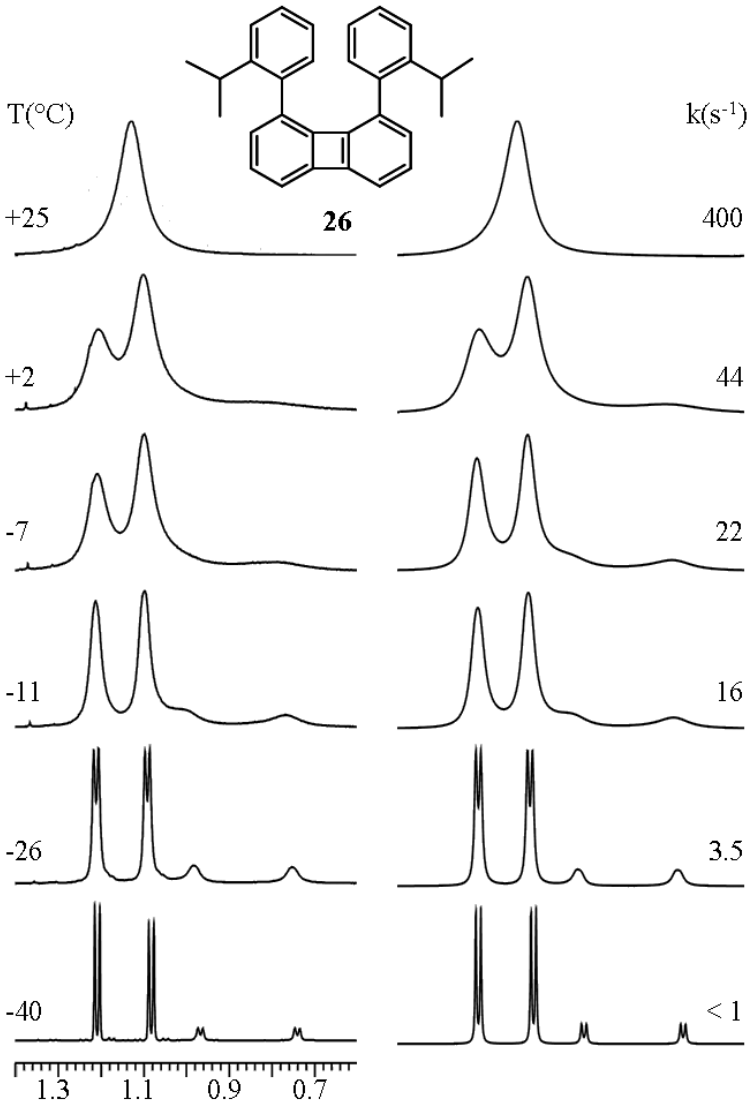

Figure 56: **Left: Temperature dependence of the ^{1}H methyl signal (600 MHz in CD_2Cl_2) of compound *26*. Right: line shape simulation obtained with the rate constants reported.**

As conceivable, the barrier increases further in the *tert*-butyl derivative **27**, although the proportion of the more stable conformer *anti*[77] does not increase accordingly in that, surprisingly, it is lower than in the case of **26**: solvent effects might be responsible for this feature. The lower proportion of the conformer *anti* observed in compound **27** with respect to **26** might be also interpreted as the consequence of a statistic effect, due to the possibility of having both the *anti-in* and *anti-out* situations in the case of **26**, whereas solely a single *anti* form occurs in **27**.

Contrary to the case of **24**, the single crystal X-ray diffraction of **27** shows that the *anti* conformation is adopted in the solid state, a result which agrees with the computations predicting the *anti* to be more stable by 1.1 kcal mol^{-1} than the *syn* (*Figure 57*): also the DFT calculations of chemical shifts confirm such an assignment.

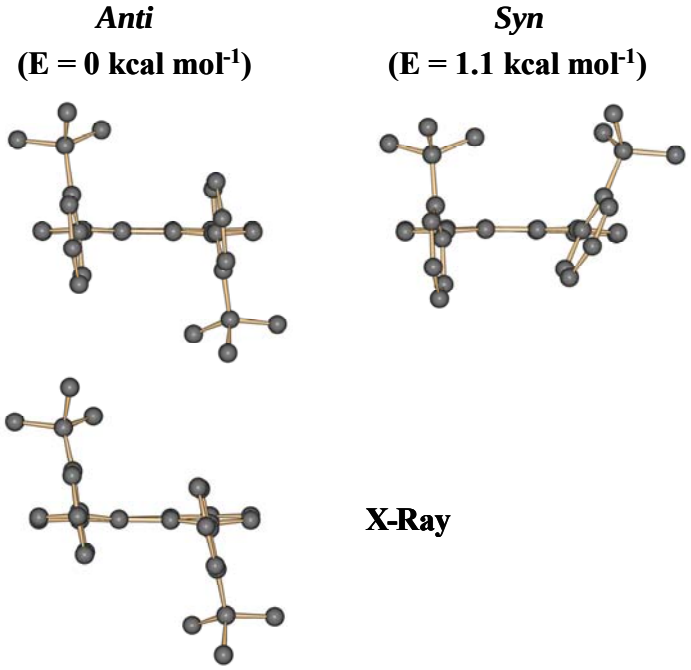

Figure 57: **Top: DFT computed structures of the *syn* and *anti* conformers of *27*. Bottom: experimental structure obtained by single crystal X-ray diffraction (the hydrogen atoms are omitted for convenience).**

According to computations the dihedral angle between the aryl rings and the biphenylene moiety (+81°) is very close to +90°, thus only one type of conformer *anti* occurs in **27**, because the *anti-in* and *anti-out* conformations of *Figure 51* become essentially indistinguishable when the planes are nearly orthogonal: the same value for this dihedral angle is also found in the X-ray structure (*Figure 57*).

The barrier measured for **27** (17.0 kcal mol^{-1}) indicates that even the presence of the large *tert*-butyl group in the *ortho* position of the benzene rings is not sufficient to allow a

physical separation of the *anti* and *syn* forms at ambient temperature, in that the lifetime of the corresponding conformers is exceedingly short ($t_{½} \approx 0.3$ second at +25 °C).

Such a separation could be however achieved in the case of compound **29**, were two 2–methylnaphthyl rings are bonded to the biphenylene moiety in the 1,8 positions: computations predict, in fact, a barrier as high as 34.7 kcal mol^{-1} (*Table 7*) for the corresponding naphthyl-biphenylene rotation process. The two isomers, indicated as **29a** and **29b**, in fact, have been isolated at ambient temperature by HPLC on a C18-phase, and their structural assignment is carried out with an alternative NOE approach, which is found more appropriate for the present case.

Following the procedure reported[78] for the assignment of symmetric isomers, the ^{13}C satellites of the methyl signals of **29a** and of **29b** (both with J_{CH} = 126.7 Hz) was irradiated at a temperature of 0 °C. The temperature of 0 °C was selected in order to obtain a better signal to noise ratio in the DPFGSE-NOE experiment. In order to avoid the interference of the HDO signal (present as an impurity in our $CDCl_3$) with the signals of **29b**, the spectrum of the latter is obtained in acetone-d_6 (the impurity of HDO in our acetone-d_6 lies in a position that does not interfere with the signals of **29b**).

As shown in *Figure 58*, simultaneous irradiation of the two ^{13}C-satellite lines of the isomer having the lower field methyl signal at 2.08 ppm (**29a**) yields a NOE effect on the ^{13}C central line, indicating that this signal must be that of the isomer *syn*, where the hydrogens of the two methyl groups are sufficiently close to experience a reciprocal NOE enhancement.

On the other hand, irradiation of the satellites of the compound having the higher field methyl signal at 1.52 ppm (**29b**) does not produce any NOE effect, indicating that this signal corresponds to the isomer *anti*,[44] where the hydrogens of the two methyl groups are too far apart to experience a reciprocal NOE enhancement. In this way an unambiguous assignment could be achieved for the isomers **29a** (*syn*) and **29b** (*anti*).

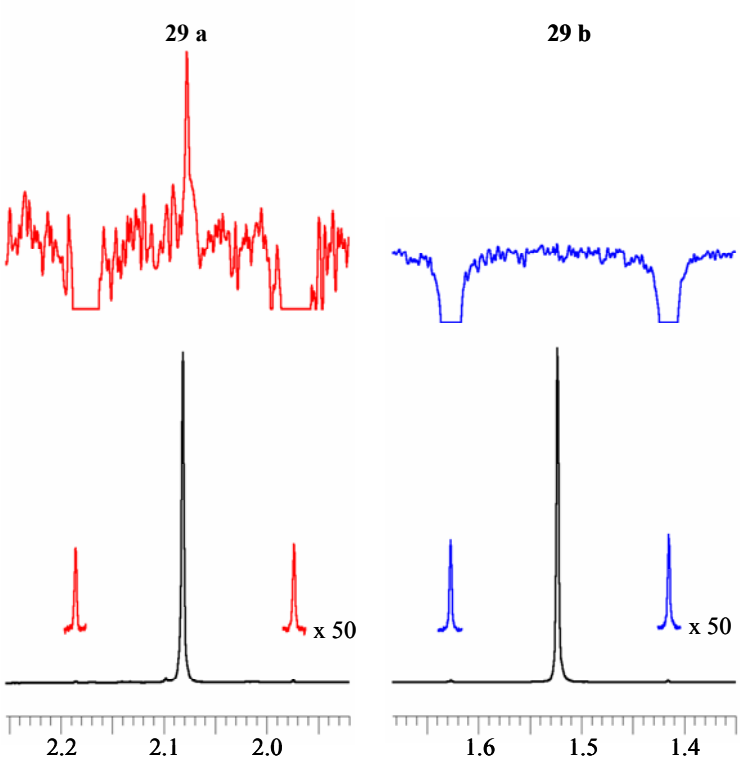

Figure 58: **Left: methyl signal of *29a* (600 MHz in $CDCl_3$ at 0 °C) with the amplified ^{13}C satellites (red) in the inset of the lower trace. The NOE effect, obtained by irradiating the ^{13}C satellites, is displayed in the top trace (red). Right: methyl signal of *29b* (600 MHz in aceton-d_6 at 0 °C) with the amplified ^{13}C satellites (blue) in the inset of the lower trace. The absence of NOE effect, on irradiation of the ^{13}C satellites, is clearly evident in the top trace (blue).**

The process leading to the interconversion of the configurationally stable isomers of **29** is followed by monitoring the time dependence of the NMR methyl signal of the pure *syn* isomer (**29a**) in DMSO at +140 °C. The intensity of the original methyl line of **29a** decreases, while that of the *anti* isomer **29b** begins to appear at higher field with an intensity which increases until an equilibrium, corresponding to a *syn* : *anti* ratio of 36:64 (*Figure 59* and *Table 7*), is reached (as in the case of compounds **25-28** the *anti* is more stable than the *syn* in equilibrium conditions).

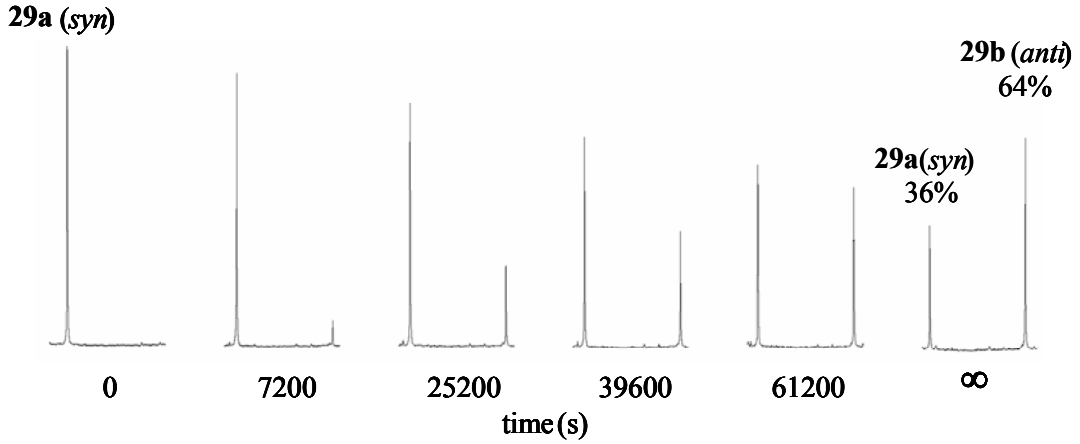

Figure 59: **Time dependence of the 600 MHz ^{1}H NMR methyl signal for the interconversion process of *29* in DMSO at +140 °C.**

From the first order kinetics equation for a process at the equilibrium, the appropriate rate constants are obtained (*Figure 60*) and the barrier for exchanging the more (*anti*, **29b**) into the less (*syn*, **29a**) stable isomer is derived ($\Delta G^{\neq}$ =34.5 kcal mol^{-1}).

time (s)	x(29b)	ln(x_e -x)
0	0	-0,4463
3600	0,050	-0,5276
7200	0,083	-0,5854
10800	0,119	-0,6520
14400	0,152	-0,7174
18000	0,185	-0,7875
25200	0,250	-0,9416
32400	0,301	-1,0818
39600	0,356	-1,2588
46800	0,398	-1,4188
61200	0,468	-1,7603
75600	0,516	-2,0875

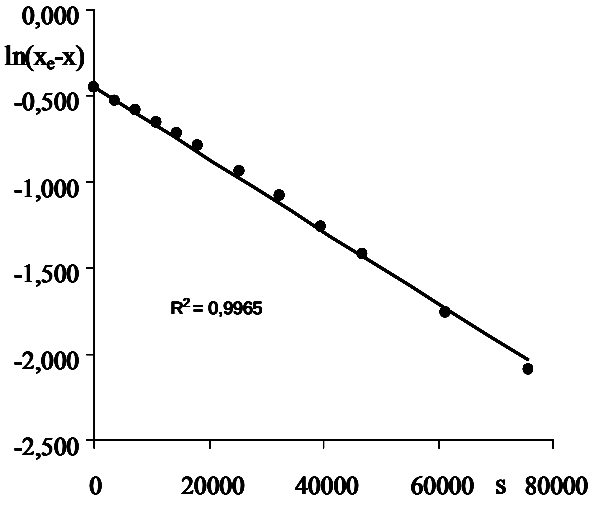

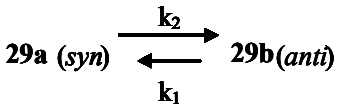

$\Delta G_1^{\#} = 34.5$ kcal mol

$\Delta G_2^{\#} = 34.0$ kcal mol

$\ln(x_e\text{-}x) = \ln x_e - (k_1+k_2)t$

$k_1+k_2 = 1.34 \cdot 10^{-5}\ s^{-1}$

$k_2/k_1 = 1.78$

$k_2 = 8.58 \cdot 10^{-6}\ s^{-1}$

$k_1 = 4.82 \cdot 10^{-6}\ s^{-1}$

Figure 60: **Kinetics for the interconversion process of the *syn* (29a) and *anti* isomers (29b) of compound 29 in DMSO at +140 °C.**

The result agrees well with the DFT computed value (34.7 kcal mol^{-1}) reported in *Table 7*.

The *syn* isomer **29a** (C_s point group), having two equal stereogenic axes with opposite (*M,P*) handedness, corresponds to a meso form, whereas the *anti* isomer **29b** (C_2 point group) exists as a pair of enantiomers (*M,M* and *P,P*),[79,80] as illustrated in *Scheme 9*.

Scheme 9: **Schematic Representation of the *Syn* (Meso) *29a*, and *Anti* (Racemic), *29b* Isomers of Compound *29*.**

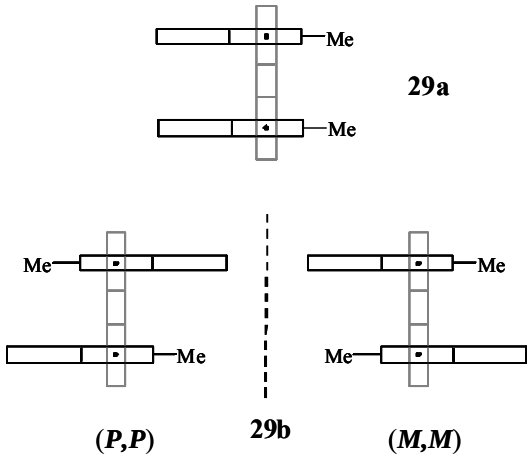

The two enantiomers of **29b** are separated by enantioselective HPLC on a Chiralcel OJ-H 250x4.6 mm column, at a flow rate of 1.0 mL/min, using hexane/iPr-OH 95:5 v:v as eluent. The corresponding CD spectra display the two opposite signed traces shown in *Figure 61*.

The intense band at ≈ 215 nm is due to the ^{1}B transition of naphthalene, and that at ≈ 255 nm is that of the biphenylene moiety.

In order to assign the absolute configuration (AC), the TD-DFT approach was used: the CD spectrum of one enantiomer is calculated by theoretical methods and its shape (and intensity) compared with that of the experimental spectrum. If they match, the AC assumed in the calculations should then be assigned to the enantiomer whose experimental spectrum has been recorded.

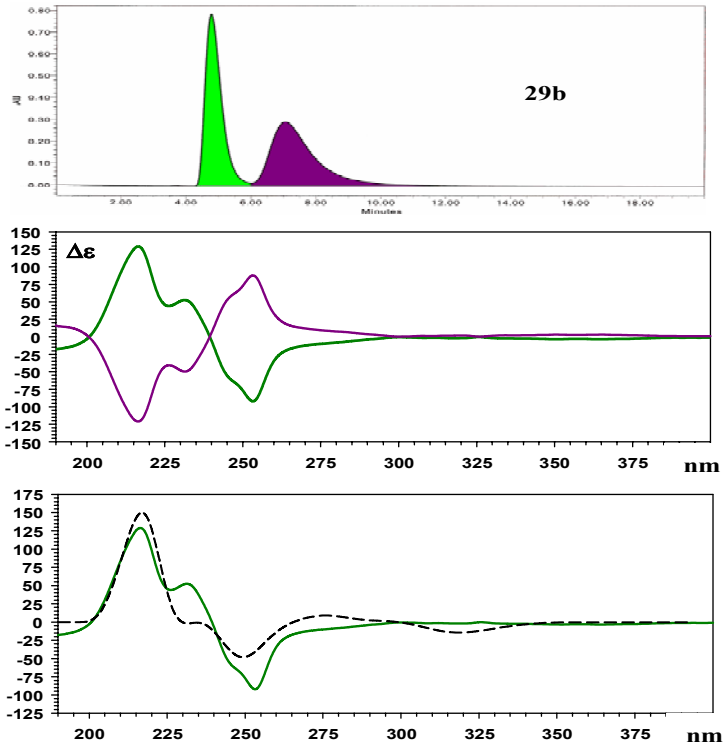

Figure 61: **Top: Enantioselective HPLC trace of the two enantiomers of the *anti* isomer *29b*. Middle: CD spectra of the two enantiomers. Bottom: Computed CD spectrum (blue shifted by 7 nm, dashed trace) for the *M,M* configuration, compared with the experimental spectrum (green) of the first eluted enantiomer.**

As shown in *Figure 61*, the CD spectrum calculated by assuming the *M,M* configuration has a shape analogous to that of the spectrum of the first eluted enantiomer, with a significant positive Cotton effect at lower wavelengths (≈ 220 nm), as well as a significant negative effect at higher wavelengths (≈ 255 nm). Accordingly, the first eluted enantiomer has the *M,M* configuration and, as a consequence, the *P,P* configuration must be assigned to the second eluted enantiomer.

3.2 Conclusions

Dynamic NMR spectroscopy allowed, for the first time, the determination of the π-barriers responsible for the enantiomerisation processes in derivatives bearing two aryl substituents bonded to a planar framework: this could be achieved in the case of 1,8-di-*m*-tolylbiphenylene (**22**) and 1,8-di-*m*-xylylbiphenylene (**23**). In compound **22**, the three possible conformers predicted by DFT computations (*anti-in*, *syn*, and *anti-out*) was detected, and in addition, the steric barrier responsible for their interconversion could be measured.

Anti and *syn* conformers, due to restricted sp^2-sp^2 bond rotation, are also detected in hindered 1,8-diarylbiphenylenes, the aryl moieties being phenyl groups bearing *ortho* alkyl substituents such as Me (**24**), Et (**25**), *i*-Pr (**26**), *t*-Bu (**27**). By means of low temperature NOE experiments the corresponding structures are assigned and are found to be in agreement with the results of single crystal X-ray diffraction. The interconversion barriers of these conformers was determined by line shape simulation of the variable temperature NMR spectra and the experimental values are reproduced satisfactorily by DFT calculations. In the case of the bulkiest aryl substituent investigated (i.e. 2-methylnaphthalene, **29**) the *syn* and *anti* atropisomers are amenable to be separated at ambient temperature. The two enantiomers (*M,M* and *P,P*) of the isomer *anti* are also isolated by enantioselective HPLC and the theoretical interpretation of the corresponding CD spectrum allowed the absolute configuration to be assigned.

3.3 Experimental Section

3.3.1 *1,8-Dibromobiphenylene*[81], *1,3-dibromo-2-iodobenzene*[82] and *2-methylnaphthylboronic acid*[83] were prepared according to the literature; *2-tert-butylphenylboronic acid* was prepared following known procedures[84] *3-methylphenyl boronic acid*, *3,5-dimethylphenyl boronic acid*, *2-methylphenylboronic acid***,** *2-ethylphenylboronic acid***,** *2-isopropylphenylboronic acid* and *2,3-dimethylphenylboronic acid* were commercially available.

3.3.2 General Procedure for 22 and 23. To a solution of 1,8-dibromobiphenylene (0.062 g, 0.2 mmol, in 2 ml of benzene), K_2CO_3 (2M solution, 1.0 ml), the appropriate boronic acid (0.5 mmol, suspension in 2 ml of ethanol), and $Pd(PPh_3)_4$ (0.046 g, 0.04 mmol) were added at room temperature. The stirred solution was refluxed for 2-3 h, the reaction being monitored by GC-MS, to confirm the first coupling. After cooling to room temperature, a second amount of boronic acid (0.5 mmol, suspension in 2 ml of ethanol), and $Pd(PPh_3)_4$ (0.046 g, 0.04 mmol) were added, and the solution refluxed again for 2 h. Subsequently $CHCl_3$ and H_2O were added and the extracted organic layer was dried (Na_2SO_4) and evaporated. The crude products were pre-purified by chromatography on silica gel (Hexane/Et_2O 10:1) to obtain mixtures containing the target compounds, together with biphenylene, 1-bromobiphenylene, 1-aryl-biphenylene and 1-aryl-8-bromobiphenylene as impurities. Analytically pure samples of **22-28** were obtained by semi-preparative HPLC on a C18 column (5µm, 250x10 mm, 5 ml/min, ACN/H_2O). Crystals suitable for X-ray analysis were obtained from chloroform, by slow evaporation, in the cases of **24** and **27**.

1,8-di-(3-methylphenyl)-biphenylene (**22**): ^{1}H-NMR (600 MHz, $CDCl_3$, 25°C, TMS): δ 1.88 (6H, s), 6.65 (2H, bs), 6.67 (2H, d, J = 4.3, 3.2 Hz), 6.85-6.86 (4H, m), 6.91 (6H, m). ^{13}C-NMR (150.8 MHz, $CDCl_3$, 25°C, TMS): δ 21.0 (CH_3), 115.4 (CH), 124.2

(CH), 127.5 (CH), 127.8 (CH), 128.6 (CH), 129.3 (CH), 129.4 (CH), 133.0 (q) 137.4 (q), 137.7 (q), 148.1 (q), 151.4 (q). HRMS(EI): m/z calcd for $C_{26}H_{20}$: 332.1565; found 332.1566. HPLC: 5 ml/min, ACN/H_2O 95:5 v:v, RT = 16.62 min.

1,8-di-(3,5-dimethylphenyl)-biphenylene (**23**): ^{1}H-NMR (600 MHz, $CDCl_3$, 25°C, TMS): δ 1.97 (12H, s), 6.61 (4H,bs), 6.65 (2H, dd, J = 5.6, 2.0 Hz), 6.74 (2H, bs), 6.82-6.86 (4H, m). ^{13}C-NMR (150.8 MHz, $CDCl_3$, 25°C, TMS): δ 20.9 (CH_3), 115.3 (CH), 125.9 (CH), 128.5 (CH), 128.8 (CH), 129.4 (CH), 133.0 (q) 137.2 (q), 137.7 (q), 148.1 (q), 151.3 (q). HRMS(EI): m/z calcd for $C_{28}H_{24}$: 360.1878; found 360.1873. HPLC: 5 ml/min, ACN/H_2O 90:10 v:v, RT = 35.06 min.

1,8-di(*o*-tolyl)biphenylene (24) :^{1}H NMR (600 MHz, $CDCl_3$, 25°C, TMS): δ 1.89 (6H, s), 6.66 (6H, m), 6.80 (6H, m), 6.93 (2H, td, *J* = 7.4, 1.6 Hz). ^{13}C NMR (150.8 MHz, $CDCl_3$, 25°C, TMS): δ 19.7 (CH_3), 115.6 (CH), 124.8 (CH), 127.1 (CH), 128.2 (CH), 128.2 (CH), 129.4 (CH), 130.3 (CH), 132.5 (q), 135.0 (q), 137.6 (q), 149.6 (q), 150.8 (q). HRMS(EI): *m/z* calcd for $C_{26}H_{20}$: 332.15650; found 332.1564. HPLC: 4 ml/min, ACN/H_2O 95:5 v:v, RT = 13.68 min.

Crystal Data

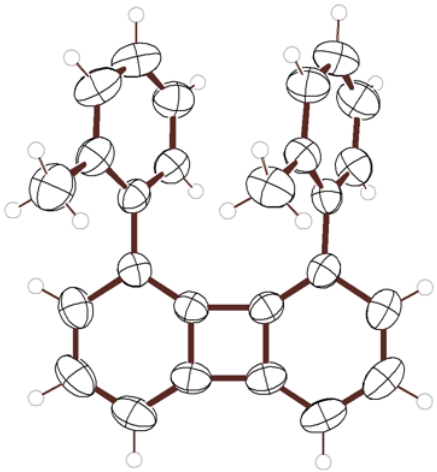

Crystals obtained from $CHCl_3$, molecular formula: $\mathbf{C_{26}H_{20}}$, M_r = 332.42, monoclinic, space group $P2_1/c$ (No. 14), a = 9.0552(9), b = 28.655(3), c = 7.5307(3) Å, β = 108.552(1), V = 1852.5(3) Å^3, T = 298(2) K, Z = 4, ρ_c = 1.192 g cm^{-3}, $F(000)$ = 704, graphite-monochromated $Mo_{K\alpha}$ radiation (λ = 0.71073 Å), $\mu(Mo_{K\alpha})$ = 0.067 mm^{-1}, colourless plate (0.5 × 0.2 × 0.2 mm^3), empirical absorption correction with SADABS (transmission factors: 0.9867 – 0.9671), 2400 frames, exposure time 10 s, $2.37 \leq \theta \leq 28.61$, $-11 \leq h \leq 12$, $-38 \leq k \leq 37$, $-10 \leq l \leq 10$, 21086 reflections collected, 4485 independent reflections (R_{int} = 0.0264), solution by direct methods (SHELXS97[32]) and subsequent Fourier syntheses, full-matrix least-squares on F_o^2 (SHELX97[32]), hydrogen atoms refined with a riding model, data / restraints / parameters = 4485/ 0 / 237, $S(F^2)$ = 1.047, $R(F)$ = 0.0709 and $wR(F^2)$ = 0.1401 on all data, $R(F)$ = 0.0465 and $wR(F^2)$ = 0.1268 for 3056 reflections with $I > 2\sigma(I)$, weighting scheme $w = 1/[\sigma^2(F_o^2) + (0.0635P)^2 + 0.0000P]$ where $P = (F_o^2 + 2F_c^2)/3$, largest difference peak and hole 0.180 and –0.155 e Å^{-3}.

1,8-bis(2-ethylphenyl)biphenylene (25) :^{1}H-NMR (600 MHz, $CDCl_3$, 25°C, TMS): δ 0.91 (6H, t, J = 7.6 Hz), 2.24 (4H,bs), 6.63 (2H, d, J = 8.5 Hz), 6.67 (2H, d, J = 6.8 Hz), 6.71 (2H, d, J = 7.7 Hz), 6.76 (4H, m), 6.80 (2H, dd, J = 8.2, 6.9 Hz), 6.97 (2H, m). ^{13}C-NMR (150.8 MHz, $CDCl_3$, 25°C, TMS): δ 14.7 (CH_3), 25.8 (CH_2), 115.5 (CH), 124.8 (CH), 127.3 (CH), 127.5 (CH), 128.1 (CH), 128.6 (CH), 130.5 (CH), 132.4 (q), 137.1 (q), 141.0 (q), 149.5 (q), 150.8 (q). HRMS(EI): m/z calcd for $C_{28}H_{24}$: 360.18780; found 360.1877. HPLC: 5 ml/min, ACN/H_2O 90:10 v:v, RT = 14.74 min.

1,8-bis(2-isopropylphenyl)biphenylene (26):^{1}H-NMR (600 MHz, $CDCl_3$, 25°C, TMS): δ 1.13 (12H, bs), 3.10 (2H,bs), 6.43 (4H,bs), 6.60 (2H, d, J = 8.4 Hz), 6.67 (2H, d, J = 6.8 Hz), 6.77 (2H, dd, J = 8.2, 6.8 Hz), 6.98 (2H, t, J = 7.3 Hz), 7.08 (2H, d, J = 7.3 Hz). ^{13}C-NMR (150.8 MHz, $CDCl_3$, 25°C, TMS): δ 24.1 (CH), 29.3 (CH_3), 115.5 (CH), 124.6 (CH), 124.7 (CH), 127.4 (CH), 127.5 (CH), 129.2 (CH), 130.8 (CH), 132.6 (q), 136.4 (q),

145.1 (q), 149.3 (q), 151.3 (q). HRMS(EI): m/z calcd for $C_{30}H_{28}$: 388.21910; found 388.2190. HPLC: 5 ml/min, ACN/H_2O 97:3 v:v, RT = 18.61 min.

1,8-bis(2-*tert*-butylphenyl)biphenylene (27) :^{1}H-NMR (600 MHz, $C_2D_2Cl_4$, 0°C) δ 1.10 (4.6 H, s, minor isomer), 1.26 (13.4H, s, major isomer), 6.57-6.61 (5 H, m, major + minor isomer), 6.66 (2H, d, J = 6.8 Hz, major + minor isomer), 6.70-6.74 (3 H, m, major + minor isomer), 6.89 (1.5 H, ddd, J= 8.1, 6.3, 2.7 Hz, major isomer), 7.01 (0.5H, ddd, J= 8.3, 5.9, 3.0 Hz, minor isomer), 7.16 (2H, d, J = 8.2 Hz). ^{13}C-NMR (150.8 MHz, $C_2D_2Cl_4$, 0°C): major isomer: δ 32.77 (CH_3), 36.2 (q), 115.6 (CH), 124.55 (CH), 126.4 (CH), 126.7 (CH), 127.1 (CH), 131.1 (CH), 131.4 (CH), 135.6 (q), 136.5 (q), 146.4 (q), 149.5 (q), 150.5 (q); minor isomer (two CH lines are overlapped to those of the major isomer): δ 32.74 (CH_3), 36.1 (q), 115.3 (CH), 124.50 (CH), 126.8 (CH), 131.7 (CH), 131.8 (CH), 136.0 (q), 136.8 (q), 146.6 (q), 149.1 (q), 150.3 (q). HRMS(EI): m/z calcd for $C_{32}H_{32}$: 416.25040; found 416.2503. HPLC: 5 ml/min, ACN/H_2O 97:3 v:v, RT = 19.97 min.

Crystal Data

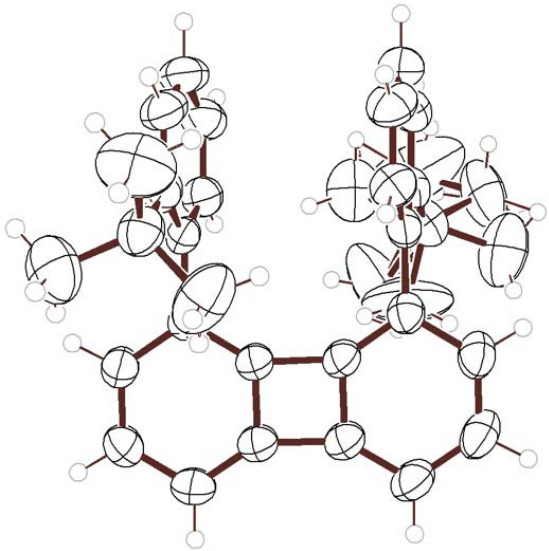

Crystals obtained from $CHCl_3$, molecular formula: $\mathbf{C_{32}H_{32}}$, M_r = 416.58, monoclinic, space group $P2_1/c$ (No. 14), a = 10.132(6), b = 11.507(6), c = 21.320(12) Å, β

= 95.982(7), V = 2472.0 (20) Å^3, T = 298(2) K, Z = 4, ρ_c = 1.119 g cm^{-3}, F(000) = 896, graphite-monochromated $Mo_{K\alpha}$ radiation (λ = 0.71073 Å), $\mu(Mo_{K\alpha})$ = 0.063 mm^{-1}, colourless brick (0.3 × 0.3 × 0.1 mm^3), empirical absorption correction with SADABS (transmission factors: 0.9938 – 0.9814), 2400 frames, exposure time 15 s, $1.92 \leq \theta \leq 27.77$, $-13 \leq h \leq 13$, $-15 \leq k \leq 15$, $-27 \leq l \leq 27$, 27469 reflections collected, 5731 independent reflections (R_{int} = 0.0303), solution by direct methods (SHELXS97[32]) and subsequent Fourier syntheses, full-matrix least-squares on F_o^2 (SHELX97[32]), hydrogen atoms refined with a riding model, data / restraints / parameters = 5731/ 6 / 335, $S(F^2)$ = 1.028, $R(F)$ = 0.0830 and $wR(F^2)$ = 0.1464 on all data, $R(F)$ = 0.0518 and $wR(F^2)$ = 0.1278 for 3781 reflections with $I > 2\sigma(I)$, weighting scheme $w = 1/[\sigma^2(F_o^2) + (0.0618P)^2 + 0.4145P]$ where $P = (F_o^2 + 2F_c^2)/3$, largest difference peak and hole 0.149 and –0.166 e Å^{-3}. One of two t-butyl group was disordered and treated as two independent parts, each one populated by 50%.

1,8-bis(2,3-dimethylphenyl)biphenylene (28): ^{1}H-NMR (600 MHz, $C_2D_2Cl_4$, +70°C): δ 1.79 (6H, s), 1.99 (6H, s), 6.66 (2H, d, J = 8.4 Hz), 6.70 (2H, d, J = 6.7 Hz), 6.79 (4H, m), 6.84 (2H, d, J = 7.6 Hz), 6.89 (2H, d, J = 7.0). ^{13}C-NMR (150.8 MHz, $C_2D_2Cl_4$, +70°C): δ 16.0 (CH_3), 20.1 (CH_3), 115.4 (CH), 124.5 (CH), 126.4 (CH), 128.2 (CH), 128.9 (CH), 130.8 (CH), 133.2 (q), 134.1 (q), 136.5 (q), 138.1 (q), 149.9 (q), 150.7 (q). HRMS(EI): m/z calcd for $C_{28}H_{24}$: 360.18780; found 360.1879. HPLC: 5 ml/min, ACN/H_2O 97:3 v:v, RT = 14.92 min.

3.3.3 1,8-bis(2-methylnaphthalen-1-yl)biphenylene (29). To a solution of 1,8-dibromobiphenylene (0.062 g, 0.2 mmol, in 2 ml of benzene), K_2CO_3 (2M solution, 1.0 ml), 2-methylnaphtylboronic acid (0.5 mmol, suspension in 2 ml of ethanol), and $Pd(OAc)_2$ (0.009 g, 0.04 mmol) were added at room temperature. The stirred solution was refluxed for 48 h, the reaction being monitored by GC-MS to confirm the first coupling had

achieved. Subsequently $CHCl_3$ and H_2O were added and the extracted organic layer was dried (Na_2SO_4) and evaporated. The crudes was pre-purified by chromatography on silica gel (Hexane/Et_2O 10:1) to obtain a mixture, that was further purified by preparative HPLC on a C18 column (10μm, 250x21.2 mm, 24 ml/min, ACN/H_2O 90:10 v/v), to obtain 0.052 g (60%) of 1-bromo-8-(2-methylnaphthalen-1-yl)biphenylene. To a solution of this intermediate, (0.052 g, 0.12 mmol, in 2 ml of benzene), K_2CO_3 (2M solution, 1.0 ml), 2-methylnaphtylboronic acid (0.5 mmol, suspension in 2 ml of ethanol), and $Pd(PPh_3)_4$ (0.046 g, 0.04 mmol) were added, and the solution stirred for 48 h, the reaction being monitored by GC-MS. Subsequently $CHCl_3$ and H_2O were added and the extracted organic layer was dried (Na_2SO_4) and evaporated. The crude was pre-purified by chromatography on silica gel (Hexane/Et_2O 10:1) to obtain purified mixtures containing the title compound and 1-(2-methylnaphthalen-1-yl)biphenylene as impurity. Separation of the two isomers **29a** and **29b** was obtained in two steps: the pair was first separated from the impurity by preparative HPLC on a C18 column (10μm, 250x21.2 mm, 24 ml/min, ACN/H_2O 95:5 v/v), then the separation of the two isomers was obtained by joining a C18 and a C8 semipreparative HPLC columns (first column: Kromasil C18, 5μm, 250x10 mm; second column: Luna C8(2), 5μm, 250x10 mm, 5 ml/min, ACN/H_2O 90:10 v/v). A total amount of 0.015 g of the *anti* isomer **29b** (first eluted) and 0.005 g of the *syn* isomer **29a** (second eluted) were obtained.

1,8-bis(2-methylnaphthalen-1-yl)biphenylene, *syn* isomer (29a): ^{1}H NMR (600 MHz, $CDCl_3$, 25°C, TMS): δ 2.09 (6H, s), 6.51 (2H, d, J = 8.2 Hz), 6.75-6.84 (10H, m), 7.17-7.23 (6H, m). ^{13}C NMR (150.8 MHz, $CDCl_3$, 25°C, TMS): δ 20.5 (CH_3), 115.9 (CH), 123.8 (CH), 125.0 (CH), 125.05 (CH), 127.1 (CH), 127.2 (CH), 127.3 (CH), 128.3 (CH), 129.9 (q), 130.98 (q), 131.0 (q), 131.4 (CH), 131.8 (q), 133.1 (q), 150.8 (q), 151.3 (q). HRMS(EI): *m*/*z* calcd for $C_{34}H_{24}$: 432.18780; found 432.1876. HPLC: 1 ml/min, ACN/H_2O 90:10 v:v, RT = 43.16 min.

1,8-bis(2-methylnaphthalen-1-yl)biphenylene, *anti* isomer (29b) :^{1}H NMR (600 MHz, acetone-d_6 25°C): δ 1.55 (6H, s), 6.33 (2H, d, *J* = 8.4 Hz), 6.50 (2H, d, *J* = 8.1 Hz), 6.87 (2H, d, *J* = 6.7 Hz), 6.92 (2H, dd, *J* = 8.1, 6.9 Hz), 7.27 (2H, d, *J* = 8.4 Hz), 7.31-7.37 (4H, m), 7.44 (2 H, d, *J* = 8.2 Hz), 7.67 (2H, d, *J* = 8.0 Hz). ^{13}C NMR (150.8 MHz, acetone-d_6, 25°C): δ 19.7 (CH_3), 116.5 (CH), 124.3 (CH), 125.2 (CH), 125.5 (CH), 127.3 (CH), 127.6 (CH), 128.1 (CH), 128.9 (CH), 130.2 (q), 131.0 (CH), 131.72 (q), 131.74 (q), 132.5 (q), 133.1 (q), 150.8 (q), 151.6 (q). HRMS(EI): *m*/*z* calcd for $C_{34}H_{24}$: 432.18780; found 432.1877. HPLC: 1 ml/min, ACN/H_2O 90:10 v:v, RT = 41.12 min.

3.4 Enantioselective HPLC and CD spectra

Separation of the two enantiomers of **29b** was achieved at 25°C on a Chiralcel OJ-H 250x4.6 mm column, at a flow rate of 1.0 mL/min, using hexane/iPr-OH 95:5 v:v as eluent. In order to have the sufficient amount to record the CD spectra, 10 injections (50 μg each one) were collected. UV detection was fixed at 225 nm. UV absorption spectra were recorded at 25 °C in hexane on the racemic mixture, in the 190-400 nm spectral region. The cell path length was 0.1 cm, concentration was $1.43 \cdot 10^{-4}$ mol L^{-1}. Maximum molar absorption coefficient was recorded at 218 nm (ε = 66670). CD spectra were recorded at 25°C in hexane, with the same path lengths of 0.1 cm, in the range 190-400 nm; reported Δε values are expressed as L $mol^{-1}cm^{-1}$.

3.5 NMR Spectroscopy

The spectra were recorded at 600 MHz for ^{1}H and 150.8 MHz for ^{13}C. The assignments of the ^{1}H and ^{13}C signals were obtained by bi-dimensional experiments (edited-gHSQC[33] and gHMBC[34] sequences). The samples for obtaining spectra at temperatures lower than –100 °C were prepared by connecting to a vacuum line the NMR tubes containing the compound and a small amount of C_6D_6 (for locking purpose), and condensing therein the gaseous CHF_2Cl and $CHFCl_2$ (4:1 v/v) under cooling with liquid

nitrogen. The tubes were subsequently sealed in vacuo and introduced into the precooled probe of the spectrometer. Temperature calibrations were performed before the experiments, using a Cu/Ni thermocouple immersed in a dummy sample tube filled with isopentane, and under conditions as nearly identical as possible. The uncertainty in the temperatures was estimated from the calibration curve to be ±1 °C. The line shape simulations were performed by means of a PC version of the QCPE program DNMR 6 n° 633, Indiana University, Bloomington, IN. Kinetic equilibration of compound **29** was obtained by heating a NMR sample of pure **29a** in DMSO-d_6 into a thermostatic oil bath, kept at +140 °C. NMR spectra were then recoded at regular times until the equilibrium was reached.

3.6 Calculations

Geometry optimization were carried out at the B3LYP/6-31G(d) level by means of the Gaussian 03 series of programs[15]: the standard Berny algorithm in redundant internal coordinates and default criteria of convergence were employed. The reported energy values are not ZPE corrected. Harmonic vibrational frequencies were calculated for all the stationary points. For each optimized ground state the frequency analysis showed the absence of imaginary frequencies, whereas each transition state showed a single imaginary frequency. Visual inspection of the corresponding normal mode was used to confirm that the correct transition state had been found. NMR chemical shift calculations were obtained with the GIAO method at the B3LYP/6-311++G(2d,p)//B3LYP/6-31G(d) level. TMS, calculated at the same level of theory, was used as reference to scale the absolute shielding value. TDDFT calculations on the M,M enantiomer of **29b** were obtained at the B3LYP/6-31+G(d,p)//B3LYP/6-31G(d) level. In order to cover the whole 190-400 nm range, 60 transition were calculated. The CD spectrum was then obtained applying a 0.3 eV Gaussian bandshape.[85]

Chapter 4

4.1 Anthrones, Anthraquinones and Anthracenes: Structures, Stereodynamics and Absolute Configurations

It has been recognized that π-stacking interactions of aromatic substituents bonded in appropriate positions to planar (or quasi-planar) frameworks[86] play an important role in a great number of chemical properties, including stereocontrolled reactions,[87] molecular recognitions,[88] nucleic acid and protein structures,[89] and crystal packing.[90] Depending on the hindrance of the aryl substituents and on the type of the planar framework the resulting atropisomers can be either stereolabile or configurationally stable, as seen in some examples in *Chapter 3*. This type of atropisomer should be also observable when anthrone or anthraquinone are used as a framework to which connect the appropriate aryl substituents (*Scheme 10*).

Scheme 10

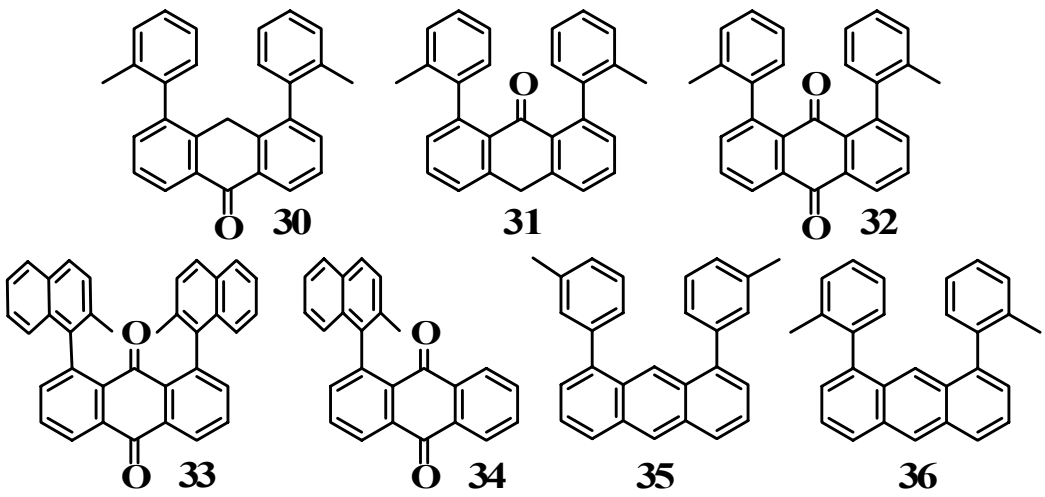

The interest for synthesizing and studying these derivatives is due to the fact that they can be further functionalized quite easily, owing to the presence of the carbonyl

moiety, whereas the compounds investigated in the previous *Chapter 3* are less prone to undergo further modification, and the compounds **35** and **36** could be an example of the reduction of these carbonyls.

In these kind of compounds, DFT computations[15] predict in each case the existence of two energy minima, corresponding to the *syn* and *anti* atropisomers generated by the restricted sp^2-sp^2 rotation. As an example the *syn* and *anti* forms computed (at the B3LYP/6-31G(d) level), for compound **30** are displayed in *Figure 62*: they are predicted to have essentially the same energy. From this picture it is evident that the two methylene hydrogens of the *anti* conformer experience the same environment, being related by the 2-fold symmetry axis of the molecule (C_2 point group), whereas the two methylene hydrogens (labelled H_a and H_b) of the *syn* conformer (C_s point group) experience different environments, and are therefore diastereotopic.[91]

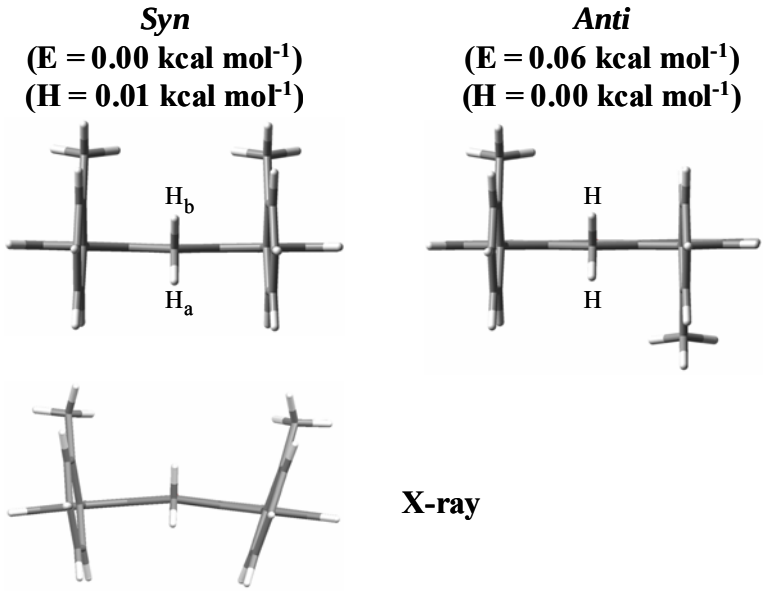

Figure 62: **Top: DFT Computed Structures of the Two Conformers of *30*; Bottom: Experimental X-ray Structure.**

The ^1H NMR signal of the CH_2 hydrogens of **30** (upper trace of *Figure 63*) displays, in fact, the four lines of an AB-type spectrum (J_{gem} = -24.0 Hz) along with a

single line, due to the chiroptic methylene of the *syn* and to the achiroptical methylene of the *anti* conformer, in a 50:50 ratio, respectively.

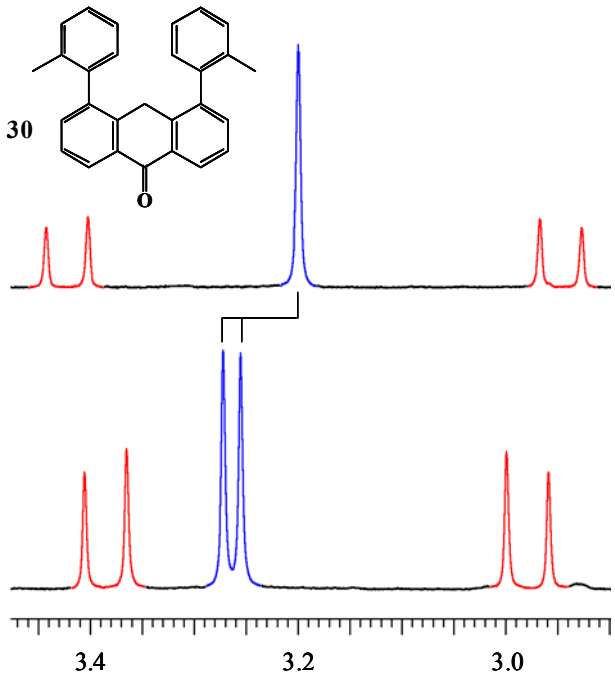

Figure 63: **Top: ^{1}H methylene spectrum (600 MHz in CD_2Cl_2 at –40 °C) of *30*. Bottom: in a chiral environment it is observed the splitting of the single line (blue) of the *anti* (chiral) conformer but not of the four line spectrum (red) of the *syn* (achiral) conformer.**

An analogous spectrum is also observed for the CH_2 hydrogens of **31** (i.e. a single line and an AB-type spectrum with J_{gem} = -20.7 Hz, as in *Figure 64*).

In the case of compound 30 it is also obtained the X-ray structure (*Figure 62*, bottom), which shows that solely the *syn* form is populated in the solid state. From *Figure 62* it is evident that the central ring of anthrone is bent in the crystalline structure, while is planar in both the *anti* and *syn* calculated structures.

This finding is apparently anomalous, because in the cases of 31 and 32 the DFT calculations indicate that the corresponding ground states have the central ring bent (*Figure 65*).

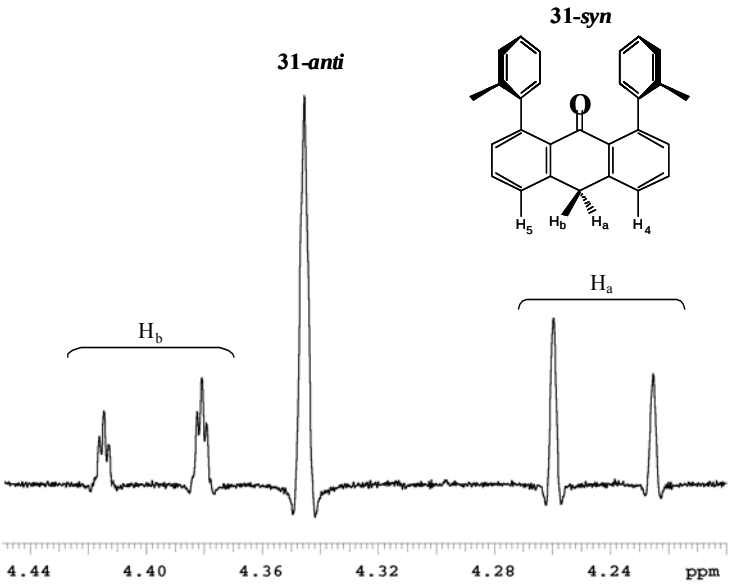

Figure 64: **Resolution enhanced ^{1}H spectrum (600 MHz in $CDCl_3$) of the CH_2 signals of compound 31, displaying a ^{2}J coupling of -20.7 Hz between H_a and H_b, and a ^{4}J coupling (0.95 Hz) with H_4,H_5 solely for the downfield signal (i.e. the one corresponding to H_b) of the *syn* conformer. The assignment of the downfield signal to H_b derives from the relative shifts predicted by DFT computations.**

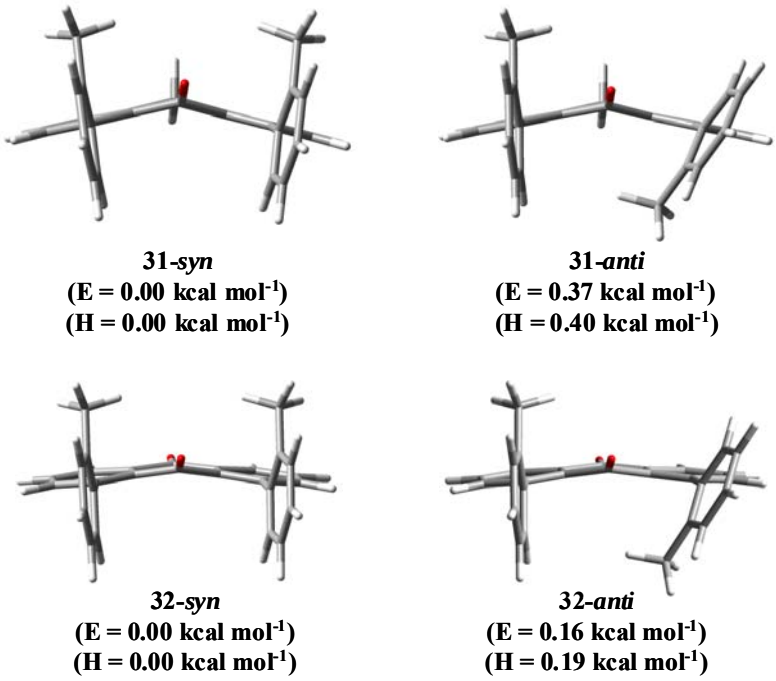

Figure 65: **DFT calculated structures for the two conformers of *31* and *32*.**

To check whether the discrepancy depends upon the inadequacy of the theoretical approach, calculations at higher levels (PBE1PBE/6-31+G(d,p), HF/6-31+G(d,p) and B3LYP/6-31++G(d,p)) are carried out on the **30**-*syn* conformation: in all cases, however, the central ring results invariably planar.

Two experimental observations in solution actually support the theoretical prediction of a planar structure of the anthrone ring in **30**:

i) the large geminal coupling has been reported[92] to be a function of the dihedral angle ϕ, defined as the angle between the π orbital and an imaginary line passing through both protons of the methylene group. In the case of the calculated planar structure of **30**-*syn*, this dihedral angle is exactly 0°, thus this coupling reaches its maximum value.[92] In the case of **31**, the bent geometry of the central ring causes the dihedral angle ϕ to become about 23° (according to DFT calculations), thus reducing the value of the *J*-coupling, as experimentally observed (i.e. -24.0 and -20.7 Hz in **30** and 3**1**, respectively). The observed difference between these two J_{gem}-couplings (24.0 – 20.7 = 3.3 Hz for ϕ = 0° and ϕ = 23°, respectively) is consistent with the differences reported in reference 92 (e.g. 23.6 – 18.1 = 5.5 Hz for ϕ = 0° and for ϕ = 45°, respectively).

ii) in the case of **31**, the low-field hydrogen signal of the AB-system displays a small additional ^4J coupling (0.95 Hz) with the two hydrogens in position 4 and 5 of the anthrone ring, whereas the high-field hydrogen signal does not display such a coupling (*Figure 64*). This implies that in compound **31** H_a and H_b have different dihedral angles with the two ortho hydrogens, therefore confirming the bent geometry of the anthrone ring. These considerations are further supported by the DFT calculated *J*-couplings (including the Fermi contact term) for the two *syn* conformers of **30** and **31**: in the case of planar **30**, in fact, the calculated J_{gem} for the *syn* conformer is actually predicted to be larger than that of **31** (-28.5 and -22.5 Hz, respectively). In addition, these calculations predict that H_b of compound **31** (computed to have the lower field signal) is coupled with the hydrogens in position 4 and 5 of anthrone (^4J = -1.34 Hz), in agreement with the experimental 0.95 Hz

value. On the other hand, H_a is predicted to have a negligible ^4J coupling (-0.02 Hz), as experimentally observed.

The presence of two enantiomers in the *anti* form can be demonstrated by the NMR spectrum taken in a chiral environment. In these conditions for instance, (the temperature of -40 °C is used to increase the separation of the lines; 10 Hz at 600 MHz, see *Figure 66*)[50] the single signal of the CH_2 moiety of **30** splits into a pair of lines due to the *M,M* and *P,P* enantiomers, whereas the CH_2 signals of the achiral *syn* conformer are not further split (*Figure 63, bottom trace*): these methylene hydrogens, in fact, are already diastereotopic in the achiral solvent.

Each of the two (blue) lines in the bottom trace of *Figure 63* corresponds to the two identical (isochronous) methylene hydrogens within each enantiomer of the *anti* conformer. If the two hydrogens had been anisochronous, an AB-type spectrum, with a geminal *J* coupling, would have been observed.[93] This issue has to be addressed in that two enantiotopic groups of an achiral molecule also split their signal in a chiral environment.[94] In compound **30**, in fact, not only the methyl signal of the *anti*, but also the methyl signal of the *syn* conformer splits in this experiment, because the methyl groups of the latter are enantiotopic in the achiral environment, contrary to the corresponding CH_2 hydrogens that are already diastereotopic (see *Figure 68*).

The same behaviour is also observed in the corresponding ^{13}C spectrum of the two CH_2 lines: the signal at higher field splits, in fact, into a pair of lines, due to the *M,M* and *P,P* enantiomers, whereas that at lower field does not (*Figure 66*). This allows one to assign the up-field line to the *anti* (chiral) and the down-field line to the *syn* (achiral) conformer.

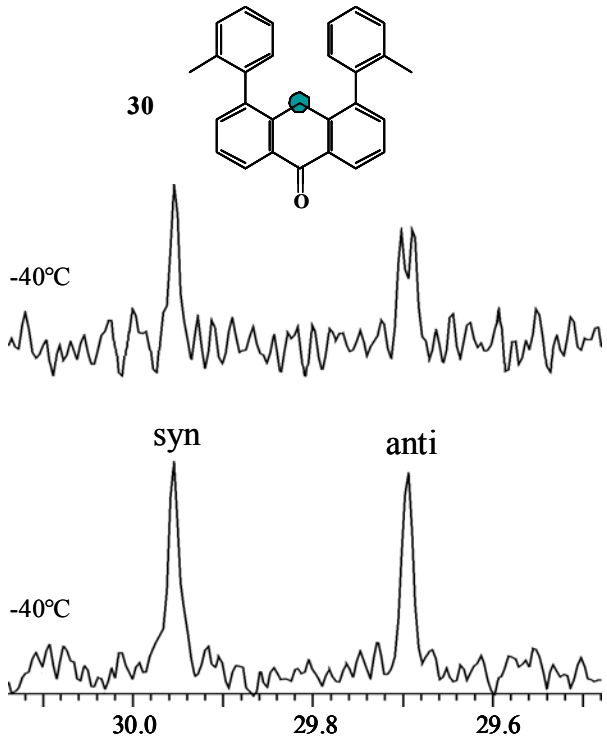

Figure 66: **Bottom: ^{13}C NMR signals (150.8 MHz in CD_2Cl_2 at –40 °C) of the methylene carbon (indicated by the green spot) of the *syn* and *anti* conformers of *30*. Top: spectrum taken in the chiral environment[50] displays the splitting of the up-field line of the *anti* (chiral) conformer but not of the downfield line of the *syn* (achiral) conformer.**

In the spectrum of compound **31** (bottom trace of *Figure 67*) the intensity of the single line of the *anti* is slightly higher than the intensity of the four line spectrum of the *syn* (ratio 53:47). This result, apparently, is not matched by DFT computations that predict an energy lower (ΔE and ΔH^0 = 0.37 and 0.40 kcal mol^{-1}, respectively) for the *syn* with respect to the *anti* (*Figure 65*). The ratio of the conformers actually depends upon the free energy $\Delta G° = \Delta H° - T\Delta S°$. DFT computations yield acceptable values for the enthalpy, but they are known to produce unreliable values for the entropy factor when low frequency normal modes (< 900 cm^{-1}) are taken into account, as it happens in the present cases.[95] For this reason it is preferred to estimate the entropy contribution on the basis of the molecular symmetry. It has to be taken into account, however, that the *anti* form is favoured (by RT

ln2) by the entropy of mixing, since the *anti* comprises two enantiomers whereas the *syn* does not.[96,90]

Accordingly, the relative computed enthalpy of the *syn* has to be corrected, at ambient temperature, by an entropic factor of RT ln2 = 0.41 kcal mol^{-1} with respect to the *anti*. When this effect is taken into account, the *anti* is expected to have essentially the same population of the *syn* (in fact ΔG^0 is 0.40 – 0.41 = –0.01 kcal mol^{-1}), therefore accounting for the nearly equal population experimentally observed (if the experimental errors are considered, the 53:47 ratio does not differ significantly from 50:50). It should be also outlined that the *syn* has a C_s and the *anti* a static C_1 symmetry (assuming it has a bent geometry), as a consequence, both have an equal symmetry number (σ = 1),[90,96] causing this contribution to the entropic factor to be the same, thus irrelevant. When the same argument is applied to the case of compound **30**, the *anti* conformer should be likewise expected to be more populated than the *syn*, but in this case the *anti* has a C_2 symmetry, whereas the *syn* has C_s symmetry. As a consequence, the former is favoured by the entropy of mixing, but it is disfavoured by RTln2 because of the different symmetry number (σ = 1 for C_s and σ =2 for C_2): the two entropic effects act in opposite directions and therefore cancel out.

The enthalpy difference, accordingly, remains the same as that (-0.01 kcal mol^{-1}) computed in *Figure 62* and such a negligible difference accounts for the equal population experimentally observed.

The simulated spectrum (*Figure 67*, bottom and *Figure 68,* top) at +25 °C is composed by the signals of the two conformers *syn* and *anti*. The *anti* conformer has enantiotopic H signals, and correspond to the singlet.

The *syn* conformer has diastereotopic hydrogens, with a geminal coupling of -20.7 Hz. Therefore the simulation is that of a singlet exchanging with an AB system.

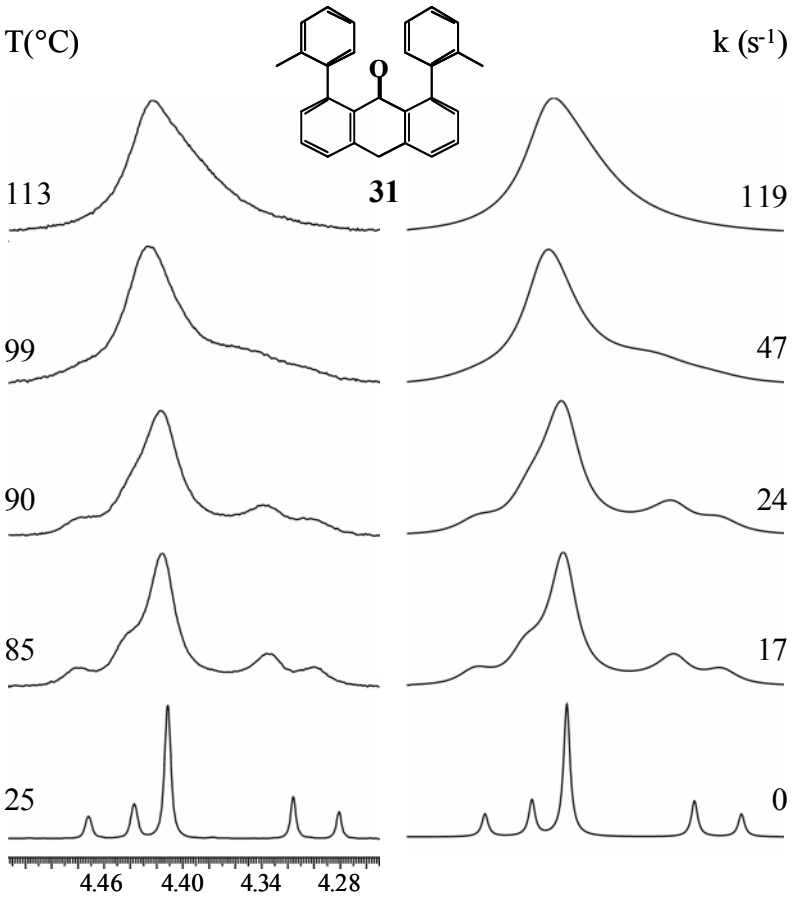

Figure 67: **Temperature dependence of the ^{1}H NMR methylene signal (600 MHz in $CDCl_2$-$CDCl_2$) of 31 (left). On the right the simulation with the rate constants indicated.**

In the DNMR6 input file reported are considered the *anti* conformer (signal 1) with two identical chemical shifts (72.9 Hz from the left edge of the spectrum), the *syn* conformer where 2' and 2" are the chemical shifts of the two diastereotopic hydrogens, (48.0 and 139.3 Hz, respectively), and the exchanged *syn* conformer (3' and 3", 139.3 and 48.0 Hz, respectively), in which the chemical shifts of the hydrogens have been reversed, in order to account for the AB system exchange. To simulate the spectra at higher temperatures, the direct exchange between the AB system of the *syn* conformer (i.e. $k_{2\text{-}3}$) is always 0, and only $k_{1\text{-}2}$ and $k_{1\text{-}3}$ are optimized, with values corresponding to one half of that used for methyl simulation at the same temperature.

This exchange matrix corresponds, in practice, to exchange the *anti* conformer with the *syn* by rotation of a single aromatic ring, and *viceversa*.

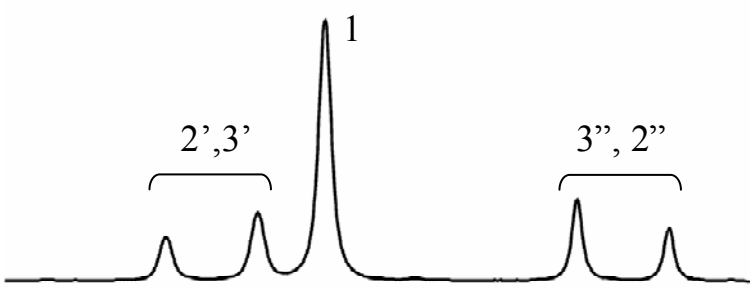

Simulated spectrum of compound **31** at +25°C

```
                                    ant-25.frq
                                    273
                                    1,2,3,0,2,0,1
Anti conformation 1          →      72.9,72.9      Singlet
                                    0.0
Syn conformation 2 (2' and 2")  →   48.,139.3
                                    -20.7          AB system
Exchanged Syn conformation 3 (3' and 3")  →  139.3,48.
                                    -20.7
                                    .53,.235,.235
                                    .093,.096,.096
k1-2  →                             0.
k1-3  →                             0.
k2-3  →                             0.
```

Figure 68: **Exchange matrix used in the simulation of the CH_2 signal of compound 31.**

On raising the temperature, the CH_2 signals of **31** display a line broadening effect due to the exchange of the *syn* and *anti* conformers (*Figure 67*): eventually these signals merge into a single line when the interconversion process becomes fast (above +110 °C). This exchange process can be also followed by monitoring the temperature dependence of the two single lines of the methyl groups (*Figure 69*), where the more intense line of the *anti* (53%) is at higher field than that of the *syn* conformer (47%). The methyl line of the *anti* is at higher field than that of the *syn* because it lies above the plane of the other aromatic ring, thus experiencing the well known effect of the aromatic ring currents.[44]

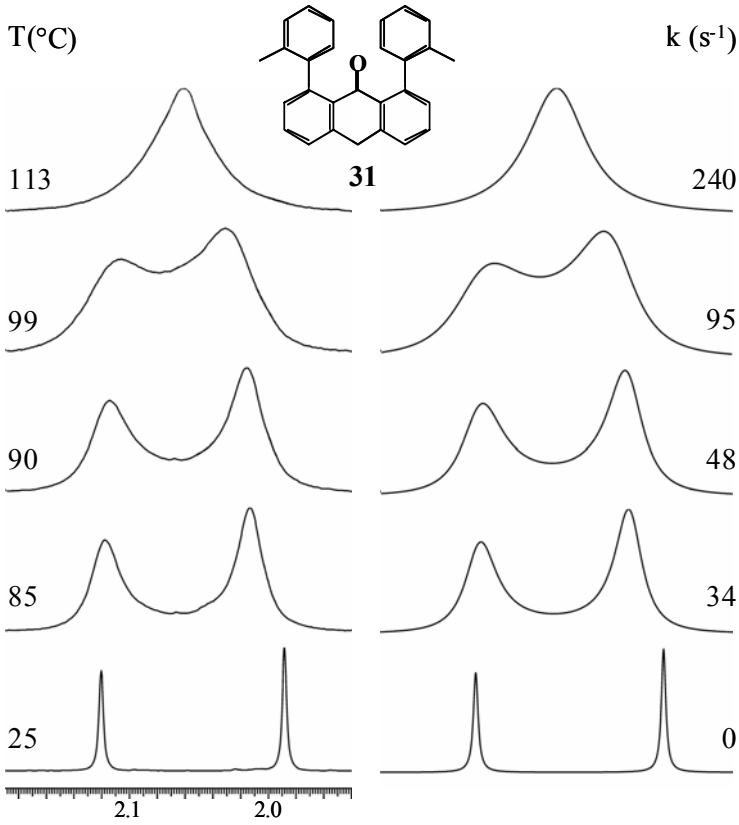

***Figure 69**:* **Left: Temperature dependence of the CH_3 signals (600 MHz in $CDCl_2$-$CDCl_2$) of *31*; Right: spectral simulation with the rate constants indicated.**

From the rate constants used to simulate the exchange process of the methyl lines (*Figure 69*), a $\Delta G^{\neq}$ value of 18.6 kcal mol^{-1} is obtained. As often observed in conformational processes, the free energy of activation is found independent of temperature within the errors, indicating a negligible value of $\Delta S^{\neq}$.[65c] This barrier corresponds to the interconversion of the *anti* into the *syn* conformer that, however, can take place *via* a rotation of either of the two tolyl rings. In order to obtain the barrier corresponding to the rotation of a single tolyl ring, the values of the rate constants reported should be divided by two:[24,97] the corresponding barrier is, accordingly, 0.5 kcal mol^{-1} higher ($\Delta G^{\neq}$ = 19.1 kcal mol^{-1} as in *Table 8*).

Table 8: **Conformer Ratio and *Anti* to *Syn* Interconversion Barrier (in kcal mol^{-1})[a] for Compounds *30-32*.**

Compd.	30	31	32
***Anti* : *Syn* ratio**	50: 50	53: 47	57 : 43
***Anti* to *Syn* barrier[a]**	20.7 (21.2) 20.3[b] (20.8)	18.6 (19.1)	18.7 (19.2)

a) The values in parenthesis refer to the rotation barrier of a single tolyl ring (see text).

b) Data obtained from 1D-EXSY experiments

Since the exchange of methylene hydrogens corresponds to two subsequent single rotations of the tolyl rings, this explains why the rate constants, introduced in the matrix for simulating the spectrum of *Figure 67*, are one half than those of *Figure 69* at the same temperature. In the case of **30**, where the methyl signals are accidentally coincident, the corresponding *anti* to *syn* interconversion barrier could be obtained, by dynamic NMR approach, only by monitoring the methylene signals (*Figure 70*).

The direct *anti* to *syn* interconversion can be also obtained by means of an independent method, based upon the use of the saturation transfer approach (1-D EXSY), which allows one to perform experiments at lower temperatures and to achieve rate constants much smaller than those obtainable by the DNMR method. This is accomplished by saturating the single CH_2 line of the *anti* conformer whereas observing the increasing of the CH_2 lines of the *syn* conformer. In this way (see as an example *Figure 71*) rate constants of 0.30, 0.44, 0.64 and 0.92 s^{-1} (at +59 °C, +63 °C, +67 °C and +72 °C, respectively) are determined for the *anti* to *syn* interconversion, corresponding to a $\Delta G^{\neq}$ value of 20.3 ± 0.2 kcal mol^{-1}. Within the experimental error, this value agrees with that obtained by the DNMR technique (*Table 8*).

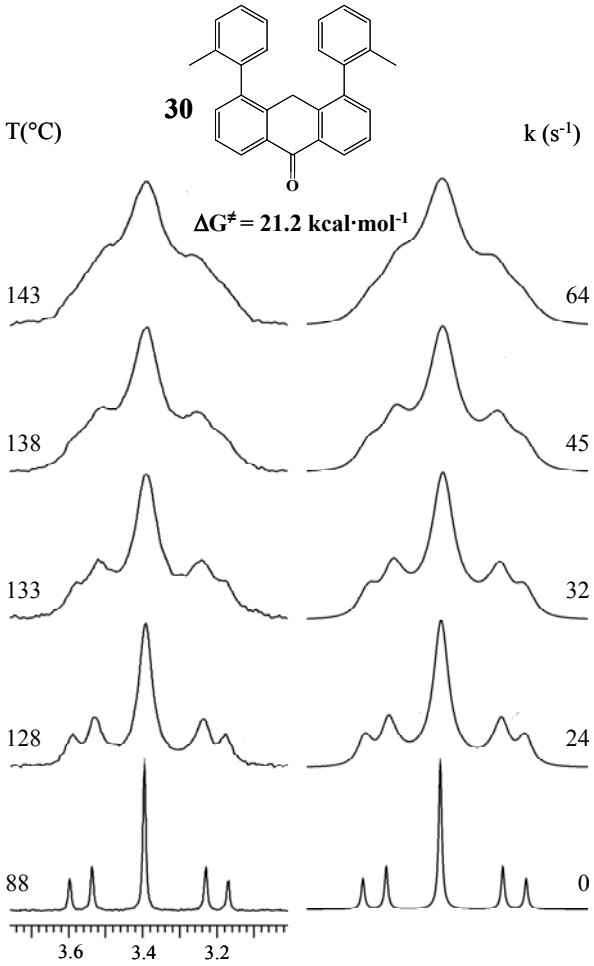

Figure 70: **Left: Temperature dependence of the CH_2 signal (400 MHz in $CDCl_2$-$CDCl_2$) of compound *30;* Right: spectral simulation with the rate constants indicated.**

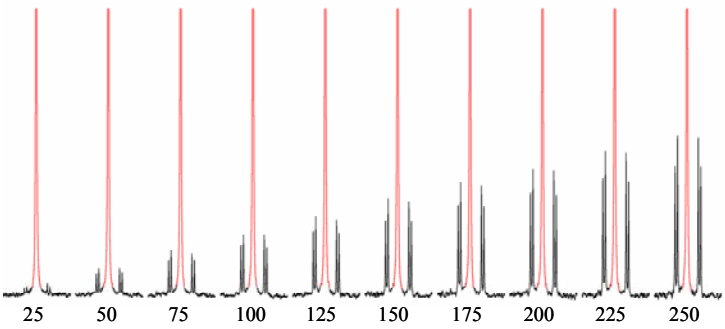

Figure 71: **Saturation transfer experiment (1D-EXSY) for compound *30* at +72 °C (600 MHz in $CDCl_2$-$CDCl_2$). The AB-type CH_2 spectrum (black trace) of the *syn* conformer grows when raising the mixing time (in ms), after saturation of the CH_2 *anti* single line (red signal).**

Also in compound 32 two atropisomers with different proportions (57:43) are observed at ambient temperature. Line shape simulation of the two methyl signal as function of temperature yields the corresponding interconversion barrier (*Figure 72*).

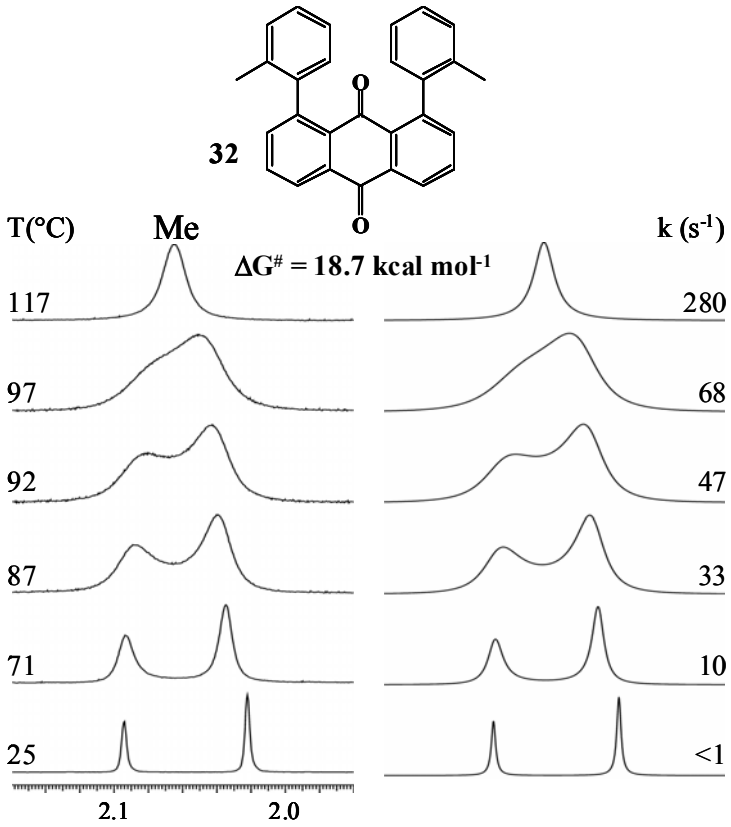

Figure 72: **Left: Temperature dependence of the Me signal (600 MHz in $CDCl_2$-$CDCl_2$) of compound *32*; Right; Spectral simulation with the rate constants indicated.**

In order to establish unambiguously whether in **32** the *anti* or the *syn* is more populated, a NOE experiment is performed (the temperature of –10 °C is used in order to avoid the effects of saturation transfer). Irradiation of the methyl signal of the *syn* conformer is expected to enhance two groups of signals, i.e. those of the hydrogens in positions 2,7 of the anthraquinone moiety and those of the hydrogens in position ortho to the methyl group (indicated as 3,3' in *Figure 73*).

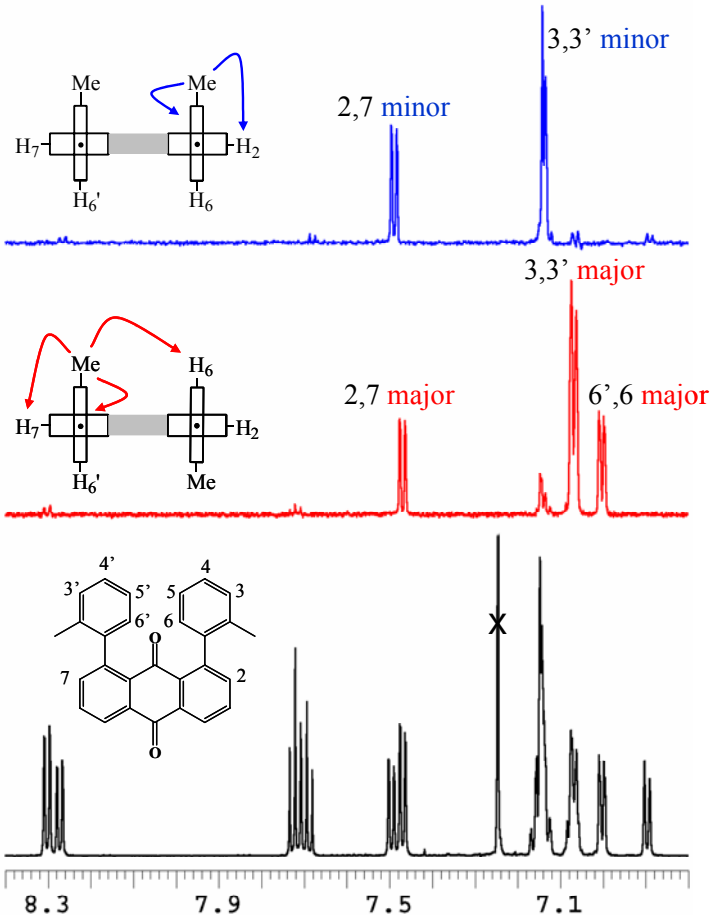

Figure 73: **Bottom trace, black: Aromatic spectral region (600 MHz at –10 °C in $CDCl_3$) of compound *32*; Middle trace, red: NOE experiments due to the irradiation of the major methyl signal at 1.98 ppm; Top trace, blue: NOE experiments due to the irradiation of the minor methyl signal at 2.08 ppm.**

Irradiation of the methyl signal of the *anti* conformer would enhance the same signals and, in addition, those of the hydrogens in positions 6' and 6 of the facing ring: in the *anti* atropisomer, in fact, the methyl in position 2 of one tolyl ring is close to the hydrogen in position 6' of the other tolyl ring (likewise the methyl in position 2' is close to the hydrogen in position 6 of the other tolyl). Since irradiation of the major methyl signal displays three significant NOE effects (red middle trace of *Figure 73*), the corresponding conformation is established to be *anti*. Whereas, the irradiation of the minor methyl signal, (top trace, blue) displays two significant NOE effects, which are attributed at the

hydrogens in positions 2,7 and 3,3'; therefore the corresponding conformation is established to be *syn*.

Again the DFT computations[15] of **32** predict the *syn* to have an enthalpy lower (by 0.19 kcal mol^{-1}) than the *anti* (*Figure 65*), but the mentioned correction for the entropy of mixing (RTln2) accounts for the greater population observed for the *anti* form: in this case, in fact, the ΔG^0 of the *anti* results to be lower (by 0.19 – 0.41 = –0.22 kcal mol^{-1}) than that of the *syn*.

In *Table 8* are summarised the results obtained for compounds **30-32**. The barriers of **31** and **32** are equal within the experimental error (± 0.2 kcal mol^{-1}), because in both cases the interconversion involves the passage of the tolyl ring across the C=O moiety. On the other hand the barrier of **30** is significantly higher because the corresponding interconversion requires the passage of the ring across the bulkier CH_2 moiety.

Configurationally stable atropisomers with the anthraquinone skeleton are quite interesting since this moiety can be easily functionalized, as seen above, so we synthesized an anthraquinone derivate bearing 2-methyl-1-naphtyl substituents in the 1,8 positions (compound **33** of *Scheme 10*).

This compound exists as the *syn* isomer (**33a**), which is a meso form (C_s point group), and the *anti* isomer (**33b**), which is racemic (C_2 point group), as shown in *Scheme 11*.

Scheme 11

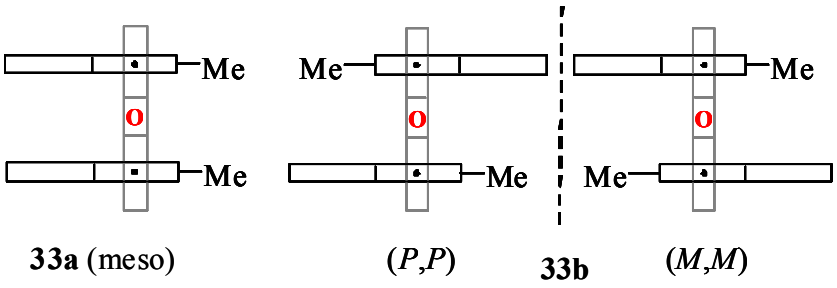

According to DFT calculations,[15] the barrier for the *anti* (**33b**) to *syn* (**33a**) interconversion is expected to be as high as 33.5 kcal mol^{-1}. Computations indicate the *anti*

to be 0.35 kcal mol^{-1} more stable than *syn* conformer. In the transition state required to accomplish their interconversion, the methyl group of one naphthalene ring crosses over the C=O moiety. The alternative transition state, where the methyl group crosses over the position 2 of anthraquinone, has a higher computed energy (37.7 kcal mol^{-1}) so that the corresponding pathway is not expected to take place.

In keeping with this prediction, these derivatives might be separated at ambient temperature using HPLC. It is worth noting that the two isolated isomers show different colours, the first eluted being red and the second eluted yellow. This particular behaviour is probably due to different interactions between the two naphthalene rings, that are face to face in the *syn*, but not in the *anti* isomer.

Structural assignment in solution is unambiguously achieved by ^{1}H NMR spectroscopy, making use of the NOE effect. This approach requires that the ^{13}C satellites of the methyl signal (J_{CH} = 126.3 Hz in both isomers) be simultaneously irradiated.[65c,78]

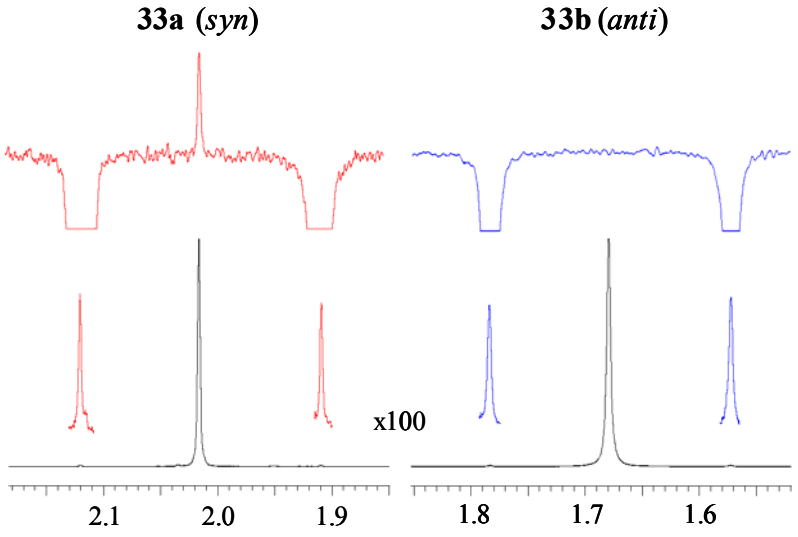

Figure 74: **Left: ^{1}H methyl signal of 33a (600 MHz in $CDCl_3$) with the 100-fold amplified ^{13}C satellites in the inset of the lower trace. The NOE effect, obtained by irradiating these satellites, is shown in the top trace (red). Right: methyl signal of 33b with the amplified ^{13}C satellites. The same experiment does not yield any NOE effect here (top trace, blue).**

When applied to the red isomer, this procedure yielded a significant NOE effect at the $^{12}CH_3$ signal, as displayed on the top left side of *Figure 74*. This proves that this isomer is 33a, with the *syn* meso structure (C_s point group), because the interproton distance between the two methyl groups (averaged[98] computed value 5.13 Å) is compatible with the detection of a NOE effect. On the contrary, such an effect is not seen in the case of the other (yellow) isomer, which is assigned the *anti* racemic structure 33b (*Figure 74*, top right) since in this form the two methyl groups are too far apart (averaged[98] computed distance 7.07 Å). This attribution agrees with the trend of the ^1H shift of the corresponding methyl groups, that of 33a (2.02 ppm) being at lower field with respect to that of 33b (1.68 ppm). The latter should thus correspond to the *anti* structure since its methyl groups lie in a position where they experience the upfield shift displacement due to the aromatic ring currents.[44] Also DFT computations[15] predict an upfield methyl shift for the *anti* (1.71 ppm) with respect to the *syn* (2.16 ppm), in agreement with the observed trend.

Single crystals suitable for X-ray diffraction are obtained in the case of *syn* **33a**, the corresponding structure (*Figure 75*, bottom) being quite similar to that predicted by DFT calculations (*Figure 75*, top left). Owing to the slight distortion due to the crystal lattice, however, **33a** does not display, in the solid state, a true C_s symmetry (the dihedral angles between the anthraquinone and naphthalene rings are, in fact, -77.0° and +81.8°).

M,*M* and *P*,*P* enantiomers of the *anti* form **33b** (*Scheme 11*) are separated by HPLC on two Chiralcel OD-H 250x4.6 mm columns joint together, at a flow rate of 1.0 mL/min, using hexane/iPr-OH 98:2 v:v as eluent (*Figure 76*, top). Comparison of the ECD spectrum computed for the *M*,*M* form (obtained by the TD-DFT method as implemented in the Gaussian program[15]) with that of the first eluted atropisomer, indicated that the latter has the absolute configuration *M*,*M* (*Figure 76*, bottom traces): the *P*,*P* configuration should be, consequently, assigned to the second eluted.

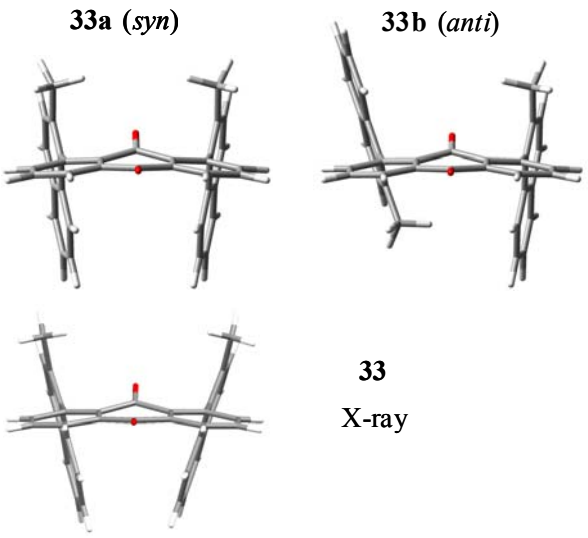

Figure 75: **Top: DFT computed ground state of the *syn* (*33a*) and *anti* (*33b*) isomers of *33*. Bottom: X-ray structure determined for *33a*.**

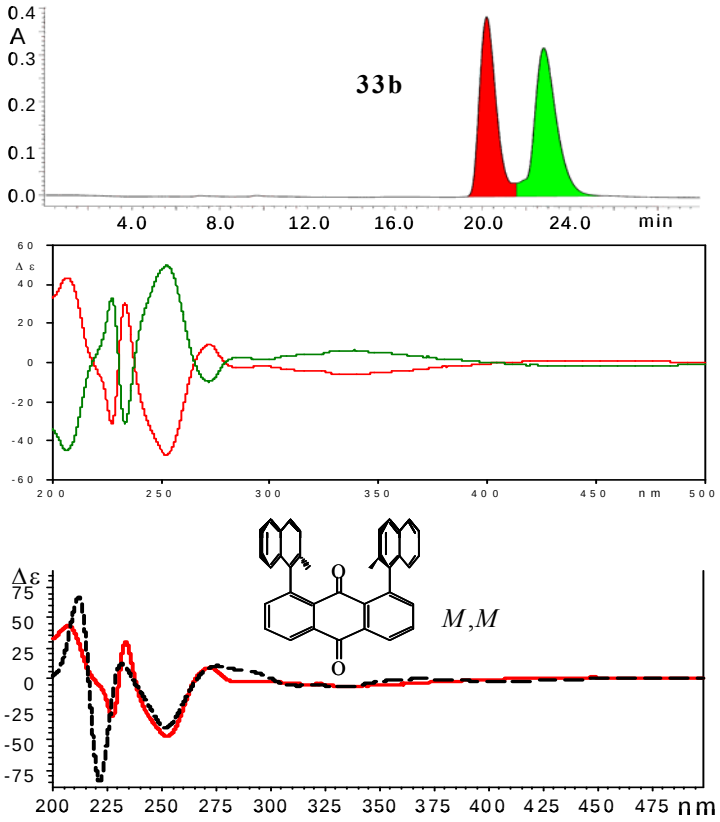

Figure 76: **Top: enantioselective HPLC trace of 33b (red, first eluted and green, second eluted atropisomer). Middle: experimental ECD spectra of the two atropisomers of 33b (red trace: first eluted; green trace: second eluted). Bottom traces: DFT computed ECD spectrum for the *M*,*M* configuration (dashed) and experimental spectrum (red) of the first eluted atropisomer.**

The kinetics for the *syn*/*anti* interconversion are determined by monitoring the time dependence of the NMR methyl signal of the pure *syn* isomer (33a) in a $(CDCl_2)_2$ solution, maintained at +140 °C. The signal of 33a decreases while that of the *anti* 33b begins to appear. The intensity of the latter increases until the equilibrium is reached at *anti* (33b) : *syn* (33a) = 59 : 41 (*Figure 77*). This ratio is matched by that (60/40) predicted by DFT calculations at +140°C.

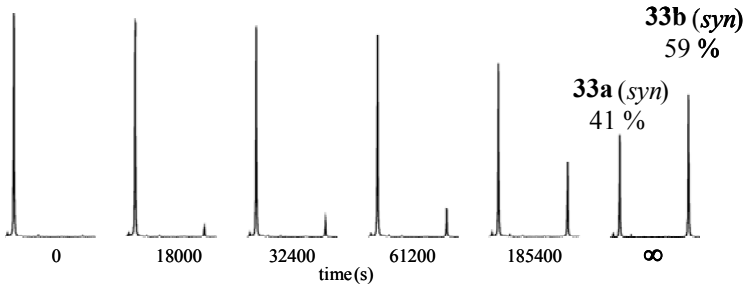

Figure 77: **Time dependence of the 600 MHz ^{1}H NMR methyl signal in $(CDCl_2)_2$ for the interconversion process at +140 °C.**

From the first order kinetics equation for a process at the equilibrium, the appropriate rate constant is obtained (details in *Figure 78*). The barrier for exchanging the more stable *anti* (**33b**) into the *syn* (**33a**) is then derived ($\Delta G^{\neq}$= 35.4 kcal mol^{-1} at +140 °C).

The mentioned computed value is in acceptable agreement with the experimental result. It has to be pointed out that the experimental interconversion is accomplished *via* the rotation of either of the two naphthalene rings, whereas the computed value is obtained assuming the rotation of only one ring. Thus, for an appropriate comparison the experimental rate constant should be divided by two.[97b,c] Accordingly, the value of the experimental barrier which actually corresponds to the rotation of a single ring becomes slightly higher, i.e. 35.9 kcal mol^{-1}.

time (s)	x	ln(xe-x)
0	0	-0.5276
3600	0.013	-0.5499
7200	0.020	-0.5621
11700	0.028	-0.5763
18000	0.038	-0.5942
25200	0.053	-0.6218
32400	0.068	-0.6501
46800	0.095	-0.7032
61200	0.119	-0.7529
128100	0.234	-1.0328
185400	0.300	-1.2379
243000	0.355	-1.4482
329400	0.420	-1.7720

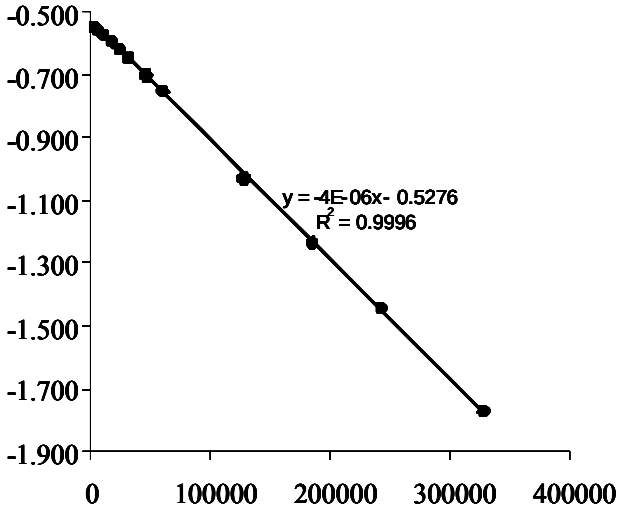

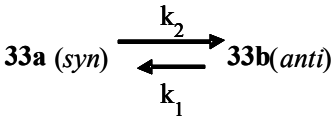

$\Delta G_1^{\#} = 35.4$ kcal mol^{-1}

$\Delta G_2^{\#} = 35.1$ kcal mol^{-1}

$\ln(x_e - x) = \ln x_e - (k_1 + k_2)t$

$k_1 + k_2 = 3.78 \cdot 10^{-6}$ s^{-1}

$k_2/k_1 = 1.439$

$k_2 = 2.23 \cdot 10^{-6}$ s^{-1}

$k_1 = 1.55 \cdot 10^{-6}$ s^{-1}

Figure 78: **Kinetics for the interconversion process of *33a* (*syn*) and *33b* (*anti*) in $(CDCl_2)_2$ at +140 °C.**

To check whether the high barrier and the configurational stability of the atropisomers of **33**, are dependent on the steric interactions between the two naphthyl groups, or whether a single naphthyl substituent is sufficiently large to allow the enantiomer separation, derivative **34** (*Scheme 10*) is also synthesized. The presence of two substituents might be responsible for the observed interconversion barrier as a consequence of a possible buttressing effect.

The ambient temperature ^{1}H NMR methyl signal of **34** (*Figure 79*) splits into two lines when recorded in the presence of a chiral solvating agent, (a separation of 5 Hz, (600 MHz at +25 °C) is observed in a CD_2Cl_2 solution when using a 37:1 molar excess of an enantiopure alcohol[50]), thus suggesting that the atropisomers of **34** are configurationally stable at ambient temperature.

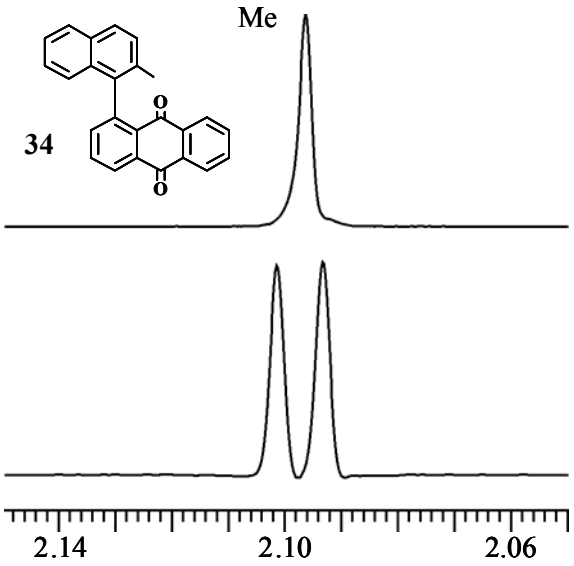

Figure 79: **Top: Single ^{1}H methyl line (600 MHz in CD_2Cl_2) of *34* Bottom: splits, at ambient temperature, into two equally intense lines in a chiral environment.**

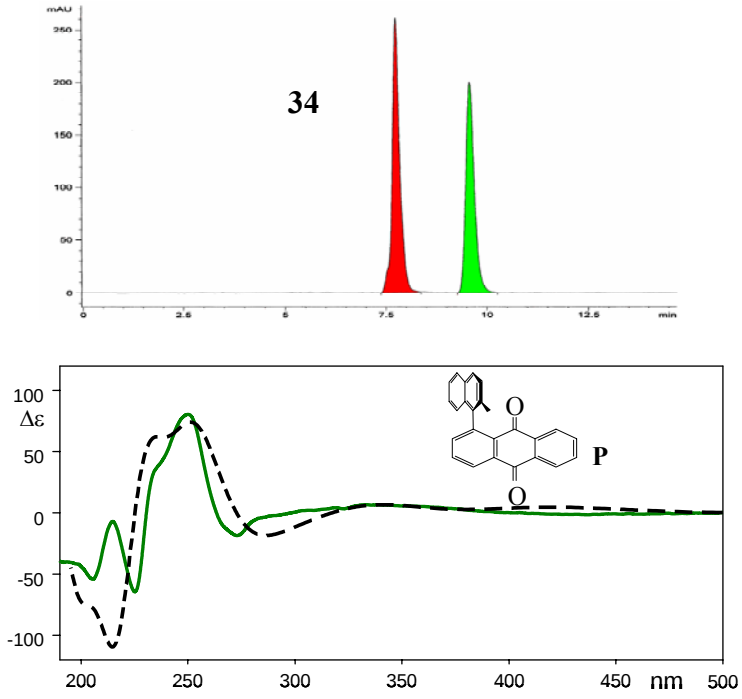

Figure 80: **Top: Enantioselective HPLC separation of the two atropisomer of *34*. Bottom: Experimental (green trace) ECD spectrum of the second eluted atropisomer, and computed (B3LYP/6-31+G(d,p)//B3LYP/6-31G(d) level) CD spectrum (dashed black line) obtained by assuming Gaussian band-shapes (σ = 0.5 eV) for the absolute configuration *P* of *34*. The calculated spectrum is red-shifted by 5 nm.**

The *P* and *M* antipodes are separated by means of HPLC on a Chiralcel AD-H column, with hexane/iPrOH 90:10 v/v as eluent and the oppositely phased ECD spectra recorded. Comparison of the computed[54] ECD trace for the *P* form with that of the second eluted atropisomer (*Figure 80*) indicates that the latter has the absolute configuration *P*.

The racemisation rate constant is determined by following the decreasing proportion of the enantiopure *P* form, kept at +140 °C in a $(CDCl_2)_2$ solution, accompanied by the increasing amount of the *M* atropisomer. The process is monitored by recording the corresponding HPLC trace on aliquotes of the solution, until the *P* and *M* peaks showed equal intensity, indicating that a complete racemisation is achieved (*Figure 81*).

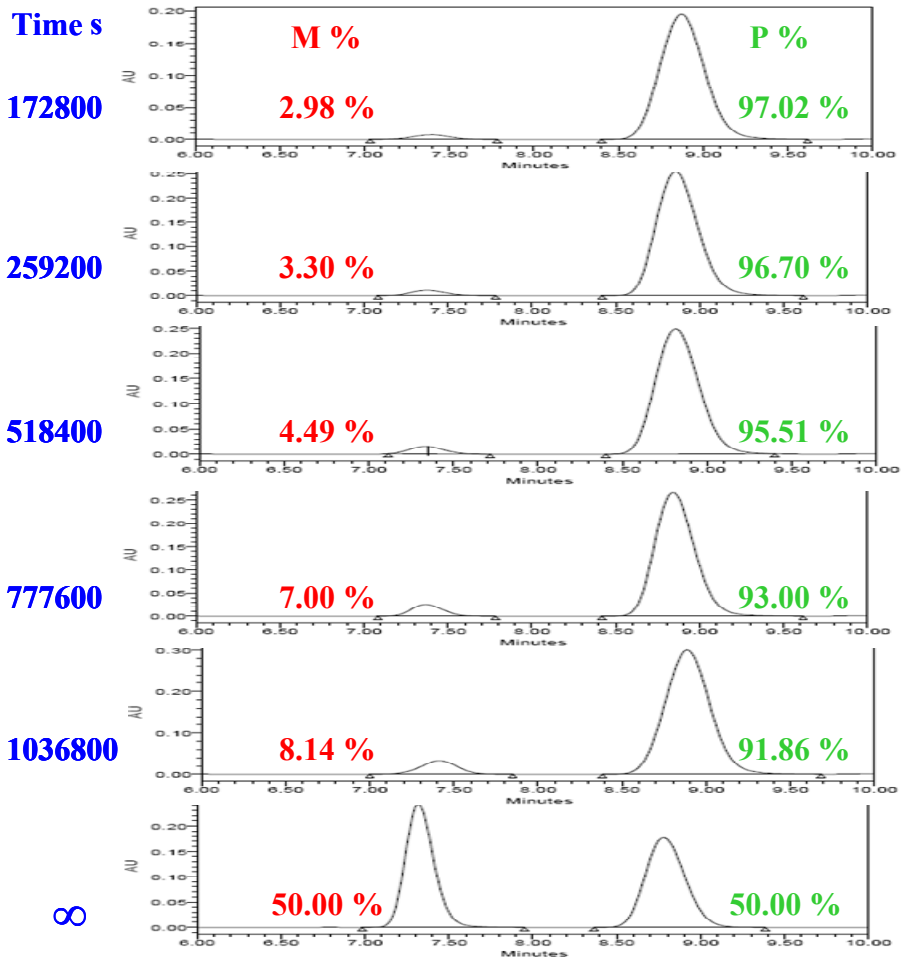

Figure 81: **Time dependence of the traces HPLC (chiralcel AD-H, 90:10 hexane/*i*PrOH v/v) for the interconversion process of *34* starting from pure *34*(*P*) in $(CDCl_2)_2$ at +140 °C.**

From the first order kinetics equation for a process at equilibrium, the appropriate rate constant is obtained (details in *Figure 82*).

time (s)	x	ln(xe-x)
0	0.0155	-0.7246
72000	0.0200	-0.7340
172800	0.0300	-0.7550
259200	0.0330	-0.7614
518400	0.0480	-0.7941
777600	0.0699	-0.8437
1036800	0.0815	-0.8711

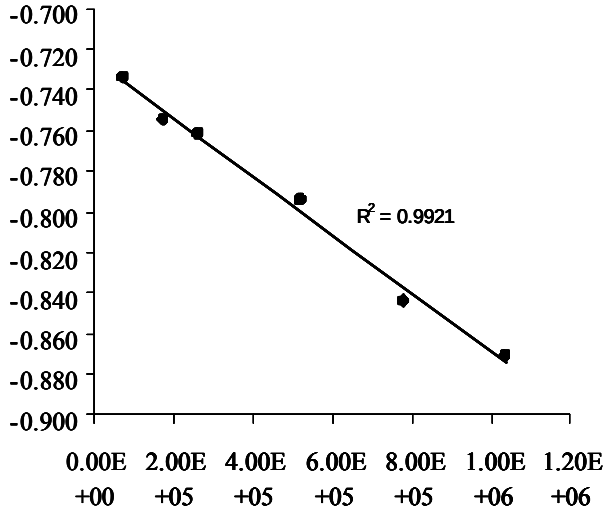

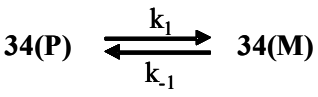

$\ln(x_e-x) = \ln x_e - (k_1+k_{-1})t$

$k_1+k_{-1} = 1.29 \cdot 10^{-7}\ s^{-1}$

$k_1 = 0.64 \cdot 10^{-8}\ s^{-1}$

$\Delta G_1^{\#} = 38.0$ **kcal mol^{-1}**

Figure 82: **Kinetics for the racemization process of *34* starting from pure *34*(*P*) in $(CDCl_2)_2$ at +140 °C.**

The experimental racemisation barrier of **34** ($\Delta G^{\neq}$ = 38.0 kcal mol^{-1} at +140 °C) is reasonably well reproduced by the computed value (35.6 kcal mol^{-1}) and is close to the interconversion barrier measured in the case of **33**. This indicates that the configurational stability of these atropisomers is essentially due to the steric interaction between a single methylnaphthyl substituent and the carbonyl group of the anthraquinone moiety, rather than to the interaction between the two substituents.

4.2 Anthracenes:

By reduction of anthraquinone moiety, anthracenes and so compounds **35** and **36** were prepared (*Scheme 10* and experimental data). Some time ago House and co-workers[99] measured, by variable temperature NMR spectroscopy, the rotation barriers of 1,8-diarylanthracene derivatives. The values, reported as activation energies derived from the Arrhenius equation, were unusually low with respect to the expectation for this type of compounds, being 5.3 and 10.4 kcal mol^{-1} for compounds **35** and **36**, respectively. The authors themselves were surprised by such incredibly low values and a few years later published a paper[100] where a possible explanation was proposed.

The energy surface of compound **35**, computed[101] by M.M. methods, as function of the anthracene-tolyl torsion angle φ (*Figure 83*), shows that the rotation pathways interconverting the trans and the *cis* conformers (indicated by red lines) run parallel to the respective axes, indicating that the two motions are independent of each other and the processes, accordingly, are not correlated.[28g,102]

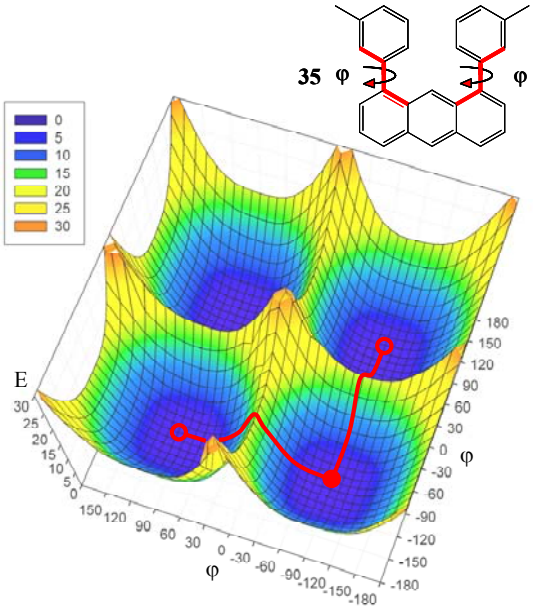

Figure 83: **Energy surface (E in kcal mol^{-1}) and rotation pathways computed[101] as function of the two torsion angles (φ) about the tolyl-anthracene bonds of derivative *35*. The full and hollow dots represent the trans and the cis conformer, respectively.**

The rotation barrier is calculated to be much larger (about 16 kcal mol^{-1}) than the reported[99] value. Such a theoretical value is refined using the more reliable DFT approach,[15] that likewise indicated the trans to be more stable than the cis (by 0.2 kcal mol^{-1} as in *Figure 84*) and predicted again the existence of a sp^2-sp^2 rotation barrier (12.2 kcal mol^{-1}) significantly larger than one reported in the literature (5.3 kcal mol^{-1}).[99] A similar value have been also calculated[103] (12.9 kcal mol^{-1}) for the sp^2-sp^3 rotation barrier in an anthracene substituted by two CF_3CHOH groups in positions 1 and 8, although in that case an experimental determination to confirm the theoretical prediction have not been provided.

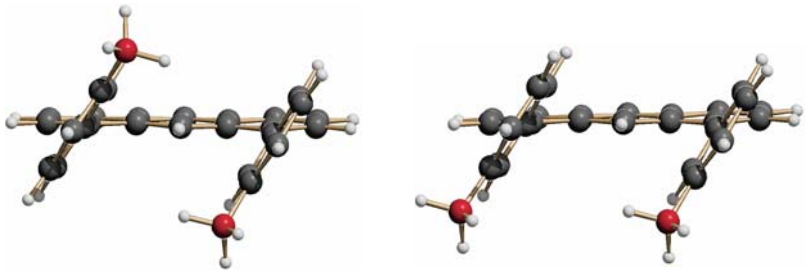

35-trans
(E = 0.0 kcal mol^{-1})

35-cis
(E = 0.2 kcal mol^{-1})

Figure 84: **DFT computed structures of the trans and cis conformers of 35: (Methyl groups are shown as red for convenience).**

Contrary to the case of biphenylenes (see *chapter 3*), the small amplitude torsion due to π-barrier of the tolyl ring about the orthogonal situation has a very small barrier (less than 1 kcal mol^{-1}), so that in the NMR time-scale the trans displays a dynamic C_2 (chiral) and the cis a dynamic C_s (achiral) symmetry.

Also the DFT computed[15] barrier of **36** (20.8 kcal mol^{-1}) turned out to be much higher than 10.4 kcal mol^{-1}.[99,100] Since the values derived from these calculations are seemingly at huge variance with the experimental data, accurate verification of the previous experiments has been carried out by taking advantage of a better instrumentation than available in the past. Compounds **35** and **36** are selected for this purpose because the

determinations of the corresponding barriers could be carried out both in the low temperature (compound **35**) and in the high temperature (compound **36**) range.

As shown in *Figure 85* (left) the ^{1}H NMR spectrum of **35** (600 MHz in CD_2Cl_2) at –77 °C displays two methyl signals with different intensities, the ratio being 63:37. The more intense downfield signal is assigned to the chiral trans conformer, following the prediction of the above mentioned DFT computations (*Figure 84*).

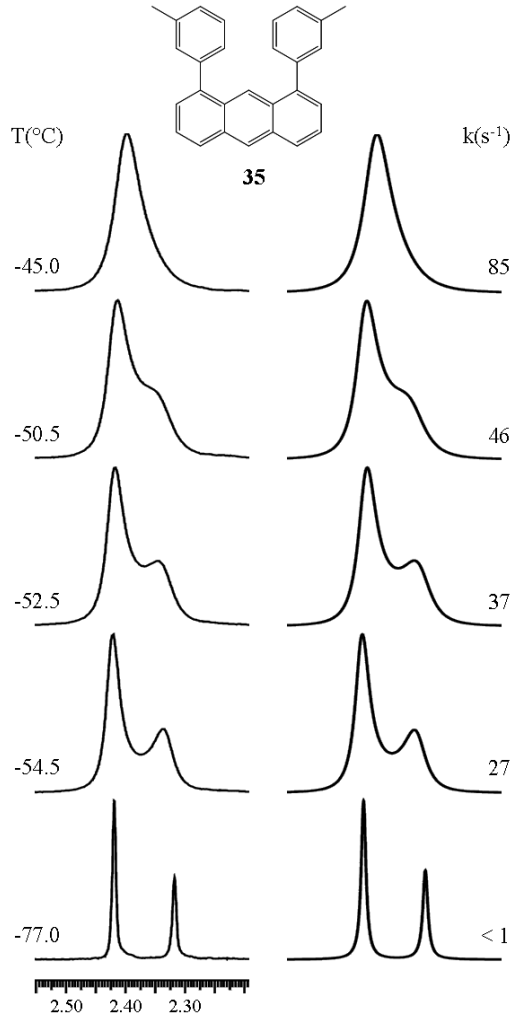

Figure 85: **Left: ^{1}H NMR methyl signals of compound *35* (600 MHz in CD_2Cl_2) as function of temperature. Right: line shape simulation obtained with the rate constants indicated.**

The computer line shape simulation[104] of these lines is performed at ten significant temperatures in the range –66 °C to –45 °C: a few selected sample traces are reported in *Figure 85* (right). Also the aromatic hydrogen in position 9 yields two signals with the same 63:37 ratio, and these are likewise simulated at the same temperatures where the methyl lines have been examined. Equal values for the rate constants are obtained in both cases, thus providing an independent check of the accuracy of the present data. The ten rate constants obtained in this way (*Table 9*) allowed us to derive the activation parameters using both the Eyring and Arrhenius equations.

Table 9: **Rate Constants (k, s^{-1}) for the trans to cis Interconversion of the Conformers of *35*, as Obtained by the Simulation of the NMR Spectra at Various Temperatures (°C).**

Temp.	-66	-61	-59	-58	-57	-55.5	-54.5	-52.5	-50.5	-45
k	6.	12.5	15.	17.	20.	23.	27.	37.	46.	85.

The corresponding data are collected in *Table 10* and, as often observed in the dynamics of conformational processes, the $\Delta S^{\neq}$ value results to be negligible[19] within the experimental uncertainty. From our experiment it is quite evident that the interconversion barrier, indicated either as $\Delta G^{\neq}$, $\Delta H^{\neq}$, or E_a, is in good agreement with the DFT calculations but is more than twice as large as the 5.3 kcal mol^{-1} of the previous experiments.[99] Since the trans to cis conversion can be accomplished by rotation of either of the two tolyl rings, the rotation rate of a single ring corresponds to half of the measured rate constants. The corresponding $\Delta G^{\neq}$, $\Delta H^{\neq}$ and E_a thus become, in this case, 0.3 kcal mol^{-1} higher (i.e. 11.5, 11.8 and 12.2 kcal mol^{-1}, respectively) and are these values that, in principle, should be compared to the theoretical rotation barrier of 12.2 kcal mol^{-1}.[97b]

Distinguishable NMR methyl signals for the *cis* and *trans* conformers of **36** are observed at ambient temperature, the up-field signal displaying a slightly higher intensity, i.e. 54% in $CDCl_3$ and 53% in dimethylformamide-d7 (DMF-d_7).

Table 10: **Experimental Activation Parameters for Compounds *35* and *36* ($\Delta G^{\neq}$, $\Delta H^{\neq}$, E_a in kcal mol^{-1}, $\Delta S^{\neq}$ in cal mol^{-1} T^{-1}). The Value in Parenthesis is the Estimated Uncertainty.**

Compound	$\Delta G^{\neq}$	$\Delta H^{\neq}$	$\Delta S^{\neq}$	E_a	Log A
35	11.22 (0.02)	11.45 (0.2)	1.1 (1.0)	11.9 (0.2)	13.3 (0.2)
36	21.30 (0.03)	21.0 (0.3)	-0.75 (1.0)	21.8 (0.3)	13.2 (0.2)

DFT calculations[15] indicate that the cis form has an energy 0.25 kcal mol^{-1} higher than the trans, suggesting again that the latter should be the more stable conformer. It should be pointed out, however, that the relative proportions of the trans and cis conformers are nearly equal in this case, thus making less reliable an assignment based solely on theoretical considerations.

Following the procedure reported[78] for the assignment of symmetric isomers, the ^{13}C satellite spectra of the methyl signals of each of the two conformers are irradiated, using the DPFGSE-NOE sequence.[105] As shown in *Figure 86* (trace b), irradiation of the satellites of the less intense low field signal yields a substantial NOE effect, indicating that this signal corresponds to the cis conformer, where the hydrogens of the two methyl groups are sufficiently close (computed average distance 4.60 Å) as to experience a reciprocal NOE enhancement.

On the other hand, irradiation of the satellites of the more intense upfield signal (trace c) does not produce any NOE effect, indicating that this corresponds to the trans conformer, where the hydrogens of the two methyl groups are too far apart (computed average distance 6.94 Å) to experience the reciprocal NOE enhancement. These experimental results confirm, therefore, the theoretical assignment.

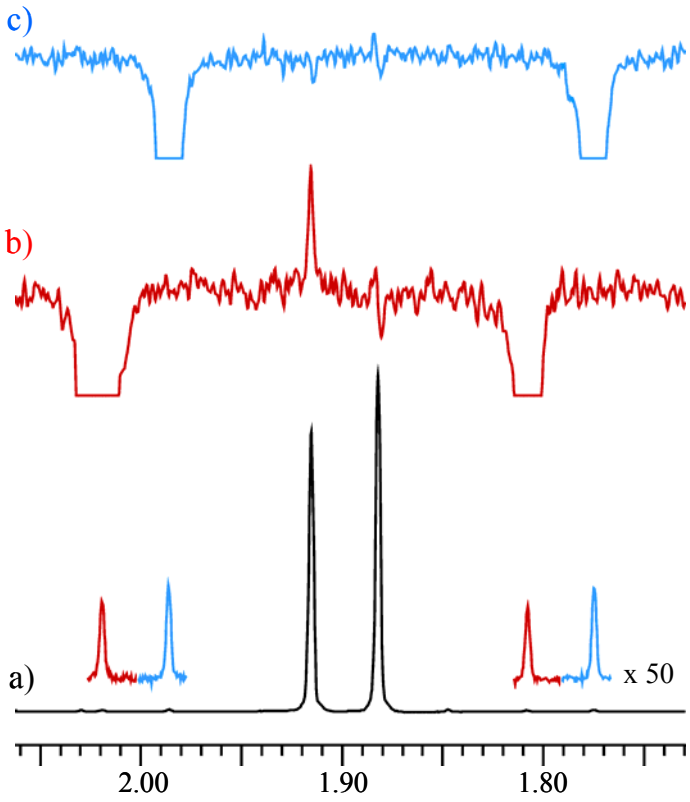

Figure 86: **Traces**

a) Methyl signals (^{1}H, 600 MHz) of *36* in $CDCl_3$ at 0°C,[13] displaying in the inset the ^{13}C satellite signals.

b) spectrum obtained by irradiating the satellites of the downfield line.

c) spectrum obtained by irradiating the satellites of the upfield line.

As shown in *Figure 87* (left), the two methyl signals of **36** broaden on raising the temperature (in DMF-d_7 as solvent), eventually coalescing into a single line. Line shape simulation (*Figure 87*, right) provides the corresponding rate constants for the trans to cis interconversion.

Twelve such rates are determined in the range +104 °C to +136 °C (*Table 11*) and from these values the activation parameters collected in *Table 10* are obtained. As discussed above, the rotation of a single tolyl group of **36** has, in this case, activation parameters 0.5 kcal mol^{-1} higher.

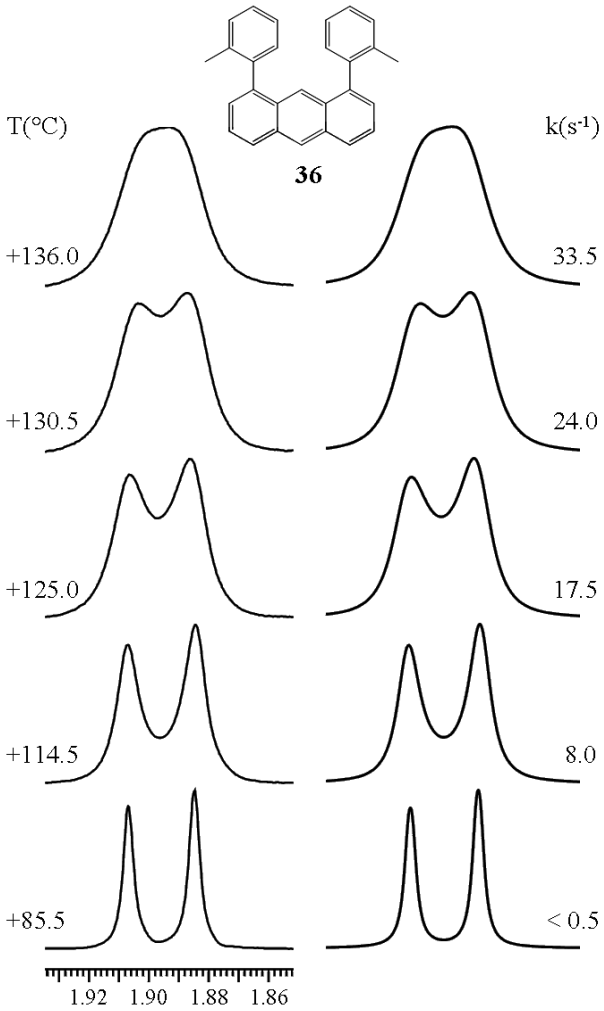

Figure 87: **Left: ^{1}H NMR methyl signals of compound *36* (600 MHz in DMF-d_7) as function of temperature. Right: line shape simulation obtained with the rate constants indicated.**

Table 11: **Rate Constants (k, s^{-1}) for the trans to cis Interconversion of the Conformers of *36*, as Obtained by the Simulation of the NMR Spectra at Various Temperatures (°C).**

Temp	+104	+107.5	+111	+114.5	+118	+121.5
k	3.3	4.7	6.3	8.	10.5	13.5

Temp	+125	+129	+130.5	+132.5	+134	+136
k	17.5	22.0	24.0	27.0	30.0	33.5

The experimental barrier, see *Table 10*, agrees well with that predicted by the DFT computations and is at least twice as large as the 10.4 kcal mol^{-1} previously reported.[99,100]

It is therefore demonstrated that the unusually low values quoted for the barriers of **35** and **36** are the consequence of measurements of insufficient accuracy, so that it is not necessary to propose any explanation to justify barriers that actually are in keeping with the expectations. For instance, the barrier of **35** lies in the same range as that of biphenyls bearing a single substituent of analogous size in the ortho position,[37] and that of **36** lies in the same range as that of biphenyls bearing two substituents of analogous size in the ortho, ortho' positions.[25]

4.3 Conclusions

Syn and *anti* conformers in similar proportions are observed at ambient temperature for compounds **30**, **31**, **32**. The conformational assignment of the two anthrones is obtained by the observation of different multiplicity of the methylene NMR signals, whereas that of the anthraquinone derivative is determined by NOE experiments. The *anti* to *syn* interconversion barriers are obtained by line shape simulation of the temperature dependent NMR spectra, and by saturation transfer experiments. In one case the X-ray diffraction indicated that the *syn* is the only structure observed in the crystals.

Anthraquinone substituted by 2-methyl-1-naphthyl groups in positions 1,8 (**33**) yields *syn* (meso) and *anti* (racemic) isomers (red and yellow colored, respectively) that interconvert with a barrier of 35.4 kcal mol^{-1} in solution.

Their structures are identified by NOE experiment in solution and X-ray diffraction in the solids. The racemic *anti* form (C_2 point group) entails two atropisomers that are separated by enantioselective HPLC: the absolute configuration is assigned by TD-DFT simulation of the ECD spectrum. Two atropisomers are also separated and assigned in the case of anthraquinone bearing a single 2-methyl-1-naphthyl substituent in position 1 (**34**).

The rotation barriers of two 1,8-ditolylanthracene derivatives (**35**, **36**) have been measured by accurate line shape simulation of their variable temperature NMR spectra. Both values are found to be more than twice as large as those previously reported in the literature.

4.4 Experimental Section

4.4.1 Preparation of 1,8-di-(o-tolyl)anthracene-9,10-dione (32). To a solution of 1,8-dichloroanthraquinone (0.277 g, 1.0 mmol, in 10 ml of benzene), K_2CO_3 (2M solution, 5.0 ml), ortho-tolylboronic acid (2.0 mmol, suspension in 2 ml of ethanol), and $Pd(PPh_3)_4$ (0.23g, 0.2 mmol) were added at room temperature. The stirred solution was refluxed for 2-3 h, the reaction being monitored by GC-MS to confirm the first coupling had been achieved. After cooling to room temperature, a second amount of K_2CO_3 (2M solution, 5.0 ml), ortho-tolylboronic acid (2.0 mmol, suspension in 2 ml of ethanol), and $Pd(PPh_3)_4$ (0.12g, 0.1 mmol) were added, and the mixture was refluxed again and monitored by GC-MS, until the mono-chloro intermediate disappeared. On the cooled mixture $CHCl_3$ and H_2O were added and the extracted organic layer was dried (Na_2SO_4) and evaporated. The crude was prepurified by chromatography on silica gel (Hexane/Et_2O 10:1) to obtain a mixture containing the target compound contaminated by 1-(o-tolyl)-anthraquinone and 1-chloro,8-(o-tolyl)-anthraquinone. Analytically pure **32** was obtained by semipreparative HPLC on a C18 column (10μm, 250x21.2 mm, 24 ml/min, ACN/H_2O 90/10 v/v).

1,8-di-(o-tolyl)anthracene-9,10-dione (32) ^{1}H NMR (600 MHz, $CDCl_3$, 25°C, TMS): δ 1.95 (3.66H, s), 2.05 (2.76H, s), 6.90 (0.88H, d, *J* = 6.9 Hz), 7.00 (1.23H, m), 7.07 (2.12H, m), 7.15 (4.25H, m), 7.47 (1.14H, dd, *J* = 7.6, 1.3 Hz), 7.50 (0.86H, dd, *J* = 7.6, 1.2 Hz), 7.69 (0.86H, t, *J* = 7.6 Hz), 7.72 (1.14H, t, *J* = 7.6 Hz), 8.27 (0.86H, dd, *J* = 7.7, 1.2 Hz), 8.30 (1.14H, dd, *J* = 7.7, 1.2 Hz). ^{13}C NMR (150.8 MHz, $CDCl_3$, 25°C,

TMS): δ 20.27 (CH_3), 20.31 (CH_3), 125.2 (CH), 125.3 (CH), 126.2 (CH), 126.4 (CH), 127.1 (CH), 127.2 (CH) 127.8 (CH), 128.6 (CH), 129.6 (CH), 129.8 (CH), 131.8 (CH), 132.3 (CH), 133.89 (q), 133.91 (q) 134.2 (q), 134.4 (q), 134.6 (q), 134.8 (q), 137.21 (CH), 137.27 (CH), 140.3 (q), 140.6 (q), 142.48 (q), 141.54 (q), 184.0 (CO), 184.1(CO), 184.6 (CO), 185.5 (CO) HRMS(EI): *m/z* calcd for $C_{28}H_{20}O_2$: 388.14633; found 388.1462. HPLC: 5 ml/min ACN/H_2O 90/10 v/v RT = 10.96 min.

4.4.2 4,5-di-(o-tolyl)-anthracen-9(10H)-one (30) and **1,8-di-(o-tolyl)-anthracen-9(10H)-one (31)** were obtained by the Wolf-Kishner reduction[106] of **32**: Hydrazine hydrate (1 mL) and KOH (50 mg, solid) were added to a solution of 1,8-di-(o-tolyl)-anthracene-9,10-dione (100 mg, 0.257 mmol) in a flask equipped with a Dean-Stark apparatus. The stirred solution was refluxed in a oil bath kept at 200°C for about 3 hours, removing the water during the reaction. The brown cooled mixture was extracted with Et_2O, and the extracted organic layer was dried (Na_2SO_4) and evaporated. The crude was pre-purified by chromatography on silica gel (Hexane/Et_2O 1:1) to obtain a mixture containing the target compounds (in a 1:4 ratio, yield 55%) together with the starting product. Analytically pure samples of **30** and **31** were obtained by semipreparative HPLC on a C18 column (5µm, 250x10 mm, 5 ml/min, ACN/H_2O). Crystals of **30** suitable for X-ray analysis were obtained by slow evaporation of a $CHCl_3$ solution.

4,5-di-(o-tolyl)-anthracen-9(10H)-one (30): ^{1}H NMR (600 MHz, $CDCl_3$, 25°C, TMS): δ 1.94 (3H, s), 2.08 (3H, s), 4.23 (0.5H, d, *J* = -20.7 Hz), 4.34 (s, 1H), 4.39 (0.5H, d, *J* = -20.7 Hz), 6.85 (1H, d, *J* = 7.6 Hz), 6.98-7.18 (9H, m), 7.40-7.50 (4H, m). ^{13}C NMR (150.8 MHz, $CDCl_3$, 25°C, TMS): δ 20.51 (CH_3), 20.54 (CH_3), 34.3 (CH_2), 34.4 (CH_2), 124.84 (CH), 124.87 (CH), 126.56 (CH), 126.57 (CH), 126.6 (2CH), 126.8 (2CH), 128.0 (CH), 128.7 (CH), 129.2 (CH), 129.6 (CH), 129.8 (CH); 129.9 (CH), 130.2 (CH), 130.8 (CH), 133.3 (q), 134.1 (q), 134.9 (q), 135.2 (q), 139.6 (q), 139.8 (q), 140.9 (q), 141.5 (q),

141.8 (q), 142.2 (q), 185.9 (CO), 187.2 (CO). HRMS(EI): *m/z* calcd for $C_{28}H_{22}O$: 374.16707; found 374.1674. HPLC: RT = 14.39 min

Crystal Data

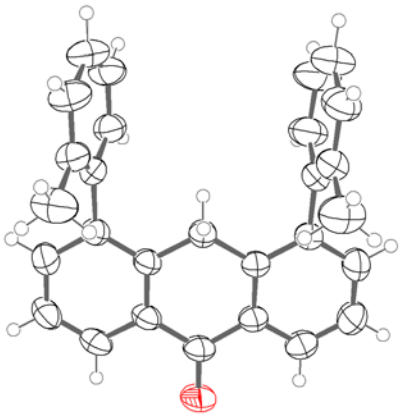

Molecular formula: $C_{28}H_{22}O$, M_r = 374.17, Triclinic, space group P-1 (No. 2), a = 7.5933(10), b = 10.1784(13), c = 15.0517(19) Å, α= 71.664(2), β=76.411(2), γ=72.426(2). V = 1040.0(2) Å^3, T = 295(2) K, Z = 2, ρ_c = 1.285 g cm^{-3}, F(000) = 424, graphite-monochromated Mo$_{K\alpha}$ radiation (λ = 0.71073 Å), μ(Mo$_{K\alpha}$) = 0.078 mm^{-1}, colourless plate (0.2 × 0.2 × 0.1 mm^3), empirical absorption correction with SADABS (transmission factors: 0.9922 – 0.9845), 2400 frames, exposure time 20 s, $1.44 \le \theta \le 28.64$, $-10 \le h \le 10$, $-13 \le k \le 13$, $-19 \le l \le 19$, 12113 reflections collected, 4876 independent reflections (R_{int} = 0.0220), solution by direct methods (SHELXS97[32]) and subsequent Fourier syntheses, full-matrix least-squares on F_o^2 (SHELX97[32]), hydrogen atoms refined with a riding model, data / restraints / parameters = 4876 / 0 / 283, $S(F^2)$ = 1.065, $R(F)$ = 0.0833 and $wR(F^2)$ = 0.2009 on all data, $R(F)$ = 0.0606 and $wR(F^2)$ = 0.1818 for 3384 reflections with $I > 2\sigma(I)$, weighting scheme $w = 1/[\sigma^2(F_o^2) + (0.1029P)^2 + 0.1627P]$ where $P = (F_o^2 + 2F_c^2)/3$, largest difference peak and hole 0.422 and –0.274 e Å^{-3}. The unit cell contains also 10-hydrazinyl-4,5-dio-tolylanthracen-9(10H)-one as co-crystallized impurity, that was taken

into account as a separate part of the main molecule, and refined using anisotropic displacement parameters restraints.

1,8-di-(o-tolyl)-anthracen-9(10H)-one (31): ^{1}H NMR (600 MHz, $CDCl_3$, 25°C, TMS): δ 1.907 (3H, s), 1.911 (3H, s), 3.14 (0.5H, d, *J* = -24.0 Hz), 3.34 (s, 1H), 3.51 (0.5H, d, *J* = -24.0 Hz), 6.94 (2H, m), 7.06-7.18 (6H, m), 7.40 (2H, dt, *J* = 7.3, 1.7 Hz), 7.52 (2H, t, *J* = 7.7 Hz), 8.40 (2H, d, *J* = 8.4 Hz). ^{13}C NMR (150.8 MHz, $CDCl_3$, 25°C, TMS): δ 19.57 (CH_3), 19.59 (CH_3), 29.6 (CH_2), 29.8 (CH_2), 125.6 (CH), 125.7 (CH), 126.6 (CH), 126.8 (CH), 127.6 (2CH), 128.6 (CH), 128.7 (CH), 129.8 (CH), 129.9 (CH), 132.03 (q), 132.04 (q), 133.4 (2CH) 135.0 (q), 135.2 (q), 138.7 (q), 138.8 (q), 139.04 (q), 139.05 (q), 141.45 (q), 141.47 (q), 184.79 (CO), 184.83(CO). HRMS(EI): *m*/*z* calcd for $C_{28}H_{22}O$: 374.16707; found 374.1672. HPLC: RT = 12.26 min.

4.4.3 1,8-bis(2-methylnaphtyl)anthraquinone (33). To a solution of 1,8-dichloroanthraquinone (0.056 g, 0.2 mmol, in 3 ml of benzene) K_2CO_3 (2M solution, 1.0 ml), 2-methylnaphthylboronic acid[107] (0.6 mmol, 0.110 g, suspension in 3 ml of ethanol), and $Pd(PPh_3)_4$ (0.046 g, 0.04 mmol) were added at room temperature. The stirred solution was refluxed for 2-3 h, the reaction being monitored by GC-MS until the first coupling was complete. After cooling to room temperature, a second amount of boronic acid (0.6 mmol), K_2CO_3 (2M solution, 1.0 ml) and $Pd(PPh_3)_4$ (0.046 g, 0.04 mmol) were added, and the solution refluxed again for 2-3 h. Subsequently $CHCl_3$ and H_2O were added and the extracted organic layer was dried (Na_2SO_4) and evaporated. The crudes were pre-purified by chromatography on silica gel (Hexane/Et_2O 8:2) to obtain purified mixtures containing the target compounds, and some by-products as impurities. Pure samples of meso **33a** (red crystals) and racemic **33b (**yellow powder) were obtained by semi-preparative HPLC on a C18 column (5μm, 250x10 mm, 5 ml/min, ACN/H_2O 90/10). Single crystals of **33a**, suitable for X-ray diffraction, were obtained by slow evaporation of a chloroform solution.

***Anti*-1,8-bis(2-methylnaphtyl)anthraquinone, (33b)** : m.p. 255-257 (dec.), ^{1}H-NMR (600 MHz, $CDCl_3$, 25°C, TMS): δ 1.69 (6H, s), 6.96 (2H, d, J = 8.4 Hz), 7.02 (2H, d, J = 8.5 Hz), 7.18 (2H, t, J = 7.6 Hz), 7.32 (2H, d, J = 7.4 Hz), 7.41 (2H, d, J = 7.6 Hz), 7.53 (2H, d, J = 8.5 Hz), 7.73 (2H, d, J = 8.1 Hz), 7.78 (2H, t, J = 7.6 Hz), 8.43 (2H, d, J = 7.9 Hz). ^{13}C-NMR (150.8 MHz, $CDCl_3$, 25°C, TMS): δ 20.6 (2 CH_3), 124.4 (2 CH), 125.3 (2 CH), 125.7 (2 CH), 126.88 (2 CH), 126.89 (2 CH), 128.0 (2 CH), 128.4 (2 CH), 132.0 (2 q), 132.25 (2 q), 132.26 (2 q), 132.9 (2 CH), 134.4 (2 q), 134.5 (2 q), 136.6 (2 q), 138.5 (2 CH), 140.9 (2 q), 183.1 (C=O), 184.6 (C=O). HRMS(EI): m/z calcd for $C_{36}H_{24}O_2$: 488.17763; found 488.1779. HPLC: 1 ml/min, ACN/H_2O 90/10, RT = 10.64 min.

***Syn*-1,8-bis(2-methylnaphtyl)anthraquinone, (33a)** :m.p. 294-296, ^{1}H-NMR (600 MHz, $CDCl_3$, 25°C, TMS): δ 2.02 (6H, s), 6.82 (2H, d, J = 8.4 Hz), 6.95 (2H, ddd, J = 1.3, 6.7, 8.4 Hz), 7.13 (2H, ddd, J = 1.1, 6.7, 8.4 Hz), 7.17 (2H, d, J = 8.4 Hz), 7.38 (2H, dd, J = 1.3, 7.6 Hz), 7.51 (2H, d, J = 8.3 Hz), 7.55 (2H, d, J = 8.3 Hz), 7.77 (2H, t, J = 7.6 Hz), 8.43 (2H, dd, J = 1.3, 7.6 Hz). ^{13}C-NMR (150.8 MHz, $CDCl_3$, 25°C, TMS): δ 20.6 (2 CH_3), 124.2 (2 CH), 124.7 (2 CH), 125.7 (2 CH), 126.72 (2 CH), 126.74 (2 CH), 127.5 (2 CH), 128.0 (2 CH), 131.51 (2 q), 131.56 (2 q), 131.8 (2 q), 132.7 (2 CH), 133.9 (2 q), 134.3 (2 q), 136.7 (2 q), 138.4 (2 CH), 140.8 (2 q), 182.6 (C=O), 184.4 (C=O). HRMS(EI): m/z calcd for $C_{36}H_{24}O_2$: 488.17763; found 488.1773. HPLC: 1 ml/min, ACN/H_2O 90/10, RT = 10.17 min.

Crystal Data

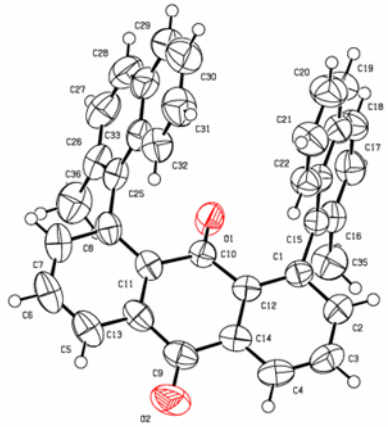

Molecular formula: $C_{36}H_{24}O_2$, M_r = 292.40, Monoclinic, space group $P2_1/C$ (No. 14), a = 14.2858(16), b = 9.2432(11), c = 19.143(2), β = 92.451(2) Å, V = 2525.4(5) Å^3, T = 295(2) K, Z = 4, ρ_c = 1.285 g cm^{-3}, $F(000)$ = 1024, graphite-monochromated $Mo_{K\alpha}$ radiation (λ = 0.71073 Å), $\mu(Mo_{K\alpha})$ = 0.078 mm^{-1}, red brick (0.5 × 0.5 × 0.2 mm^3), empirical absorption correction with SADABS (transmission factors: 0.9845 – 0.9619), 2400 frames, exposure time 10 s, 1.43 ≤ θ ≤ 28.72, –19 ≤ h ≤ 18, –12 ≤ k ≤ 12, –25 ≤ l ≤ 25, 28390 reflections collected, 6152 independent reflections (R_{int} = 0.0230), solution by direct methods (SHELXS97[32]) and subsequent Fourier syntheses, full-matrix least-squares on F_o^2 (SHELX97[32]), hydrogen atoms refined with a riding model, data / restraints / parameters = 6152 / 0 / 345, $S(F^2)$ = 1.567, $R(F)$ = 0.0679 and $wR(F^2)$ = 0.1426 on all data, $R(F)$ = 0.0471 and $wR(F^2)$ = 0.1339 for 4378 reflections with $I > 2\sigma(I)$, weighting scheme $w = 1/[\sigma^2(F_o^2) + (0.0681P)^2 + 0.3413P]$ where $P = (F_o^2 + 2F_c^2)/3$, largest difference peak and hole 0.166 and –0.160 e Å^{-3}.

1-(2-Methylnaphtyl)anthraquinone (34) was prepared using the same procedure described for **33**, using 1-chloroanthraquinone instead of 1,8-dichloroanthraquinone. m.p. 269-271 (dec.), ^{1}H-NMR (600 MHz, $CDCl_3$, 25°C, TMS): δ 2.14 (3H, s), 7.11 (1H, d, J = 8.6 Hz), 7.23 (1H, ddd, J = 1.3, 6.7, 8.6 Hz), 7.38 (1H, ddd, J = 1.1, 6.7, 8.0 Hz), 7.47 (1H, d, J = 8.4 Hz), 7.54 (1H, dd, J = 1.4, 7.6 Hz), 7.66 (1H, ddd, J = 1.4, 7.3, 7.6 Hz), 7.73 (1H,

ddd, J = 1.4, 7.3, 7.6 Hz), 7.87 (3H, m), 7.97 (1H, ddd, J = 0.5, 1.2, 7.8 Hz), 8.30 (1H, ddd, J = 0.5, 1.2, 7.9 Hz), 8.52 (1H, dd, J = 1.4, 7.8 Hz). ^{13}C-NMR (150.8 MHz, $CDCl_3$, 25°C, TMS): δ 20.8 (CH_3), 125.0 (CH), 125.1 (CH), 126.1 (CH), 127.0 (CH), 127.4 (CH), 127.6 (CH), 127.7 (CH), 128.4 (CH), 128.8 (CH), 131.8 (q), 132.1 (q), 132.2 (q), 132.3 (q), 133.2 (q), 133.90 (CH), 133.95 (CH), 134.40 (CH), 134.43 (q), 135.3 (q), 137.9 (q), 138.5 (CH), 142.0 (q), 182.9 (C=O), 183.7 (C=O). HRMS(EI): m/z calcd for $C_{25}H_{16}O_2$: 348.11503; found 348.1151. HPLC: 1 ml/min, ACN/H_2O 90/10, RT = 5.68 min.

4.4.4 1,8-dibromoanthracene[103] was prepared according to the literature; o- and m- tolylboronic acids were commercially available, as well as the $Pd(PPh_3)_4$ catalyst.

4.4.5 1,8-di-*m*-tolylanthracene (35) and 1,8-di-*o*-tolylanthracene (36):[99] To a solution of 1,8-dibromoanthracene (0.336 g, 1 mmol in 6 ml of benzene), K_2CO_3 (2 M solution, 1.25 ml), *m*-tolylboronic acid for **35** and *o*-tolylboronic acid for **36** (0.340 g, 2.5 mmol, suspension in 6 ml of ethanol), and $Pd(PPh_3)_4$ (0.231 g, 0.2 mmol) were added at room temperature. The stirred solution was refluxed for 2-3 hours, the reaction being monitored by GC-MS. After the first coupling was complete, a second amount of *m*-tolylboronic acid (0.340 g, 2.5 mmol, suspension in 6 ml of ethanol), and $Pd(PPh_3)_4$ (0.231 g, 0.2 mmol) were added at room temperature, and the solution refluxed again for 3 hours. Then $CHCl_3$ and H_2O were added and the extracted organic layer was dried (Na_2SO_4) and evaporated. The crude product was pre-purified by chromatography on silica gel (hexane/Et_2O 50:1) to yield 0.28 g of a mixture containing mainly 1-bromo-8-*m*-tolylanthracene, 1-*m*-tolylanthracene and compound **35**. Analytically pure samples of **35** were obtained by semi-preparative HPLC on a Luna C18(2) column (5µm, 250x10 mm, 4 ml/min, ACN/H_2O 90:10 v:v).

1,8-di-*m*-tolylanthracene (35):

^{1}H NMR (600 MHz, CD_2Cl_2, 25°C, δ 5.31): δ 2.38 (6H, s), 7.18-7.20 (2H, m), 7.29-7.34 (6H, m), 7.38 (2H, dd, *J* = 6.8, 1.1 Hz), 7.52 (2H, dd, J = 8.5, 6.8 Hz), 8.03 (2H, d, J = 8.5 Hz), 8.55 (1H, s), 8.63 (1H, s). ^{13}C NMR (150.8 MHz, CD_2Cl_2, 25°C, δ 54.2): δ 22.0 (CH_3), 124.6 (CH), 126.1 (CH), 126.9 (CH), 127.5 (CH), 127.8 (CH), 128.3 (CH), 128.68 (CH), 128.70 (CH), 130.9 (q), 131.4 (CH), 132.6 (q), 138.7 (q), 141.2 (q), 141.4 (q). HPLC: RT = 22.05 min.

1,8-di-*o*-tolylanthracene (36):

^{1}H NMR (600 MHz, $CDCl_3$, 25°C, TMS): δ 1.87 (3H, s), 1.91 (3H, s), 7.06-7.22 (8H, m), 7.27-7.30 (4H, m), 7.48-7.53 (3H, m), 8.02 (2H, d, *J* = 8.6 Hz), 8.52 (1H, d, J = 2.6 Hz). ^{13}C NMR (150.8 MHz, $CDCl_3$, 25°C, TMS): δ 19.96 (CH_3), 19.97 (CH_3), 124.0 (CH), 124.2 (CH), 125.16 (2CH), 125.20 (CH), 125.3 (CH), 125.5 (CH), 125.6 (CH), 126.4 (CH), 126.5 (CH), 127.31 (CH), 127.32 (CH), 127.36 (CH), 127.38 (CH), 129.4 (CH), 129.6 (CH), 130.11 (CH), 130.14 (CH), 130.6 (q), 130.7 (q), 131.57 (q), 131.62 (q), 136.4 (q), 136.5 (q), 139.64 (q), 139.66 (q), 140.2 (q), 140.3 (q). HPLC: RT = 20.38 min.

4.5 NMR Spectroscopy

The spectra were recorded at 600 MHz for ^{1}H and 150.8 MHz for ^{13}C. Variable temperature spectra of **30** were obtained at 400 MHz. The assignments of the ^{1}H and ^{13}C signals were obtained by bi-dimensional experiments (edited-gsHSQC[33] and gsHMBC[34]). The NOE experiments on **32** were obtained by means of the DPFGSE-NOE[57] sequence. To selectively irradiate the desired signal, a 50 Hz wide shaped pulse was calculated with a refocusing-SNOB shape[58] and a pulse width of 37 ms. The mono-dimensional NOE experiments of **31** were obtained in $CDCl_3$ at 0 °C[108] by means of the DPFGSE-NOE[57] sequence. To selectively irradiate the two ^{13}C satellites, a double-frequency[109] 10 Hz wide shaped pulse was calculated with a refocusing-SNOB shape[58] and a pulse width of 185 ms. Mixing time was set to 1.5 s. Saturation transfer experiments[110] (1D-EXSY) of **30** were

obtained using the same DPFGSE-NOE pulse sequence,[57] raising the mixing time from 25 to 500 ms. Temperature calibrations were performed before the experiments, using a Cu/Ni thermocouple immersed in a dummy sample tube filled with 1,1,2,2-tetrachloroethane, and under conditions as nearly identical as possible. The uncertainty in the temperatures was estimated from the calibration curve to be ± 1 °C. The line shape simulations were performed by means of a PC version of the QCPE program DNMR 6 n° 633, Indiana University, Bloomington, IN.

4.6 HPLC separation and ECD spectra

Separation of the two atropisomers of **33b** was achieved at 25°C using two Chiralcel OD-H 250x4.6 mm columns joined together, at a flow rate of 1.0 mL/min, using hexane/iPr-OH 98:2 v:v as eluent. UV detection was fixed at 254 nm. Separation of the two atropisomers of **34** was achieved at 25°C using a Chiralcel AD-H 250x20 mm, at a flow rate of 20.0 mL/min, using hexane/iPr-OH 90:10 v:v as eluent. UV detection was fixed at 254 nm. UV absorption spectra were recorded at 25°C in acetonitrile on the racemic mixtures, in the 200-500 nm spectral region. The cell path length was 0.1 cm, concentration was $8.2 \cdot 10^{-5}$ mol L^{-1} for **33b** and $7.2 \cdot 10^{-5}$ mol L^{-1} for **34**. Maximum molar absorption coefficient was recorded at 223 nm for **33b** (ε = 86950) and 226 nm for **34** (ε = 96660). ECD spectra were recorded at 25°C with the same path lengths of 0.1 cm, in the range 500-200 nm; reported $\Delta\varepsilon$ values are expressed as L mol^{-1} cm^{-1}.

4.7 Kinetics

Equilibration of the two isomers of **33** was obtained by heating a NMR sample of pure **33a** in $(CDCl_2)_2$ into a thermostatic oil bath, kept at +140 °C. At regular intervals the sample was taken out from the oil bath, and the NMR spectrum recorded at +25 °C, until the equilibrium was reached. Racemization of the atropisomers of **34** was obtained by heating a sample of enantiopure (P)-**34** in $(CDCl_2)_2$ into a thermostatic oil bath, kept at +140 °C. At regular intervals an aliquot of the sample was taken out from the oil bath,

diluted with iPrOH and analyzed by HPLC on a Chiralcel AD-H column (250x4.6 mm, 1.0 mL/min, hexane/iPr-OH 90:10 v:v), until the equilibrium was reached.

4.8 Calculations

Geometry optimizations were carried out at the B3LYP/6-31G(d) level by means of the Gaussian 03 series of programs[15]. In the case of **30**-syn, geometry optimization was also carried out at the B3LYP/6-31++G(d,p), PBE1PBE/6-31+G(d,p) and HF/6-31+G(d,p) level. The standard Berny algorithm in redundant internal coordinates and default criteria of convergence were employed in all the calculations. Reported energies include unscaled ZPE and thermal correction to enthalpy. Harmonic vibrational frequencies were calculated for all the stationary points. For each optimized ground state the frequency analysis showed the absence of imaginary frequencies. Visual inspection of the corresponding normal mode was used to confirm that the correct transition state had been found. NMR chemical shift calculations were obtained with the GIAO method at the B3LYP/6-311++G(2d,p)//B3LYP/6-31G(d) level. TMS, calculated at the same level of theory, was used as reference to scale the absolute shielding value. TD-DFT calculations on the *M*,*M* atropisomer of **33b** and the *P* atropisomer of **34** were obtained at the B3LYP/6-31+G(d,p)//B3LYP/6-31G(d) level. In order to cover the whole 500-200 nm range, 90 transition were calculated in both cases. The CD spectra were then obtained by applying a 0.3 eV Gaussian bandshape.[85]

Chapter 5

5.1 Studying E and Z Conformers of 2-Naphthylalkylsulfoxides

The chirality of sulfoxides has been widely investigated[111] and a number of reactions aiming to the synthesis of these compounds with a satisfactory enantiomeric excess have been reported.[112] The absolute configuration of sulfoxides can be determined in the solid state by means of the anomalous dispersion of X-ray crystallography[113] and in solution by means of the theoretical interpretation of Electron Circular Dicroism (ECD)[114] or Vibrational Circular Dicroism (VCD)[114e,115] spectra. In particular, DFT computations yield quite reliable prediction of ECD and VCD spectra, allowing a meaningful comparison with the experimental CD traces to be performed.[54s]

In the case of molecules adopting more than one conformation like, for instance, some arylalkylsulfoxides, it is important to know the structures and populations of their conformers,[114d,115b] because different conformers might give substantially different contributions to the ECD spectra.[114c] In the case of sulfoxides reliable information concerning the conformer population can be obtained by low temperature NMR spectra,[28f,113b,c,116] that yield distinguishable traces for different conformers.

Here we investigate a series of 2-naphthylalkylsulfoxide not previously reported (*Scheme 12*) by making use of the information derived from dynamic NMR experiments, ECD spectroscopy, DFT computations and anomalous dispersion of X-ray crystallography.

All the compounds of *Scheme 12* display NMR signals that broaden on cooling and eventually split, below –100 °C, into two groups of signals, with different intensity.

Scheme 12: **Synthetic scheme for the preparation of the 2-naphthylalkylsulfoxides (*37-41*) investigated.**

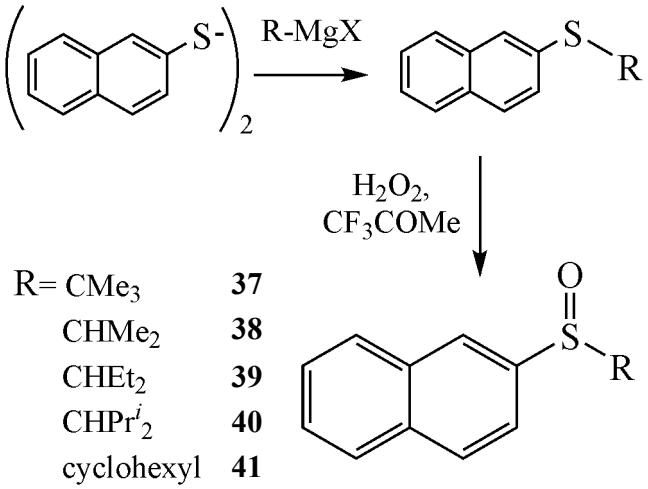

This feature is a consequence of the restricted rotation process about the naphthyl-SO bond, which shows the existence of the two conformers (Z, synperiplanar and E, antiperiplanar) displayed in *Scheme 13*. This type of conformers have been observed also in the case of 1-naphthyl alkylsulfoxides where, however, the existence of larger interconversion barriers, due to the greater steric hindrance, allowed the corresponding splitting of the NMR signals to be detected at substantially higher temperatures.[113b,116a]

Scheme 13*:* **Representation of the E and Z conformers for the 2-naphthyl alkyl sulfoxides**

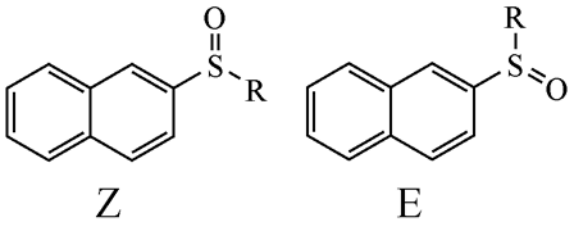

As an example, is reported the ^{13}C NMR signal of the carbon in position 3 of 2-naphthyl-*tert*-butyl sulfoxide **37** which splits into two lines (separated by 2.8 ppm at –114 °C) with a 55/45 intensity ratio (*Figure 88*).

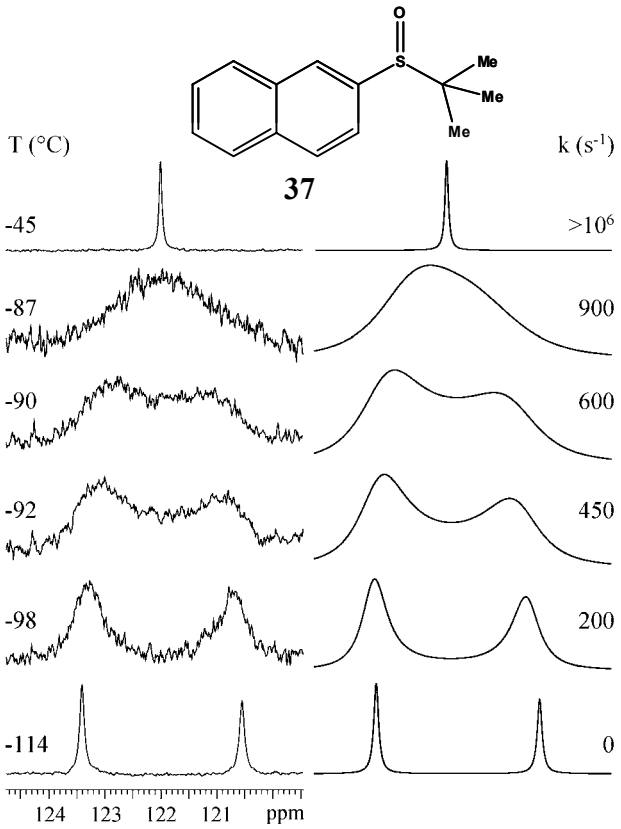

Figure 88: **Left: Temperature dependence of the ^{13}C NMR signal (150.8 MHz in $CHF_2Cl/CHFCl_2$) of carbon in position 3 (identified by bi-dimensional COSY and HSQC sequences) of 2 naphthyl *tert*-butylsulfoxides, *37*. Right: line shape simulation with the corresponding rate constants (k).**

The computer line shape simulation allowed the determination of the rate constants for the interconversion of the major into the minor conformer; from these values the corresponding barrier due to the Ar-SO rotation ($\Delta G^{\neq} = 8.2 \pm 0.15$ kcal mol^{-1}) was obtained (*Table 12*).

Table 12: **NMR determined conformer ratios and barriers ($\Delta G^{\neq}$) for the Z to E interconversion. In parenthesis the DFT computed barriers.**

Compounds	Z/E ratio	$\Delta G^{\neq}$ (kcal mol^{-1})
37, R = CMe_3	55/45	8.2 (9.0) 5.5 [a] (4.5) [a]
38, R = $CHMe_2$	70/30	6.0 (5.5)
39, R = $CHEt_2$	67/33	5.9
40, R = $CHPr^i_2$	97/3	6.3 (6.2)
41, R = cyclohexyl	54/46	6.0

a) Barriers for the S-CMe_3 rotation

On further cooling, a second exchange process, due to the restricted rotation about the S-CMe_3 bond, becomes visible when monitoring the ^{13}C signal of the methyl groups. Three groups of signals with a 1/1/1 relative intensity are eventually detected at –159 °C. At this temperature, in fact, the three methyl groups of the *tert*-butyl moiety become diastereotopic, thus yielding three anisochronous signals. This diastereotopicity is expected to occur in both the Z and E conformers, so that each of the three diastereotopic methyl groups should yield a pair of lines, with the mentioned 55/45 intensity ratio. However the corresponding shift separation is sufficiently large to be observed only for the methyl signal at higher field, which thus appears as a 55/45 doublet, whereas the two signals at lower field (i.e., at 23 and 25 ppm) could not be resolved (*Figure 89*). From the rate constants derived by line shape simulation, the rotation barrier for the *tert*-butyl moiety was found to be equal to 5.5 kcal mol^{-1} (*Table 12*).

The DFT calculations[15] predict that the Z conformer of **37** has an energy 0.20 kcal mol^{-1} lower than that of E. On this basis it is reasonable to assign the Z structure to the more stable of the two conformers.

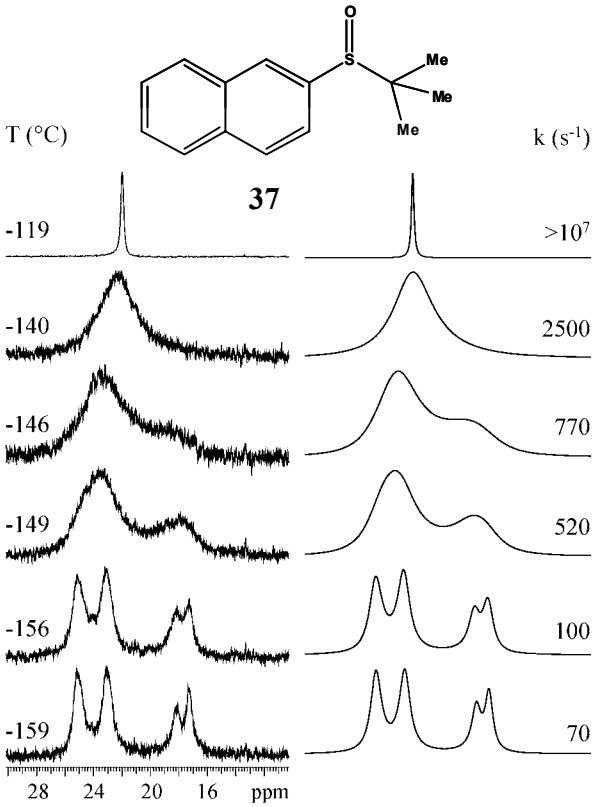

Figure 89: **Left: Temperature dependence of the ^{13}C-NMR signal (150.8 MHz in $CHF_2Cl/CHFCl_2$) of the methyl carbons of 2-naphthyl *tert*-butyl-sulfoxide, *37*; Right: line shape simulation obtained with the rate constants (k) indicated.**

Further support to this assignment is offered by the DFT calculated values of the ^{1}H chemical shifts. The chemical shift of the hydrogen in position 1 (i.e. H-1) is predicted by DFT calculation to be at lower field in the Z (predicted value 8.84 ppm) with respect to the E conformer (predicted value 7.81 ppm): the S=O moiety, in fact, is known to move downfield the signal of the hydrogens in a *syn* relationship. In the experimental spectrum at –114 °C, where separate signals are observed for the two conformers, the downfield signal of H-1 (at 8.23 ppm) is actually more intense (55%) than its upfield companion (45% at 7.83 ppm). The same calculations predict an opposite trend for the shifts of the hydrogen in position 3 (i.e. H-3) and, indeed, the upfield H-3 signal (7.33 ppm) is more intense (55%) than its downfield companion (45% at 7.78 ppm) in the spectrum at –114 °C. These DFT computations are quite reliable in that they also predict that the Z to E interconversion

barrier is 9.0 kcal mol^{-1} and that the *tert*-butyl rotation barrier is 4.5 kcal mol^{-1}, both in satisfactory agreement with the experimental measurements (*Table 12*).

It should be also noticed that the relationship between ^{1}H and ^{13}C spectra, obtained at –114 °C *via* the bi-dimensional HSQC pulse sequence (*Figure 90*), proved that the trend of the corresponding ^{13}C shifts for the carbon at position 3 (i.e. C-3) in the Z and E conformers is opposite to that of the corresponding ^{1}H signals mentioned above.

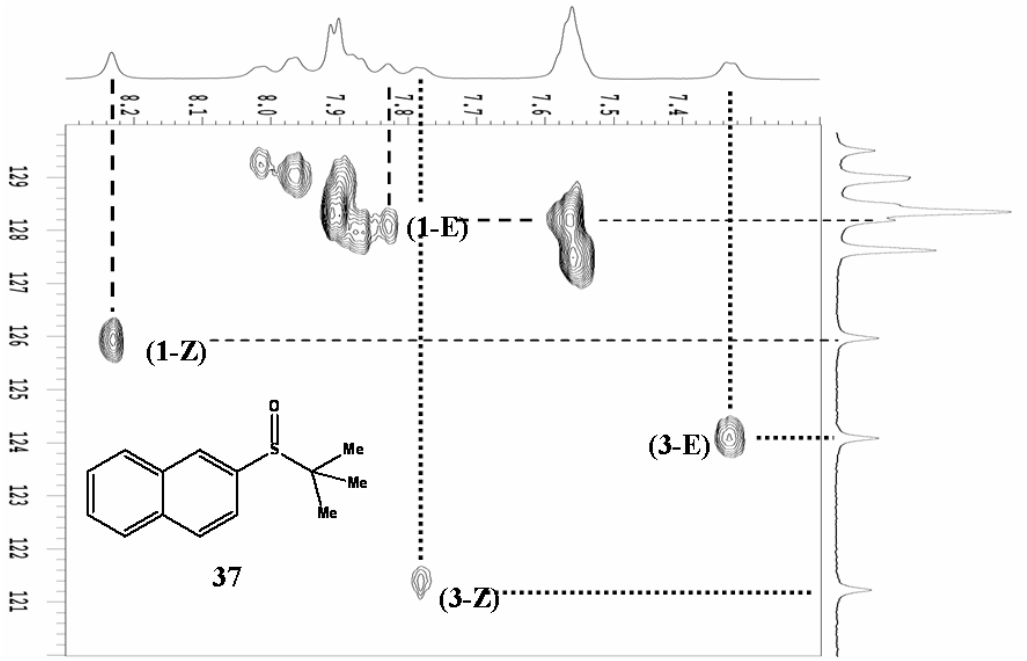

Figure 90: **Bi-dimensional HSQC spectrum (600 MHz in CD_2Cl_2 at –114 °C) of the aromatic region of 2-naphthyl *tert*-butylsulfoxide, *37*, showing separate ^{1}H and ^{13}C signals of the atoms in position 1 and 3 for the E and Z conformers.**

Therefore, the more intense downfield C-3 signal (123.4 ppm), observed in the –114 °C spectrum of *Figure 88*, must correspond the Z conformer and its less intense upfield companion (120.6 ppm) to the E conformer.

An independent conformational assignment can be also achieved on the basis of NOE experiments. In the Z conformer the DFT computed average distance of the *tert*-butyl hydrogens from H-1 (4.65 Å) is larger than that from H-3 (4.38 Å), the ratio being 1.06. In

the E conformer the situation is reversed in that these distances are, respectively, 4.44 and 4.60 Å, the ratio being 0.96. Due to the reciprocal 6th power relationship between distances and NOE effects, the ratio of the enhancements experienced by the *tert*-butyl line on irradiation of the H-3 and H-1 signals should be, therefore, $(1.06)^6 = 1.42$ for the Z conformer, but $(0.96)^6 = 0.78$ for the E conformer. In the case of exactly equal proportions of the two conformers, the ratio of the NOE enhancements experienced by the *tert*-butyl line should be, accordingly, (1.42+0.78)/2 = 1.10. Therefore a ratio larger than 1.10 (and smaller than 1.42) would indicate that the population of the Z conformer at the equilibrium is greater than that of the E conformer, whereas a ratio smaller than 1.10 (and larger than 0.78) would indicate a preference for the E conformer. The experimental enhancement of the *tert*-butyl line, observed when irradiating the H-3, is larger than when irradiating the H-1 signal, the ratio being 1.21 ± 0.02. Likewise, irradiation of the *tert*-butyl line enhances the H-3 more than the H-1 signal, the experimental ratio being 1.23 ± 0.02 (*Figure 91*). All these theoretical and experimental data thus indicate that the Z is undoubtedly more populated than the E conformer in sulfoxide **37**.

When the synthesis of 2-naphthyl*tert*-butylsulfoxide, **37** was performed according to the reaction of Kagan,[112b] a 90% e.e. was obtained. The major was separated from the minor enantiomer by making use of an enantioselective HPLC column (Daicel Chiralcel OJ-H): the ECD spectrum of the major, corresponding to the second eluted enantiomer, is displayed in *Figure 92*. Since the structure and the ratio of the two conformers were well established by NMR, we used this information to calculate, by means of the TD-DFT approach,[15,53,54] the theoretical ECD spectrum for the configuration S. The shape of the computed spectrum is in substantial agreement with the experimental one, as shown in *Figure 92*. Thus to the major, second eluted enantiomer the S configuration could be assigned: as a consequence the R configuration must be attributed to the first eluted minor enantiomer.

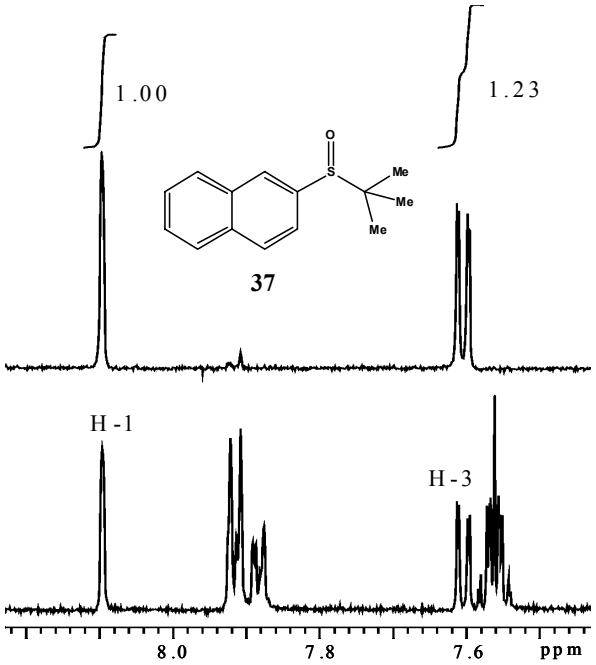

Figure 91: **Bottom trace: 600 MHz NMR spectrum of the aromatic region of 2-naphthyl*tert*-butylsulfoxide, *37* in $CDCl_3$ at +25 °C. Upper trace: NOE experiment obtained by irradiation of the *tert*-butyl line (at 1.20 ppm) showing that the enhancement of the H-3 signal is larger than that of the H-1 signal, the relative amounts being 1.23/1.00.**

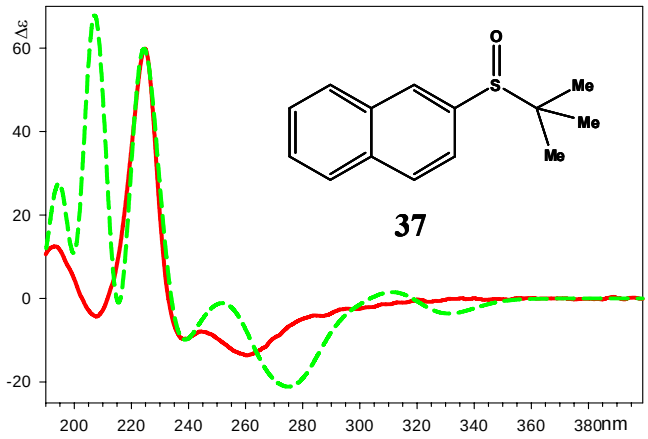

Figure 92: **Experimental (full red trace) and DFT computed (S configuration, dashed green trace, blue shifted by 5 nm) ECD spectrum of the second eluted (Daicel Chiralcel OJ-H column) enantiomer of 2-naphthyl-*tert*-butylsulfoxide, *37*, corresponding to the enantiomer obtained in the 90 % e.e. Calculate ECD spectra result from the weight average of E and Z conformers.**

In order to obtain an unambiguous proof of this conclusion, single crystals of the second eluted major enantiomer were grown and submitted to X-ray diffraction. As shown in *Figure 93* the conformer observed in the solid state has indeed the Z structure as well as the absolute configuration S, the latter having been determined by the anomalous dispersion methodology. This experimental result thus indicates that the TD-DFT interpretation of the ECD spectra of these sulfoxides is quite reliable for determining the absolute configurations, particularly when supported by an experimental NMR determination of the structure and population of the conformers involved.

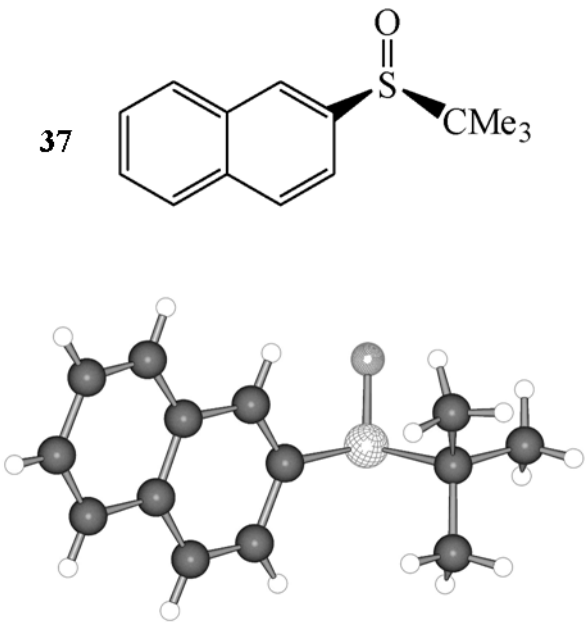

Figure 93: **Single crystal X-ray structure (conformer Z and absolute configuration S, as obtained by anomalous dispersion) determined for the 90% e.e. enantiomer (corresponding to the second eluted on the Daicel Chiralcel OJ-H column) of 2 naphthyl-*tert*-butylsulfoxide, *37***

This result also offers an experimental proof of the absolute configuration assignment that was deduced by Kagan for the analogous phenyl-*tert*-butylsulfoxide on the basis of a synthetic scheme involving two inversions of configuration[112b] (the present

assignment also agrees with that proposed in the case of two similar 2-naphthylalkyl sulfoxides[114c])

Also in the case of 2-naphthyl-isopropylsulfoxide **38** (synthesized *via* a non enantioselective procedure) two conformers were detected in the ^{13}C NMR spectrum: in *Figure 94*, for instance, each of the two the quaternary carbons C-9 and C-10 displays, at –157 °C, two signals with a 70 : 30 intensity ratio.

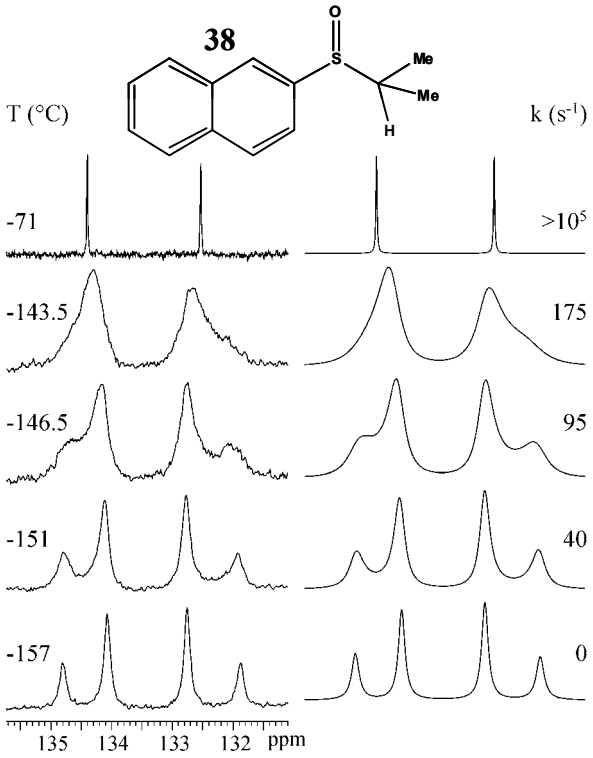

Figure 94: **Left: Temperature dependence of the ^{13}C NMR signals (150.8 MHz in $CHF_2Cl/CHFCl_2$) of the quaternary carbons in positions 9 and 10 (identified by a bi-dimensional HMBC pulse sequence) of 2-naphthyl-isopropylsulfoxide, *38*; Right: line shape simulation with the corresponding rate constants (k).**

In this case an even lower temperature had to be reached since the interconversion barrier, determined by line shape simulation, is quite lower (6.0 kcal mol^{-1}), owing to the presence of an alkyl substituent (isopropyl) less bulky than the *tert*-butyl group of **37**. Again the major form must correspond to the Z conformer since, as in the case of **37**, the

^{13}C line of C-3 at lower field (120.9 ppm in the –157 °C spectrum) is more intense than its companion at higher field (120.0 ppm). It should be also pointed out that the greater population of conformer Z, experimentally observed in **37** and **38** (and also in **3-5**, as in *Table 12*), is at variance with the report of reference [117] where it was suggested that E was the preferred conformer in the case of two similar 2-naphthylalkylsulfoxides.

The greater amount of Z conformer present at the equilibrium in compound **38** (70%) with respect to **37** (55%) explains why the corresponding ECD spectra are appreciably different. This is because the individual conformers E and Z are predicted by computations to yield quite different ECD traces, so that a change in their relative proportion substantially affect the resulting spectrum. An independent determination of the conformers ratio is therefore required in order to obtain a reliable computed spectrum for assessing the absolute configuration.

On the basis of the present NMR conformational analysis, the theoretical ECD spectrum for the R configuration of **38** was computed by the DFT approach. The enantiomers present in the racemic mixture of **38** were separated using an enantioselective HPLC column (Daicel Chiralcel OB-H) and the ECD spectrum of the second eluted enantiomer (*Figure 95*) was found to correspond to that computed for the enantiomer R.

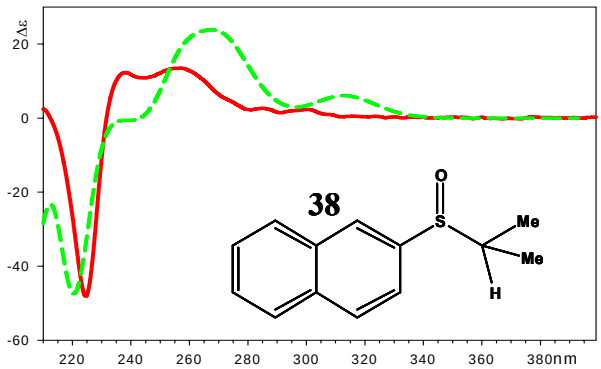

***Figure 95**:* **Experimental (full red trace) and DFT computed (R configuration, dashed green trace, blue shifted by 7 nm) ECD spectrum of the second eluted (Daicel Chiralcel OB-H column) enantiomer of 2-naphthyl-isopropylsulfoxide, *38*. Calculate ECD spectra result from the weight average of E and Z conformers.**

This is opposite to what observed in the case of **37**, where the R configuration corresponded to the first eluted enantiomer: the reason is that in the OJ-H column, needed to obtain a good separation of the enantiomers of **37**, the elution times are reversed with respect to the OB-H column, which had to be employed to obtain a satisfactory separation of the enantiomers of **38**. Proof of the reversal of the peak separation is obtained when the 90% e.e. enriched mixture of **37** is injected into the OB-H column: in this case, in fact, the major enantiomer becomes the first eluted, although the time difference between the peaks is too small for allowing the physical recovery when this column is employed.

The same elution trend of **38** was also observed (when using the same OB-H column) for the separation of the enantiomers of compounds **39-41**, where again the R configuration was found to correspond to that of the second eluted enantiomer.

The proportion of the E conformer of 2-naphthyldiisopropylmethylsulfoxide **40** is very small if compared to the amounts detected in the other cases: for this reason the ^{13}C NMR signals of the E conformer could not be observed, owing to the insufficient signal to noise ratio. However the ^{1}H spectrum of the four diastereotopic methyl groups[41] of **40** shows how the most upfield signal splits, at -157 °C, into two lines with a 97:3 intensity ratio, indicating that the proportion of the E conformer is as low as 3% (*Figure 96*).

On the basis of this result, the ECD spectrum of **40** is expected to correspond essentially to that of its Z conformer, and indeed the experimental spectrum appears to be quite different from those of **37** and **38**. Once more it has to be stressed that an independent knowledge of the conformer ratio is required in order to obtain a reliable computed spectrum for assigning the absolute configuration. *Figure 97* displays the ECD spectrum of the first eluted (Daicel Chiralcel OB-H column) enantiomer of **40** which has a shape in agreement with the computed spectrum, if the S configuration is assumed and if a 3% proportion of the E conformer, as determined by the NMR measurements, is taken into account.

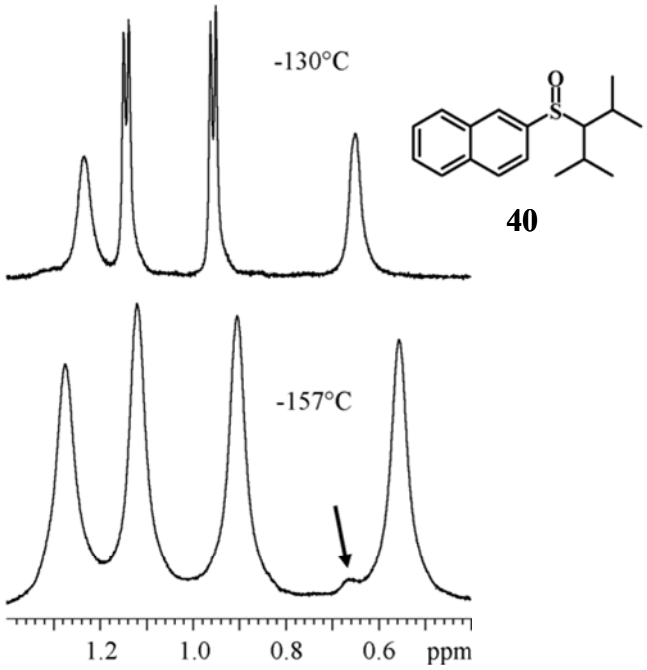

Figure 96: **Top: 600 MHz ^{1}H NMR signals of the four diastereotopic methyl groups of 2-naphthyl-di-isopropylmethylmethylsulfoxide, *40* in $CHF_2Cl/CHFCl_2$ at -130 °C. Bottom: at -157 °C the Z to E interconversion rate becomes slow enough as to split the upfield methyl signal into two lines, the minor one (≅ 3%, indicated by an arrow) corresponding to the conformer E.**

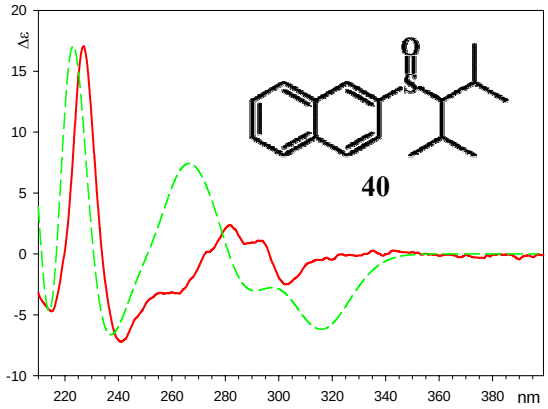

Figure 97: **Experimental (Full red trace) and DFT computed (S configuration, dashed green trace blue shifted by 3 nm) ECD spectrum of the first eluted (Daicel Chiralcel OB-H column) enantiomer of 2-naphthyl-di-isopropylmethylsulfoxide, *40*. Calculate ECD spectra result from the weight average of E and Z conformers.**

5.2 Conclusions

The low temperature dynamic NMR spectra allowed the structure and the ratio of the E and Z conformers of the 2-naphthylalkylsulfoxides **37-41** to be determined. On the basis of this result, the theoretical ECD spectra of the R and S enantiomers were calculated by means of the DFT approach. The enantiomers were separated by enantioselective HPLC and the comparison of the theoretical with the experimental ECD spectra, allowed the absolute configuration to be assigned. In the case of the 2-naphthyl-*tert*-butyl sulfoxide **37** the absolute configuration, derived from the interpretation of the ECD spectrum, was also confirmed in the basis of the anomalous dispersion effects of X-ray crystallography. Although the compounds examined are very similar their ECD spectra appear to be different, owing to the different ratio of the Z and E conformers, as determined by NMR. This observation outlines the usefulness of obtaining an independent determination of the conformer ratio in order to have a reliable prediction of the ECD spectra of those compounds where more than one conformer can be appreciably populated.

5.3 Experimental Section

5.3.1 The alkyl naphthyl sulfoxides **38-41** were prepared by oxidation of the sulfides obtained by reacting the appropriate alkyl Grignard reagent with 2-naphthyl disulfide.

2-Naphthyl disulfide[118] A solution (25 ml CH_3OH, 10 mL H_2O) of 2-naphthylthiol (1.6 g, 10 mmol) was reacted with 20 ml $NaBO_3 \cdot 4H_2O$ at RT for 2h. The mixture was diluted with water, extracted 3x15ml $CHCl_3$. The collected organic layers were washed with 2x15ml NaOH 5%, dried on Na_2SO_4 and concentrated at reduced pressure to give white crystals (1.5 g, 4.7mmol) in 93% yield. mp. 139-140°C. ^{1}H NMR (300 MHz, $CDCl_3$): δ = 7.5 (m, 2H), 7.7 (dd, *J* = 8.7 *J* = 1.9 Hz, 1H), 7.8 (m, 3H), 8.0 (d, *J* = 1.9 Hz, 1H); ^{13}C NMR (75 MHz, $CDCl_3$): δ = 125.6, 126.2, 126.5, 126.7, 127.4, 127.7, 128.9, 132.4, 133.4, 134.2.

5.3.2 General procedure for the preparation of the sulfoxides 38-41.

The Grignard reagent, obtained by reacting Mg (61 mg, 2.5 mmol) and the appropriate alkyl bromide (2.6 mmol) in dry THF, was slowly added at 15°C to 2-naphthyl disulfide (640 mg, 2 mmol) in dry THF and the mixture was stirred for 2h. When the reaction was completed the mixture was quenched with water, extracted with Et_2O (3x15ml), dried and concentrated at reduced pressure to give the crude product in 60-75% yield. The sulfides were converted in the racemic sulfoxides by using a known procedure.[119]

2-(isopropylsulfinyl)naphthalene (38): ^{1}H NMR (600 MHz, $CDCl_3$): δ = 1.13 (d, *J* = 7.1 Hz, 3H), 1.24 (d, *J* = 7.1 Hz, 3H), 2.90 (m, *J* = 7.1 Hz, 1H), 7.53-7.57 (m, 3H), 7.87 (m, 1H), 7.91 (m,1H), 7.93 (d, *J* = 8.5 Hz, 1H), 8.11 (d, *J* = 1.3,Hz, 1H); ^{13}C NMR (150 MHz, $CDCl_3$): δ = 13.8 , 16.0 , 54.4, 120.7, 125.6, 127.1, 127.6, 127.9, 128.4, 128.9, 132.6, 134.4, 139.0.

2-(pentan-3-ylsulfinil)naphthalene (39): ^{1}H NMR (600 MHz, $CDCl_3$): δ = 0.91(t, *J* = 7.5 Hz, 3H), 1.06 (t, *J* = 7.5 Hz, 3H), 1.55 (m, *J* = 7.5 Hz, 1H), 1.66 (m, 1H), 1.68 (m, 1H), 1.79 (m, *J* = 7.5 Hz, 1H), 2.50(m, *J* = 5.1, 6.7, 13.8 Hz, 1H), 7.54 (dd, *J* = 8.6, *J* = 1,8 Hz, 1H), 7.57(m, 2H), 7.89 (m, 1H), 7.93 (m,1H), 7.94 (d, *J* = 8.6 Hz, 1H), 8.14 (d, *J* = 1.4 Hz, 1H); ^{13}C NMR (150 MHz, $CDCl_3$): δ = 11.1, 11.5, 18.6, 20.5, 67.6, 120.7, 125.8, 127.2, 127.6 , 128.0, 128.4, 129.0, 132.8, 134.4, 139.4. mp 45-47°C.

2-(2,4-dimethylpentan-3-ylsulfinyl)naphthalene(40): ^{1}H NMR (600 MHz, $CDCl_3$): δ = 0.87 (d, *J* = 6.9 Hz, 1H), 1.08 (d, *J* = 6.9 Hz, 1H), 1.13 (d, *J* = 6.9 Hz, 1H), 1.23 (d, *J* = 6.9 Hz, 1H), 2.27 (m, 1H), 2.38 (m, 1H), 2.45 (dd, *J* = 5.8, *J* = 3.6 Hz, 1H), 7.48 (dd, *J* = 8.6, *J* = 1.8 Hz, 1H), 7.56 (m, 2H), 7.88 (m,1H), 7.92 (m, 2H), 8.16 (d, *J* = 1.5 Hz, 1H); ^{13}C NMR (150 MHz, $CDCl_3$): δ = 19.9, 20.9, 22.3, 22.8, 25.3, 27.1, 76.9, 120.4, 125.2, 127.1, 127.4, 127.9, 128.4, 129.0, 132.9, 133.9, 142.0. mp 112-113°C.

2-(cyclohexylsulfinyl)naphthalene (41): ^{1}H NMR (600 MHz, $CDCl_3$): δ = 1.12-1.28 (m, 3H), 1.43 (m, 1H), 1.47 (m, 1H), 1.62 (m, 1H), 1.81 (m, 3H), 1.87 (m, 1H), 2.64 (m, *J* = 11.8, *J* = 3.5 Hz, 1H), 7.55-7.58 (m, 3H), 7.88 (m, 1H), 7.92 (m, 1H), 7.94 (d, *J* = 8.6 Hz, 1H), 8.11 (d, *J* =1.3 Hz, 1H); ^{13}C NMR (150 MHz, $CDCl_3$): δ = 24.0, 25.3, 25.4, 25.6, 26.4, 63.0, 120.8, 125.7, 127.2, 127.6, 128.0, 128.5, 129.0, 132.7, 134.4, 139.1. mp 111-112°C.

5.3.3 The optically enriched **37** was achieved from the 2-naphthyl-(-)-(L)-dimenthylsulfinate according to a known procedure.[112b]

2-naphthyl-(-)-(L)-dimenthylsulfinate: a 2-naphthyl Grignard solution obtained by reacting Mg (121 mg, 5 mmol) and 2-naphthyl bromide (0.7 ml, 5 mmol) in 15 ml of dry THF, was added in 40 min. to a solution, cooled to 0°C, of dimenthylsulfinate (1.79 g, 5 mmol) in dry THF (10 ml). The temperature was allowed to rise at 25°C and the reaction was completed after stirring for 2.5 hours. The mixture was quenched with water, extracted with ether, dried and the solvent removed at reduced pressure. The crude was recrystallized from hexane to give white crystals of pure sulfinate (1.4 g, 4.2 mmol) in 85% yield. ^{1}H NMR (600 MHz, $CDCl_3$): δ = 0.87 (d, *J* = 6.9 Hz, 3H), 0.88 (d, *J* = 6.6 Hz, 3H), 0.90 (d, *J* = 6.6 Hz, 3H), 1.05 (m, 1H), 1.26 (m, 1H), 1.40 (m, 1H), 1.46 (m, 1H), 1.65 (m, 1H), 1.68 (m, 1H), 2.12 (m, 1H), 2.18 (m, 1H), 4.26 (dt, *J* = 4.4, *J* = 10.9 Hz, 1H), 7.57 (m, 2H), 7.65 (dd, *J* = 1.8, *J* = 8.5 Hz, 1H), 7.8 (m, 1H), 7.95(m, 1H), 7.96 (d, *J* = 8.5 Hz, 1H), 8.11 (d, *J* =1.3 Hz, 1H); ^{13}C NMR (150 MHz, $CDCl_3$): δ = 15.7, 20.9, 21.9, 23.0, 25.5, 31.9, 33.9, 43.6, 48.2, 82.4, 120.6, 125.3, 127.1, 128.0, 128.1, 129.0, 129.2, 132.5, 134.9, 143.2.

2-(*tert*-butylsulfinyl)naphthalene (37): ^{1}H NMR (600 MHz, $CDCl_3$): δ = 1.20 (s, 9H), 7.56 (m, 2H), 7.61 (dd, *J* = 8.6, *J* = 1.6 Hz, 1H), 7.88 (m, 1H), 7.91 (d, *J* = 8.5 Hz, 1H), 7.92 (m, 1H), 8.10 (d, *J* = 1.3 Hz, 1H); ^{13}C NMR (150 MHz, $CDCl_3$): δ = 22.9, 56.2, 122.4, 126.7, 127.0, 127.6, 127.9, 128.1, 128.5, 132.4, 134.6, 137.4. mp 121-122°C.

5.4 NMR Spectroscopy

The spectra were recorded at 600 MHz for ^{1}H and 150.8 MHz for ^{13}C. The assignments of the ^{1}H and ^{13}C signals were obtained by bi-dimensional experiments (edited-gHSQC[33] and gHMBC[34] sequences). The samples for obtaining spectra at temperatures lower than –100 °C were prepared by connecting to a vacuum line the NMR tubes containing the compound and a small amount of C_6D_6 (for locking purpose), and condensing therein the gaseous CHF_2Cl and $CHFCl_2$ (4:1 v/v) under cooling with liquid nitrogen. The tubes were subsequently sealed in vacuo and introduced into the precooled probe of the spectrometer. Temperature calibrations were performed before the experiments, using a Cu/Ni thermocouple immersed in a dummy sample tube filled with isopentane, and under conditions as nearly identical as possible. The uncertainty in the temperatures was estimated from the calibration curve to be ±1 °C. The line shape simulations were performed by means of a PC version of the QCPE program DNMR 6 n° 633, Indiana University, Bloomington, IN.[4b]

5.5 Calculations

Geometry optimization were carried out at the B3LYP/6-31G(d) level by means of the Gaussian 03 series of programs[15]: the standard Berny algorithm in redundant internal coordinates and default criteria of convergence were employed. The reported energy values are not ZPE corrected. Harmonic vibrational frequencies were calculated for all the stationary points. For each optimized ground state the frequency analysis showed the absence of imaginary frequencies, whereas each transition state showed a single imaginary frequency. Visual inspection of the corresponding normal mode was used to confirm that the correct transition state had been found. NMR chemical shift calculations were obtained with the GIAO method at the B3LYP/6-311++G(2d,p)//B3LYP/6-31G(d) level. TMS, calculated at the same level of theory, was used as reference to scale the absolute shielding value. TDDFT calculations on **37-41** were obtained at the B3LYP/6-

31++G(2d,p)//B3LYP/6-31G(d) level. In order to cover the 200-400 nm range, 30 transition were calculated. The CD spectrum was then obtained applying a 0.3 eV Gaussian bandshape.[85]

5.6 Enantioselective HPLC and CD spectra

Separation of the enantiomers of **37** was achieved at 25 °C on a Chiralcel OJ-H 250x4.6 mm column, at a flow rate of 1.0 mL/min, using hexane/iPr-OH 90:10 v:v as eluent. Separation of the enantiomers of **38-41** was achieved at 25 °C on a Chiralcel OB-H 250x4.6 mm column, at a flow rate of 1.0 mL/min, using hexane/iPr-OH 92:8 v:v as eluent (hexane/iPr_2O 80:20 v:v in the case of **40**) . In order to have the sufficient amount to record the CD spectra, 10 injections (50 μg each one) were collected. UV detection was fixed at 225 nm. UV absorption spectra were recorded at 25 °C in acetonitrile on the racemic mixture, in the 200-400 nm spectral region. The cell path length was 0.1 cm, concentration was $1.0 \cdot \div 1.2 \cdot 10^{-4}$ mol L^{-1}. CD spectra were recorded at 25 °C in acetonitrile, with the same path lengths and concentrations, in the range 200-400 nm; reported Δε values are expressed as L $mol^{-1}cm^{-1}$.

Chapter 6

6.1 Rearrangement of Carbamates by N to C Aryl Migration and DFT Calculations To determinate the Cyclic Intermediate

Carbamates, or urethanes, are among the most useful protecting group for alcohols and amines.[120] These blocking groups present the advantage to be easily introduced, deactivate the nucleophilic properties of the protected heteroatom and can be readily removed when needed.

Within Prof. Clayden's group, we have studied the rearrangement of carbamates to provide a new route to α,α-arylated secondary or tertiary alcohols. This reaction is an α-arylation of benzylic alcohols by N to C aryl migration in lithiated carbamates. The presence of an acid hydrogen in α to the oxygen of carbamates permits its lithiation[121] and generates a series of nucleophilic reagents which have a versatile reactivity[122] (*Figure 98*). This provides a strategically uncommon route to secondary and tertiary alcohols.

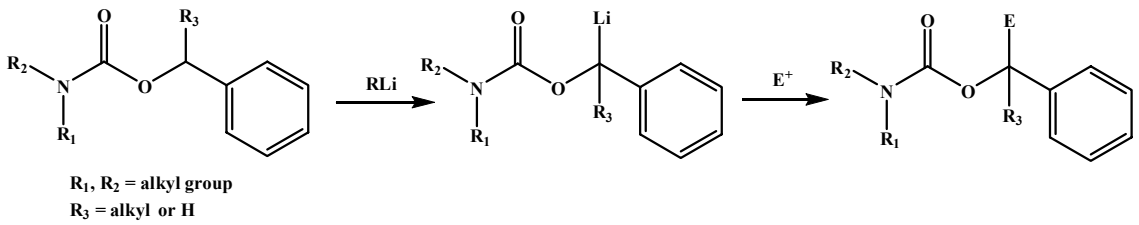

***Figure 98*:Versatile reactivity of lithiated carbamates.**

Less hindered carbamate, having for example $R_1 = R_2 = Et$ are too unstable at -78 °C and for that take place a rearrangement by 1,2-acyl transfer from O to C provides α-hydroxyamides (*Figure 99*).[123]

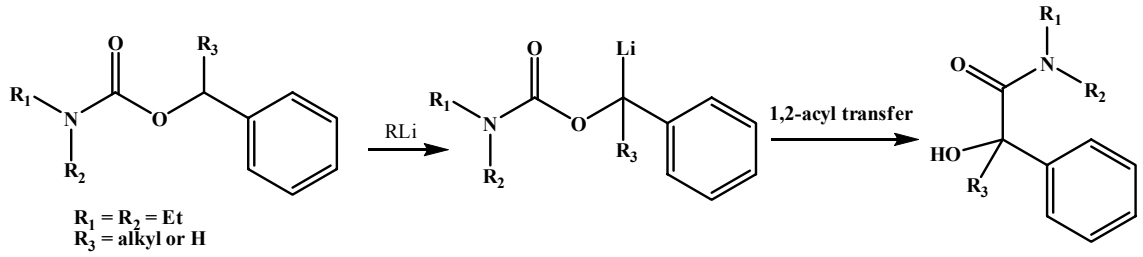

Figure 99: **Reaction of less hindered carbamates by 1,2-acyl transfer**

When an alkyl group (R_1 or R_2) tied to N is substituted with an aryl group, the electrophilic attack takes place intramolecularly, resulting in a migration of the aryl group through a cyclic intermediate (*Figure 100*).

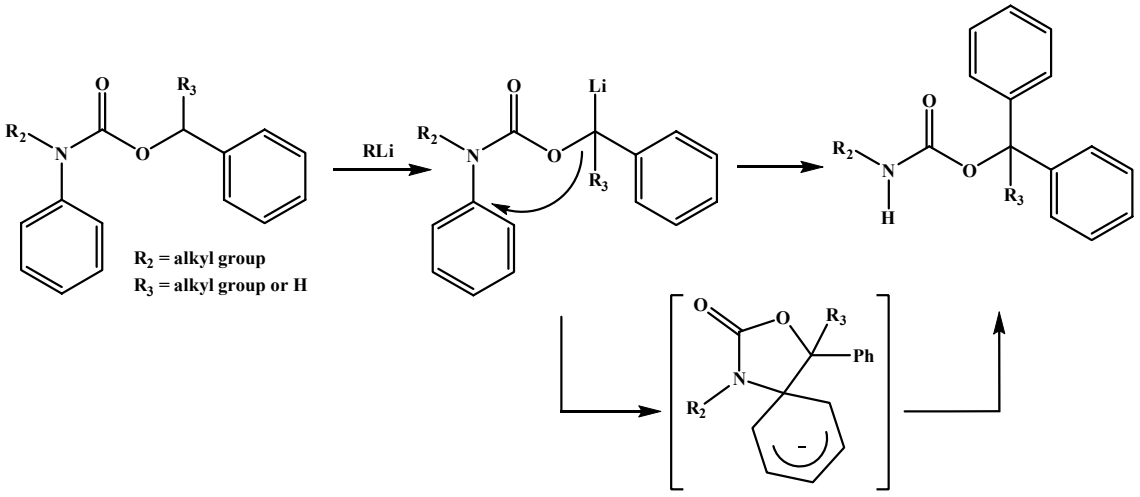

***Figure 100*:Mechanism proposed to 1,4-aryl transfer: cyclic intermediate.**

The hypothesis of the intermediate formation is suggest by a similar rearrangement in lithiated ureas, studied by Clayden,[124] in which the intermediate was isolated by oxidation resulting in a crystalline enone (*Figure 101*).

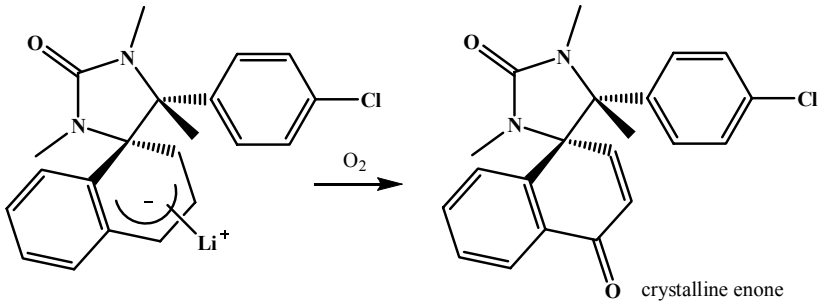

***Figure 101*: Rearrangement in lithiated ureas: the oxidation permit the crystallization of corresponding enone.**

Hence our goal was the optimization of this rearrangement. The best reaction conditions were achieved by treating the carbamate with LDA (2.5 eq.) in Et_2O/DMPU[125] (4:1) at -78 °C; the solution became orange-red and after work up with MeOH the product was obtained in good yield. (*Figure 102*). Once reaction conditions have been optimized we made a series of related carbamates from α-methylated benzylic alcohols and the products were isolated in good to excellent yield (*Table 13*).

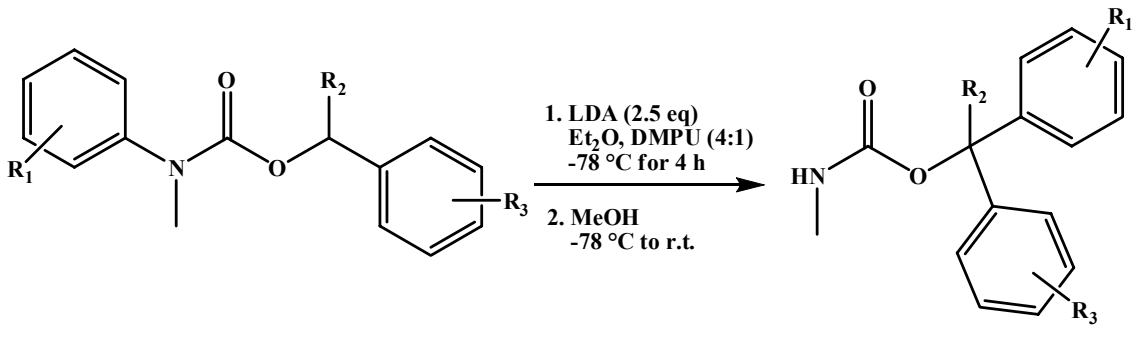

42 **43**

***Figure 102*: Aryl transfer in lithiated carbamates.**

Table 13: **Rearrangements of carbamates 42.**

S.M. 42	R_1	R_2	R_3	43 (yield)
42a	p-Me	H	H	**43a (62 %)**
42b	o-Me	H	H	**43b (55 %)**
42c	p-F	H	H	**43c (40 %)**
42d	p-Me	Me	H	**43d (84 %)**
42e	o-Me	Me	H	**43e (72 %)**
42f	o-i-Pr	Me	H	**43f (67 %)**
42g	p-Me	Me	p-Cl	**43g (82 %)**

The easy deprotection to give the alcohols **44** was done for the compounds **43a**, **43b** and **43c** by treatment of carbamates with sodium ethoxide in ethanol by refluxing for 2 h (*Figure 103* and results in *Table 14*).

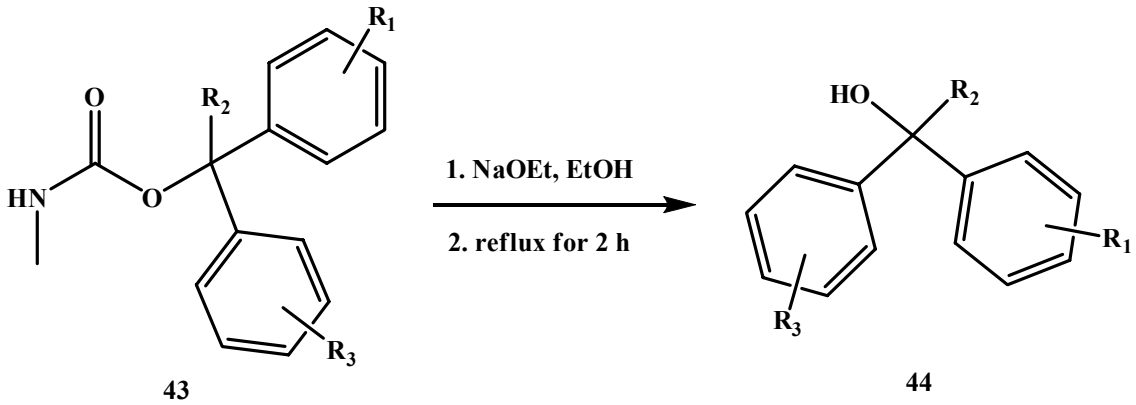

43 **44**

Figure 103**: Diary-alcohols by deprotection of carbamates 43.**

Table 14: **Deprotection of carbamates 43**

S.M. 43	R_1	R_2	R_3	44 (yield)
43a	p-Me	H	H	**44a (68 %)**
43b	o-Me	H	H	**44b (83 %)**
43c	p-F	H	H	**44c (67 %)**

A further support to the suggest of mechanism rearrangement is given by DFT calculations. Two competition transfer could be investigated: the 1,2-acyl shift and 1,4-aryl transfer (*Figure 104*).

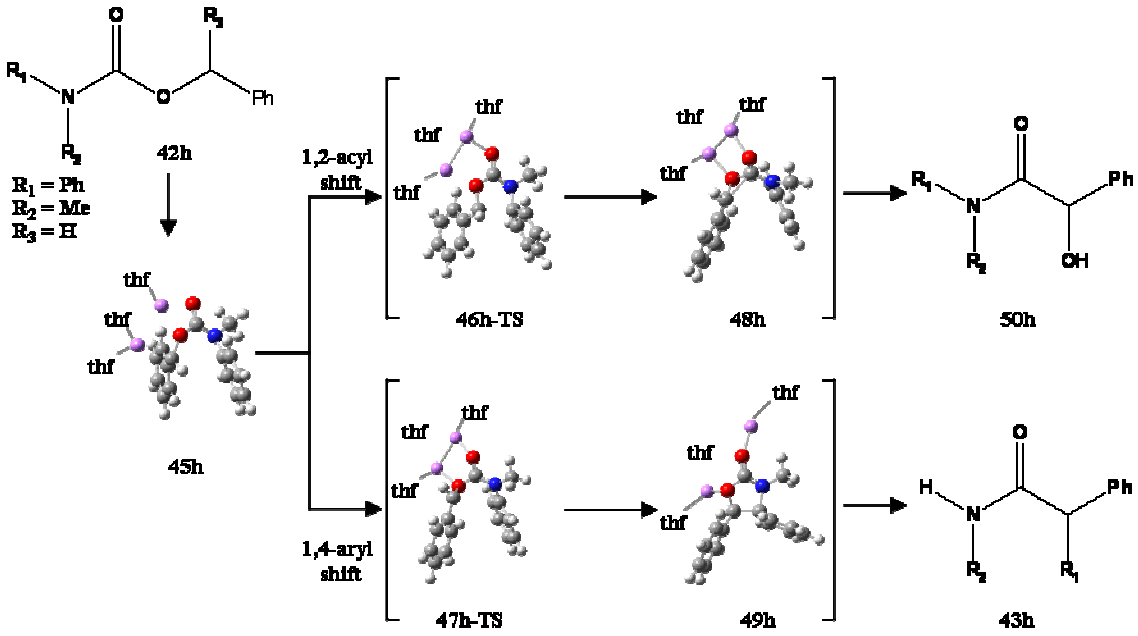

Figure 104: **Mechanism and Selectivity: 1,4-aryl vs. 1,2-acyl transfer.**
Li = fuchsia; N = blue; O = red; C = grey; H = white.

The stationary structures involved in the conversion of the organolithium **45h** to both cyclic intermediate **48h** (1,2-acyl transfer) and **49h** (1,4-aryl transfer) were

determined using DFT calculations (further details in *sect. 6.5*).[15] A simple carbamate **42h** with R_1 = Ph, R_2 = Me and R_3 = H was chosen as the substrate. The anionic intermediate **45h** was coordinate with two Li^+ cations and three THF solvent molecules; in addition solvent effect was introduced by using a continuum bulk model. The structures **46h-TS** and **47h-TS** were identified like transition state and the calculated free energy barrier are reported in *Figure 105*.

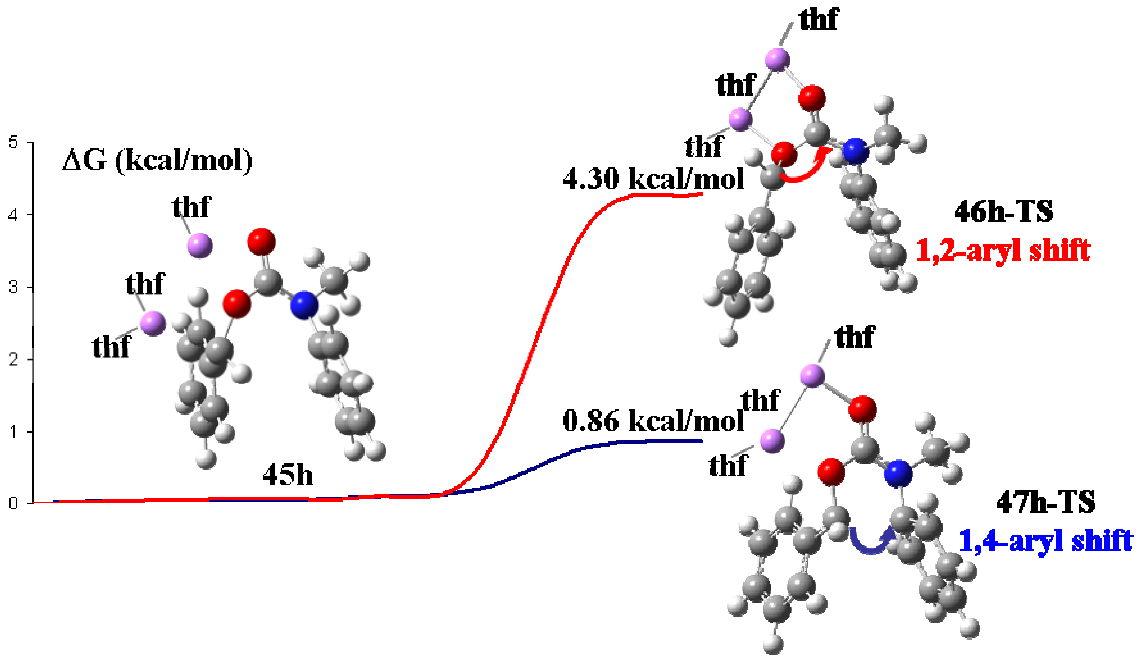

Figure 105: **Rearrangement's pathway of organolithium *45h* (stationary state) en route to *46h-TS* (1,2-acyl shift) and *47h-TS* (1,4-aryl shift)**

The calculated free energy barrier for the attack on the aromatic ring (1,4-aryl shift $\Delta G^{\#}$ = 0.86 kcal mol^{-1}) is considerably lower (by 3.74 kcal mol^{-1}) than the barrier for the attack on the carbonyl group (1,2-acyl shift $\Delta G^{\#}$ = 4.30 kcal mol^{-1}).

For a 1,2-acyl shift of an N,N-dimethyl carbamate (R_1 = R_2 = Me, undergoing a similar reaction as substrate in *Figure 99*), the corresponding barrier (5.42 kcal mol^{-1}) is close to the value for the conversion of **45h**. This shows that the N-phenyl group R_1 favours aryl transfer simply by opening up an alternative pathway rather than by disfavouring the 1,2-acyl shift.

6.2 Conclusions

Within Prof. Clayden's group, we have studied the rearrangement of carbamates **42**. We discovered that this kind of compounds, carrying an N-aryl substituent, on lithiation the N-aryl group is transferred cleanly from N to C, through an 1,4-aryl transfer. This aryl migration in lithiated carbamates provides a new route to α,α-arylated secondary or tertiary alcohols. The best condition was found treating the carbamate **42** with LDA (2.5 eq) in Et_2O/DMPU (4:1) at -78 °C, obtaining the compound **43** in good yields. The deprotection to obtain the corresponding alcohol was done with NaOEt in EtOH in good yields.

The theoretical studies with DFT calculations confirm the 1,4-aryl shift as the favourite mechanism. The latter having a significantly lower energy pathway than the 1,2-aryl transfer.

6.3 Experimental Section

6.3.1 Procedure for preparation of carbamates 42

The aryl isocyanate (1 equiv.) was added in one portion to a solution of the benzylic alcohol (1 equiv.) and triethylamine (2 equiv.) in anhydrous DCM (0.2 M) stirred at room temperature. The solution was stirred for 24 hours. The reaction was concentrated and the product was then purified by flash column chromatography on silica.

NaH (60% in mineral oil, 2 equiv.) was added to a stirred solution of carbamate in THF (0.2 M) at room temperature. After 30 min. methyl iodide (2.5 equiv.) was added and the reaction left to stir for 24 h. Water was added and the reaction mixture was extracted with diethyl ether. The organic layers were then repeatedly washed with water, dried with $MgSO_4$, filtered and evaporated under reduced pressure. The crude product was purified by flash column chromatography on silica.

Methyl p-tolyl carbamic acid 1-benzyl ester 42a

Flash column chromatography (SiO_2; 9:1 Petrol:EtOAc) gave the title compound as a colourless oil (88 %). Rf 0.26; IR νmax ($CHCl_3$)/cm^{-1} 1708 (C=O); ^{1}H-NMR ($CDCl_3$, 400 MHz) δ 7.26-7.22 (m, 5H), 7.09-7.06 (m, 4H), 5.08 (s, 2H), 3.22 (s, 3H, N-CH_3), 2.27 (s, 3H, p-CH_3); ^{13}C-NMR ($CDCl_3$, 100 MHz) δ 155.6 (C=O), 140.6 (C), 136.8 (C), 135.9 (C), 129.5 (2 CH), 128.4 (2 CH), 127.8 (2 CH), 127.7 (CH), 125.7 (2 CH), 67.2 (CH_2), 37.9 (NCH_3), 21.0 (p-CH_3); MS (EI+) m/z 255 (M+), 211, 120, 91 (100%); HRMS (EI+) calcd for $C_{16}H_{17}NO_2$ (M+): 255.1259, found: 255.1257.

Methyl o-tolyl carbamic acid 1-benzyl ester 42b

Flash column chromatography (SiO_2; 9:1 Petrol:EtOAc) gave the title compound as a colourless oil (89 %). Rf 0.26; IR νmax ($CHCl_3$)/cm^{-1} 1708 (C=O); ^{1}H-NMR ($CDCl_3$, 500 MHz) 2 conformers: *a* 27.3 %, *b* 72.7 % δ 7.48-7.13 (m, 9H *a* + *b*), 5.24 (br s, 2H, *b*), 5.15 (d, 1H, J = 13.0, *a*), 5.05 (d, 1H, J = 13.0, *a*), 3.25 (s, 3H, N-CH_3, *b*), 3.23 (s, 3H, N-CH_3, *a*), 2.25 (s, 3H, o-CH_3, *b*), 2.17 (s, 3H, o-CH_3, *a*); ^{13}C-NMR ($CDCl_3$, 125 MHz) δ 155.7 (C=O), 141.6 (C), 136.8 (C), 135.6 (C), 130.9 (CH), 128.3 (CH), 128.0 (CH), 127.7 (CH), 127.6 (2 CH), 126.9 (CH), 67.0 (CH_2), 37.4 (NCH_3), 17.4 (o-CH_3); MS (EI+) m/z 255 (M+), 120, 106, 91 (100%); HRMS (EI+) calcd for $C_{16}H_{17}NO_2$ (M+): 255.1259, found: 255.1261.

Methyl p-fluorophenyl carbamic acid 1-benzyl ester 42c

Flash column chromatography (SiO_2; 9:1 Petrol:EtOAc) gave the title compound as a colourless oil (85 %). Rf 0.22; IR νmax ($CHCl_3$)/cm^{-1} 1707 (C=O), 1509 (C-F); ^{1}H-NMR ($CDCl_3$, 400 MHz) δ 7.26-7.13 (m, 7H), 6.98-6.94 (m, 2H), 5.08 (s, 2H), 3.22 (s, 3H, N-CH_3); ^{13}C-NMR ($CDCl_3$, 100 MHz) δ 161.9 (CF), 159.5 (C=O), 155.5 (C), 139.2 (C), 136.5 (CH), 128.5 (2 CH), 128.3 (CH), 128.0 (CH), 115.8 (2 CH), 115.6 (2 CH), 67.4

(CH_2), 38.0 (N-CH_3) MS (EI+) m/z 255 (M+), 211, 120, 91 (100%); HRMS (EI+) calcd for $C_{15}H_{14}FNO_2$ (M+): 259.1009, found: 259.1012.

Methyl p-tolyl carbamic acid 1-phenylethyl ester 42d

Flash column chromatography (SiO_2; 9:1 Petrol:EtOAc) gave the title compound as a colourless oil (87 %). Rf: 0.28; IR νmax ($CHCl_3$)/cm^{-1} 1702 (C=O); ^{1}H-NMR ($CDCl_3$, 400 MHz) δ 7.20-7.14 (m, 5H), 7.05-7.00 (m, 4H), 5.74 (q, 1H, J = 6.5), 3.17 (s, 3H, N-CH_3), 2.24 (s, 3H, p-CH_3), 1.38 (br s, 3H, CH_3); ^{13}C-NMR ($CDCl_3$, 100 MHz) δ 155.1 (C=O), 142.4 (C), 140.8 (C), 135.7 (C), 129.4 (2 CH), 128.4 (2 CH), 127.5 (CH), 125.8 (2 CH), 125.7 (2 CH), 73.6 (CH), 37.8 (N-CH_3), 22.9 (CH_3), 21.0 (p-CH_3); MS (EI+) m/z 269, 225, 166, 121 (100%), 105 (100%) 91, 77; HRMS (EI+) calcd for $C_{17}H_{19}NO_2$ (M+): 269.1416, found: 269.1410.

Methyl o-tolyl carbamic acid 1-phenylethyl ester 42e

Flash column chromatography (SiO_2; 9:1 Petrol:EtOAc) gave the title compound as a colourless oil (86 %). Rf 0.27; IR νmax ($CHCl_3$)/cm^{-1} 1702 (C=O); ^{1}H-NMR ($CDCl_3$, 400 MHz) 3 conf: *a* 50%, *b* 14.3%, *c* 35.7%, δ 7.45-7.06 (m, 9H, *a*+*b*+*c*), 5.90 (br s, 1H, *b*), 5.83 (q, 1H, J = 6.5, *a*+*c*), 3.28 (s, 3H, N-CH_3, *b*), 3.20 (s, 3H, NCH_3, *a*), 3.20 (s, 3H, N-CH_3, *c*), 2.30 (s, 3H, o-CH_3, *a*), 2.09 (s, 3H, o-CH_3, *b*), 2.06 (s, 3H, o-CH_3, *c*), 1.64 (d, 3H, J = 6.5, CH_3, *c*), 1.40 (m, 3H, CH_3 *a*+*b*); ^{13}C-NMR ($CDCl_3$, 100 MHz) 155.3, 155.1 (C=O), 142.6, 142.4 (C), 141.8 (C), 135.6 (C), 130.7 (CH), 128.3 (2 CH), 127.6 (CH), 127.5, 127.4 (CH), 127.3 (CH), 126.8 (CH), 125.7 (CH), 125.4 (CH), 73.4, 73.2 (CH), 37.2, 37.1 (CH_3), 23.2, 22.9 (N-CH_3), 17.5, 17.4 (o-CH_3); MS (EI+) m/z 269, 210, 166, 121, 105 (100%), 91, 77; HRMS (EI+) calcd for $C_{17}H_{19}NO_2$ (M+): 269.1416, found: 269.1406.

Methyl o-isopropylphenyl carbamic acid 1-phenylethyl ester 42f

Flash column chromatography (SiO_2; 9:1 Petrol:EtOAc) gave the title compound as a colourless oil (83 %). Rf 0.32; IR νmax ($CHCl_3$)/cm^{-1} 1705 (C=O); ^{1}H-NMR ($CDCl_3$, 400 MHz) 3 conformers: *a* 37.8 %, *b* 11.8 %, *c* 50.4 % δ 7.46-7.05 (m, 9H, *a*+*b*+*c*), 5.91-5.79 (m, 3H, CH *a*+*b*+*c*), 3.28 (s, 3H, N-CH_3, *b*), 3.22 (s, 3H, N-CH_3, *a*), 3.21 (s, 3H, N-CH_3, *c*), 3.15 (sep, 1H, J = 7.0, *c*), 2.96 (sep, 1H, J = 7.0, *a*), 2.84 (sep, 1H, J = 7.0, *b*), 1.64 (br s, 3H, MeiPr, *b*), 1.40 (br s, 3H, MeiPr,, *a*), 1.27 (br s, 3H, MeiPr,, *c*), 1.16 (d, 3H, J = 7.0, CH_3, *c*), 1.05 (d, 3H, J = 7.0, CH_3, *b*), 0.97 (d, 3H, J = 7.0, CH_3, *a*); ^{13}C-NMR ($CDCl_3$, 100 MHz) 155.6, 155.4 (C=O), 146.25, 146.2 (C), 142.6, 142.1 (C), 140.5, 140.3 (C), 128.3 (2CH), 128.2, 128.1 (CH), 128.0 (CH), 127.8 127.7 (CH), 127.4, 127.3 (CH), 126.5, 126.5 (CH), 125.8 (CH), 125.4 (2CH), 73.5, 73.3 (CH), 38.3, 38.2 (CH3), 27.8, 27.6 (N-CH_3), 24.3, 24.2, 23.6, 23.2, 23.1, 22.7 (MeiPr,); MS (EI+) m/z 297, 193, 148, 133, 117, 105 (100%), 91, 77; HRMS (EI+) calcd for $C_{19}H_{23}NO_2$ (M+): 297.1729, found: 297.1720.

Methyl p-tolyl carbamic acid 1-(p-chlorophenyl)ethyl ester 42g

Flash column chromatography (SiO_2; 9:1 Petrol:EtOAc) gave the title compound as a colourless oil (80 %). Rf 0.27; IR νmax ($CHCl_3$)/cm^{-1} 1708 (C=O); ^{1}H-NMR ($CDCl_3$, 500 MHz) δ 7.29 (m, 2H), 7.17 (m, 4H), 7.12 (m, 2H), 5.82 (q, 1H, J = 6.5), 3.29 (s, 3H, N-CH_3), 2.38 (s, 3H, p-CH_3), 1.48 (br s, 3H, CH_3); ^{13}C-NMR ($CDCl_3$, 125 MHz) δ 154.9 (C=O), 140.9 (C), 140.6 (C), 136.0 (C), 133.3 (C), 129.4 (2 CH), 128.6 (2 CH), 127.3 (2 CH), 125.8 (2 CH), 72.9 (CH), 37.8 (N-CH_3), 22.8 (CH_3), 22.0 (p-CH_3); MS (EI+) m/z 303, 259, 166, 139 (100%), 121 (100%), 103, 91; HRMS (EI+) calcd for $C_{17}H_{18}ClNO_2$ (M+): 304.1021, found: 303.1022.

6.3.2 Procedure for Lithiation of Carbamates 43

LDA (17.5 mmol) was added to a solution of the carbamate (7 mmol) in diethyl ether (70 ml) and DMPU (18 ml) at -78 °C under N_2. The reaction was stirred for 4 hours at -78 °C. The reaction was then quenched with MeOH (10 ml), diluted with diethyl ether (200 ml) and washed with water (2 x 50 ml). The organics were dried over $MgSO_4$, concentrated under reduced pressure and the residue purified by flash silica chromatography.

Methylcarbamic acid p-tolyl-(phenyl)methyl ester 43a

By general procedure, carbamate **43a** (724 mg, 2.84 mmol) gave, after flash column chromatography (SiO_2; 4:1 Petrol:EtOAc), the title compound as a colourless oil (449 mg, 62 %). Rf 0.28; IR νmax ($CHCl_3$)/cm^{-1} 3395 (N-H), 1696 (C=O); ^{1}H-NMR ($CDCl_3$, 400 MHz) δ 7.22-7.12 (m, 7H), 7.04 (d, 2H, J = 8.0), 6.69 (s, 1H), 4.77 (br s, 1H, N-H), 2.67 (d, 3H, J = 5.0, N-CH_3), 2.23 (s, 3H, p-CH_3); ^{13}C-NMR ($CDCl_3$, 100 MHz) δ 156.4 (C=O), 140.9 (C), 137.8 (C), 137.6 (C), 129.2 (2 CH), 128.4 (CH), 127.7 (2 CH), 127.2 (2 CH), 126.9 (2 CH), 77.3 (CH), 27.6 (N-CH_3), 21.2 (p-CH_3); MS (EI+) m/z 255 (M+), 198, 180 (100%), 165; HRMS (EI+) calcd for $C_{16}H_{17}NO_2$ (M+): 255.1259, found: 255.1249.

Methylcarbamic acid o-tolyl-(phenyl)methyl ester 43b

By general procedure, carbamate **43b** (833 mg, 3.26 mmol) gave, after flash column chromatography (SiO_2; 4:1 Petrol:EtOAc), the title compound as a colourless oil (458 mg, 55 %). Rf 0.32; IR νmax ($CHCl_3$)/cm^{-1} 3345 (N-H), 1700 (C=O); ^{1}H-NMR ($CDCl_3$, 400 MHz) δ 7.39-7.27 (m, 6H), 7.24-7.14 (m, 3H), 6.99 (s, 1H), 4.82 (m, 1H, N-H), 2.80 (d, 3H, J = 5.0, N-CH_3), 2.31 (s, 3H, o-CH_3); ^{13}C-NMR ($CDCl_3$, 100 MHz) δ 156.3 (C=O), 139.8 (C), 138.5 (C), 135.7 (C), 130.6 (CH), 128.4 (2 CH), 127.8 (CH), 127.7 (CH), 127.4 (2 CH), 126.7 (CH), 126.0 (CH), 74.7 (CH), 27.6 (N-CH_3), 19.4 (o-

CH_3); MS (EI+) m/z 255 (M+), 198, 180 (100%), 165, 152, 91; HRMS (EI+) calcd for $C_{16}H_{17}NO_2$ (M+): 255.1254, found: 255.1246.

Methylcarbamic acid p-fluorophenyl-(phenyl)methyl ester 43c

By general procedure, carbamate **43c** (767 mg, 2.96 mmol) gave, after flash column chromatography (SiO_2; 4:1 Petrol:EtOAc), the title compound as a white solid (307 mg, 40 %). Rf 0.28; M.P. 88-90 °C; IR νmax ($CHCl_3$)/cm^{-1} 3342 (N-H), 1700 (C=O), 1509 (C-F); ^{1}HNMR ($CDCl_3$, 400 MHz) δ 7.37-7.28 (m, 7H), 7.06-7.00 (m, 2H), 6.80 (s, 1H), 4.84 (br s, 1H, N-H), 2.82 (d, 3H, J = 5.0, N-CH_3); ^{13}C-NMR ($CDCl_3$, 100 MHz) δ 162.3 (d, C-F, JC-F = 246.5), 156.2 (C=O), 140.4 (C), 136.6 (C), 129.0 (CH), 128.5 (2 CH), 127.9 (2 CH), 126.9 (2 CH), 115.3 (2 CH), 76.7 (CH), 27.6 (N-CH_3); MS (EI+) m/z 259 (M+), 201, 183, 164, 48 (100%); HRMS (EI+) calcd for $C_{15}H_{14}FNO_2$ (M+): 259.1009, found: 259.0998.

Methylcarbamic acid 1-(p-tolyl)-1-phenylethyl ester 43d

By general procedure, carbamate **43d** (839 mg, 3.1 mmol) gave, after flash column chromatography (SiO_2; 4:1 Petrol:EtOAc), the title compound as a colourless oil (702 mg, 84 %). Rf 0.26; IR νmax ($CHCl_3$)/cm^{-1} 3351 (N-H), 1700 (C=O); ^{1}H-NMR ($CDCl_3$, 400 MHz) δ 7.22-7.19 (m, 4H), 7.16-7.11 (m, 3H), 7.02 (m, 2H), 4.73 (br s, 1H, N-H), 2.61 (d, 3H, J = 5.0, N-CH_3), 2.23 (s, 3H, p-CH_3), 2.14 (s, 3H, CH_3); ^{13}C-NMR ($CDCl_3$, 100.6 MHz) δ 155.5 (C=O), 146.4 (C), 143.1 (C), 136.6 (C), 128.8 (2 CH), 128.0 (2 CH), 127.0 (CH), 125.9 (2 CH), 125.85 (2 CH), 83.7 (CH), 27.5 (CH_3), 27.3 (N-CH_3), 21.1 (p-CH_3); MS (EI+) m/z 269, 212, 194 (100%), 178, 165; HRMS (EI+) calcd for $C_{17}H_{19}NO_2$ (M+): 269.1416, found: 269.1419.

Methylcarbamic acid 1-(o-tolyl)-1-phenylethyl ester 43e

By general procedure, carbamate 43e (807 mg, 3.1 mmol) gave, after flash column chromatography (SiO_2; 4:1 Petrol:EtOAc), the title compound as a white solid (581 mg, 72 %). Rf 0.26; M.P. 154-156 °C; IR νmax ($CHCl_3$)/cm^{-1} 3344 (N-H), 1700 (C=O); ^{1}H-NMR ($CDCl_3$, 400 MHz) δ 7.56 (m, 1H), 7.19-7.12 (m, 7H), 6.99 (d, 1H, J = 7.5 Hz), 4.68 (br s, 1H, N-H), 2.62 (d, 3H, J = 4.5, N-CH_3), 2.11 (s, 3H, CH_3), 1.86 (s, 3H, o-CH_3); ^{13}C-NMR ($CDCl_3$, 100 MHz) δ 155.2 (C=O), 146.8 (C), 141.7 (C), 136.4 (C), 132.3 (CH), 127.9 (2 CH), 127.8 (CH), 127.4 (CH), 126.7 (CH), 125.3 (CH), 125.2 (2 CH), 84.4 (C), 29.7 (CH_3), 27.3 (N-CH_3), 21.2 (o-CH_3); MS (EI+) m/z 269, 212, 194, 178 (100%), 165; HRMS (EI+) calcd for $C_{17}H_{19}NO_2$ (M+): 269,1410, found: 269.1406.

Methylcarbamic acid 1-(o-isopropylphenyl)-1-phenylethyl ester 43f

By general procedure, carbamate **43f** (918 mg, 3.09 mmol) gave, after flash column chromatography (SiO_2; 4:1 Petrol:EtOAc), the title compound as a white solid (618 mg, 67 %). Rf 0.31; M.P. 180-182 °C; IR νmax ($CHCl_3$)/cm^{-1} 3384 (N-H), 1693 (C=O); ^{1}H-NMR ($CDCl_3$, 400 MHz) δ 7.68 (m, 1H), 7.36-7.21 (m, 8H), 4.78 (br s, 1H, N-H), 3.07 (sep, 1H, J = 6.5, CHipr), 2.72 (d, 3H, J = 5.5, N-CH_3), 2.22 (s, 3H, CH_3), 1.02 (d, 3H, J = 6.5, CH_3-ipr"), 0.56 (d, 3H, J = 6.5, CH_3-ipr'); ^{13}C-NMR ($CDCl_3$, 100 MHz) δ 155.3 (C=O), 148.0 (C), 147.6 (C), 140.3 (C), 128.2 (CH), 127.9 (2 CH), 127.7 (CH), 127.3 (CH), 126.6 (CH), 125.1 (2 CH), 124.9 (CH), 84.3 (C), 30.2 (CH_3), 29.2 (CHipr), 27.2 (N-CH_3),24.6 (CH_3-ipr"), 22.9 (CH_3-ipr'); MS (EI+) m/z 297, 240, 222, 206 (100%), 191, 178; HRMS (EI+) calcd for $C_{19}H_{23}NO_2$ (M+): 297.1729, found: 297.1720.

Methylcarbamic acid 1-(p-tolyl)-1-(p-chlorophenyl)ethyl ester 43g

By general procedure, carbamate **43g** (1.003 g, 3.3 mmol) gave, after flash column chromatography (SiO_2; 4:1 Petrol:EtOAc), the title compound as a white solid (0.822 mg, 82 %). Rf 0.31; M.P. 108-110 °C; IR νmax ($CHCl_3$)/cm^{-1} 3351 (N-H), 1700 (C=O); ^{1}H-

NMR ($CDCl_3$, 500 MHz) δ 7.17 (m, 4H), 7.08 (m, 2H), 7.02 (m, 2H), 4.73 (br s, 1H, N-H), 2.63 (d, 3H, J = 5.0 Hz, N-CH_3), 2.24 (s, 3H, p-CH_3), 2.11 (s, 3H, CH_3); ^{13}C-NMR ($CDCl_3$, 125 MHz) δ 155.3 (C=O), 144.9 (C), 142.8 (C), 136.9 (C), 132.8 (C), 128.9 (2 CH), 128.2 (2 CH), 127.4 (2 CH), 125.7 (2 CH), 83.3 (C), 27.4 (CH_3), 27.3 (N-CH_3), 21.0 (p-CH_3); MS (EI+) m/z 303, 246, 228 (100%), 212, 193, 178; HRMS (EI+) calcd for $C_{17}H_{18}ClNO_2$ (M+): 303.1021, found: 303.1018.

6.3.3 Procedure for the deprotection of carbamates 44

The carbamates **43** was dissolved in EtOH and NaOEt (21% solution in EtOH, 10 equiv.) was added. The solution was heated to 78 °C until TLC control showed full conversion (6 to 24 h). The solution was cooled to RT, neutralised with AcOH and the solvent was evaporated. The crude product was purified by flash chromatography (silica, petroleum ether/EtOAc 12:1).

p-Methylphenyl(phenyl)methanol 44a[126]

Following the general procedure, carbamate **43a** (17 mg, 0.07 mmol) was treated with NaOEt (21 % in EtOH, 0.22 mL, 0.7 mmol). The crude product was purified by flash column chromatography (SiO_2; 12:1 Petrol:EtOAc) giving the title compound as a colourless oil (9 mg, 68 %). The experimental data (^{1}H- and ^{13}C-NMR, EI-MS) were identical to that previously reported.[127]

o-Methylphenyl-(phenyl)methanol 44b

Following the general procedure, carbamate **43b** (85 mg, 0.33 mmol) was deprotected using NaOEt (21 % in EtOH, 1.1 mL, 3.3 mmol). The crude product was purified by flash column chromatography (SiO_2; 12:1 Petrol:EtOAc) giving the title compound as a white solid (55 mg, 83 %). The experimental data (^{1}H- and ^{13}C-NMR, EI-MS) were identical to that previously reported.[127]

p-Fluorophenyl-(phenyl)methanol 44c

Following the general procedure, carbamate **43c** (21 mg, 0.08 mmol) was deprotected using NaOEt (21 % in EtOH, 0.27 mL, 0.8 mmol). The crude product was purified by flash column chromatography (SiO_2; 12:1 Petrol:EtOAc) giving the title compound as a colourless oil (11 mg, 67 %). The experimental data (^{1}H- and ^{13}C-NMR, EI-MS) were identical to that previously reported.[127]

6.4 NMR Spectroscopy

NMR spectra were recorded on a Varian XL 300 or a Bruker Ultrashield 300, 400 or 500 MHz spectrometer. The chemical shifts (δ) are reported in ppm downfield of trimethylsilane and coupling constants (J) reported in hertz and rounded to 0.5 Hz. Splitting patterns are abbreviated as follows: singlet (s), doublet (d), triplet (t), quartet (q), septet (sep), mulitiplet (m), broad (br), or a combination of these. Solvents were used as internal standard when assigning NMR spectra (δ H: $CDCl_3$ 7.26 ppm; δ C: $CDCl_3$ 77.0 ppm). Low and high resolution mass spectra were recorded by staff at the University of Manchester. EI and CI spectra were recorded on a Micromass Trio 2000; ES and APCI spectra were recorded on a Micromass Platform II; high resolution mass spectra (HRMS, EI and ES) were recorded on a Thermo Finnigan MAT95XP mass spectrometer. Infrared spectra were recorded on a Perkin Elmer Spectrum RX I FTIR spectrometer as a film on a sodium chloride plate. Absorptions reported are sharp and strong unless otherwise stated as broad (br), medium (m), or weak (w), only absorption maxima of interest are reported. Melting points (M.P.) were determined on a Gallenkamp apparatus and are uncorrected.

Thin layer chromatography (TLC) was performed using commercially available pre-coated plates (Macherey-Nagel alugram Sil G/UV254) and visualised with UV light at 254 nm or phosphomolybdic acid dip (5 % in ethanol). Flash chromatography was carried out using Fluorochem Davisil 40-63u 60 Å.

All reactions were conducted under an atmosphere of dry nitrogen in oven dried glassware. Tetrahydrofuran (THF) was distilled under nitrogen from sodium using benzophenone as indicator. Dichloromethane and toluene were obtained by distillation from calcium hydride under nitrogen. Petrol refers to the fraction of light petroleum ether boiling between 40-65 °C. All other solvents and commercially obtained reagents were used as received or purified using standard procedures.

6.5 Calculations

Density functional theory (DFT) calculations at the B3LYP/6-31++G** level were used to obtain structures of the anionic lithium (**45h**), and the cyclic intermediate (**48h**, **49h**) (*Figure 104*), and the corresponding transition structures (*Figure 104* and *Figure 105*). The relative free energies of these structures in bulk THF were obtained employing the CPCM method for bulk solvation, together with zero point energies calculated for the corresponding structures at the B3LYP/6-31G level. All calculations were carried out using Gaussian 03.[15]

Bibliography

1) Jackman, L.M., Cotton, F.A. eds. *Dynamic Nuclear Magnetic Resonance Spectroscopy*, Academic Press, New York, NY, **1975**.

2) Gutowsky, H.S.; Holm, C.H. *J. Chem. Phys.* **1956,** *25,* 1228.

3) Eyring, H. *Chem. Revs.* **1935**, *17*, 65.

4) a) Allerhand, A.; Gutowsky, H.S.; Jonas, J.; Meinzer, R.A. *J. Am. Chem. Soc.* **1966**, *38*, 3185; b) Binsch, G. *J. Am. Chem. Soc.* **1969**, *91*, 1304; c) Dahlqvist, K.I.; Forsen, S.; Alm, T. *Acta Chem. Scand.* **1970**, *24*, 651; d) Brown, J.H.; Bushweller, H.C. *QCPE DNMR6*, Indiana University.

5) Oki, M. *Top. Stereochem.* **1984**, *14*, 1.

6) Kuhn, R. *"Molekulare asymmetrie", Stereochemie* Frendenberg, K. Ed.; Franz Deutike, **1933**, 803.

7) Eliel, L. E.; Wilen, S. H.; *Stereochemistry of Organic Compounds*; John Wiley and Sons: New York, **1994**; chapter 14.

8) Introduction of DFT are in Young, D. *Computational Chemistry* John Wiley & Sons, New York, **2001**.

9) Hohenberg P.; Kohn, W. *Phys. Rev.* **1964**, *136*, B864.

10) Kohn, W.; Sham, *Phys. Rev.* **1965**, *140*, A1133.

11) a) Becke, A.D. *J. Chem. Phys.* **1993**, *98*, 5648; b) Lee, C.; Yang, W.; Parr, R.G. *Phys. Rev.* **1988**, *B 37*, 785.

12) a) Lynch, B. J.; Fast, P. L.; Harris, M.; Truhlar, D. G. *J. Phys. Chem. A* **2000**, *104*, 4811; b) Zhao, Y.; Tishchenko, O.; Truhlar, D. G. *J. Phys. Chem. B* **2005**, *109*, 19046; c) Tsuzuki, S.; Luthi, H. P. *J. Chem. Phys.* **2001**, *114*, 3949; d) Duncan, J. A.; Spong, M. C. *J. Phys. Org. Chem.* **2005**, *18*, 462.

13) a) Newsoroff, G. P.; Sternhell, S. *Tetrahedron Lett*. **1967**, *8*, 2539; b) Baas, J. M. A.; Sinnema, A. *Recl. Trav. Chim. Pays-Bas* **1973**, *92*, 899 ; c) Baas, J. M. A.; van der Toorn, J. M.; Wepster, B. M. *Recl. Trav. Chim. Pays-Bas* **1974**, *93*, 173. d) Landman, D.; Newsoroff, G. P.; Sternhell, S. *Aust. J. Chem.* **1972**, *25*, 109. Suezawa, H.; Wada, H.; Watanabe, H.; Yuzuri, T.; Sakakibara, K.; Hirota, M. *J. Phys. Org. Chem*. **1997**, *10,* 925; e) Anderson, S.; Drakenberg, T. *Org. Magn. Resonance* **1983**, *21,* 730; f) Lomas, J. S.; Dubois, J.-E. *J. Org. Chem.* **1976**, *41*, 3033; g) Lomas, J. S.; Luong, P. K.; Dubois, J.-E. *J. Org. Chem.* **1977**, *42*, 3394; h) Lomas, J. S.; Dubois, J.-E. *Tetrahedron* **1981**, *37*, 2273; i) Lomas, J. S.; Vaissermann, J. *J. Chem. Soc. Perkin Trans. 2* **1998**, 1777; j) Lomas, J. S. *J. Chem. Soc. Perkin Trans. 2* **2001***,* 754; k) Lomas, J. S.; Adenier, A. *J. Chem. Soc. Perkin Trans. 2* **2002***, 1264;* l) Anderson, J. E.; Bru-Capdeville, V.; Kirsch. P. A.; Lomas, J. S.

Chem. Comm. **1994**, 1077; m) Lomas, J. S.; Anderson, J .E. *J. Org. Chem.* **1995**, *60*, 3246; n) Casarini, D.; Lunazzi, L.; Mazzanti, A. *J. Org. Chem.* **1997**, *62*, 3315; o) Wolf, C.; Pranatharthiharan, L.; Ramagosa, R. B. *Tetrahedron Lett.* **2002**, *43*, 8563; p) Casarini, D.; Coluccini, C.; Lunazzi, L.; Mazzanti, A. *J. Org. Chem.* **2005**, *70*, 5098.

14) Casarini, D.; Lunazzi, L.; Mancinelli, M.; Mazzanti, A. *J. Org. Chem.* **2007**, *72*, 998.

15) Program Gaussian 03, Revision D.01, Frisch, M. J.; Trucks, G. W.; Schlegel, H. B.; Scuseria, G. E.; Robb, M. A.; Cheeseman, J. R.; Montgomery, Jr., J. A.; Vreven, T.; Kudin, K. N.; Burant, J. C.; Millam, J. M.; Iyengar, S. S.; Tomasi, J.; Barone, V.; Mennucci, B.; Cossi, M.; Scalmani, G.; Rega, N.; Petersson, G. A.; Nakatsuji, H.; Hada, M.; Ehara, M.; Toyota, K.; Fukuda, R.; Hasegawa, J.; Ishida, M.; Nakajima, T.; Honda, Y.; Kitao, O.; Nakai, H.; Klene, M.; Li, X.; Knox, J. E.; Hratchian, H. P.; Cross, J. B.; Bakken, V.; Adamo, C.; Jaramillo, J.; Gomperts, R.; Stratmann, R. E.; Yazyev, O.; Austin, A. J.; Cammi, R.; Pomelli, C.; Ochterski, J. W.; Ayala, P. Y.; Morokuma, K.; Voth, G. A.; Salvador, P.; Dannenberg, J. J.; Zakrzewski, V. G.; Dapprich, S.; Daniels, A. D.; Strain, M. C.; Farkas, O.; Malick, D. K.; Rabuck, A. D.; Raghavachari, K.; Foresman, J. B.; Ortiz, J. V.; Cui, Q.; Baboul, A. G.; Clifford, S.; Cioslowski, J.; Stefanov, B. B.; Liu, G.; Liashenko, A.; Piskorz, P.; Komaromi, I.; Martin, R. L.; Fox, D. J.; Keith, T.; Al-Laham, M. A.; Peng, C. Y.; Nanayakkara, A.; Challacombe, M.; Gill, P. M. W.; Johnson, B.; Chen, W.; Wong, M. W.; Gonzalez, C.; Pople, J. A.; Gaussian, Inc., Wallingford CT, **2004**.

16) MMX force field as in PC Model v 7.5, Serena Software, Bloomington, IN.

17) Eliel, L. E.; Wilen, S. H.; *Stereochemistry of Organic Compounds*; John Wiley and Sons: New York, **1994**; p. 21.

18) This result is at variance with the hypothesis of Schaefer *et al*., that have arbitrarily assumed conformation C to be the ground state. See: Schaefer, T.; Sebastian, R.; Penner, G.H.; Salman, S.R. *Can. J. Chem*. **1986**, *64*, 1602.

19) PC version of QCPE program DNMR 6 n° 633, Indiana University, Bloomington, IN.

20) The inversion of the relative stability of two conformers when the ethyl groups substitute the methyl groups had been well documented in analogous cases (see: Casarini, D.; Coluccini, C.; Lunazzi, L.; Mazzanti, A. *J. Org. Chem.* **2005**, *70*, 5098).

21) The existence of symmetric and asymmetric conformers due to the relative disposition of two ethyl groups has been also detected by supersonic jet mass resolved excitation spectroscopy (see: Breen, P. J.; Bernstein, E. R.; Seeman, J. I. *J .Chem. Phys*. **1987**, *87*, 3269). A situation analogous to the present one had been also observed in the case of 3-(1-naphthyl)pentan-3-ol (see: Ref. 12n).

22) As often observed in conformational process, the $\Delta G^{\neq}$ value was found independent of temperature within the experimental uncertainty of the NMR measurements. See:

Hoogosian, S.; Bushweller, C. H.; Anderson, W. G.; Kigsley, G. *J. Phys. Chem.* **1976**, *80*, 643; Lunazzi, L.; Cerioni, G.; Ingold, K. U. *J. Am. Chem. Soc.* **1976**, *98*, 7484; Forlani, L.; Lunazzi L.; Medici, A. *Tetrahedron Lett.* **1977**, *18*, 4525; Bernardi, F.; Lunazzi, L.; Zanirato, P.; Cerioni, G. *Tetrahedron*, **1977**, *33*, 1337; Lunazzi, L.; Magagnoli, C.; Guerra, M.; Macciantelli, D. *Tetrahedron Lett.* **1979,** 3031; Cremonini, M. A.; Lunazzi, L.; Placucci, G.; Okazaki, R.; Yamamoto, G. *J. Am. Chem. Soc.* **1990**, *112*, 2915; Anderson, J. E.; Tocher, D. A.; Casarini, D.; Lunazzi, L. *J. Org. Chem.* **1991**, *56*, 1731; Borghi, R.; Lunazzi, L.; Placucci, G.; Cerioni, G.; Foresti, E.; Plumitallo, A. *J. Org. Chem.* **1997**, *62*, 4924. Garcia, M. B.; Grilli, S., Lunazzi, L.; Mazzanti, A., Orelli, L. R. *J. Org. Chem.* **2001**, *66*, 6679. Garcia, M. B.; Grilli, S., Lunazzi, L.; Mazzanti, A., Orelli, L. R. *Eur. J. Org. Chem.* **2002**, 4018. Casarini, D.; Rosini, C.; Grilli, S; Lunazzi, L.; Mazzanti, A. *J. Org. Chem.* **2003**, *68*, 1815. Casarini, D.; Grilli, S.; Lunazzi, L.; Mazzanti, A. *J. Org. Chem.* **2004**, *69*, 345. Bartoli, G.; Lunazzi, L.; Massacesi, M.; Mazzanti, A. *J. Org. Chem.* **2004**, *69*, 821. Casarini, D.; Coluccini, C.; Lunazzi, L.; Mazzanti, A.; Rompietti, R. *J. Org. Chem.* **2004**, *69*, 5746.

23) Bondi, A. *J. Phys. Chem*, **1964**, *68*, 441.

24) Mazzanti, A.; Lunazzi, L.; Minzoni, M.; Anderson, J. E. *J. Org .Chem*. **2006**, *71*, 5474.

25) It should be outlined that the present result is at variance with the report of another pair of biphenyl derivatives, where the ortho-methyl substituted compound displayed a rotation barrier 0.5 kcal mol^{-1} higher than that of the corresponding chlorine derivative. See: Bott, G.; Field, L. D.; Sternhell, S. *J. Am. Chem. Soc.* **1980**, *102*, 5618.

26) Two values were indicated for the van der Waals radii of the methyl group: a minimum of 1.715 and a maximum of 2.23, see: Charton, M. *J. Am. Chem. Soc*. **1969**, *91*, 615.

27) DFT calculations of the whole energy surface exceeded the capabilities of our computing facilities, thus only the optimized singular points (ground and transition states) were computed.

28) Examples of NMR determinations of very low barriers can be found in: a) Anet. F. A. L.; Chmurny, G. N.; Krane, J. *J. Am. Chem. Soc*. **1973**, *95*, 4423. Anet, F.A.L.; Yavari I. *J. Am. Chem. Soc*. **1977**, *99*, 6752; b) Lunazzi, L.; Macciantelli, D.; Bernardi, F.; Ingold, K. U. *J. Am. Chem. Soc.* **1977**, *99*, 4573; c) Brown, J. H.; Bushweller, C. H. *J. Am. Chem. Soc*. **1992**, *114*, 8153; d) Pawar, D. M.; Noe, E. A. *J. Am. Chem. Soc.* **1998**, *120*, 41485; e) Pawar, D. M.; Wilson, K. K.; Noe, E. A. *J. Org. Chem*. **2000**, *65*, 1552; f) Casarini, D.; Grilli, S.; Lunazzi, L.; Mazzanti, A. *J. Org. Chem*. **2001**, *66*, 2757; g) Anderson J.E.; de Meijere, A.; Kozhushkov, S. I.; Lunazzi, L.; Mazzanti, S. *J. Am. Chem. Soc*. **2001**, *124*, 6706; h) Lunazzi, L.; Mazzanti, A.; Minzoni, M. *Tetrahedron*, **2005**, *61*, 6782; i) Lunazzi,

L.; Mazzanti, A.; Minzoni, M. *J. Org. Chem*. **2005**, *70*, 456; j) Pawar, D. M.; Brown II, J.; Chen, K.-H.; Allinger, N. L., Noe, E. A. *J. Org. Chem*. **2006**, *71*, 6512.

29) Lulinski, S.; Serwatowski, J. *J. Org. Chem.* **2003**, *68*, 5384.

30) Coe, P. L.; Waring, A. J.; Yarwood, T. D. *J. Chem. Soc. Perkin Trans. 1* **1995**, *21*, 2729.

31) Brown, H. C.; Grayson, M. *J. Am. Chem. Soc.* **1953**, *75*, 20.

32) Sheldrick, G. M. *SHELX97*; Universität Göttingen, Germany, 1997.

33) a) Bradley, S. A.; Krishnamurthy, K. *Magn. Reson. Chem.* **2005**, *43*, 117. b) Willker, W.; Leibfritz, D.; Kerssebaum, R.; Bermel, W. *Magn. Res. Chem.* **1993**, *31*, 287.

34) Hurd, R. E.; John, B. K. *J. Magn. Reson.* **1991**, *91*, 648.

35) Bringmann, G.; Price Mortimer, A. J.; Keller, P.A.; Gresser, M.J.; Garner, J.; Breuning, M. *Angew. Chem., Int. Ed.* **2005**, *44*, 5384 and references quoted therein.

36) Bott, G.; Field, L.D.; Sternhell, S. *J. Am. Chem. Soc.* **1980**,*102*, 5618.

37) a) Lunazzi, L.; Mazzanti, A.; Minzoni, M.; Anderson, J. E. *Org. Lett.* **2005**, *7*, 1291; b) Mazzanti, A.; Lunazzi, L.; Minzoni, M.; Anderson, J.E. *J. Org. Chem.* **2006**, *71*, 5474; c) Lunazzi, L.; Mazzanti, A.; Minzoni, M. *J. Org. Chem.* **2006**, *71*, 9297.

38) a) Casarini, D.; Lunazzi, L.; Mazzanti, A. *J. Org. Chem.* **1997**, *62*, 3315; b) Casarini, D.; Coluccini, C.; Lunazzi, L.; Mazzanti, A. *J. Org. Chem.* **2006**, *71*, 4490.

39) a) Mislow, K.; Raban, M. *Top. Stereochem.* **1967**, *1*, 1; b) Jennings, W.B. *Chem. Rev.* **1975**, *75*, 307; c) Eliel, E. L. *J. Chem. Educ.* **1980**, *57*, 52; d) Casarini, D.; Lunazzi, L.; Macciantelli, D. *J. Chem. Soc., Perkin Trans.* **1992**, *2*, 1363.

40) Meyer, W. L.; Meyer, R. B. *J. Am. Chem. Soc.* **1963**, *85*, 2171; Baitinger, W. F., Jr.; Schleyer, P. v. R.; Mislow, K. *J. Am. Chem. Soc.* **1965**, *87*, 3168.

41) Rajnikant, D.; Sharma, B.; Singh, D. *J. Chem. Crystallogr.* **2006**, *36*, 331.

42) Jackman, L. M.; Sternhell, S. *Application of NMR Spectroscopy in Organic Chemistry,* 2nd ed.; Pergamon Press: Oxford, **1969**; p. 17.

43) a) Ikeda, C.; Nagahara, N.; Motegi, E.; Yoshioka, N.; Inoue, H. *Chem. Comm.* **1999**, 1759; b) Escuder, B.; LLusar, M.; Travet, J. F. *J. Org. Chem.* **2006**, *71*, 7747.

44) Jackman, L. M.; Sternhell, S. *Application of NMR Spectroscopy in Organic Chemistry,* 2nd ed.; Pergamon Press: Oxford, **1969**; p. 95; Jennings, W.B.; Farrel, B. M.; Malone, J. F. *Acc. Chem. Res.* **2001**, *34*, 885; Wüthrich, K. *Angew. Chem. Int. Ed.* **2003**, *42*, 3340).

45) a) Howard, J. A. K.; Hoy, V. J.; O'Hagan, D.; Smith, G.T. *Tetrahedron* **1996**, *52*, 12613; b) Alkorta, I.; Rozas, I.; Elguero, J. *J. Fluorine Chem.* **2000**, *101*, 233.

46) The H-bond energy of a OH group with organo fluorine compounds is estimated to be between 2.4 kcal mol^{-1} (ref.34) and 3 kcal mol^{-1} (Bettinger, H. F. *Chem. Phys. Chem.* **2005**,

6, 1169), to be compared with the 9 kcal mol^{-1} of the H-bond with methanol (Pimentel, G. C.; McClellan, A. L. *The Hydrogen Bond*; Freeman and Co.: San Francisco **1960**; p. 99).

47) Claridge, T. D. W. *High Resolution NMR Techniques in Organic Chemistry;* Pergamon Press: Oxford **1999**; p. 36.

48) Johnson, C. S., Jr. *Prog. Nucl. Magn. Reson. Spectrosc.* **1999**, *34*, 203; Cohen, Y.; Avram, L.; Frish, L. *Angew. Chem., Int. Ed.* **2005**, *44*, 520; Pregosin, P. S.; Kumar, P. G. A.; Fernandez, I. *Chem. Rev.* **2005**, *105*, 2977. Dehner, A.; Kessler, H. *ChemBioChem* **2005**, *6*, 1550.

49) Cabrita, E. J.; Berger, S. *Magn. Reson. Chem.* **2001**, *39*, 3142; Valentini, M.; Rüegger, H.; Pregosin, P. S. *Helv. Chim. Acta* **2001**, *84*, 2833.

50) Pirkle, W. H.; Sikkenga, D. L.; Pavlin, M. S. *J. Org. Chem.* **1977**, *42*, 384.

51) Barron, L. *Molecular Light Scattering and Optical Activity;* Oxford University Press: Cambridge, U.K., 2004.

52) a) Jaffè, H. H.; Orchin, M. *The Theory and Application of UV Spectroscopy*; J. Wiley and Sons: New York, **1962**. b) Suzuki, H. *Electronic Absorption Spectra and Geometry of Organic Molecules;* Academic Press: New York, **1967**.

53) For Determination of the Absolute Configuations using DFT and ECD see: *J. Org. Chem.* **2006**, *71*, 6074. Tanaka, T.; Kodama, T. S.; Morita, H. E.; Ohno, T.; *Chyrality*, **2006**, *18*, 652. Stephensen, P. J.; Pan, J. J.; Devlin, F.; Urbanova, M.; Julinek, O.; Hajicek, J. *Chyrality*, **2008**, *20*, 454. Goerigk, L.; Grimme S. *J. Phys. Chem. A*, **2009**, *113*, 767

54) For TDDFT-CD calculations, see: a) Diedrich, C.; Grimme, S. *J. Phys. Chem. A* **2003**, *107*, 2524; b) Autschbach, J.; Ziegler, T.; van Gisbergen, S. J. A. ; Baerends, E. J. *J. Chem. Phys.* **2002**, *116*, 6930; c) Pecul, M.; Ruud, K.; Helgaker, T. *Chem. Phys. Lett.* **2004**, *388*, 110; d) Grimme, S.; Bahlmann, A. *Modern Cyclophane Chemistry* **2004**, 311; e) Braun, M.; Hohlmann, A. Rahematpura, J.; Buehne, C.; Grimme, S. *Chem. Eur. J.* **2004**, *10*, 4584; f) Furche, F.; Ahlrichs, R.; Wachsmann, C.; Weber, E.; Sobanski, A.; Voegtle, F.; Grimme, S. *J. Am. Chem. Soc.* **2000**, *122*, 1717; g) Stephens, P. J.; McCann, D. M.; Butkus, E.; Stoncius, S.; Cheeseman, J. R.; Frisch, M. J. *J. Org. Chem.* **2004**, *69*, 1948; h) Stephens, P.J.; McCann, D. M.; Devlin, F. J.; Cheeseman, J. R.; Frisch, M. J. *J. Am. Chem. Soc.* **2004**, *126*, 7514; i) Neugebauer, J.; Baerends, E. J.; Nooijen, M.; Autschbach, J. *J. Chem. Phys.* **2005**, *122*, 234305/1-234305/7; j) Pecul, M.; Marchesan, D.; Ruud, K.; Coriani, S. *J. Chem. Phys.* **2005**, *122*, 024106/1-024106/9; k) Giorgio, E.; Tanaka, K.; Ding, W.; Krishnamurthy, G.; Pitts, K.; Ellestad, G. A.; Rosini, C.; Berova, N. *Bioorg. Med. Chem.* **2005**, *13*, 5072; l) Mori, T.; Inoue, Y.; Grimme, S. *J. Org. Chem.* **2006**, *71*, 9797; m) Stephens, P. J.; McCann, D. M.; Devlin, F. J.; Smith, A. B., III *J. Nat. Prod.* **2006**, *69*, 1055; n) Salam, Y.M.A. *Chem. Phys*. **2006**, *324*, 622-630; o) Bringmann, G.; Gulder, T.;

Reichert, M.; Meyer, F. *Org. Lett*. **2006**, *8*, 1037-1040; p) Stephens, P. J.; Pan, J.-J.; Devlin, F. J.; Urbanova, M.; Hajicek, J. *J. Org. Chem.*, **2007**, *72*, 2508; q) Casarini, D.; Lunazzi, L.; Mancinelli, M.; Mazzanti, A.; Rosini, C. *J. Org. Chem.* **2007**, *72*, 7667-7676; r) Goel, A.; Singh, F.V.; Kumar, V.; Reichert, M.; Goulder, T. A. M.; Bringmann, G. *J. Org. Chem.* **2007**, *72*, 7765-7768.

55) Gilman, H.; Gorsich, R. D. *J. Am. Chem. Soc.* **1956**, *78*, 2217.

56) Lunazzi, L.; Mazzanti, A.; Minzoni, M. *J. Org. Chem.* ***2006****, 71*, 9297.

57) a) Stott, K.; Stonehouse, J.; Keeler, J.; Hwand, T.-L.; Shaka, A.J. *J. Am. Chem. Soc.* **1995**, *117*, 4199. b) Stott, K.; Keeler, J.; Van, Q. N.; Shaka, A. J. *J. Magn. Resonance* **1997**, *125*, 302. c) Van, Q. N.; Smith, E. M.; Shaka, A. J. *J. Magn. Resonance* **1999**, *141*, 191. d) See also: Claridge, T.D.W. *High Resolution NMR Techniques in Organic Chemistry*; Pergamon: Amsterdam, **1999**.

58) Kupče, E.; Boyd, J.; Campbell, I. D. *J.Magn. Reson. Series B*, **1995**, *106*, 300.

59) Wu, D.; Chen, A.; Johnson, C.S. *J. Magn. Reson. A* **1995**, *115*, 260

60) Tyrrell, H.J.W; Harris, K.R. *Diffusion in Liquids*; Butter-Worth: London 1984

61) Santos, F.J.V.; Nieto de Castro, C.A.; Dymond J.H.; Dalaouti, N. K.; Assale, M. J.; Akira Nagashima, A. *J. Phys. Chem. Ref. Data* **2006**, *35*,1

62) Mitchell, R. H.; Yan, J. S. H. *Can. J. Chem*. **1980**, *58*, 2584-2587.

63) a) Clough, R. L.; Roberts, J. D. *J. Am. Chem. Soc*. **1976**, *98*, 1018-1020; b) Cozzi, F.; Cinquini, M.; Annunziata, R.; Siegel, J. S. *J. Am. Chem. Soc*. **1993**, *115*, 5330-5331; c) Cozzi, F.; Ponzini, F.; Annunziata, R.; Cinquini, M.; Siegel, J. S. *Angew. Chem. Int. Ed. Engl.* **1995**, *34*, 1019-1020; d) Zoltewicz, J. A.; Maier, N. M. ; Fabian, W. M .F. *Tetrahedron* **1996**, *52*, 8703-8706; e) Zoltewicz, J. A.; Maier, N. M. ; Fabian, W. M. F. *J. Org. Chem*. **1996**, *61*, 7018-7021; f) Thirsk, C.; Hawkes, G. E.; Kroemer, R. T.; Liedl, K. R.; Loerting, T.; Nasser, R.; Pritchard, R. G.; Steele, M.; Warren, J. E.; Whiting, A. *J. Chem. Soc. Perkin Trans. 2* **2002**, 1510-1519; g) Tumambac, G. E.; Wolf, C. *J. Org. Chem*. **2005**, *70*, 2930-2938.

64) Lai, J.-H. *J. Chem. Soc. Perkin Trans. 2* **1986**, 1667-1670.

65) a) House, H.; Hrabie, J.A.; Van Derveer, D. *J. Org. Chem*. **1986**, *51*, 920-929; b) House, H.; Holt, J.T.; Van Derveer, D. *J. Org. Chem*. **1993**, *58*, 7516-7523; c) Lunazzi, L.; Mancinelli, M.; Mazzanti, A. *J. Org. Chem*. **2007**, *72*, 5391-5394.

66) Cross, W.; Hawkes, G. E.; Kroemer, R. T.; Liedl, K. R.; Loerting, T.; Nasser, R.; Pritchard, R. G.; Steele, M.; Watkinson, M.; Whiting, A. *J. Chem. Soc. Perkin Trans. 2* **2001**, 459-467.

67) Lai, Y.-H.; Chen, P. *J. Chem. Soc. Perkin Trans. 2* **1989**, 1665-1670. Lai, Y.-H. *J. Chem. Soc. Perkin Trans. 2* **1986**, 1667-1670.

68) Anderson, J. E.; Casarini, D.; Lunazzi, L.; *Tetrahedron Lett*. **1988**, *29*, 3141-3144.

69) In a theoretical paper describing compounds analogous to **22** only one of the two possible anti conformers was, inexplicably, considered (see: Bigdeli, M. A.; Moradi, S.; Nemati, F. *J. Mol. Structure Theochem* **2007**, *807*, 125-135.).

70) The CH/π interaction is the weakest extreme of hydrogen bonds that occurs between a soft acid (CH) and a soft base (π-system) in the context of Pearson's HSAB principle. See: Nishio, M. *Tetrahedron* **2005**, *61*, 6923.

71) see: Nishio, M.; Hirota, M; Umezawa, Y. *The CH/π interaction: Evidence, Nature and Consequences;* Wiley: Weinheim, 1998.

72) see : Bonini, B. F.; Grossi, L.; Lunazzi, L. *J.Org.Chem*. **1986**, *51*, 517-522.

73) See, for instance: a) Jackson, W. R.; Jennings, W. B. *Tetrahedron Letters*, **1974**, *15*, 1837-1838; b) Anderson, J. E.; Casarini, D.; Ijeh, A. J.; Lunazzi, L. *J. Am. Chem. Soc*. **1997**, *119*, 8050-8057; c) Lunazzi, L.; Mazzanti, A.; Álvarez Muñoz, A. *J.Org.Chem*. **2000**, *65,* 3200-3206.

74) Dissimilarities between the conformations in solution with respect to the structures found in the solids have been reported, see: Johansen, J. T.; Vallee, B. L. *Proc. Nat. Acad. Sci. USA* **1971**, *68*, 2532-2535. Kessler, H. *Fresenius Z. Anal. Chem*. **1987**, *327*, 66-67. Burke, L. P.; DeBellis, A. D.; Fuhrer, H.; Meier, H.; Pastor, S. D.; Rihs, G.; Rist, G.; Rodebaugh, R. K.; P. Shum, S. P. *J. Am. Chem. Soc.* **1997**, *119*, 8313-8323. Paulus, E. F.; Kurz, M.; Matter, H.; Vértesy. L. *J. Am. Chem. Soc.* **1998**, *120*, 8209-8221. Coluccini, C.; Grilli, S.; Lunazzi, L.; Mazzanti, A. *J.Org. Chem*. **2003**, *68*, 7266-7273. Perry, N. B.; Blunt, J. W.; Munro, M. H. *Magn. Reson. Chem*. **2005**, *27*, 624-627.

75) Saunders, J. K.; Bell, R. A. *Can J. Chem*. **1970**, *48*, 512-513. Combrisson, S.; Roques, B.; Rigny, P.; Basselier, J. J. *Can J. Chem*. **1971**, *49*, 904-918. Neuhaus, D.; Williamson, M. *The Nuclear Overhauser Effect in Structural and Conformational Analysis*; VCH Publishers Inc.: New York N.Y., 1989; Chapter 5.

76) a) Westheimer, F. H. in *Steric Effect in Organic Chemistry*; Newman, M. S. Ed.; John Wiley and Sons, Inc.: New York N. Y., 1956; Chapter 12; b) Karnes, H. A.; Rose, M. L.; Collat, J. W.; Newman, M. S. *J. Am. Chem. Soc*. **1968**, *90*, 458-461; c) Decouzon, M.; Ertl, P.; Exner, O.; Gal, J.-F.; Maria, P.-C. *J. Am. Chem. Soc*. **1993**, *115*, 12071-12078; d) Heiss, F.; Marzi, E.; Schlosser, M. *Eur. J. Org. Chem*. **2003**, 4625-4629; e) Gorecka, J.; Heiss, C.; Scopelliti, R.; Schlosser, M. *Org. Lett*. **2004**, *6*, 4591-4593; f) Heiss, C.; Leroux, F.; Schlosser, M. *Eur. J. Org. Chem*. **2005**, 5242-5247; g) Schlosser, M.; Cottet, F.; Heiss, C.; Lefebvre, O.; Marull, M.; Masson, E.; Scopelliti, R. *Eur. J. Org. Chem*. **2006**, 729-734.

77) The conformational assignment in compounds **26** and **27** was obtained by means of the mentioned low temperature NOE experiments.

78) Irradiation of the ^{13}C satellite (1% natural abundance) of the NMR ^{1}H signals yields NOE effects on the spatially close hydrogen of the same isotopomer but not on the hydrogens of the 99% isotopomer having only ^{12}C atoms. In a DPFGSE-NOE sequenze, the latter signals are completely canceled, and it is possible, therefore, to detect NOE effect experienced by isochronous lines that would not be otherwise observable. This allows the structural assigments of symmetric isomers to be unambiguously obtaines. See: Lunazzi, L.; Mazzanti, A. *J. Am. Chem. Soc*. **2004**, *126*, 12155-12157.

79) Dell' Erba, C.; Gasparrini, F.; Grilli, S.; Lunazzi, L.; Mazzanti, A.; Novi, M.; Pierini, M.; Tafani, C.; Villani, C. *J.Org. Chem*. **2002**, *67*, 1663-1668.

80) Grilli, S.; Lunazzi, L.; Mazzanti, A.; Pinamonti, M. *Tetrahedron* **2004**, *60*, 4451-4458.

81) a)Humayun Kabir, S. M.; Hasegawa, M.; Kuwatani, Y.; Yoshida, M.; Matsuyama, H.; Iyoda, M. *J. Chem Soc. Perkin Trans. 1* **2001**, 159-165. b) For the preparation of the intermediate 2,2',6,6'-tetrabromobiphenyl see: Rajca, A.; Safronov, A.; Rajca, S.; Ross, C. R. II; Stezowski, J. J. *J. Am. Chem. Soc* **1996**, *118*, 7272-7279.

82) Leroux, F.: Schlosser, M. *Angew. Chem. Int. Ed.* **2002**, *41*, 4272-4274.

83) Pathak, R.; Nhlapo, J. M.; Govender, S.; Michael, J. P.; Van Otterlo, W. A. L.; De Koning, C. B. *Tetrahedron* **2006**, *62*, 2820-2830.

84) Thompson, W. J.; Gaudino, J. *J.Org.Chem.* **1984**, *49*, 5237.

85) a) O'Boyle, N. M. GaussSum 2.1.3, 2007. Available at http://gausssum.sf.net. b) O'Boyle, N. M.; Tenderholt, A. L.; Langner, K.M. *J. Comp. Chem.,* **2007**, DOI 10.1002/jcc.20823

86) Cozzi, F.; Annunziata, R.; Benaglia, M.; Cinquini, M.; Raimondi, L.; Baldridge, K. K.; Siegel, J. S. *Org. Biomol. Chem.* **2003**, *1*, 157.

87) Jones, G. B. *Tetrahedron* **2001**, *57*, 7999.

88) a) Diederich, F. *Angew. Chem., Int. Ed. Engl.* **1988**, *27*, 362; b) Smithrud, D. B.; Wyman, T. B.; Diederich, F. *J. Am. Chem. Soc.* **1991**, *113*, 5420; c) Conn, M. M.; Deslongchamps, G.; de Mendoza, J.; Rebek, J. *J. Am. Chem. Soc.* **1993**, *115*, 3458; d) Philip, D.; Stoddardt, J. F. *Angew. Chem., Int. Ed. Engl.* **1996**, *35*, 1154; e) Muehldorf, A. V.; Van Egen, D.; Warner, J. C.; Hamilton, A. D. *J. Am. Chem. Soc.* **1988**, *110*, 6561; f) Zimmermann, S. C.; Zeng, Z.; Wu, W.; Reichert, D. E. *J. Am. Chem. Soc.* **1991**, *113*, 183; g) Newcomb, L. T.; Gellman, S. H. *J. Am. Chem. Soc.* **1994**, *116*, 4993; h) Cochran, J. E.; Parrott, T. J.; Whitlock, H. W. *J. Am. Chem. Soc.* **1992**, *114*, 2269.

89) a) Saenger, W. *Principles of Nucleic Acid Structures*; Springer Verlag: New York, **1984**. b) Burley, S. K.; Petsko, G. A. *Science* **1985**, *229*, 23; c) Hunter, C. A.; Singh, J.; Thornton, J. M. *J. Mol. Biol.* **1991**, *218*, 837; d) Hunter, C. A. *J. Mol. Biol.* **1993**, *230*, 1025; e) Schall, O. F.; Gokel, G. W. *J. Org. Chem.* **1996**, *61*, 1149; f) Guckian, K. M.;

Schweitzer, B. A.; Ren, R. X. F.; Sheils, C. J.; Paris, P. L.; Tanmasseri, D. C.; Kool, E. T. *J. Am. Chem. Soc.* **1996**, *118*, 8182; g) Ho, T. L.; Liao, P. Y.; Wang, K. T. *J. Chem. Soc., Chem. Commun.* **1995**, 2437; h) Ranganathan, D.; Hardas, V.; Gilardi, R.; Karle, J. L. *J. Am. Chem. Soc.* **1998**, *120*, 10793; i) Chelli, F.; Gervasio, F.L.; Procacci, P.; Schettino, V. *J. Am. Chem. Soc.* **2002**, *124*, 6133; j) Chelli, F.; Gervasio, F.L.; Procacci, P.; Schettino, V. *Proteins* **2002**, *48*, 117.

90) a) Dahl, T. *Acta Chem. Scand.* **1994**, *48*, 95; b) Williams, J. H. *Acc. Chem. Res.* **1993**, *26*, 593; c) Anderson, H. L.; Bashall, A.; Henrick, K.; McPartlin, M.; Sanders, J. K. M. *Angew. Chem., Int. Ed. Engl.* **1994**, *33*, 429; d) Dance, I.; Scuddar, M. *Chem. Eur. J.* **1996**, *2*, 481; e) Wang, Z. H.; Hirose, T. Hiratani, K.; Yang, Y.; Kasuga, K. *Chem. Lett.* **1996**, 603; f) Martin, C. B.; Patrick, B. O.; Cammers-Goodwin, A. *J. Org. Chem.* **1999**, *64*, 7568; g) Nakamura, Y.; Suzuki, H.; Hayashida, Y.; Kudo, T.; Nishimura, J. *Liebigs Ann./Recl.* **1997**, 1769.

91) For an opposite situation see: Chen, C-T; Chadah, R.; Siegel, J.S.; Hardcastle, K. *Tetrahedron Lett*. **1995**, *36*, 8403-8406.

92) Renaud, R. N.; Bovenkamp, J. W.; Fraser, R. R.; Capoor, R. *Can. J. Chem*. **1977**, *55*, 2642-2648 and references quoted therein.

93) see: Fraser, R.R.; Pettit, M.A.; Miskow, M. *J. Am. Chem. Soc*. **1972**, *94*, 3253-3254. Kainosho, M.; Ajisaka, K.; Pirkle, W.H.; Beare, S. D. *J. Am. Chem. Soc*. **1972**, *94*, 5924-5926.

94) see: Casarini, D.; Davalli, S.; Lunazzi, L.; Macciantelli, D. *J.Org. Chem*. **1989**, *54*, 4616-4619. Casarini, D.; Lunazzi, L.; Verbeek, R *Tetrahedron* **1996**, 52, 2471-2480. Casarini, D.; Lunazzi, L.; Mazzanti, A. *Angew. Chem. Int. Ed*. **2001**, *40*, 2536-2539.

95) see, for instance, Ayala, P.Y; Schlegel, H.B. *J. Chem. Phys.* **1998**, *108*, 2314-2325.

96) See also: Lunazzi, L.; Mazzanti, A.; Minzoni, M. *J.Org. Chem*. **2005**, *70*, 10062-10066.

97) a) Lomas, J. S.; Cordier, C. *J. Phys. Org. Chem*. **2003**, *16*, 361-368; b) Lunazzi, L.; Mazzanti, A.; Minzoni, M. *J. Org. Chem.* **2007**, *72*, 2501-2507; c) Lunazzi L.; Mazzanti, A.; Rafi, S.; Rao, H. S. P. *J. Org. Chem.* **2008**, *73*, 678-688.

98) The average distances between the methyl hydrogens, used for comparing the NOE effects, were derived from the DFT computed structures by the relationship $\langle r^{-6} \rangle^{-1/6}$, according to: Claridge, T. D. W. *High-Resolution NMR Techniques in Organic Chemistry;* Pergamon Press: Oxford, **1999**; p 303.

99) House, H.O.; Hrabie, J.A.; VanDerveer, D. *J. Org. Chem*. **1986**, *51*, 921.

100) House, H.O.; Holt, J.T.; VanDerveer, D. *J. Org. Chem*. **1993**, *58*, 7516.

101) Molecular Mechanics approach using the MMFF force field, as in PC Model v 7.5, Serena Software, Bloomington, IN.

102) a) Grilli, S.; Lunazzi, L.; Mazzanti, A. *J. Org. Chem*. **2001**, *66*, 4444; b) Grilli, S.; Lunazzi, L.; Mazzanti, A. *J. Org. Chem*. **2001**, *66*, 5853; c) Jog, P. V.; Brown, R. E.; Bates, D. K. *J. Org. Chem*. **2003**, *68*, 8240; d) Casarini, D.; Lunazzi, L.; Mazzanti, A.; Mercandelli, P.; Sironi, A. *J. Org. Chem*. **2004**, *69*, 821.

103) Pérez-Trujillo, M.; Maestre, I.; Jaime, C.; Alvarez-Larena, A.; Pinella, J. F.; Virgili, A. *Tetrahedron: Asymmetry* **2005**, *16*, 3084.

104) PC version of the DNMR program n° 633, QCPE, Indiana University, Bloomington, IN, USA.

105) a) Stonehouse, J.; Adell, P.; Keeler, J.; Shaka, A. J. *J .Am. Chem. Soc.* **1994**, *116*, 6037; b) Stott, K.; Stonehouse, J.; Keeler, J.; Hwang, T. L.; Shaka, A. J. *J. Am. Chem. Soc.* **1995**, *117*, 4199; c) Stott, K.; Keeler, J.; Van, Q.N.; Shaka, A. J. *J. Magn. Reson.* **1997**, *125*, 302; d) Van, Q. N.; Smith, E. M.; Shaka, A. J. *J. Magn. Reson.* **1999**, *141*, 191.

106) Kishner, N. J. *Russ. Phys. Chem. Soc.* **1911***, 43*, 582. Wolff, L. *Ann.* **1912***, 394*, 86. Todd, D. *Org. React*. **1948***, 4*, 378.

107) Prepared according to: Thompson, W. J.; Gaudino, J. *J.Org.Chem.* **1984**, *49*, 5237.

108) The NOE experiment was carried out at 0 °C to avoid the possibility of a saturation transfer process between the two conformers.

109) Smallcombe, S. H. *J. Am. Chem. Soc.* **1993**, *115*, 4776; Patt, S. *J. Magn. Reson.* **1992**, *96*, 94.

110) Forsén, S.; Hoffmann, R. A. *Acta Chem. Scand.* **1963**, *17*, 1787.

111) a) Mislow, K.; Ternay, A.L. Jr; Melillo, J.T., *J. Am. Chem. Soc.* **1963**, *85*, 2329; b) Mislow, K; Green, M.M.; Laur, P.; Melillo, J.T.; Simmons, T.; Ternay, A.L. Jr, *J. Am. Chem. Soc.* **1965**, *87*, 1958; c) Jacobus, J.; Mislow, K., *J. Am. Chem. Soc.* **1967**, *89*, 5228; d) Saeva, F.D.; Rayner, D.R.; Mislow, K., *J. Am. Chem. Soc.* **1968**, *90*, 4176; e) Landini, D.; Modena, G.; Montanari, F.; Scorrano, G., *J. Am. Chem. Soc.* **1970**, *92*, 7168; f) Quintily, U.; Scorrano, G., *Chem. Comm.* **1971**, 260; g) Andersen, K.K., Stereochemistry, conformation, and chiroptical properties of sulfoxides. In: Patai, S.; Rappoport, Z.; Stirling, C.J.M., editors. The chemistry of sulfones and sulfoxides. Chichester UK:Wiley; **1988**, p 55-94.

112) a) Pitchen, P.; Duñach, E.; Deshmukh, M.N.; Kagan, H.B., *J. Am. Chem. Soc.* **1984**,*106*, 8188; b) Rebiere, F.; Samuel, O.; Ricard, L.; Kagan, H.B., *J. Org. Chem.* **1991**, *56*, 5991; c) Brunel, J-M.; Diter, P.; Dustch, M.; Kagan, H.B., *J. Org. Chem.* **1995**, *60*, 8086; d) Kagan, H.B., Asymmetric oxidation of sulfides. In: Ojima, I., editor. Catalytic asymmetric synthesis. New York: VCH; **1993** p 203-226; e) Andersen, K.K., *Tetrahedron*

Lett. **1962**, *3*, 93; f) Di Furia, F.; Modena, G.; Seraglia, R., *Synthesis* **1984**, 325; g) Andersen, K.K.; Gaffield, W; Papanikolaou, N.E.; Foley, J.W.; Perkins, R.I., *J. Am. Chem. Soc.* **1964**, *86*, 5637; h) De Lucchi, O; Lucchini, V.; Marchioro, C.; Valle, G.; Modena, G., *J. Org. Chem.* **1986**, *51*, 1457; i) Di Furia, F.; Licini, G.; Modena, G.; Motterle, R.; Nugent, W.A., *J. Org. Chem.* **1996**, *61*, 5175; l) Donnoli, M.I.; Superchi, S.; Rosini, C., *J. Org. Chem.* **1998**, *63*, 9392.

113) a) Clayden, J.; Kubinski, P.M.; Sammiceli, F.; Helliwell, M.; Diorazio, L., Tetrahedron **2004**, *60*, 4387; b) Casarini, D.; Lunazzi, L.; Gasparrini, F.; Villani, C.; Cirilli, M.; Gavuzzo, E., J. Org. Chem. **1995**, *60*, 97; c) Casarini, D.; Lunazzi, L.; Mazzanti, A.; Mercandelli, P.; Sironi, A., J. Org. Chem. **2004**, *69*, 3574.

114) a) Bendazzoli, G.L.; Palmieri, P.; Gottarelli, G.; Moretti, I.; Torre, G., *J. Am. Chem. Soc.* **1976(a)**, *98*, 2659; b) Moretti, I.; Torre, G.; Gottarelli, G., *Tetrahedron Lett.* **1976(b)**, *17*, 711; c) Rosini, C.; Donnoli, M.I.; Superchi, S., *Chem. Eur. J.* **2001(a)**, *7*, 72; d) Donnoli, M.I.; Giorgio, E.; Superchi, S.; Rosini, C., *Org. Biomol. Chem.* **2003**, *1*, 3444; e) Donnoli, M.I.; Superchi, S.; Rosini, C., *Mini Rev. Org. Chem.* **2006**, *3*, 77.

115) a) Devlin, F.J.; Stephen, P.J.; Scafato, P.; Superchi, S.; Rosini, C., *Tetrahedron: Asymmetry* **2001(b)**, *12*, 1551; b) Stephens, P.J.; Aamouche, A.; Devlin, F.J.; Superchi, S.; Donnoli, M.I.; Rosini, C., *J. Org. Chem.* **2001(c)**, *66*, 3671.

116) a) Casarini, D.; Foresti, E.; Gasparrini, F.; Lunazzi, L.; Macciantelli, D.; Misiti, D.; Villani, C., *J. Org. Chem.* **1993**, *58*, 5674; b) Jennings, W.B.; Kochanewycz, M.J.; Lunazzi, L., *J. Chem. Soc., Perkin Trans. 2* **1997**, 2271.

117) Rosini C, Donnoli MI, Superchi S. *Chem. Eur. J.* **2001**(a);*7*, 72.

118) Mc Killop, A.; Koyunçu, D. *Tetrahedron Lett.* **1990**, *31*, 5007

119) Lupatelli, P.; Ruzziconi, R.; Scafato, P.; Degl'Innocenti, A.; Paolobelli, AB. *Synth Commun* **1997**, *27*, 441.

120) Greene, T. W.; Wuts, P. G. M. *Protective Groups in Organic Synthesis*; Wiley: New York, **1999**.

121) Clayden, J. *Organolithiums: Selectivity for Synthesys*. Pergamon: Oxford, **2002**.

122) a) Hoppe, D.; Hanko, R.; Brönneke, A. *Angew. Chem. Int. Ed.* **1980**, *19*, 625; b) Hoppe, D.; Brönneke,, A. *Synthesis* **1982**, 1045; c) Peters, J. G.; Seppi, M.; Fröhlich, R.; Wibbeling, B.; Hoppe, D. *Synthesis* **2002**, 381; d) Hoppe, D. *Angew. Chem. Int. Ed.* **1984**, *23*, 932; e) Hoppe, D.; Hintze, F.; Tebben, P. *Angew. Chem. Int. Ed.* **1990**, *29*, 1422; f) Hoppe, D.; Hintze, F. *Synthesys* **1992**, 1216; g) Hoppe, D.; Hense, T. *Angew. Chem. Int. Ed.* **1997**, *36*, 2282; h) Carstens, A.; Hoppe, D. *Tetrahedron* **1994**, *50*, 6097.

123) a) Zhang, P.; Gawley, R. E. *J. Org. Chem.* **1993**, *58*, 3223; b) Superchi, S.; Sotomayor, N.; Miao, G.; Babu, J.; Campbell, M. G.; Snieckus, V. *Tetrahedron Lett.* **1996**,

37, 6061; c) Slana, G. B. C. A.; de Azevedo, M. S.; Lopes, R. S. C.; Lopes, C. C.; Cardoso, J. N. *Beilstein J. Org. Chem.* **2002**, *2*, 1.

124) Clayden, J.; Dufour, J.; Grainger, D. M.; Helliwell, M. *J. Am. Chem. Soc.* **2007**, *129*, 7488.

125) DMPU = N,N'-dimethyl-N,N'-propylideneurea. It is routinely added DMPU to reactions where it is needed to promote organolithium nucleophilicity , particularly towards aromatic rings. See: Clayden, J.; Parris, S.; Cabedo, N.; Payne, A. H. *Angew. Chem. Int. Ed.* **2008**, *47*, 5060; Clayden, J.; Knowles, F. E.; Menet, C. J. *Synlett* **2003**,

126) Huang, R.; Shaughnessy, K.H.; *Chem. Commun.*, **2005**, 4484

127) Yamamoto, T.; Ohta, T.; Ito, Y., *Org. Lett.*, **2005**, *7*, 4153